Pyrolysis of *Eucalyptus grandis*

by

Jan-Erns Joubert

Thesis presented in partial fulfilment
of the requirements for the Degree

of

Master of Science in Engineering
(Chemical Engineering)

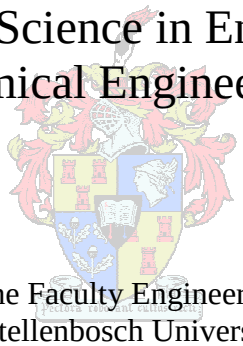

in the Faculty Engineering
at Stellenbosch University

Supervisor
Prof. J.H. Knoetze

Advisor
Dr. M. Carrier

March 2013

Declaration

By submitting this thesis electronically, I declare that the entirety of the work contained therein is my own, original work, that I am the sole author thereof (save to the extent explicitly otherwise stated), that reproduction and publication thereof by Stellenbosch University will not infringe any third party rights and that I have not previously in its entirety or in part submitted it for obtaining any qualification.

Jan-Erns Joubert — 26 February 2013

Signature — Date

ABSTRACT

In recent times, governments around the world have placed increasing focus on cleaner technologies and sustainable methods of power generation in an attempt to move away from fossil fuel derived power, which is deemed unsustainable and unfriendly to the environment. This trend has also been supported by the South African government, with clear intentions to diversify the country's power generation by including, among others, biomass as a renewable resource for electricity generation. Woody biomass and associated forestry residues in particular, could potentially be used as such a renewable resource when considering the large amount of fast growing hardwood species cultivated in South Africa. Approximately 6.3 million ton of *Eucalyptus grandis* is sold annually for pulp production while a further 7 million ton of *Eucalyptus* species are sold as round wood. With these tree species reaching commercial maturity within 7 – 9 years in the South African climate, there is real potential in harnessing woody biomass as a renewable energy source. In this study, pyrolysis was investigated as a method to condense and upgrade *E.grandis* into energy and chemical rich products.

The pyrolysis of *E.grandis* is the study of the thermal degradation of the biomass, in the absence of oxygen, to produce char and bio-oil. The thermal degradation behaviour of *E.grandis* was studied using thermo-gravimetric analysis (TGA) at the Karlsruhe Institute of Technology (KIT) in Germany and subsequently used to determine the isoconversional kinetic constants for *E.grandis* and its main lignocellulosic components. Slow, Vacuum and Fast Pyrolysis were investigated and optimised to maximise product yields and to identify the key process variables affecting product quality. The Fast Pyrolysis of *E.grandis* was investigated and compared on bench ($KIT_{0.1\ kg/h}$), laboratory ($SU_{1\ kg/h}$) and pilot plant scale ($KIT_{10\ kg/h}$), using Fast Pyrolysis reactors at Stellenbosch University (SU) in South Africa and at KIT in Germany. The Slow and Vacuum Pyrolysis of *E.grandis* was investigated and compared using a packed bed reactor at Stellenbosch University.

The TGA revealed that biomass particle size had a negligible effect on the thermal degradation behaviour of *E.grandis* at a heating rate set point of 50 °C/min. It was also shown that increasing the furnace heating rates shifted the thermo-gravimetric (TG) and differential thermo-gravimetric (DTG) curves towards higher temperatures while also

increasing the maximum rate of volatilisation. Lignin resulted in the largest specific char yield and also reacted across the widest temperature range of all the samples investigated. The average activation energies found for the samples investigated were 177.8, 141.0, 106.2 and 170.4 kJ/mol for holocellulose, alpha-cellulose, Klason lignin and raw *E.grandis*, respectively.

Bio-oil yield was optimised at 76 wt. % (daf) for the $SU_{1\ kg/h}$ Fast Pyrolysis plant using an average biomass particle size of 570 µm and a reactor temperature of 470 °C. Differences in the respective condensation chains of the various Fast Pyrolysis reactor configurations investigated resulted in higher gas and char yields for the KIT reactor configurations compared to the $SU_{1\ kg/h}$ Fast Pyrolysis plant.

Differences in the vapour residence time between Slow (>400 s) and Vacuum Pyrolysis (< 2 s) resulted in a higher liquid and lower char yield for Vacuum Pyrolysis. Local liquid yield maxima of 41.1 and 64.4 wt. % daf were found for Slow and Vacuum Pyrolysis, respectively (achieved at a reactor temperature of 450 °C and a heating rate of 17 °C/min). Even though char yields were favoured at low reactor temperatures (269 – 300 °C), the higher heating values of the char were favoured at high reactor temperatures (29 – 34 MJ/kg for 375 – 481 °C). Reactor temperature had the most significant effects on product yield and quality for the respective Slow and Vacuum Pyrolysis experimental runs. The bio-oils yielded for SP and VP were found to be rich in furfural and acetic acid.

OPSOMMING

Regerings regoor die wêreld het in die afgelope tyd toenemende fokus geplaas op skoner tegnologie en volhoubare metodes van kragopwekking in 'n poging om weg te beweeg van fossielbrandstof gebasseerde energie, wat geag word as nie volhoubaar nie en skadelik vir die omgewing. Hierdie tendens is ook ondersteun deur die Suid-Afrikaanse regering, met 'n duidelike bedoeling om die land se kragopwekking te diversifiseer deur, onder andere, biomassa as 'n hernubare bron vir die opwekking van elektrisiteit te gebruik. Houtagtige biomassa en verwante bosbou afval in die besonder, kan potensieel gebruik word as so 'n hernubare hulpbron, veral aangesien ‘n groot aantal vinnig groeiende hardehout spesies tans in Suid-Afrika verbou word. Ongeveer 6,3 miljoen ton *Eucalyptus grandis* word jaarliks verkoop vir pulp produksie, terwyl 'n verdere 7 miljoen ton van *Eucalyptus* spesies verkoop word as paal hout. Met hierdie boom spesies wat kommersiële volwassenheid bereik binne 7 - 9 jaar in die Suid-Afrikaanse klimaat, is daar werklike potensiaal vir die benutting van houtagtige biomassa as 'n hernubare energiebron. In hierdie studie is pirolise ondersoek as 'n metode om *E.grandis* te kondenseer en op te gradeer na energie en chemikalie ryke produkte.

Die pirolise van *E.grandis* is die proses van termiese afbreking van die biomassa, in die afwesigheid van suurstof, om houtskool en bio-olie te produseer. Die termiese afbrekingsgedrag van *E.grandis* is bestudeer deur gebruik te maak van termo-gravimetriese analise (TGA) by die Karlsruhe Instituut van Tegnologie in Duitsland en daarna gebruik om die kinetiese konstantes vir die iso-omskakeling van *E.grandis* en sy hoof komponente te bepaal. Stadige, Vakuum en Snel pirolise is ondersoek en geoptimiseer om produk opbrengste te maksimeer en die sleutel proses veranderlikes wat die kwaliteit van die produk beïnvloed te identifiseer. Die Snel Pirolise van *E.grandis* is ondersoek en vergelyk op bank- ($KIT_{0.1\ kg/h}$), laboratorium- ($SU_{1\ kg/h}$) en proefaanlegskaal ($KIT_{10\ kg/h}$) deur gebruik te maak van Snel pirolise reaktore by die Universiteit van Stellenbosch (US) in Suid-Afrika en die Karlsruhe Instituut van Tegnologie (KIT) in Duitsland. Die Stadige en Vakuum Pirolise van *E.grandis* is ondersoek en vergelyk met behulp van 'n gepakte bed reaktor aan die Universiteit van Stellenbosch.

Die TGA studie het openbaar dat biomassa deeltjiegrootte 'n onbeduidende uitwerking op die termiese afbrekingsgedrag van *E.grandis* het by 'n verhittings tempo van 50 ° C / min. Dit is

ook bewys dat die verhoging van die oond verwarming tempo die termo-gravimetriese (TG) en differensiële termo-gravimetriese (DTG) kurwes na hoër temperature verskuif, terwyl dit ook die maksimum tempo van vervlugtiging laat toeneem het. Lignien het gelei tot die grootste spesifieke houtskool opbrengs en het ook oor die wydste temperatuur interval gereageer van al die monsters wat ondersoek is. Die gemiddelde aktiveringsenergieë vir die monsters wat ondersoek is, was 177,8, 141,0, 106,2 en 170,4 kJ / mol, onderskeidelik vir holosellulose, alpha-sellulose, Klason lignien en rou *E.grandis*.

Bio-olie opbrengs is geoptimeer teen 76 wt. % (DAF) vir die $SU_{1\ kg\ /\ h}$ Snel Pirolise aanleg met behulp van 'n gemiddelde biomassa deeltjiegrootte van 570 µm en 'n reaktor temperatuur van 470 ° C. Verskille in die onderskeie kondensasie kettings van die verskillende Snel Pirolise aanlegte wat ondersoek is, het gelei tot hoër gas- en houtskool opbrengste vir die KIT reaktor konfigurasies in vergelyking met die $SU_{1kg/h}$ FP plant.

Verskille in die damp retensie tyd tussen Stadige (> 400 s) en Vakuum pirolise (<2 s) het gelei tot 'n hoër vloeistof en laer houtskool opbrengs vir Vakuum Pirolise. Plaaslike vloeistof opbrengs maksima van 41,1 en 64,4 wt. % (daf) is gevind vir Stadig en Vakuum pirolise onderskeidelik, bereik by 'n reaktor temperatuur van 450 ° C en 'n verhittingstempo van 17 ° C / min. Selfs al is houtskool opbrengste bevoordeel by lae reaktor temperature (269 - 300 ° C), is die hoër warmte waardes van die houtskool bevoordeel deur hoë reaktor temperature (29 - 34 MJ / kg vir 375 - 481 ° C). Reaktor temperatuur het die mees beduidende effek op die produk opbrengs en kwaliteit vir die onderskeie Stadige Pirolise en Vakuum Pirolise eksperimentele lopies gehad. Die bio-olies geproduseer tydens Stadige en Vakuum Pirolise was ryk aan furfuraal en asynsuur.

ACKNOWLEDGEMENTS

The author would like to extend words of thanks and acknowledgement towards his supervisors, Professor Hansie Knoetze and Doctor Marion Carrier of the Department of Process Engineering at the University of Stellenbosch for their guidance and support throughout the course of this degree. A special word of thanks is extended toward PAMSA (Paper Manufacturers Association of South Africa) and Mondi South Africa for providing the financial support required for the study. Thank you to Doctor Ralph Stahl and the rest of the team at the Karlsruhe Institute of Technology (KIT) in Germany for making the visit to KIT possible and for assisting me in the lab. Thank you to Hanlie Botha and the laboratory technicians for their assistance with laboratory analyses for the work conducted in South Africa.

I would like to thank my friends and family, in particular Laura, Joan and Erns, for their emotional support and encouragement throughout the entire duration of my studies. Finally, I would like to thank my heavenly Father for providing for me and guiding me every step of the way.

TABLE OF CONTENTS

LIST OF FIGURES

LIST OF TABLES

ABBREVIATIONS AND NOMENCLATURE

Symbol	Definition	Unit
BET	Brunauer, Emmett and Teller surface area	[m^2/g]
C_i	Component i in the condensation chain	[-]
COD	Chemical Oxygen demand	[mg/l]
HHV	Higher Heating Value	[MJ/kg]
ID	Internal Diameter	[mm]
$M_{biomass\ (daf)}$	Mass of biomass fed on a dry and ash free basis	[g]
$M_{Biomass\ fed\ (daf)}$	Mass of biomass fed to reactor on a dry and ash free basis	[kg]
$M_{biomass\ moisture}$	Mass of initial moisture in the biomass used	[g]
$M_{bulk\ liquid}$	Mass of bulk liquid	[g]
MC	Moisture Content	[wt%]
$M_{char\ pots}$	Mass of char in char pots	[g]
MC_i	Mass of product from component i in the condensation chain	[g]
MC_{io}	Empty mass of component i in the condensation chain	[g]
$M_{condenser\ Liquid}$	Mass of liquid recovered from condenser	[g]
M_{ESP}	Mass of ESP product	[kg]
M_{Filter}	Dry mass of char recovered from ethanol washing	[g]
$M_{gas\ i}$	Mass of gas i detected by GC	[kg]
M_{K1}	Mass of product from K1	[kg]
M_{K2}	Mass of K2 product	[kg]
$M_{K2\ init}$	Starting inventory mass for K2	[kg]
$M_{reactor}$	Mass of reactor after experiment	[g]
$M_{reactor\ content}$	Mass of reactor contents	[g]
$M_{reactor\ o}$	Empty mass of reactor	[g]
M_{sand}	Mass of initial sand bed	[g]
$M_{tarry\ phase}$	Mass of tarry phase after acetone evaporation	[g]
n	Total number of gas species detected with GC	[-]
TOC	Total Organic Carbon	[mg/l]
x	Elemental Mass Fraction	[-]

x_{ash}	Mass fraction of ash	[-]
x_C	Mass fraction of elemental carbon	[-]
$x_{char\ K1}$	Char mass fraction of K1product	[-]
x_H	Mass fraction of elemental hydrogen	[-]
$x_{liquid\ K1}$	Liquid fraction of K1 product	[-]
x_N	Mass fraction of elemental nitrogen	[-]
x_O	Mass fraction of elemental oxygen	[-]
x_S	Mass fraction of elemental sulphur	[-]
Y_{char}	Char Yield	[wt. % daf]
Y_{gas}	Gas Yield	[wt. % daf]
Y_{liquid}	Liquid Yield	[wt. % daf]
α	Conversion Factor	[-]

Abbreviation	**Definition**
A	Pre-exponential Constant
a.r.	As Received
AKTS	Advanced Kinetics and Technology Solutions
BFBR	Bubbling Fluidised Bed Reactor
C	Elemental Carbon
daf	Dry ash-free
DOE	Design of experiments
DTG	Differential Thermo-thermogravimetric
E.grandis	*Eucalyptus grandis*
E_a	Apparent Activation Energy
ESP	Electrostatic Precipitator
FP	Fast Pyrolysis
GC	Gas Chromatography
GC-MS	Gas Chromatography coupled with Mass Spectroscopy
H	Elemental Hydrogen
HPLC	High Performance Liquid Chromatography
K1	Condenser 1 (10 kg/h PDU at KIT)
K2	Condenser 2 (10 kg/h PDU at KIT)

KF	Karl Fischer
KIT	Karlsruhe Institute of Technology
$KIT_{0.1\ kg/h}$	Karlsruhe Institute of Technology 0.1 kg/h Fast Pyrolysis Plant
N	Elemental Nitrogen
n.a.	Not Applicable
O	Elemental Oxygen
O/C	Oxygen to Carbon Ratio
PDU	Process Demonstration Unit
S	Elemental Sulphur
SP	Slow Pyrolysis
SU	Stellenbosch University
$SU_{1\ kg/h}$	Stellenbosch University 1 kg/h Fast Pyrolysis Plant
TCD	Thermal Conductivity Detector
TG	Thermo-gravimetric
TGA	Thermo Gravimetric Analysis
TGA-MS	Thermo Gravimetric Analysis coupled with Mass Spectroscopy
TSR	Twin Screw Reactor
UV	Ultra Violet
VP	Vacuum Pyrolysis
wt. %	Weigh percentage
wt. % daf	Weight percentage on a dry and ash free basis
wt. % dry	Weight percentage on a dry basis
XRF	X-Ray Fluorescence

1 Introduction

In light of the current economic climate, the energy crisis and concerns about weather pattern changes, the global tendency is towards reducing the impact of everyday life on the ecosystem through cleaner technologies, lower emissions and focussing on renewability and sustainability with regard to energy production and usage. Of specific concern is the possible depletion of fossil fuels and the adverse effects the use of these fuels can have on the environment. Consequently, steps have been taken by the South African government to ensure that energy generation is diversified over the next 20 years in such a way as to facilitate climate change mitigation. These commitments, as stated in the Integrated Resource Plan 2010 report, have been revised and updated accordingly on May 6, 2011 (Peters, 2011). Of specific interest are the incentives towards using biomass as a source of renewable energy in an attempt to alleviate the energy shortage and to stimulate sustainable development.

Eucalyptus species are preferred as the hardwood feedstock for the paper and pulp industry not only in South Africa, but globally. The main reason for this is the low production costs, the rapid growth (especially in the South African climate) and the favourable fibre qualities exhibited for pulping (Da Silva *et al.* 2009). A typical *E.grandis* clone can be harvested for paper and pulp manufacture within 7-8 years of planting the clone, compared to the ± 70 years of growth required in the Northern hemisphere before a hardwood can be harvested (Cox, 2011). Approximately 7 million ton of the round wood sales in South Africa are made up by eucalyptus species, while 6.3 million ton of *E.grandis* is sold annually as pulpwood (Godsmark, 2010). This amounts to a substantial volume of biomass, without even taking the waste biomass such as roots, branches and leaves into account. These facts make the use of fast growing hardwoods such as *E.grandis* an attractive option to consider as a possible resource in the attempts to diversify South Africa's energy supply.

Pyrolysis has been shown to be an effective method for condensing bulky biomass such as wood into valuable and easily transportable products. The liquid and solid phases resulting from the pyrolysis process are of particular interest. The liquid phase product, widely referred to as bio-oil or bio-crude, contains various valuable chemicals and can also be utilised as a fuel in burners and boilers (Bridgwater, 2004; Czernik and Bridgwater 2004). The solid phase product is referred to as char and has been shown to have application as a

solid fuel (Elyounssi *et al.* 2010), activated carbon (Tancredi *et al.* 1996) and in soil amendment as biochar (Lehmann *et al.* 2003). Research has also focussed on using pyrolysis as an intermediate step to gasification and the production of synthetic fuels (Henrich *et al.*, 2009).

Pyrolysis data can be found in the literature for various Eucalyptus species such as *E.globulus, E.regnans, E.loxophelba* and forestry wastes such as branches, stumps, bark, etc., but almost no data is available for the Pyrolysis of *E.grandis*. The data that are available for *E.grandis* are not easily comparable with other literature due to limited information regarding the reactor configurations, the scale of the operations and the process parameters employed in the various studies. In most instances it is also unclear whether optimum conditions were employed to generate the pyrolysis data.

1.1 Objectives and scope

The purpose of this study is to investigate and compare the yields of products and their properties resulting from the Slow, Vacuum and Fast Pyrolysis of *E.grandis*. In order to achieve this goal, six sub-objectives were set. The main objectives of this study were:

1. To identify and understand the parameters which influence the product yields and quality of woody biomass pyrolysis as researched in scientific literature.
2. To characterise the biomass in terms of its chemical and lignocellulosic composition and to extract the main lignocellulosic components of the biomass for thermo-gravimetric analysis.
3. To understand the thermal degradation behaviour of *E.grandis* by using thermo-gravimetric analysis (TGA) and to compare the results to that of the major lignocellulosic compounds as chemically extracted from the raw biomass.
4. To experimentally investigate the influences of reactor temperature and biomass particle size on the product yields and product properties of bio-oil and char resulting from the Fast Pyrolysis of *E.grandis* using a 1 kg/h bubbling fluidised bed reactor.
5. Investigate and compare the Fast Pyrolysis of *E.grandis* using 3 different reactor configurations at different scale (0.1 kg/h, 1 kg/h and 10 kg/h).

6. To experimentally investigate, compare and optimise the influence of reactor temperature and heating rate on the product yields and product properties bio-oil and char resulting from the Slow and Vacuum Pyrolysis of *E.grandis* using a packed bed reactor.

1.2 Mind map

Figure 1-1 illustrates the logical path way that was followed in order to achieve the objectives set in section **1.1.**

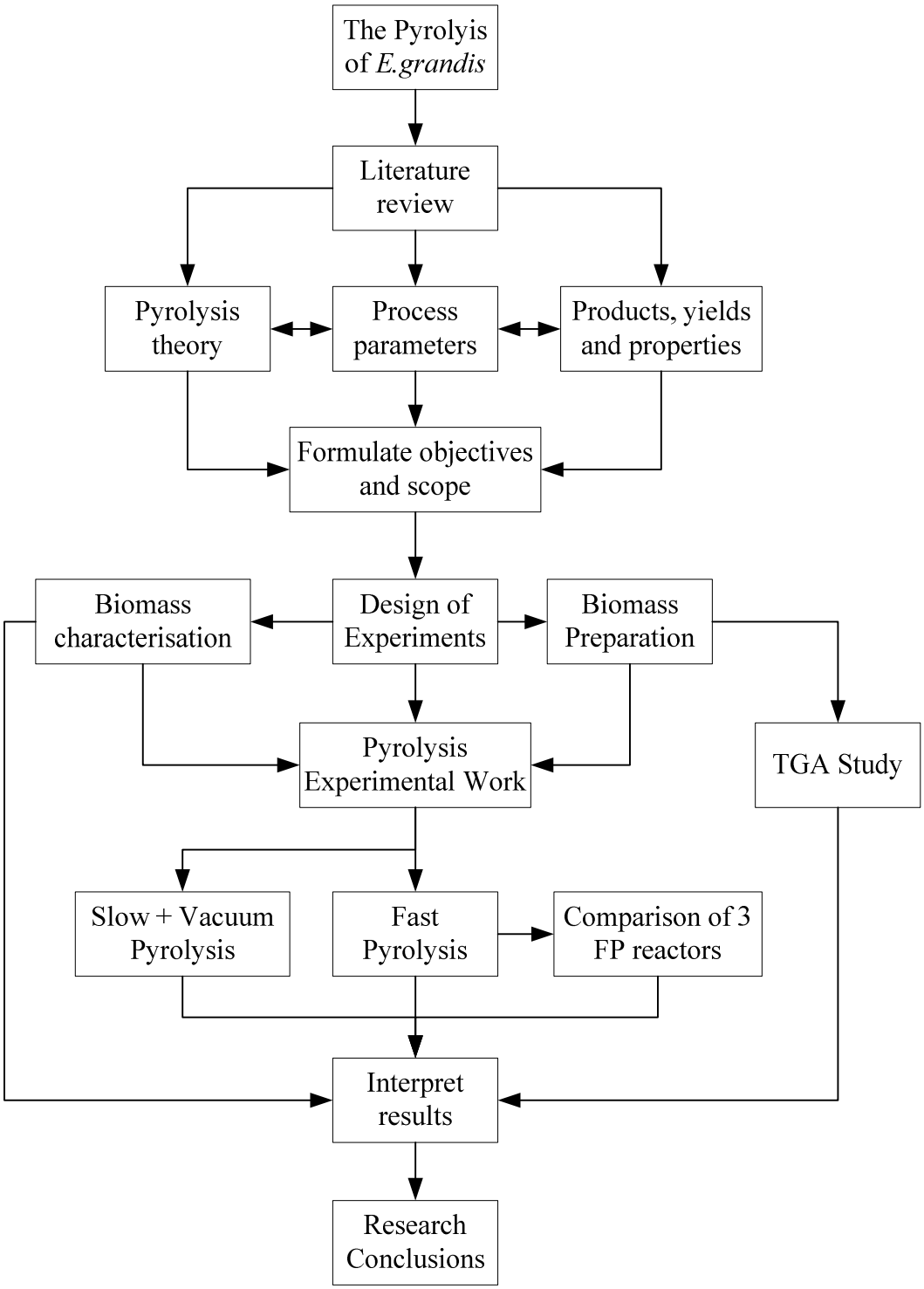

Figure 1-1: Mind map for the pyrolysis of *E.grandis*

2 Literature

2.1 Chemical composition of woody biomass

Wood consists of five major components present in different proportions based on species, environmental factors and sampling position within a specific tree. The components cellulose, polyoses, lignin, extractives and ash, make up the chemical composition of a given wood species. **Figure 2-1** gives a schematic representation of the typical chemical composition of wood and the classification of these lignocellulosic components in general.

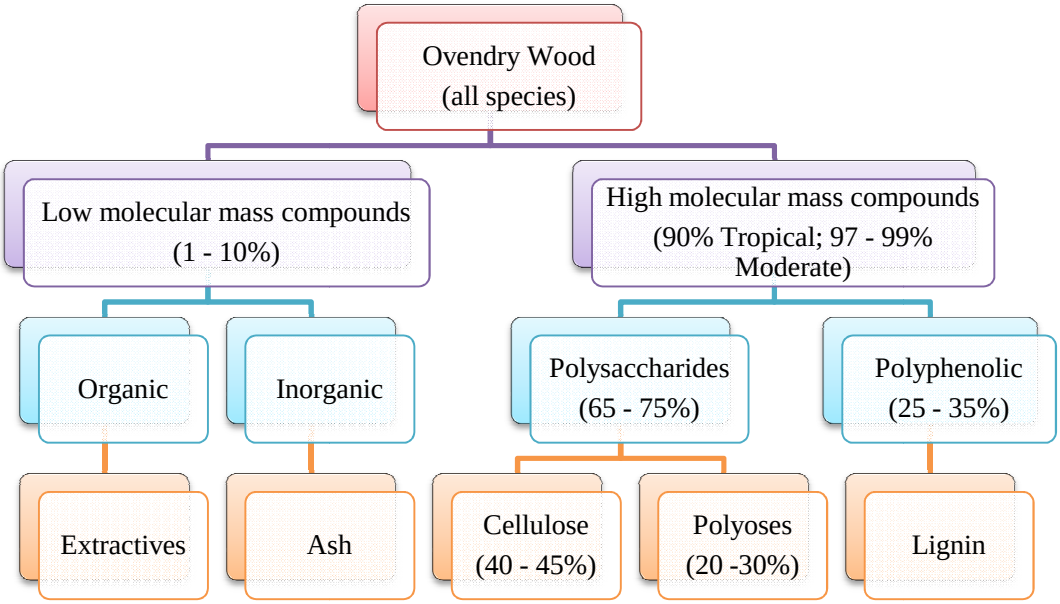

Figure 2-1: Typical woody biomass composition (Redrawn from Fengel and Wegener, 2003)

Many factors which affect the chemical composition for woody biomass have been reported, illustrating the fact that inherent differences can be expected for the composition and properties of a specific biomass. These variations may be found when considering the same species of tree with regard to its geographical origin, the climate in which the tree was grown and even the soil quality and elevation above sea level. Studies suggested that differences in chemical composition may be observed when considering different parts of the tree (such as the stem, branches, bark and leaves etc.) as well as the different types of wood formed (such as sapwood, heartwood, earlywood and latewood and even reaction wood) throughout the life of a specific tree. (Fengel and Wegener, 2003).

These variations were illustrated in an unpublished study, conducted at the Department of Forestry at Stellenbosch University, aimed specifically on four hardwood species commercially used in the South African paper and pulp industry, (Swart, J 2011). In the study 10 trees of each species (*Acacia mearnsii, Eucalyptus dunnii, E.grandis and E.macathurii*) were sampled from 5 different locations in the plantation, North, East, South, West and Centre. The results revealed a significant variation in the chemical composition of the individual species selected across the changes in sampling locality. Furthermore, it was also evident that species belonging to the same genus (Eucalyptus) can vary substantially from each other even when originating from the same plantation. **Figure 2-2** shows the notched box plots for the chemical composition of the 4 species investigated where the notches demarcate approximate 95% confidence intervals for the medians.

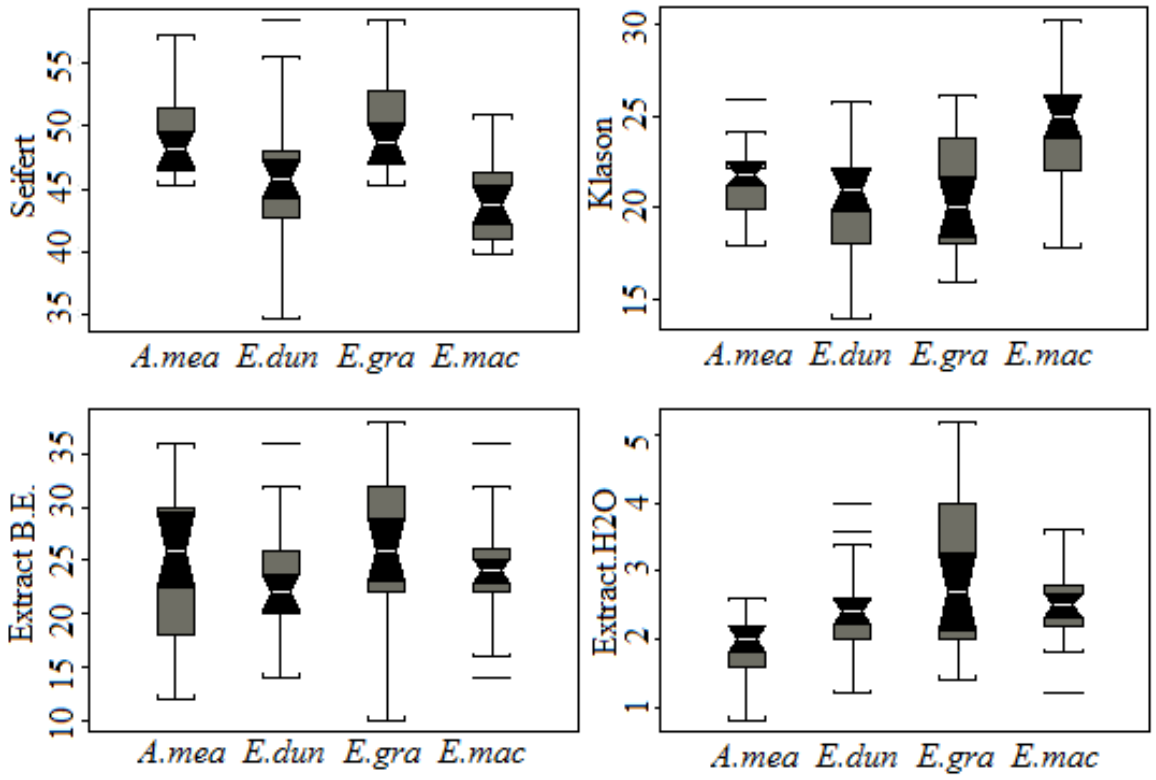

Figure 2-2: Boxplots for Seifert cellulose content (upper left panel), Klason lignin content (upper right panel), Benzene-Ethanol extractives (lower left panel) and H_2O extractives (lower right panel) (Swart, J 2011).

Furthermore, it is important to note that the determination of the chemical composition of biomass is never truly exact, as all the major lignocellulosic compounds (cellulose, polyoses

and lignin) are intimately bonded together within the cell wall. It is therefore difficult to isolate and analyse one component without partially or even completely degrading the other components in the cell wall structure. Various standard methods have been developed to isolate individual components for chemical characterisation of a woody biomass and are described in great detail by among others Browning (1967), the Technical Association of the Pulp and Paper Industry (TAPPI) and National Renewable Energy Laboratory (NREL).

2.1.1 Cellulose

Cellulose makes out the largest portion of wood cell structure contributing 40-50% of the wood on a dry basis. Cellulose is an organic polymer with anhydroglucopyranose units as building blocks. These sugar units are bonded together by β-(1-4)-glycosidic bonds, resulting in every second anhydroglucopyranose unit to be flipped 180° about the main axis. The actual recurring unit for cellulose is therefore taken as cellobiose, consisting of two anhydroglucopyranose units (Fengel and Wegener, 2003).

Strong hydrogen bonding exists in cellulose chains both intermolecular (with other cellulose chains) and intra-molecular (within the same chain) resulting in a cellulose supramolecular structure with definite crystalline properties. Both crystalline and amorphous sections may be found in the cellulose supramolecular structure in various proportions depending on the treatment or method used to isolate the cellulose. The crystalline sections within a cellulose micro-fibril (supramolecular structure) are known to be more resistant to chemical, microbial and thermal degradation than the amorphous cellulose sections (Fengel and Wegener, 2003).

2.1.2 Polyoses

Polyoses, also known as hemicelluloses, are polysaccharide structures containing various different sugar units as building blocks. Unlike cellulose, polyoses contain branched side chains which results in an amorphous supramolecular structure which makes polyoses easier to degrade through chemical and microbial attack pathways. The naming of a polyoses is determined by the most abundant monomer making out the main/backbone chain of the overall polyoses structure. Xylan is the most common type of polyoses found in hardwood species, making up the majority of the overall polyoses content in this biomass class. Xylan contains mainly xylose units in the backbone chain, while mannan (in softwood species)

contains predominantly mannose in the backbone chain. Other polyoses commonly found in wood are glucans, galactans and pectins. (Fengel and Wegener, 2003)

2.1.3 Lignin

The true structure of lignin is not yet fully understood, but it is commonly accepted that the main building blocks of the lignin structure are p-coumaryl alcohol, coniferyl alcohol and sinapyl alcohol. These phenylpropane units are bonded to each other at random via a multitude of possible bonds to create an intricate superstructure. The phenyl rings making up the structure of the individual building blocks are not easily broken and provide entry points for chemical bonds with other molecules. Other that the phenyl ring, the functional groups attached to it also provide additional entry points for bonding, especially in the α and β carbon positions (carbon 1 and 2 respectively in the propane chain) and the lone pair electrons associated with all the oxygen containing functional groups (Fengel and Wegener, 2003).

2.1.4 Extractives

Extractives are groups of compounds that can be extracted from the wood with either aqueous or organic solvents such as ethanol and cyclohexane respectively. These compounds include among others, terpenes and terpenoids, fats, waxes, fatty acids, alcohols and phenols. Although thousands of different extractive compounds may be present in a specific wood species, the relative contribution of the total extractives family to the total chemical composition of wood is very small and typically constitutes less than 10% of the dry biomass (Fengel and Wegener, 2003).

2.1.5 Ash

Ash is a term used to define all the inorganic compounds found in wood. These compounds are absorbed from the soil and are present as alkali and alkali-earth metals, minerals and silica. Ash is known to have a profound blunting effect on cutting and chipping tools during wood processing when present in high quantities. Ash, like extractives, makes out a very small fraction of the total chemical composition of wood and varies greatly between different biomass species and growing environments (Fengel and Wegener, 2003).

2.1.6 Lignocellulosic composition of *E.grandis*

Literature values for the chemical composition of *E.grandis* are given in **Table 2-1**. Of specific interest are the values reported in the unpublished study of the Forestry Department at Stellenbosch University as the biomass used in that investigation originated from the South Afrcan east coast, similar to the biomass used in this investigation. As evident from **Table 2-1**, there is some variation in the results reported by different researchers highlighting the typical variation that can be expected when working with a specific biomass species. Such variations within a specific species and genus can be atributed to, amongst others, climatic and geographical parameter that directly influence the growth conditions of the biomass such as rainfall, altitude above sea level, soil quality and exposure to sunlight (Fengel and Wegener, 2003).

Table 2-1: Literature values of the Lignocellulosic composition of *E.grandis*

	Emmel *et al.* (2003) [wt. % daf]	Forestry Dept. [wt. % daf]	Oasmaa *et al.* (2010) [wt. % daf]
Biomass origin	Brazil	South Africa	Brazil
Moisture (wt. %)	-	-	7.6
Ash (wt. % dry)	-	-	0.4
Extractives	3.3 [a]	5.6 [b]	-
Lignin	25.8	21.0	± 27
α-cellulose	44.7	49.9	± 51
Hemicelluloses	15.3	-	± 10

[a] Benzene ethanol extraction; [b] benzene ethanol + water extraction

2.2 Pyrolysis

Pyrolysis is the thermal degradation of a substance (usually organic) in the complete absence of oxygen. The pyrolysis of whole biomass is a complex process and the true mechanism is not yet fully understood. There is however consensus in literature on the degradation pathway for cellulose, the most abundant compound in lignocellulosic biomass. It is believed

that the pyrolytic degradation of cellulose occurs according to the Waterloo mechanism as shown in **Figure 2-3**.

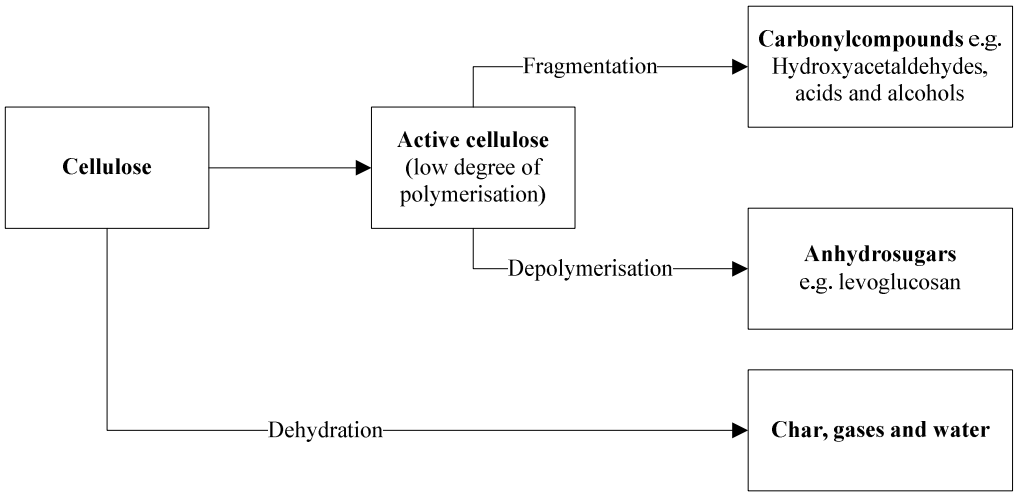

Figure 2-3: The Waterloo-mechanism for the thermal degradation of cellulose redrawn from Van de Velden *et al.* (2010)

Three product phases are formed during pyrolysis, a liquid phase bio-oil resulting from the condensation of pyrolysis vapours, solid phase, referred to as char, and an incondensable gas phase. Various methods of pyrolysis are employed in literature, but the main focus falls on Fast Pyrolysis (FP), Slow Pyrolysis (SP) and Vacuum Pyrolysis (VP) (Bridgwater, 2003). The key differences among these various methods of pyrolysis, with regard to the process parameters employed and the typical product yields, have been highlighted in a review by Bridgwater, (2003), and are summarised in **Table 2-2**. Unfortunately, no values were reported by Bridgwater, (2003) for the typical char and gas yields found for Vacuum Pyrolysis. Product yields for the Vacuum Pyrolysis of woody biomass have however, been reported by Murwanashyaka *et al.*, (2001) and Garcia-Perez *et al.*, (2007) for birch wood and hardwood residue rich in fibre respectively. These results have been added to **Table 2-2** as an indication of the typical product yields that can be expected for the Vacuum Pyrolysis of woody biomass.

Table 2-2: Comparison of product yields for Fast, Slow and Vacuum Pyrolysis (wt. % dry) as reviewed by Bridgwater, (2003).

	Process parameters	Liquid Yield	Char Yield	Gas Yield
Fast Pyrolysis	Short residence time (vapour and solid) High heating rate	75	12	13
Slow Pyrolysis	Long residence time (vapour and solid) Low heating rate	30	35	35
Vacuum Pyrolysis	Long solid residence time	35 – 50	-	-
	Short vapour residence time	63 [a]	25 [a]	12 [a]
	Low heating rate	54 [b]	26 [b]	20 [b]

[a] Murwanashyaka et al., (2001); [b] Garcia-Perez et al., (2007)

The most significant distinction among the different processes comes in with the reactor temperatures, heating rates, the vapour residence times and the solid residence times. From **Table 2-2** it is clear that Vacuum Pyrolysis lay between Fast and Slow Pyrolysis with regard to the expected product yields as it combines a slow heating rate associated with Slow Pyrolysis with the short vapour retention time of Fast Pyrolysis.

There are many different parameters that influence both the yield and the physical and chemical properties (or quality) of the products. A distinction may be made between process related parameters and non-process related parameters. Process related parameters are those which stem directly from the reactor configuration and process conditions chosen, such as reactor temperature, residence time, separation techniques/equipment, reactor type, feed rate, condensation system etc., while non-process related factors include external parameters to the reactor setup and relates to the feedstock, such as the lignocellulosic composition of the biomass used, physical preparation of biomass (milling and sieving), particle size, water content, ash content etc., which cannot be changed as readily as most of the process related parameters. Both these types of parameters will be discussed in detail later in this chapter.

2.3 Thermo-gravimetric analysis of biomass

Thermo-gravimetric analysis (TGA) and differential scanning calorimetry (DSC) are useful tools for determining the pyrolysis kinetics of lignocellulosic materials. Studies have been conducted on a variety of biomass, as well as the individual lignocellulosic and inorganic

components making up biomass, for kinetic purposes (Aboyade *et al.* 2011; Carrier *et al.* 2011b; Graham *et al.* 1994; Orfão *et al.* 1999; Raveendran *et al.* 1995; Raveendran and Ganesh 1996; Raveendran *et al.* 1996; Stenseng *et al.* 2001; Órfão and Figueiredo 2001). From the thermo-gravimetric (TG) and differential thermo-gravimetric (DTG) data obtained, it has been shown that the thermal behaviour of biomass can be predicted and modelled using both simple and complex kinetic rate equations.

However, due to the complex nature of biomass it is important to realise that although the apparent kinetics might be approximated by simple reaction models (such as first order and third order power law rate expressions), the true nature of the chemical reactions taking place are much more complex and not limited to a single reaction phase. The recent trend in literature has consequently been towards the "model free" approach such as the isoconversional method of determining pyrolysis reaction kinetics (Aboyade *et al.* 2011; Vyazovkin *et al.* 2011).

Studies by Orfão *et al.* (1999) and Raveendran *et al.* (1996) showed that a summative approach with simple first order kinetics could describe the kinetic behaviour of lignocellulosic thermal decomposition. It was however stressed by Raveendran *et al.* (1996) that the individual compounds used to make up a representative pseudo-biomass were critical and that both the composition and structure of the individual components had to be representative of the biomass used. These specifications pertained to the degree of polymerisation and the crystallinity index of the cellulose component, the main building blocks and macro structure of the hemicelluloses component (e.g. xylan for hardwood and mannan for softwood species) and the chemical composition of the ash component. It was shown that relative fractional contributions of the respective lignocellulosic compounds outweighed the influence of the intermolecular bonds existing between these compounds in the biomass cellular structure - a pseudo biomass could be made up to follow the degradation behaviour of the true biomass very closely when using individual components that are representative of that found in the true biomass (Raveendran *et al.* 1996).

Vasile *et al*. (2009) reported a change in the thermal decomposition behaviour between the raw biomass and the unbleached Kraft pulp (brown stock) from the same batch of *E.globulus*. Although the lignin content and total carbohydrates fractions were reported for the raw biomass and the Kraft pulp, no mention was made regarding the state or the relative contributions of the hemicelluloses and cellulose components for the biomass or the pulp.

The lignin content of the brown stock (1.0 – 1.7 wt. %) was significantly lower than that of the biomass chips (24.5 - 27.6 wt. %). Consequently, for all the heating rates investigated in the kinetic study, it was observed that the initiation temperature was higher while the maximum temperature of volatilisation was lower for all of the differential thermo gravimetric (DTG) curves of the brown stock pulp compared to that of the raw biomass. Furthermore it was observed that for all the heating rates investigated, the rate of thermal decomposition was higher for the brown stock pulp than for the raw biomass. These findings correlate well with the work of Raveendran *et al.* (1996) suggesting that lignin decomposes across a wider temperature range and that the rate of decomposition is much lower than that of cellulose and hemicelluloses.

A study conducted by Stenseng *et al.* (2001) pointed out the importance of sample size and the properties of the biomass used when conducting TGA. Cellulose from three different suppliers was considered in the study and was compared with washed and unwashed wheat straw. The pure component (cellulose) was shown to have a greater sensitivity toward the sample size used for TGA and DSC, while the results for the wheat straw remained fairly constant for both washed and unwashed samples. Significant variation was furthermore observed for the cellulose from different suppliers with regard to the heat of reaction, the temperature at maximum volatilisation rate and the final char yield. It was postulated that differences in the ash content, the crystallinity and the degree of polymerisation of the various cellulose samples could explain these variances although it was not explicitly investigated in the study.

A recent study by Barneto *et al.* (2011) investigated the pyrolysis kinetics of eucalyptus, specifically with regard to the differences in species and origin (*E.globulus* from Chile and Spain, and *E.grandis* from Uruguay), as well as the lignocellulosic composition of the biomass. The study showed that biomass of the same species, but different geographical origins behaved differently when subjected to TGA and DSC under both inert and oxygenated atmospheres. It was also reported that the extractives component of biomass overlapped the hemicelluloses and cellulose fractions' volatilisations (200 - 350 °C) and yielded proportionally more char than these fractions, similar to the findings of Raveendran *et al.* (1996). The higher relative char yield was ascribed to the extractives compounds with similar molecular structures to the phenylpropane building blocks of lignin.

Isoconversional reaction kinetics has been the topic of discussion in recent literature (Aboyade *et al.* 2011; Vyazovkin *et al.* 2011). It has been shown that by following recommendations set for the isoconversional method, the reaction kinetics of complex materials such as lignocellulosic biomass can be determined and modelled, as elaborately discussed by Vyazovkin *et al.* (2011). An advantage of using the isoconversional method lies in the fact that no initial assumptions need to be made regarding the kinetic model used to fit the data, as it has been shown that various reaction models could fit a specific apparent dataset with sufficient satisfaction without necessarily being the correct kinetic model (Aboyade *et al.* 2011).

Ozawa and Friedman's plots are graphical tools used to explain and obtain the kinetic parameters of isoconversional systems. A Friedman's plot is very similar to the Arrhenius plot used in conventional kinetic modelling for the determination of the activation energy (E_a) and pre-exponential constant (A) of a reaction. In both instances the natural logarithm of the reaction rate is plot against the inverted reactor temperature to yield a straight line from which the activation energy can be determined from the slope of the line and the pre-exponential constant from the intercept on the y-axis (Aboyade *et al.* 2011; Vyazovkin *et al.* 2011. A Friedman's plot typically shows several trends on the same axes, one for each heating rate investigated. These trends are then connected with straight tie-lines which indicate points of equal conversion on the respective trends, called isoconversional tie-lines. These isoconversional tie-lines are then used to calculate the activation energy as well as the pre-exponential constant as a function of conversion (Aboyade *et al.* 2011; Vyazovkin *et al.* 2011. An Ozawa plot shows this dependency graphically by plotting activation energy as a function of conversion, while also indicating the correlation coefficient between the actual and model predicted values (Aboyade *et al.* 2011; Vyazovkin *et al.* 2011. A correlation coefficient of -1 indicates a 100 % correlation, while a value of 0 indicates 0 % correlation between the experimental and predicted values.

2.4 Fast Pyrolysis

2.4.1 Overview

It is the general consensus in literature that the overall Fast Pyrolysis (FP) reaction should take place within 2 seconds after subjecting the biomass particle to the reactor conditions (Bridgwater, 2003; Bridgwater, 2011; Commandre *et al.*, 2011; Graham *et al.*, 1994; Garcia-Perez *et al.*, 2008; Maggi and Delmon, 1993; Nowakowski *et al.*, 2010; Van de Velden *et al.* 2010). After volatilisation and secondary cracking of the product vapours, the vapour and solid phases are separated, before rapid quenching of the vapour phase to yield liquid product called bio-oil. Although literature agrees on the simplified abovementioned 'recipe' for FP, there are many factors/parameters that influence the quality and the yield of the products obtained. These factors will be discussed the following subsections of paragraph **2.4**. **Table 2-3** summarises literature product yields and process conditions such as reactor size and type, reactor temperature, biomass used and biomass particle size, as reported for the Fast Pyrolysis of woody biomass.

Table 2-3: Typical product yields for woody biomass

Authors	Process conditions	Liquid Yield	Char Yield	Gas Yield
Azeez *et al.* (2010)	0.3 g/h FBR 465 – 470 °C Beech (*Fagus sylvatica*) 300 – 500 µm	70 wt. %	10 wt. % (daf)[b]	23 wt. %
Azeez *et al.* (2010)	0.3 g/h FBR 465 – 470 °C Spruce (*Picea abies* L.) 300 – 500 µm	70 wt. %	10 wt. % (daf)[b]	23 wt. %
Fahmi *et al.*, (2008)	0.15 kg/h RBR 507 °C Willow 250 – 355 µm	69 wt. % (dry)	21 wt. % (dry)	9 wt. % (dry)
Garcia-Perez *et al.*, (2008)	2 kg/h BFBR 350 – 600 °C *E.loxophelba* 100 – 600 µm	54 – 63 wt. % (dry)	12 – 27 wt. % (dry)	11 – 25 wt. % (dry)
Oasmaa *et al.*, (2010)	20 kg/h TBR[a] 480 – 520 °C *E.grandis* 3 – 5 mm	71 wt. % (dry)	-	29 wt. % (dry)

[a] Transport Bed Reactor, [b] dry and ash free

2.4.2 Reactor configurations

The principles of Fast Pyrolysis and the reactor configurations accompanying it have received a lot of attention in literature and have been reviewed by various authors (Bridgwater, 2003; Bridgwater, 2011; Meier and Faix 1999; Mohan *et al.* 2006). The fluidised bed reactor is the most common type of FP reactor used both in industry and for research purposes, possibly due to the good heat transfer and mixing that can be achieved with these reactors and the relative ease of scaling-up. Other reactor configurations used include among others, transported bed, circulating fluidised bed, rotating cone, ablative, screw and microwave reactors (Bridgwater, 2011). Each reactor configuration provides its own advantages and disadvantages, but in essence they all have to adhere to the requirements set for Fast Pyrolysis:

- Moderate reactor temperatures (typically around 500 °C);
- Vapour residence times below 2 seconds;
- High particle heating rates (> 10^2 K/min);
- Short solid residence times; and
- Rapid quenching of product vapours to yield bio-oil.

2.4.3 Reactor temperature

Temperature is one of the key variables affecting the pyrolysis reaction. Fast Pyrolysis is generally conducted in the temperature range 400°C - 600°C (Bridgwater, 2011; Mohan *et al.,* 2006; Van de Velden *et al.,* 2010), where the liquid phase (condensed product vapours) makes out the main product yielding between 60 wt.% and 70 wt.% on a dry basis. From kinetic data however, it is known that the thermal degradation of hemicelluloses and cellulose may start at lower temperatures (section **2.2**), but a higher reactor temperature is needed to ensure a steep temperature gradient within the biomass particle and to ensure the required particle heating rate can be achieved. At high reactor temperatures (> 600 °C) the thermal decomposition of the biomass continues to such an extent that the resulting products are mainly incondensable gas and char (Azeez *et al.* 2010). Above 750 °C gasification starts dominating and gas becomes the main product (Bridgwater, 2011). Reactor temperature has also been shown to not only affect the yield, but also the quality of the pyrolysis products in fast pyrolysis (Garcia-Perez *et al.* 2008; Demirbas, 2007).

2.4.4 Vapour residence time

Vapour residence time plays an important role in the extent of the thermal degradation of product vapours during pyrolysis. Residence time below two seconds limits secondary reactions of the vapour (Van de Velden *et al.,* 2010) and is a typical criterion for fast pyrolysis processes where the main product focus falls on the liquid component (Meier and Faix, 1999). When char is the desired product of the study, long residence times are employed (Bridgwater, 2003). It is believed that the char formed during pyrolysis could have catalytic effects on the vapour phase condensation reactions (Bridgwater, 2011) and should therefore be separated from the vapour phase immediately after formation. Graham *et al.,* (1994) however, showed that the vapour phase cracking of cellulose (the most abundant compound in lignocellulosic biomass) was the rate determining step in the overall thermal degradation pathway of cellulose.

2.4.5 Heating rate and particle size

The particle heating rate refers to the dynamic heat transfer within a biomass particle during pyrolysis and can be manipulated by changing the size of the biomass feed, the heat transfer medium used to heat the particle, or by altering the reactor temperature. The heating rates for Fast Pyrolysis are normally a few orders of magnitude greater than that for Slow Pyrolysis and are usually estimated based on the reactor temperature, the particle size and the residence time of the particle within the reactor. As mentioned, in Fast Pyrolysis, the vapour residence time must be short (typically 2 seconds or less) to achieve a high liquid product yield and limit secondary cracking; therefore the particle heating rate must be as high as possible after entering the reactor.

Van de Velden *et al.,* (2010) showed that the heating rate of the particle depends greatly on the Biot number of the particle and that, theoretically, the biomass particle size used for pyrolysis should not exceed 200 µm. From a practical side, however, it is the consensus that biomass particle sizes should not exceed 2-6 mm depending on the scale of the operation (Meier and Faix, 1999). Laboratory and bench scale studies however report the use of particle sizes ranging from 100 µm to 3000 µm (Bridgwater, 2011; Garcia-Perez *et al.,* 2008; Guerrero *et al.,* 2008a; Mourant *et al.,* 2005; Oasmaa *et al.,* 2010). Shen *et al.,* (2009) investigated the effect of particle size of *E.loxophelba* on the yield and composition of the bio-oil produced with a bubbling fluidised bed reactor (BFBR). It was found that an increase in the particle size decreased the yield of bio-oil between 300 µm and 1500 µm, but further increases in the particle size did not further decrease the bio-oil yield significantly (Mourant

et al., 2005). It was postulated by the authors that the increase in particle heating rate, associated with decreasing particle size, as well as the partial destruction of the biomass cell walls resulting from the mechanical forces applied in reducing the particle size, were the main reasons for the increased bio-oil yield observed at 300 µm compared to the larger particle sizes investigated. It has also been shown that the particle size used affects the yield of pyrolytic water formed under Fast Pyrolysis where larger particles tend to increase the pyrolytic water yield (Garcia-Perez *et al.*, 2008; Shen *et al.*, 2009).

Studies have also shown that char produced under high heating rates are more reactive to oxygen and has larger surface areas and more reactive sites (Guerrero *et al.*, 2005; Guerrero *et al.*, 2008a; Guerrero *et al.*, 2008b), while the liquid yield was also improved under a rapid heating rate (Meier and Faix, 1999). Furthermore, the level of mixing that can be achieved in Fast Pyrolysis (FP) reactors has been shown to be strong functions of the particle size used and that smaller particles improved both the heating rate of the particle as well as the overall mixing within a BFBR (dos Santos and Goldstein Jr., 2008; Meier and Faix, 1999).

2.5 Slow Pyrolysis

2.5.1 Overview

Slow Pyrolysis (SP) has been used for many years in charcoal manufacture and is therefore also commonly referred to as carbonisation, or conventional pyrolysis (Bridgwater, 2003; Mohan *et al.*, 2006). With the exception of limited oxygen in charcoal manufacture, Slow Pyrolysis takes place in the complete absence of oxygen, where the main product of interest is (usually) the char. In some cases however, the use of a carrier gas is not explicitly mentioned. These omissions lead the reader to assume that the experimental work was conducted in the absence of an inert atmosphere and that thermal convection and smoke/vapour generation were the only driving forces used for the transport of the vapour phase from the reactor to the condensation chain (Kumar *et al.*, 2010; Pimenta *et al.*, 1998). Packed bed reactors are typically employed for SP experimental work and are run under nitrogen, or similar inert atmospheres (Guerrero *et al.*, 2005; Kumar *et al.*, 2010; Pindoria *et al.*, 1998). Slow heating rates (typically < 25 °C/min) and long vapour residence times (typically a few seconds or even minutes) are preferred for SP to produce a char product rich

in carbon. The char remains in the heated zone of the reactor for the entire duration of the experiment, which usually consists of a dynamic heating phase followed by a soak/holding phase at constant reactor temperature (Carrier *et al.*, 2011a; Kumar *et al.*, 2010; Kumar *et al.*, 1992). The effects of the main process parameters have been investigated in literature and will be discussed in the following subsections in more detail.

2.5.2 Reactor temperature

A wide range of reactor temperatures have been investigated in literature for Slow Pyrolysis ranging from ± 300 °C to ± 600 °C in most cases (Carrier *et al.*, 2011a; Elyounssi *et al.*, 2010; Kumar *et al.*, 2010; Martins *et al.*, 2007), but for some, even as high as 900 °C and 1000 °C (Demirbas, 2007; Guerrero *et al.*, 2005; Kumar *et al.*, 1992). Studies have shown that the reactor temperature used for SP has a significant effect on the product yields where the char yield decreases with increasing reactor temperature (300 – 500 °C) and the bio-oil yield first increases and then decreases above 450 °C for the same temperature range (Carrier *et al.*, 2011a; Kumar *et al.*, 2010; Şensöz, 2003).

Although a decrease in the char yield is observed with increasing reactor temperature, it has been shown that the quality of the char product is improved with increasing reactor temperature, especially with regard to the BET surface area, calorific value and fixed carbon content of the char (Carrier *et al.*, 2011a; Della Rocca *et al.*, 1999; Guerrero *et al.*, 2005; Kumar *et al.*, 1992). A study by Martins *et al.*, (2007) showed that by using low temperature SP (< 500 °C), char can be produced from *E.grandis* that exhibits good absorption qualities, without activation, which could be considered as a promising precursor for activated carbon.

Although the main focus of Slow Pyrolysis falls on the production and characterisation of the solid product (char), it has been shown that the reactor temperature also influences the chemical composition of the bio-oil produced. A study by Demirbas, (2007) showed that the formation of acidic compounds decreased with increasing reactor temperature while production of phenolic and neutral compounds increased with increasing reactor temperatures (350 – 550 °C).

2.5.3 Heating rate

When considering Slow Pyrolysis, the heating rate refers to that of the reactor environment and not to the particle heating rate as would be the case for Fast Pyrolysis. It is generally

accepted that the temperature gradient within the biomass particle becomes negligible when the reactor heating rate is low and that the overall particle temperature follows the temperature profile of the surrounding environment closely. A recent optimisation study on the Slow Pyrolysis of *E.globulus* by Kumar *et al.*, (2010) highlighted the significance of the reactor heating rate as higher heating rates resulted in increased bio-oil yield and decreased char yield. A similar observation was made by Kumar *et al.*, (1992) for *acacia nilotica* and *eucalyptus globulus*, and by Carrier *et al.*, (2011a) for sugarcane bagasse, where higher heating rates decreased the overall char yield. It was however also reported that the heating rate was statistically insignificant toward the liquid yield and various other product properties such as calorific value, BET surface area of the char and the water content of the bio-oil (Carrier *et al.*, 2011a).

2.5.4 Hold time

Hold time refers to the duration under which the solid phase is subjected to the maximum temperature of that specific experimental run. During a typical Slow Pyrolysis experiment, the biomass is heated until the desired (maximum) reactor temperature is reached. Once this maximum temperature is reached, the reactor and its contents are allowed to 'soak' for a pre-determined hold time at the maximum temperature before allowing the system to cool down. Recent work by Elyounssi *et al.*, (2010) showed that under isothermal pyrolysis conditions the hold time had a significant effect on the char yield, but only up to 120 minutes. After 120 minutes it was found that the char yield only increased marginally for the isotherms investigated (330, 360, 390 and 420 °C). Kumar *et al.*, (1992) also showed that the hold time has a very small effect on the char yield and composition above 800 °C. A fixed hold time is generally used in literature and is commonly found to be at least 60 minutes (Carrier *et al.*, 2011a; Guerrero *et al.*, 2005; Kumar *et al.*, 2010; Kumar *et al.*, 1992; Martins *et al.*, 2007).

2.6 Vacuum Pyrolysis

Vacuum Pyrolysis (VP) is seen as the combination between Slow and Fast Pyrolysis whereby slow heating rates and long residence times are employed for the biomass/char, while product vapours are swept from the heated zone immediately after formation resulting is very short vapour residence times. Few studies have been conducted on the VP of woody biomass

(Garcìa-Pérez *et al.,* 2007; Ismadji *et al.,* 2005; Murwanashyaka *et al.,* 2001; Roy *et al.,* 1992), and up to now, no VP data could be found for *eucalyptus* species.

Roy *et al.,* (1992) investigated the Vacuum Pyrolysis (VP) of fast growing Aspen Poplar, with specific emphasis on the role that extractives play on the products of VP. Approximately 30 g of biomass was pyrolysed at a an absolute reactor pressure of 0.13 to 0.47 kPa, a heating rate of 10 K/min and final reactor temperatures ranging from 200 to 550 °C. After reaching the desired reactor temperature a hold time of 30 minutes was employed for each experiment before cooling. Similarly extractives free biomass, chlorite extracted holocellulose and commercial Avicel cellulose samples were pyrolysed and compared. In general it was observed that a plateau in the liquid yield was reached above a reactor temperature of 350 °C. It was also reported that by removing the extractives fraction from the biomass, the bio-oil yield and pyrolytic water produced could be improved from 60.7 to 68 wt. % and 14.1 to 10.1 wt. %, respectively. Furthermore the gas yield decreased from 10.8 to 5.5 wt. % while the char yield increased from 14.4 to 16.5 wt. %. The extractive content was also found to promote the formation of formic acid from the wood cellulose content, but inhibited the formation of levoglucosan.

A stepwise approach to Vacuum Pyrolysis was employed by Murwanashyaka *et al.,* (2001) where it was shown that by targeting specific reactor temperatures the phenol content of the resulting bio-oil could be manipulated. A hold time of 1 hour, an absolute reactor pressure of 0.7 kPa and condensers at -72 °C were used as constant process parameters. It was shown in the study that the most reactive temperature range for the Birch-derived biomass was between 275 and 350 °C, which also corresponded to the highest pyrolytic water and phenols yields relative to the other temperature ranges investigated.

Ismadji *et al.,* (2005) showed that the char yielded from the Vacuum Pyrolysis of teak sawdust at 7 kPa and 600 °C was a suitable precursor for activated carbon and that this char had a higher BET surface area compared to the activated carbon produced using Slow Pyrolysis at atmospheric pressure. The BET surface area of the char was found to be 342 m^2/g before activation and 1150 m^2/g after steam activation at 850 °C for 5 hours.

A study by Garcìa-Pérez *et al.,* (2007) evaluated the pyrolysis of two forestry wastes, one hardwood rich in fibres and the other mainly softwood bark. It was shown that based on the origin of the biomass, and therefore the differences in chemical composition with regard to extractives and lignin content, the products formed were distinctly different. The liquid

phase products received a lot of attention in the investigation and was characterised in great detail. It was suggested that the presence of more extractives in the softwood bark compared to that of the hardwood fibres resulted in the phase separation of the softwood bark bio-oil. For the softwood bark the waxy top layer of the liquid product amounted to 16 wt. % of the total liquid yield, compared to the 1.3 wt. % of the hardwood fibre liquid yield. It was furthermore concluded that the bottom layer of the hardwood residue liquid product was the most promising fraction for fuel applications based on the overall characterisations of the liquid products.

2.7 Non-process parameters influencing pyrolysis

2.7.1 Lignocellulosic composition

The chemical composition of the biomass used proves to be a crucial parameter influencing pyrolysis products yield and quality (Garcìa-Pérez *et al.,* 2007; Oasmaa and Czernik, 1999; Sipilä *et al.,* 1998). As mentioned in section **2.1**, great variance is found in different biomass species with regard to chemical composition. It has been suggested that the relative fractional contributions of the respective lignocellulosic compounds making up a specific biomass, outweighs the influence of the intermolecular bonds existing between these compounds (Raveendran *et al.,* 1996).

It should however be remembered that the hemicelluloses and lignin, as lignocellulosic groups, are not uniform like cellulose, and their structures are not fully understood (Fengel and Wegener, 2003). The building blocks of these super-molecular structures, however, are known and well-defined which can indicate to some extent the expected products that might result from pyrolysis. The significance of the chemical composition of a biomass is further illustrated in literature when the kinetics of individual components, as well as that of the original biomass is considered (section **2.2**). The lignocellulosic composition of the biomass used can therefore greatly assist the understanding of how the whole biomass might behave kinetically.

A recent study by Lv *et al.,* (2010) investigated the effects of the lignocellulosic composition of 6 different types of biomass using a thermo-gravimetric analyser (TGA). Two distinct

reaction phases were observed which were attributed to the volatilisation of the cellulose (rapid) and the lignin (slow) components of the biomass, respectively. It was furthermore reported that as the cellulose content of the biomass increased, the liquid yield also increased and the reaction rate increased while the opposite was observed for the lignin content. Alkali and alkaline earth metals were found to increase the char reactivity under gasification.

2.7.2 Influence of inorganic compounds

From literature it is known that ash has a significant effect on both the yield and the quality of pyrolysis products, even in small quantities (Agblevor *et al.*, 2010; Fahmi *et al.*, 2008; Raveendran *et al.*, 1995). It has also been shown that certain ash compounds like potassium and calcium catalyse char formation reactions (Agblevor *et al.*, (2010) and that de-ashing biomass has shown to increase liquid yield as well as the liquid quality of the bio-oil (with regard to water content and heating value) (Raveendran *et al.*, (1995). Azeez *et al.*, (2010) showed that the differences in minerals content of African soils compared to that of European soils influenced the ash composition for the specific biomass specimens (phytoremediation principle - uptake of minerals from the soils by the plant) and therefore also the pyrolysis products resulting from the respective specimens.

2.8 Application of pyrolysis products

Of the three product phases typically resulting from various pyrolysis pathways, the liquid (bio-oil) and solid (char) have received the most attention in research to date. The gas stream commonly contains CO, CO_2, methane, and ethane, with C3-C5 chains present in trace amounts in some cases and is therefore only mentioned but not investigated in many instances.

2.8.1 Bio-oil

Various researchers have conducted review studies on Fast Pyrolysis, the properties of the bio-oil, the upgrading of bio-oil and the applications thereof (Bridgwater, 2003; Bridgwater, 2011; Czernik and Bridgwater, 2004; Meier and Faix, 1999; Yaman, 2004; Zhang, 2007). Bio-oil is complex in nature as it is made up of hundreds of different components depending on the process parameters and biomass used. This also gives rise to subsequently deviation

with regard to the physical and chemical properties of the oil. The typical properties of pyrolysis bio-oil have been compared to that of heavy fuel oil by Czernik and Bridgwater (2004), as given in **Table 2-4**. The impact of the differences highlighted has been discussed in great detail by the authors in the same paper.

Table 2-4: Typical properties of wood pyrolysis bio-oil and heavy fuel oil (Czernik and Bridgwater, 2004)

Property	Bio-oil	Heavy fuel oil
Moisture content [wt. %]	15-30	0.1
pH	2.5	-
Specific gravity	1.2	0.94
Elemental composition [wt. %]		
C	54-58	85
H	5.5-7.0	11
O	35-40	1.0
N	0-0.2	0.3
Ash	0-0.2	0.1
HHV [MJ/kg]	16-19	40
Viscosity at 50 °C [cP]	40-100	180
Solids [wt. %]	0.2-1	1
Distillation residue [wt. %]	Up to 50	1

A substantial amount of work has been done on the utilisation of bio-oil as a liquid fuel for combustion in burner/furnace and burner/boiler systems, as well as in internal combustion engines, combustion in turbines and combustion in Sterling engines (Czernik and Bridgwater, 2004). Bio-oil is also a potential source of valuable chemicals of which acetic acid, hydrogen, levoglucosan, furfural and phenols make out only a few (Bridgwater, 2003). It has been suggested that by introducing a specific set of standards the utilisation of bio-oil as a liquid fuel could be promoted (Bridgwater, 2003).

2.8.2 Char

Key possible applications of char are solid fuels, activated carbon and biochar for soil amendment (Lehmann *et al.*, 2003). Studies have shown that high heating rates favour pore formation in pyrolysis chars and that under the correct operating conditions char may be produced that exhibit favourable BET surface areas, good absorptive properties and high reactivity for combustion (Guerrero *et al.*, 2005; Martins *et al.*, 2007 ;Ismadji *et al.*, 2005)

2.9 Pyrolysis of *E.grandis*

Data for pyrolysis of *E.grandis* are not as readily available as that of other eucalyptus species. Studies by Pimenta *et al.* (1998) and Rencoret *et al.* (2007) have, however, focussed specifically on *E.grandis*. In both instances the main focus of the studies was not explicitly on pyrolysis, however, but rather formed part of a bigger investigation aimed at using pyrolysis as method to produce desired products, or applying pyrolysis as an analytical tool, respectively. No data has, up to now, been recorded for vacuum pyrolysis of *E.grandis*.

Product yield data for Slow Pyrolysis of 7-10 year old *E.grandis* were reported in the study by Pimenta *et al.* (1998) and are shown in **Table 2-5**. As mentioned earlier, Pimenta *et al.* (1998) only used pyrolysis as a method to produce the products needed for the study. The data given are therefore not necessarily generated using optimal process conditions to favour product quality or product yield. A heating rate of 0.94˚C/min was used to heat the biomass in a furnace up to 450 ˚C. No mention was made with reference to the use of any inert carrier gas, which leads the reader to believe that the system contained air at the start of the reaction. A further limitation of the data is the fact that only room temperature condensation of product vapours was used which could have resulted in some of the lighter product vapour fractions not being condensed and were subsequently reported as incondensable gas. Finally it was also not explicitly specified on which basis the final product yields were reported, i.e. it is not clear if the initial moisture and ash content of the biomass were considered in the calculations.

Table 2-5: Slow pyrolysis product yield (Pimenta *et al.* 1998).

	Char Yield [wt. %]	**Liquid Yield [wt. %]**	**Gas Yield[a] [wt. %]**
Debarked *E.grandis*	38.5	45.5	16.0

[a] determined by difference

A recent study by Oasmaa *et al.* (2010) focussed on Fast Pyrolysis of various types of feedstock, of which *E.grandis* was one. Brazilian *E.grandis* was pyrolysed in a 20 kg/h transported bed reactor with a reactor temperature between 480°C and 520°C and a vapour residence time between 0.5 and 2 seconds. In a transported bed reactor the sand, with char formed during pyrolysis, is re-circulated via a combustion reactor to burn off the char and reheat the sand for pyrolysis. In light of the reactor design, no data was generated for the solid or gas phase products and the yield of these phases were calculated by difference. A total liquid product yield of 70.8 wt% based on dry feed was reported in the study.

2.10 Conclusions

From literature it may be concluded that:

- Woody biomass is complex in its structure and it may have different chemical compositions even when the same genus, or in fact, the same species of the tree is considered. Both environmental as well as biological factors are known to affect the lignocellulosic composition of a specific biomass. These conclusions substantiate the need for the lignocellulosic characterisation of the biomass prior to use (Chapter 3).

- The pyrolysis kinetics resulting from thermo gravimetric analysis is crucial in understanding how a specific biomass behaves under thermal degradation, motivating the need to investigate the thermal degradation characteristics of the biomass and its major lignocellulosic components (Chapter 4). It has been shown that both model based and model-free (isoconversional) kinetics yield valuable information from which pyrolysis behaviour can be extrapolated. It has been shown that the lignocellulosic composition of a specific biomass greatly affects the product yields and overall kinetics of the biomass.

- Although the effects of process parameters have been studied across Slow, Fast and Vacuum Pyrolysis for various types of biomass, the data available for eucalyptus is scarce, and even more so for *E.grandis*. Where pyrolysis results have been published for *E.grandis* it is either unclear if optimisation was employed for the process parameters, or the data were incomplete. No work has, up to now, been found for the Vacuum Pyrolysis of any eucalyptus species. These conclusions justify the need to

investigate the Slow, Vacuum and Fast Pyrolysis of E.grandis and to compare the findings (Chapters 5 and 6).

- Many researchers have compared and reviewed different reactor configurations, especially for Fast Pyrolysis, but the specific comparison and subsequent influences of the different condensation chains used for different reactor configurations are lacking. This motivates the investigation of the Fast Pyrolysis of *E.grandis* using 3 different reactor configurations of different scale (Chapter 5).

3 Materials and Methods

3.1 Biomass origin and background

The biomass used in this investigation was provided by the Richards Bay mill of Mondi South Africa, situated on the eastern coastline of South Africa. The paper and pulp industry of South Africa uses mainly *Eucalyptus grandis* for hardwood pulping due to its favourable fibre qualities, low lignin content and rapid growth (Godsmark, 2010). Originally, pure *E.grandis* seeds were imported from Australia, and subjected to careful selection after being planted. Genetically superior specimens were then isolated and cloned for future use in the plantations. In regions where the climate, altitude, proneness to disease, or soil quality was not favourable for pure *E.grandis*, hybrids of *E.grandis* with *E.camaldulensis* or *E.urophylla* (more recently) were used with *E.grandis* as the maternal plant.

In total, 24 million plants are cloned to be planted in the approximately 350'000 hectare plantations feeding the Mondi Richards Bay pulp mill. The Kwambonambi Nursery produces roughly 11 million clones per year from a 40 hectare site in Zululand, amongst the Mondi plantations. New closed loop hydroponic technology allows the nursery to clone vast quantities of preselected superior tree specimens with a 50 % success rate, compared to old methods of using seedlings and conventional green houses. Cloning ensures uniformity of the trees with regard to bole form, crown shape and wood density which streamlines the harvesting of the trees and transporting of the biomass to the pulp mill (Cox, 2011).

After being felled, the trees are debarked on site and then transported to the wood yard by truck or rail as soon as possible. The majority of the felling and debarking operations are fully mechanised. The debarked timber is then fed directly to 3 separate hardwood chipping lines for processing before screening and chip storage. Depending on the origin, the availability and the means of transport used to deliver the logs to the wood yard a variation in the moisture content of the biomass is found. In general, however, the logs received have a high moisture content. The bark, branches, leaves, old stumps and roots are left at the plantations to degrade over time and replenish the soil with some of the nutrients and minerals absorbed during growth. It is common practice to allow tree stumps to coppice and grow out for one rotation after felling before new clones are planted in their place. With each coppice rotation the fibre quality of the tree deteriorates, reducing the pulp yield and

therefore the profitability of the biomass compared to planting new clones and killing the old stumps (Cox, 2011).

The biomass used in this investigation was provided in three different batches by Mondi's Richards Bay Mill on the Kwa-Zulu Natal coastline. The biomass was received as bags of fresh wood chips, sampled directly from the wood yard at the Richards Bay Mill. It is important to note that the biomass provided was sampled from the wood yard and not from individually selected trees and that the individual batches of biomass were not personally sampled by the author of this thesis, but by mill's operational staff. This fact creates some uncertainty regarding the exact hybrid species of the biomass provided in each batch, as well as the representativeness of the sample seeing that no definite sampling techniques were reported by the sample provider. As mentioned before, however, it is certain that if the biomass sampled was not pure *E.grandis,* that *E.grandis* would have made out the maternal plant of the cloned hybrid in question.

3.2 Biomass preparation and characterisation

The three batches will from henceforth be referred to as batch 1-3. Batches 1 and 2 were used for the experimental work done in South Africa while batch 3 was used for the experimental work done in Germany at the Karlsruhe Institute of Technology (KIT).

3.2.1 Biomass preparation (SA)

3.2.1.1 Biomass drying

Batches of wet biomass were received in big plastic bags and opened on arrival to facilitate drying. Batch 1 was received early in 2010 and was allowed to dry in a dark room at ambient conditions for approximately 7 months before use. After the initial Fast Pyrolysis test runs were conducted, it was found that the mass of biomass required for each experimental run would have to be increased from 0.5 to 1 kg. The increased biomass feed would ensure that enough bio-oil and char were produced for analysis and that steady state operation could be achieved for each run. Batch 1 would therefore have been insufficient to complete all the experimental work planned for Fast Pyrolysis and additional biomass was needed. Batch 2 was received early in 2011 dried in a ventilated greenhouse. The dried biomass was mixed

and stored indoors at ambient conditions before being used for analysis and experimental work. The biomass was considered air dry at a moisture content of ± 10 wt.%.

3.2.1.2 Milling and particle size selection

Wood chips were milled using a SM 100 Retsch mill, first with a 4 mm sieve and then with a 2 mm sieve. An AS 200 Retsch shaker was used to remove the fines (< 250 µm) and oversize (> 2000 µm) fractions. Two biomass particle size ranges were chosen for the Fast Pyrolysis experimental work conducted in South Africa, +250 – 1000 µm (Hugo, 2010) and +1000 – 2000 µm. Biomass was fractionated at an amplitude of 1 mm for 10 - 15 minutes. The average particle size and typical particle size distributions were determined using the weighted average of the middle point values of the selected sieve sizes.

3.2.2 Biomass preparation at KIT

On arrival in Germany, batch 3 was found to have a high moisture content of ± 26 wt. %. The biomass was milled using a Neue Herbold mill to reduce the particle size to below 5 mm. The mill consisted of a shredder followed by a scratching chain conveyor, a magnetic separator and finally a granulator. The majority of the milled biomass (± 200 kg) was stored in open plastic bags inside an outdoor shed for the duration of the visit due to limited indoor storage capacity. Only approximately 40 kg of biomass could be stored and dried indoors. Due to the cold and wet conditions in Germany during the winter months, the biomass could not be dried in the outdoor shed effectively on large scale, which made controlling the moisture content of the biomass difficult.

A subsample of biomass was selected for bench scale Fast Pyrolysis experiments (approximately 2 kg). Further biomass particle size reduction was achieved using a Pulverisette granulator from Fritsch with a 2 mm and 1 mm sieve respectively. These samples were stored in plastic air tight sample bottles.

3.2.3 Lignocellulosic characterisation

The lignocellulosic characterisation of the biomass served two purposes, firstly for the quantification and characterisation of the biomass and secondly to fractionate the biomass into its main lignocellulosic components for the thermo-gravimetric analysis of the biomass and its components in **Chapter 4**.

Subsamples were taken from the individual batches according to the cone and quartering technique as described in "Solid biofuels – Methods for sample preparation", CEN/TS 14780:2005, and subjected to chemical analysis at the Forestry Department at Stellenbosch University. The selected samples were milled and sieved using a SM 100 Retsch mill and an AS 200 Retsch shaker, isolating the biomass particle size range +250 µm and -425 µm for lignocellulosic characterisation. Analyses were done in accordance with the TAPPI standard methods for characterising woody biomass (T264 om-88, T211 om-85), and the standard methods described in Browning 1967. Full lignocellulosic characterisation was conducted for batch 1, while the lignocellulosic characterisation of batches 2 and 3 were limited to the moisture, ash, extractives and Klason lignin content determination. A full breakdown of the aforementioned analyses conducted at Stellenbosch will follow in sections **3.2.3.1** to **3.2.3.4**.

3.2.3.1 Moisture and ash determination

The biomass moisture content was determined by drying the biomass in an oven at 105 ± 2 °C in accordance to T264 om-88 of the TAPPI standard methods. The biomass ash content was determined using a muffle furnace set to 575 ± 25 °C in accordance with T211 om-85 of the TAPPI standard methods.

3.2.3.2 Extractives

The biomass extractive content was determined in accordance to T264 om-88 of the TAPPI standard methods. Approximately 5 g of biomass was extracted with a 1:2 volume ratio of (at least) 95% ethanol and cyclohexane (instead of benzene as prescribed in the standard method), followed by distilled water extraction. Each extraction was allowed to run for 8 hours under full reflux with an extractor siphoning rate of at least 4 times per hour. The extracted biomass was allowed to air dry before continuing with further analysis.

3.2.3.3 Klason lignin and poly-saccharides content

Air dry and extractives free biomass was used for Klason lignin determination. After primary hydrolysis of the biomass with 72 % sulphuric acid (H_2SO_4), the T 222 om-88 TAPPI standard method specifies secondary hydrolysis (3 % H_2SO_4) to take place for 4 hours under full reflux using a reflux condenser. This step was replaced by secondary hydrolysis (3 % H_2SO_4) for 1 hour in an autoclave at 1.25 bar and 122 °C, based on the experience of the Forestry Department's wood chemistry laboratory. After secondary hydrolysis the sample

was vacuum filtered and dried on a No. 3 filtering crucible. The filtrate was analysed with HPLC according to standard method described by Sluiter *et al.*, (2005) to determine the biomass poly-saccharide content and Ultra Violet (UV) spectrometry at 280, 240 or 205 nm to determine the acid soluble lignin fraction of the biomass (Fengel and Wegener, 2003). The relative abundance of the different sugar species in the filtrate may be used approximate the relative contributions of the original cellulose and polyoses in the biomass. Due to the heterogeneous nature of polyoses and the fact that these compounds may also contain significant quantities of anhydroglucopyranose units as building blocks, no definite determination can be made using this technique. The detected Xylose, Arabinose and Mannose concentrations may, however, be used to approximate the total hemicelluloses fraction of the biomass.

3.2.3.4 Holocellulose and alpha-cellulose extraction

The exact procedure followed for the extraction of alpha-cellulose and holocellulose is described in much detail in Browning, 1967. Holocellulose was extracted using 5 g of extractives free biomass in a beaker with 160 ml of demineralised water set in a water bath at 70 - 80 °C, glacial acetic acid and reagent grade $NaClO_2$. 0.5 ml of glacial acetic acid and 1.5 ± 0.1 g of $NaClO_2$ were added to the heated flask under a fume hood and stirred occasionally. A second and third dose of said chemicals were added at 1 hour intervals with occasional stirring. After 3 hours of chloriting, the flask was placed in an ice bath to cool the contents to below 10 °C before filtering the contents with a coarse filter crucible. Minimal ice water was used to transfer the contents from the flask to the filtration crucible. The crucible content was washed with instrument grade acetone, followed by 100 ml of 95 % ethanol and finally by ice water before drying in an oven at 105 °C.

The same procedure was followed as the first step of alpha-cellulose extraction, but with the exception of the ethanol extraction step. 3 g of the prepared sample and 35 ml of a 17.5 % NaOH solution were added to the beaker and allowed to soak for 5 minutes before stirring and then letting the sample soak for a further 10 minutes. The sample was placed in a water bath set at 20 °C while an additional 40 ml of the caustic soda solution was added in equal portions (15 ml every 10 minutes) with occasional stirring. The sample was diluted with 75 ml of distilled water under continuous stirring before being vacuum filtered using a filtration crucible. With the suction removed, 40 ml of 10 % acetic acid was added to the crucible and

allowed to soak for 5 minutes before filtering the liquid off. The sample was finally rinsed with distilled water (under suction) before it was dried overnight in an oven set to 102 °C.

3.3 Additional biomass characterisation from KIT

On arrival, and during the course of the experimental work done in Germany, biomass samples (from batch 3) were analysed for water content, ash content, calorific value and elemental composition. Water content was determined as described in **3.2.3.1**, while the ash content was determined using a Leco 701 thermo gravimetric analyser (TGA) in an oxidative environment at three different temperatures (550, 815 and 1000 °C). The higher heating value (HHV) of the biomass was determined using a IKA, model C 5000, control bomb calorimeter. Elemental analysis of the biomass was done using a TruSpec CHN Vario EL III Leco Elementar elemental analyser.

3.4 Thermo-gravimetric analysis

All thermal gravimetric analyses (TGA) were conducted using a NETZSCH STA 409C/CD thermo-gravimetric analyser at the Karlsruhe Institute of Technology (KIT) in Germany. Four different heating rates (10, 20, 30 and 50 °C/min) were considered for both the whole biomass (*E.grandis*) as well as the individual lignocellulosic components investigated. The following samples were investigated: raw *E.grandis*, extractives free *E.grandis*, Klason lignin, holocellulose and alpha-cellulose. The particle sizes considered for the thermo-gravimetric study fell into the same particle size range used in the bench/lab scale pyrolysis investigations in this study of + 250 and – 1000 µm (Chapters 5 and 6). By using similar particle sizes for the pyrolysis and the TGA work, the mass and heat transfer for both the kinetic study as well as the pyrolysis work could be assumed as similar, especially when using lower heating rates as would be the case for Slow and Vacuum Pyrolysis (Chapter 6). For the comparison of the TGA data of the lignocellulosic components and the whole biomass, a single particle size range was chosen (+ 250 - 425 µm).

This specific particle size range was used seeing that this was the size range used for the chemical characterisation of the biomass and subsequently also the approximate size range of the extracted holocellulose and alpha-cellulose particles. Biomass from batch 1 was used for

the TGA work conducted on the virgin/raw biomass as well as the extracted lignocellulosic components of the biomass. Biomass from batch 3 was used to determine the effect of biomass particle size on the TGA results due to the limited stock of batch 1 that was available at the time.

For all TGA experiments a nitrogen flow rate of 60 ml/min was used for the protective gas in the balance chamber, while 15 ml/min was used in the oven to provide an inert environment for the sample. A constant sample size of 150.0 mg was used and all temperature measurements were recorded using the thermocouple supporting the crucible. The temperature program used for the TGA experimental work is given in **Table 3-1**. According to the prescribed methods by Vyazovkin *et al.*, (2011) at least 16000 data points are needed to obtain good data for isoconversional analysis. Seeing that the dynamic section of the temperature program for each TGA experiment was of specific interest for determining the kinetic parameters via the isoconversional method, the thermogravimetric analyser's software was set to acquire the maximum possible number of data points (600 points per minute) during the heating phase. This resulted in the acquisition of at least 16000 data points for each heating rate during the dynamic phase of the temperature program, except for a heating rate of 50 °C/min. At 50 °C/min the analyser software only managed to record between 9 000 and 10 000 data points.

Table 3-1: Temperature program for TGA

	Temperature [°C]	**Heating rate** [°C/min]	**Data point acquisition rate** [pt/min]	**Hold time** [min]
--START--				
1. Isothermal	20	0	60	30
2. Dynamic	20 – 850	(10; 20; 30; 50)	600	-
3. Isothermal	850	0	100	40
4. Dynamic	850 – 20	- 40	80	-
--END IF--	> 900			

The isoconversional method was used in determining the kinetic parameters for the obtained TGA data, using AKTS Thermokinetics software at the Department of Process Engineering at the University of Stellenbosch, South Africa. For all imported data the differential TG curves were integrated using a linear baseline and normalised accordingly, expressing the weight loss of the sample in terms of conversion (between 0 and 1) rather than the measured

sample mass. A conversion of 0 denoted the mass of the sample at the start of the peak's baseline, while a conversion of 1 (or 100 %) represented the mass of the residue measured at the end of the baseline. The generated curves were smooth enough when using the default AKTS Thermokinetics software settings at 60 milliseconds differentiation filter and therefore did not need any additional smoothing. All measured heating rates reported are average values as determined by the AKTS Thermokinetics software based on the slope of the temperature curve measured during the heating phase of each run.

3.4.1 Proximate analysis of *E.grandis*

The proximate analyses for batch 1 were derived from the thermo-gravimetric analysis results generated using a NETZSCH STA 409C/CD thermogravimetric analyser, as mentioned above. For each run, approximately 150 mg of biomass was used and the point values obtained at 200 and 845 °C were taken as the data points where all the moisture and all the organic volatiles have respectively been volatilised from the original biomass. The analyser was not programmed to introduce an oxidative atmosphere at the end of each temperature program for the thermo-gravimetric experimental work which meant that the ash content could not be determined for each sample. The reported fixed carbon therefore included the ash fraction present in the biomass as shown in .

Equation 3-1 Fixed Carbon + Ash = 100 % - Volatiles

3.5 Fast Pyrolysis

Fast Pyrolysis was investigated using three separate reactor configurations in two parts, one part at Stellenbosch University (SU) in South Africa, and the other at the Karlsruhe Institute of Technology (KIT) in Germany. A 1 kg/h Fast Pyrolysis plant was used for the experimental work conducted at Stellenbosch University, while two plants, a 0.1 kg/h bench scale plant and a 10 kg/h Process Demonstration Unit (PDU), were used for the experimental work conducted at KIT. A brief overview of the pyrolysis equipment used and the chosen process conditions will be discussed in this section.

3.5.1 $SU_{1\ kg/h}$ bubbling fluidised bed reactor

A schematic representation of the 1 kg/h Fast Pyrolysis plant at Stellenbosch University ($SU_{1\ kg/h}$) is shown in **Figure 3-1**. The FP plant can be divided into three sections: the biomass feeding unit, the furnace housing the Bubbling Fluidised Bed Reactor (BFBR) with two cyclone separators, and the condensation chain.

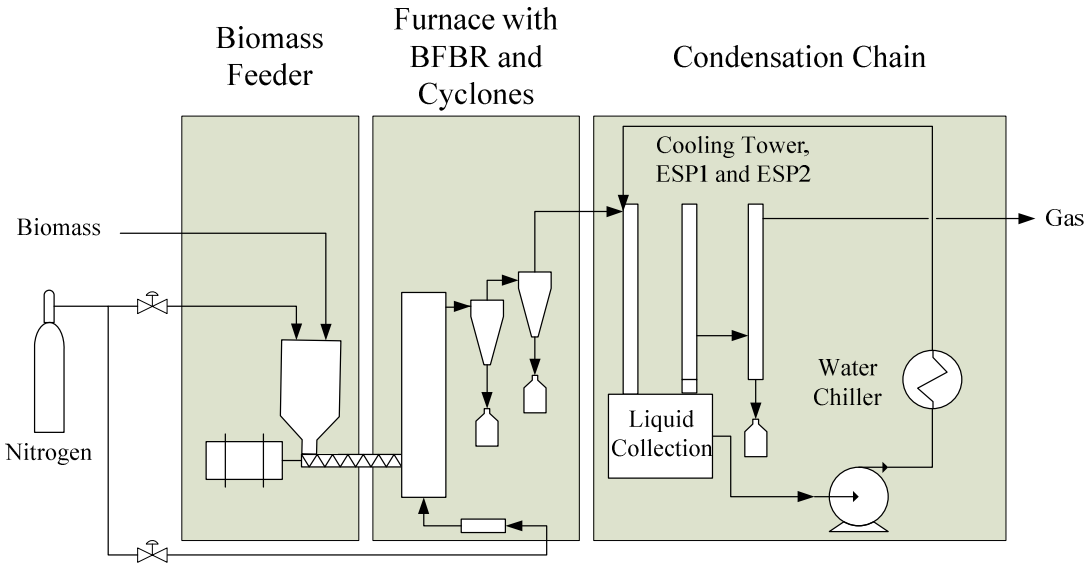

Figure 3-1: Stellenbosch University Fast Pyrolysis plant ($SU_{1\ kg/h}$).

The biomass feeding unit consisted of a hopper with a screw feeder which introduced biomass into the reactor. The hopper was supplied with a slight nitrogen overpressure (± 0.02 bar gauge) to prevent hot gas and product vapour pushing back from the reactor into the feeding system.

A 6.6 kW cylindrical furnace housed a 75 mm (ID) by 680 mm tall stainless steel BFBR, followed by two cyclones in series for solid and vapour separation. Sand (AFS 45 fused silica, from Consol minerals) was used as the heat carrier inside the reactor. The cylindrical furnace was divided into two sections, top and bottom, which met at the feeder inlet. The bottom section was controlled at an offset temperature ± 160 °C higher than the furnace set point temperature, and was thermally shielded from the top section by a thick layer of thermal wool. This offset temperature in the bottom section enabled the pre-heating of the carrier gas via a stainless steel heat exchanger filled with steel balls to facilitate the heat transfer to the carrier gas (98-SE, High Purity nitrogen from AFROX) before entering the reactor.

Pyrolysis product vapours left the furnace via a heated pipe (maintained at 400 °C to prevent intermediate condensation) before entering the cooling tower. A rope heater was previously used to heat the pipe, but was replaced by a more robust, fixed coil electric heating element during the testing phase of this investigation. The new heater improved the operation of the plant and prevented interruptions previously caused by malfunction of the more fragile rope heaters.

The condensation chain consisted of a spray cooling tower followed by two electrostatic precipitators (ESPs) in series, set to 14 and 12 kV respectively. An iso-paraffinic hydrocarbon (Isopar from Engen Petroleum Limited) was used as direct contact quenching medium in the spray cooling tower. Isopar was used as it was immiscible with the liquid product formed during pyrolysis and was circulated within the quenching system via a closed loop. A 13 kW Daikin water chiller was used to control the temperature of the water bath which, in turn, maintained the Isopar circulation loop at the desired set point temperature. All incondensable gasses were purged to atmosphere. A detailed description of the design and commissioning of this 1 kg/h Fast Pyrolysis plant has been given in by Hugo, (2010). Nitrogen was supplied to the reactor from a nitrogen cylinder and not via a fixed nitrogen line, limiting the overall duration of the run (including start-up, shut down and cool-off periods). The full operating procedure for the 1 kg/h FP plant was given by Hugo, (2010).

3.5.1.1 Design of experiments for Fast Pyrolysis conducted at Stellenbosch

Reactor temperature and the biomass particle feed size were chosen as the manipulated variables for the experiment. Other parameters such as biomass and nitrogen feed rates, condenser temperatures, heat carrier and condenser quenching medium were left unchanged and in the prescribed ranges of design specifications given by Hugo, (2010). **Table 3-2** briefly summarises the process conditions used for the 1 kg/h FP plant in South Africa ($SA_{1\ kg/h}$).

Table 3-2: Process conditions for the $SA_{1\ kg/h}$ plant

	Unit	Setting	Comments
Reactor Temperature	°C	440 - 530	
Biomass particle size	µm	+250 -1000	2 mm Retsch mill
	µm	+1000 -2000	4 mm Retsch mill
Biomass feed rate	kg/h	± 0.85	
Nitrogen flow rate	m^3/h	2.4	
Average gas residence time	S	< 2	
Heat carrier	-	Nitrogen	High purity
Pipe heater	°C	400	
Isopar temperature	°C	13 °C ± 5	

A 2 factor experimental design was used for the statistical analysis of the $SU_{1\ kg/h}$ FP plant, with reactor temperature at 3 levels (440, 470 and 530°C) and average biomass particle size at 2 levels (570 and 1200 µm) as given in **Table 3-3**. Initial test runs performed using approximately 0.5 kg of biomass fed at 1 kg/h, proved to be too short to achieve steady state operating conditions in the reactor. Consequently, the duration of the experimental runs were lengthened to approximately 60 minutes by reducing the feeding rate from 1 kg/h to 0.85 kg/h, and increasing the mass of biomass fed to approximately 0.85 kg per run. These changes helped to minimise the mass of biomass used per run, while also ensuring that each experimental run was long enough to reach steady state and to produce sufficient product quantities for analytical purposes. Even with these changes, however, it was required to conduct some of the experimental runs with an additional batch of biomass, denoted batch 2 in **Table 3-3**.

Table 3-3: DOE for Fast Pyrolysis

Run #	Reactor Temperature °C	Biomass particle size µm
12	440	570 [batch 2]
8	470	570 [batch 1]
9	470	570 [batch 1]
15	470	570 [batch 2]
5	530	570 [batch 1]
6	530	570 [batch 1]
11	440	1200 [batch 2]
13	470	1200 [batch 2]
7	530	1200 [batch 1]

3.5.1.2 Product yields

Product yields were calculated on a dry and ash free weight basis (% wt. daf) for the biomass used for each experimental run. The total char yield was calculated as the sum of the mass of char from the two cyclone char pots, and the difference in mass of the reactor contents (char and sand) and the initial sand added to the reactor, as shown in **Equation 3-2**. It was assumed that no sand was entrained from the reactor and that all the char was separated out by the two cyclone separators in series. These assumptions were verified with visual inspection after each run. A further check was done when combusting the char samples for ash content determinations.

Equation 3-2

$$Y_{char} = \frac{M_{char\ pots} + (M_{reactor\ content} - M_{sand})}{M_{biomass\ (daf)}} * 100\ \%$$

The total liquid yield was calculated by adding the mass of liquid product recovered from the cooling tower reservoir and the liquid recovered from the acetone wash as shown in **Equation 3-3.** The bulk liquid from the cooling tower reservoir was transferred to a separation funnel and allowed to separate into two layers (bio-oil and residual Isopar). After removal of the bulk liquid, the entire condensation chain was rinsed with technical grade acetone (500 – 1000 ml), removing all the visible tarry phase from the system. The resulting acetone wash was then weighed and stored in a fume hood at ambient conditions to evaporate the acetone off. The content of the beaker (tarry phase and acetone) was weighed daily until the relative change in sample mass was less than ± 5 %. The remaining mass was then recorded as the tarry phase liquid product resulting from the acetone wash. The ± 5 % threshold was determined by a sudden change in the evaporation rate of the mixture, indicating that the more volatile acetone was depleted and that only bio-oil was left in the beaker (please refer to **Figure 5-5**).

Equation 3-3

$$Y_{Liquid} = \frac{M_{bulk\ liquid} + M_{tarry\ phase}}{M_{biomass\ (daf)}} * 100\%$$

The viscous tar resulting from the acetone wash was not mixed back into the bulk liquid and not subjected to further analysis. The tar was found to make out only a small fraction of the total liquid yield and it was assumed that by evaporating the acetone, some of the volatile organic fractions of the tar phase were also lost but in negligible quantities.

After separation, the bulk liquid product (bio-oil) was carefully decanted from the separation funnel, avoiding visible Isopar contamination into 1 litre glass sample bottles. A protective layer of heavy duty aluminium foil was inserted between the screw top's rubber seal and the bottle opening to prevent possible corrosion from the acidic content and subsequent contamination of the bulk liquid. Gas yield was calculated by difference as shown in **Equation 3-4**.

Equation 3-4 $$Y_{Gas} = 100\% - Y_{Liquid} - Y_{Solid}$$

3.5.1.3 General materials and startup

Heat carrier

The detailed composition of the AFS 45 foundry sand used as heat transfer medium in the 1 kg/h BFBR at SU, as detected via X-ray fluorescence (XRF), is given in **Table 3-4**.

Table 3-4: XRF of AFS 45 fused silica sand

Compound	[wt. %]	Element	[ppm]
Al_2O_3	0.05	Al	265
CaO	0.01	Ca	71
Cr_2O_3	0	Cr	0
Fe_2O_3	0.07	Fe	490
K_2O	0	K	0
MgO	0	Mg	0
MnO	0	Mn	0
Na_2O	0	Na	0
P_2O_5	0	P	0
SiO_2	97.66	Si	456531
TiO_2	0.05	Ti	300
Loss on Ignition	0.35		
H_2O	0.21		

Start-up and test runs

Before attempting an experimental run, feeder calibrations were carried out for both biomass particle size distributions chosen for experimental work. It was found that the feeder could feed the material well with good repeatability of the average feeding rate achieved (data not shown). Due to the fibrous nature of the milled biomass, it was found that biomass bridging occurred over the screw, but the bridges could easily be broken using a manual agitator and tapping the sides of the hopper.

3.5.2 $KIT_{0.1\ kg/h}$ bubbling fluidised bed reactor

A 0.1 kg/h Fast Pyrolysis plant ($KIT_{0.1\ kg/h}$) was used for initial pyrolysis testing at the Karlsruhe Institute of Technology in Germany, before conducting experimental runs on a larger scale 10 kg/h Process Demonstration Unit (PDU). The main focus of this bench scale plant was to evaluate the mass balance and general behaviour of a specific biomass before conducting a much larger scale investigation on the PDU. This bench scale plant is shown schematically in **Figure 3-2**, and consisted of a biomass feeding unit, a furnace containing the bubbling fluidised bed reactor (BFBR) with cyclone, and a condensation chain followed by a volumetric gas flow meter.

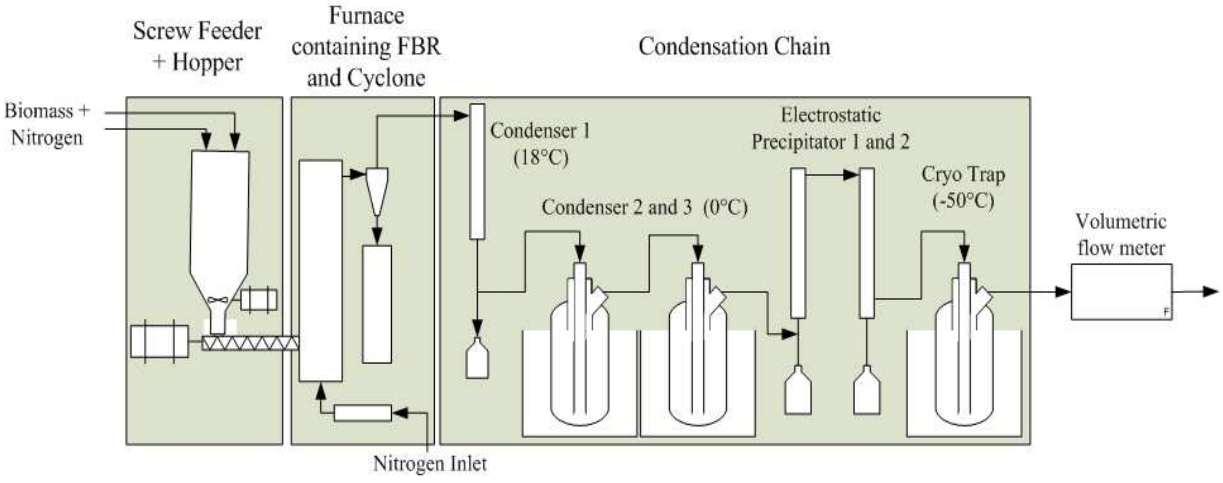

Figure 3-2: KIT bench scale Fast Pyrolysis plant ($KIT_{0.1\ kg/h}$)

The biomass feeding unit consisted of a hopper and screw feeder, where the biomass hopper was supplied with nitrogen to maintain a slight overpressure in the feeding system. Inside the furnace a single cyclone separator followed the 40 mm ID bubbling fluidised bed reactor

(BFBR). Silica sand was used as heat transfer medium in the reactor and nitrogen as the carrier gas which was supplied via a fixed line.

The product vapour exiting the cyclone was first cooled down to room temperature by a single pass, counter-current, shell and tube heat exchanger at 18 °C, before passing through two well insulated condensers maintained at 0 °C with crushed ice and water. After the first three condensers, the vapour stream was passed through two electrostatic precipitators (ESPs) in series, at 8 and 4 kV respectively for ESP 1 and ESP 2, and then through a cryogenic trap. The cryogenic trap was kept at -50 °C using ethanol and dry ice. Finally, the incondensable gas was passed through a Ritter Trommel-Gaszähler volumetric flow meter and purged to atmosphere. Gas samples were taken after the cryogenic trap at 15 minute intervals with glass syringes for analysis using gas chromatography. These samples were analysed at an external laboratory.

3.5.2.1 Design of experiments for Fast Pyrolysis conducted at KIT using a 0.1 kg/h bench scale plant

Initial moisture content and biomass particle feed size were chosen as the process variables for this reactor configuration. Both of these parameters could easily be manipulated due to the small mass of biomass needed per run (± 100 g) and the high moisture content of the biomass as received (± 26 wt.%). The two biomass particle sizes chosen were those resulting from 1 mm and 2 mm sieve milling of the biomass using a Pulverisette granulator from Fritsch. Two initial moisture contents were chosen: as received and oven dry. The oven dry samples were prepared by drying the milled samples over night at 105 °C and then letting the sample cool down to room temperature in a desiccator before use. Please refer to **Table 3-5** for a summary of the experimental conditions used for the $KIT_{0.1\ kg/h}$ Fast Pyrolysis plant.

Table 3-5: $KIT_{0.1\ kg/h}$ Fast Pyrolysis plant operating conditions

Run #	**Particle size** mm	**Initial moisture** wt. %
4,5	1	24.8
1,2,3	2	24.8
6,7	1	9.4
8,9	1	0.8
10,11	2	0.8

An intermediate moisture content of ± 10 wt. % (ambient equilibrium moisture content) was used for an additional run using only one particle size (**Table 3-5**). The intention was to have an additional datum point in the experimental design to see if it would fit in with the general trend observed. Furthermore, this datum point would give a reasonable idea of how comparable the results achieved for the reactor configuration in question would be to the results achieved with the $SU_{1\ kg/h}$ Fast Pyrolysis plant (also a bubbling fluidised bed reactor) at a similar reactor temperature. The intermediate moisture content was achieved by oven drying a sample overnight at 105 °C and then leaving the sample open at ambient laboratory conditions for another day to reach equilibrium before use. All the experimental runs using the bench scale FP plant at KIT were conducted at 505 ± 2 °C and at a constant biomass feed rate in order to feed approximately 0.1 kg/h. Experimental runs were conducted in duplicate for repeatability.

3.5.2.2 Product yields and characterisation

All product yields were calculated on a dry and ash free basis (% wt. daf) of the initial biomass fed. The individual components making up the FP plant were weighed before and after each run, accurate to 2 decimal places, using a laboratory micro balance. After weighing all the components the condensation chain was washed with technical grade ethanol to remove all visible traces of organic contamination. The resulting ethanol wash was filtered and dried overnight in an oven at 105 °C. The solid residue left on the filter paper was used to correct the mass balance for char carried over from the reactor into the condensation chain.

The total char yield was calculated as the sum of the mass of char remaining in the char pot, the difference in mass of the reactor contents (char and sand) and the initial sand added to the reactor, and the residue found after the ethanol wash and filtration as shown in **Equation 3-5**. The total liquid yield was calculated as the sum of the liquid fractions obtained from each component in the condensation chain as given by **Equation 3-6**. A further correction was made for the volatile fraction trapped by the cryogenic trap. The cryo-trap was weighed both in the frozen and thawed state to quantify the mass of volatile components in the gas phase not trapped by the condensers and electrostatic precipitators. Gas yield was calculated by difference as shown in **Equation 3-7**.

Equation 3-5 $$Y_{char} = \frac{M_{Char\ pot} + (M_{Reactor\ content} - M_{Sand}) + M_{Filter}}{M_{Biomass\ (daf)}} * 100\ \%$$

Equation 3-6 $$Y_{Liquid} = \frac{\sum M_{Condenser\ Liquid}}{M_{Biomass\ (daf)}} * 100\%$$

Equation 3-7 $$Y_{Gas} = 100\% - Y_{Liquid} - Y_{Char}$$

The characterisation of the products obtained from the $KIT_{0.1\ kg/h}$ FP plant was typically limited due to the small quantities of products obtained per run as well as limited laboratory time and resources at the time. Furthermore, the liquid product was fractionated across 6 condensers, each fraction with its own physical and chemical properties. It should be stressed again that this bench scale plant's main purpose was to evaluate the mass balance and biomass behaviour associated with FP and was not focussed on the characterisation of the products. The liquid products from experimental runs conducted at the same process conditions were therefore grouped together according to each respective component in the condensation chain and analysed as such. This was done to increase the sample volumes from the respective condensing stages, allowing individual analysis of the liquid yield from each of the respective condensing stages. The liquid fractions resulting from condensers 2 and 3 were furthermore combined as these condensers were kept at the same temperature. This increased the liquid volumes for analytical purposes and reduced the overall number of samples sent for analysis. Product characterisation for the $KIT_{0.1\ kg/h}$ FP plant was limited to water content, pH, total organic carbon (TOC) and chemical oxygen demand (COD) for the liquid fraction, while gas samples were analysed using gas chromatography. Please refer to section **3.7.2** for the details regarding the equipment used for these analyses. No analysis was conducted for the char from this reactor configuration.

3.5.3 $KIT_{10\ kg/h}$ Lurgi® twin-screw reactor (TSR)

A schematic representation of the 10 kg/h Lurgi® Twin-Screw reactor, also referred to as the Process Demonstration Unit (PDU), is shown in **Figure 3-3**. The PDU was designed to use steel balls of various sizes as the heat transfer medium for achieving pyrolysis inside a Lurgi® Twin-Screw reactor (TSR). For this investigation a mixture of 1 and 1.5 mm steel balls was used. Milled biomass (5 mm) was introduced at the far left side of the twin-screw reactor while the hot steel balls (550 °C) were introduced at an offset as shown in **Figure 3-3**.

The steel balls and biomass were mixed by the rapidly revolving twin screws (60 - 240 RPM) and pyrolysis was initiated in the range of 500 to 530 °C. Product vapours and char formed in the reactor were entrained with nitrogen to the first condenser K1, a single pass shell and tube heat exchanger equipped with an automated scraping mechanism to remove char and tar build-up on the inner walls of the condenser. The over-size char particles and steel balls were re-cycled via the heated bucket elevator system at 600 °C. At the time, the hot cyclone which typically follows the reactor to facilitate solid separation was removed. Consequently, the product resulting from the collection vessel of K1 was a mixture of liquid and solid phases, with the ratio of liquid to solid being a function of the operating temperature of K1. Colder operating temperatures for K1 would typically favour vapour condensation in K1 and would result in a higher liquid-solid ratio. The inlet coolant temperature of K1 was controlled at 20 °C, the default set point.

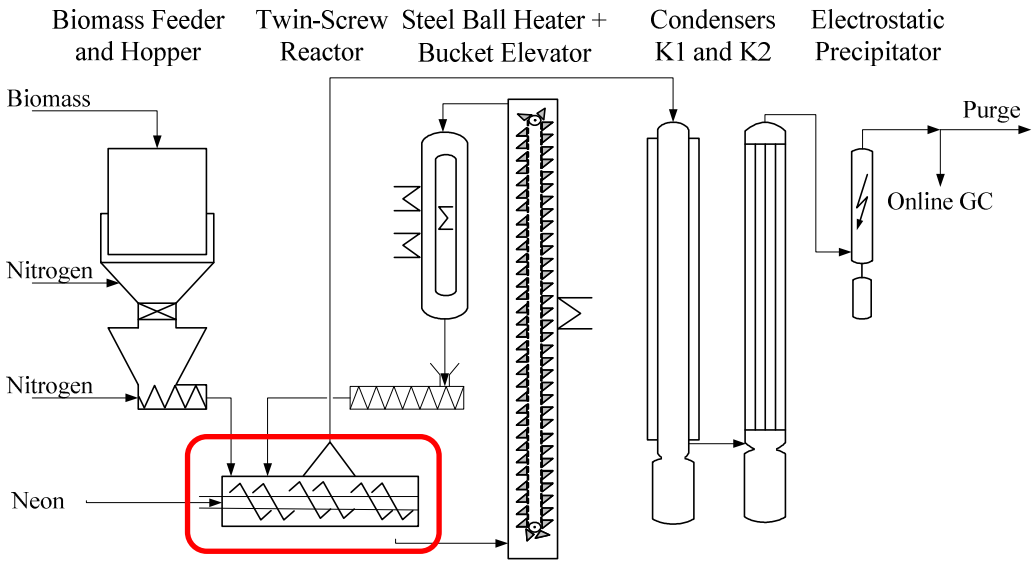

Figure 3-3: KIT 10 kg/h Process Demonstration Unit (PDU)

The uncondensed vapour and gas exiting K1 (50 – 70 °C) passed through a second shell and tube heat exchanger, K2, with an inlet coolant temperature of 10°C. K2 made use of direct contact quenching on the tube side as well as shell side cooling to maximise condensate formation and ensure temperature control. For the first run of a particular biomass investigated, approximately 5.5 litre of clean water is used as the circulating quenching medium inside K2. The watery condensate resulting from run 1 was then analysed and reused as the starting inventory of K2 for run 2 and so forth, accumulating organic condensates and pyrolytic water with each run. The accumulation of organic matter as well

as well as pyrolytic water for run 1 could then be determined by difference to the starting inventory of run 1 (fresh water). Approximately 5.5 litres of condensates (of known water and organic content) was kept aside as starting inventory for run 2 and the rest was discarded. The accumulation of organics and water condensates from run 2 could then be determined by difference to the known composition of the starting inventory of run 2 etc. The After condenser K2, the remaining vapours and gas stream was passed through an electrostatic precipitator (20 kV) before being analysed by an online GC/MS and finally purged to atmosphere.

3.5.3.1 Design of experiments for Fast Pyrolysis conducted at KIT using 10 kg/h demonstration scale plant

Due to limited indoor drying area and time constraints, only 2 of the total 5 runs' biomass could be dried to acceptable levels which were comparable to that of the FP work conducted in South Africa as mentioned in section **3.2.2**. Based on past experience, it was suggested by the plant operators to keep the reactor temperature constant, at the optimum temperature found for most biomass species tested (500 - 530 °C), as the plant is known to become difficult to control at temperatures outside of the design specification. The reactor temperature was therefore maintained at ± 500 °C. Parameters that could be manipulated were the condenser temperature of K1 (by changing the inlet coolant temperature), and the type of heat carrier used inside the reactor. It was decided to keep the heat carrier constant (steel balls at 1200 kg/h) and to vary the temperature of K1. K2 was already set to the lowest possible set point and was therefore not regarded as a process parameter that could be varied. Furthermore it was decided to keep the biomass feed rate constant as far as possible. In total, 5 experimental runs could be completed in the allocated timeframe. An overview of the operating conditions used is given in **Table 3-6**.

Table 3-6: Design of experiments for $KIT_{10\ kg/h}$

	Unit	Run 1	Run 2	Run 3	Run 4	Run 5
Moisture content	wt. %	10.6	21.7	23.4	22.4	9.5
K 1 Inlet temperature	°C	20	20	40	40	60
Reactor temperature	°C	500	500	500	500	500
Biomass feed	kg	39.2	39.0	37.6	37.7	36.9
Avg. biomass feed rate	kg/h	8.1	8.8	9.5	8.8	8.0
Steel balls feed rate	kg/h	1200	1200	1200	1200	1200
Length of run	h	4.8	4.4	4.0	4.3	4.6

3.5.3.2 Product yields

The mass balance of the solid and liquid products were solved by analysing samples taken from K1 (during the course of the experimental run), from K2 after each experimental run, and finally adding the contribution from the electrostatic precipitator (ESP). Methanol extraction was applied to the samples taken from K1 to determine the solid (char) fraction within the sample. The overall char yield was calculated based on the average mass fraction of char found for each of the 3-4 samples taken per run as shown in **Equation 3-8**. Karl-Fischer titration was used to determine the water content of the K1 liquid phase. The organic condensates yield of K1 was then determined by difference.

Equation 3-8 $$\mathbf{Y_{char}} = \frac{\mathbf{x_{charK1} * M_{K1}}}{\mathbf{M_{Biomass\ fed\ (daf)}}} * \mathbf{100}\%$$

Karl-Fischer (KF) titration was further employed to determine the water content of the liquid product from K2 after each experimental run. As the initial inventory of K2 was clean water for run 1, the organic liquid and pyrolytic water yields could be determined by difference of the final and starting inventory masses, assuming negligible evaporation losses. The organic condensate fraction was determined by conducting a water balance over the final and starting inventory, using the results from KF titration. The overall liquid yield was determined as the sum of the relative liquid product mass obtained from K1, K2 and the ESP, as given by **Equation 3-9.**

Equation 3-9 $$Y_{liquid} = \frac{(x_{liquidK1} * M_{K1}) + (M_{K2} - M_{K2\ init}) + M_{ESP}}{M_{Biomass\ fed\ (daf)}} * 100\%$$

An online GC-MS was used to analyse the gas phase throughout each experimental run at an interval of 10 – 15 minutes, with neon gas as internal standard (please refer to section **3.7.2**). The sum of the average volumetric measurements (converted to mass basis) for each gas species detected, was used to calculate the overall gas yield as shown in **Equation 3-10.**

Equation 3-10 $$Y_{gas} = \frac{\sum_i^n M_{gas\ i}}{M_{Biomass\ fed\ (daf)}} * 100\%$$

3.6 Slow and Vacuum Pyrolysis

3.6.1 Fixed bed Slow/Vacuum Pyrolysis plant

Slow and Vacuum Pyrolysis was carried out in a fixed bed reactor which was externally heated by an electrical furnace, as schematically shown in **Figure 3-4**. The reactor was made of quartz glass with an inner diameter of 60 mm and a heated zone length of 460 mm. The reactor configuration could be modified to allow operation at atmospheric pressure, using a nitrogen feed, or at a vacuum by attaching a vacuum pump to the condensation chain as shown in **Figure 3-4**. The condensation chain was kept constant for both the Slow and Vacuum Pyrolysis runs and consisted of a condenser at atmospheric temperature, 2 glass condensers kept at 0 °C using crushed ice and 2 glass cryogenic traps. The cryogenic traps were kept between -30 °C and -40 °C throughout the duration of each experimental run using dry ice and ethanol.

A pressure gauge was fitted to the first condenser which was used to measure the vacuum generated inside the reactor for the Vacuum Pyrolysis runs. The pressure gauge indicated 30 kPa (gauge) at ambient conditions and therefore needed calibration. The 30 kPa mark was taken as 101kPa (absolute) and the -70 kPa mark, as the corresponding 0 kPa absolute marker. A good vacuum was established when a reactor/system pressure of 15 kPa absolute or less could be maintained under operation. An absolute pressure of 5-7 kPa could typically be maintained according to the gauge calibration.

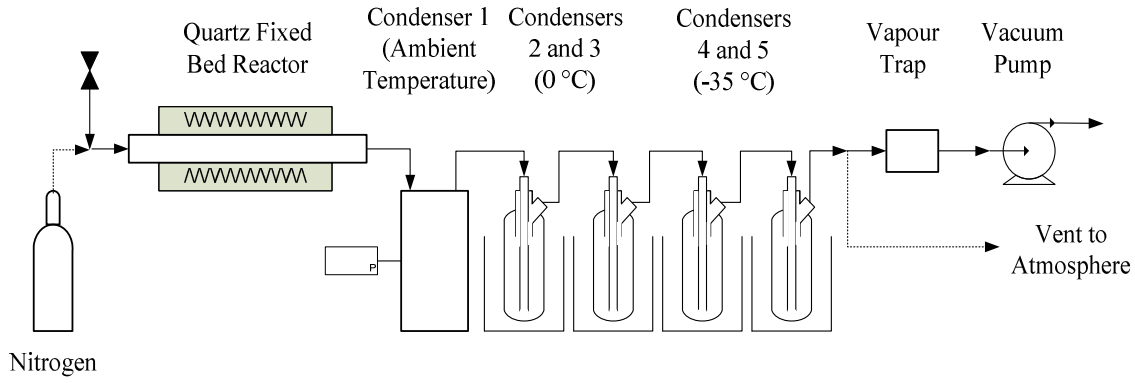

Figure 3-4: SU Fixed bed Slow/Vacuum Pyrolysis plant

Slow Pyrolysis was conducted under a constant nitrogen flow of 40 ml/min. At 40 ml/min the maximum residence times were calculated to fall between 400 and 725 seconds for reactor temperatures of 269 and 481 °C respectively, based on an empty heated zone volume. The true residence times would, however, have been considerably lower under experimental

conditions seeing that the effective open volume of the reactor would have been reduced by the volume of biomass charged to the reactor. Without the exact volume of the biomass and the porosity of the packed bed it was impossible to calculate the true vapour residence time accurately.

The nitrogen flow rate was regulated using a needle valve and calibrated before and after each run with a bubble flow meter. Due to the low flow rate used, the pressure integrity of the plant was checked using the vacuum pump. Before each run a vacuum was induced in the system (< 15 kPa) to check for leaks and then flushed with nitrogen when no leaks were detected. The Nitrogen flow was maintained at the normal operating flow rate of 40 ml/min while the vacuum pump was removed to ensure that the biomass was kept under an inert environment.

Approximately 70 g of biomass was used for each experiment with a biomass particle size range of + 250 µm – 1000 µm and an average particle size of 570 µm. The biomass was inserted and positioned very carefully with a plastic piston to ensure sufficient headroom above the biomass for gas and vapour flow. Furthermore it was ensured that the biomass was positioned within the boundaries of the furnace's heated zone and that the bed of biomass had a uniform height throughout the length of the heated zone as shown in **Figure 3-5**.

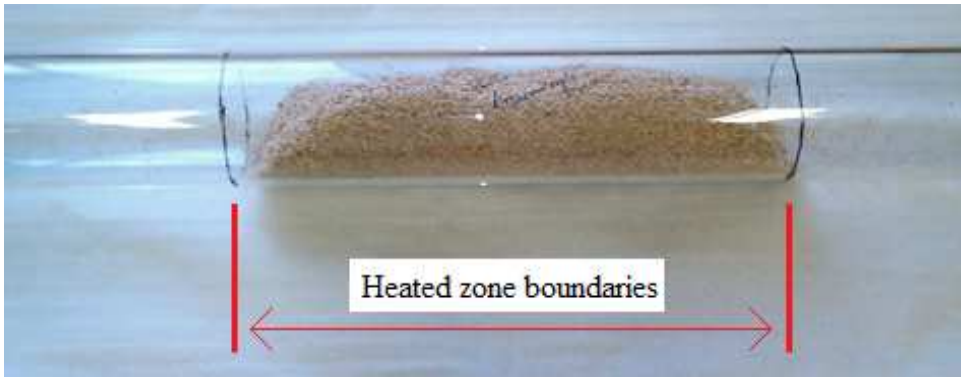

Figure 3-5: Biomass loading for Slow and Vacuum pyrolysis

The samples used for Slow and Vacuum Pyrolysis were selected from Batch 1 early in 2010 and stored (as wood chips) in plastic bags until the experimental work could be conducted in October 2011. The biomass used for both the Slow and Vacuum Pyrolysis runs were regarded as a single sample with an average biomass moisture content of 10.22 wt. % and an ash content of 0.33 wt. % on a dry basis. These average values were used for all the yield calculations in this section. The milled biomass was kept in sealed zip-lock bags for the

duration of the experimental runs to prevent any changes in the moisture content. All temperature measurements taken for Slow and Vacuum Pyrolysis were measured using a type-K thermocouple, inserted directly into the centre of the biomass bed, right in the middle of the heated zone boundaries. This ensured good representation of the packed bed temperature during the experimental run.

3.6.2 Design of experiments for Slow and Vacuum Pyrolysis conducted at Stellenbosch

From the results achieved in Chapter 4 it was decided to conduct the Slow and Vacuum Pyrolysis experiments in the range of temperatures exhibiting the highest rates of volatilisation under TGA conditions. The heating rate and reactor temperature were varied while the hold time (60 minutes) and biomass particle size were kept constant. A central composite design was used for the design of experiments for both the Slow and Vacuum Pyrolysis runs using Statistica version 10. The specified operating conditions and run sequence according to the experimental design for both SP and VP are given in **Table 3-7**.

Table 3-7: DOE for Slow and Vacuum Pyrolysis

Run #	**Reactor Temperature** °C	**Heating Rate** °C/min
5	269	12
7	375	5
3	450	7
2	300	17
6	481	12
8	375	19
9 (c)	375	12
10 (c)	375	12
4	450	17
1	300	7

3.6.3 Product yields

All product yields were calculated on the dry and ash free basis of the biomass fed for each experimental run. The liquid yield was calculated by weighing all the components of the condensation chain (C_i) before and after each experiment and then correcting for the initial water content of the biomass as shown in **Equation 3-11**. Similarly the solid yield was calculated by weighing the quartz tube reactor before (empty) and after each run as shown in **Equation 3-12**. The gas yield was calculated by difference of the liquid and char yields to 100 %.

Equation 3-11
$$Y_{liquid} = \frac{\sum(MC_i - MC_{i0}) - M_{biomass\ moisture}}{M_{biomass\ (daf)}} * 100\%$$

Equation 3-12
$$Y_{char} = \frac{Mreactor\ - Mreactor_0}{M_{biomass\ (daf)}} * 100\ \%$$

3.6.4 Characterisation of SP and VP products

For both the Slow (SP) and Vacuum Pyrolysis (VP) experiments, small volumes of liquid product was produced due to the limitation on the mass of biomass that could be loaded for each run (± 70 g). Furthermore, as a result of the configuration of the condensation chain and the short vapour residence times, the liquid product yielded for the Vacuum Pyrolysis plant was fractionated across multiple condensers. The overall pyrolytic water yield was subsequently calculated as the weighted sum of the water contents of all the respective liquid yields from the different condensers. Slow Pyrolysis did not result in the same fractionation as the linear velocities in the condensation chain were significantly lower than for the Vacuum Pyrolysis runs. For the SP runs, a single fraction of watery bio-oil was collected from the first condenser, with almost no liquid product resulting from the glass condensers. These factors limited the analysis of the SP and VP products to water content determination via Karl-Fischer titration and the organic compounds identification via GC/MS for the liquid products, and calorific value and BET surface area determination for the char products (section **3.7.1**)

3.7 Pyrolysis products analysis

3.7.1 Pyrolysis products analyses for Stellenbosch

Water content was determined by using a Metrohm KF Titrino (ASTM E871). The calorific value (HHV) of the liquid product was determined using an IKA C200 bomb calorimeter with benzoic acid tablets as calibration standard. A 509900 Utech Instruments pH probe was used to measure the pH of the liquid product. The ash content of the liquid product was determined by weighing the residue after combustion of a 2 ml liquid sample in a muffle furnace at 575 ± 5 °C. Liquid product viscosity was determined using a rheometer (Physica MCR 501, Anton Paar). The molecular composition of the liquid was determined with gas chromatography coupled with mass spectroscopy (GC/MS) using a Zebron G006-11 capillary column. Oven temperature was set to 260 °C with helium as the carrier gas at a total flow rate of 33.3 ml/min. Initially no suitable internal standard was available and consequently the analysis done for the Fast Pyrolysis oils could not be compared directly between runs. The ratios of the respective chemical families could however be compared.

High purity heptane (99 % HPLC), from Sigma-Aldrich, was used as an internal standard for the relative quantification of the bio-oil compositions resulting from the Slow and Vacuum Pyrolysis experiments. For each run the liquid product (fractions were mixed together in the case of VP) was diluted with high purity acetone in a ratio of 1.00 g of bio-oil to 10 ml of acetone. A 900 µl sample of the well mixed solution was then transferred to a sample vial and spiked with 100 µl of Heptane standard solution. The internal standard solution was prepared by weighing precisely 0.033 g of Heptane and diluting it with high purity acetone to make up a 50 ml standard solution in a volumetric flask.

Only components detected with a probability of 70 % and more were further considered in the analysis of the bio-oil. Similar to the treatment of the Fast Pyrolysis bio-oil samples, the compounds detected a probability of + 70 % were grouped according to chemical families. Seeing that a suitable internal standard had been identified for the analysis, the contribution of each compound could be expressed relative to the total peak area of the chromatogram, or relative to the total peak area of the +70 % compounds, or as a ratio to the peak area of the internal standard.

The BET surface area of the char was determined using a Micrometrics ASAP 2010 system. Char ash content was determined by weighing the residue after combustion of a 1 g char sample in a muffle furnace at 575 ± 5 °C. The HHV of the char was measured using a DDS

CP500 automatic calorific processor from Digital Data Systems, with a CP501-A solid state cooler and a DDS CP502 filling station.

3.7.2 Pyrolysis products analysis for KIT

The bio-oil water content was determined using a Metrohm 774 KF Titrino. A Metrohm pH lab 827 probe was used to measure the pH of the liquid product. The calorific value (HHV) was determined using an IKA, model C 5000 control bomb calorimeter. A TruSpec CHN Vario EL III Leco Elementar elemental analyser was used for ultimate analysis. The calorific values reported for liquid products of the $KIT_{10\ kg/h}$ FP plant were calculated using the Channiwala correlation as shown in **Equation 3-13**, where the subscript 'x' refers to the elemental mass fraction of the organic substance (relating to carbon, hydrogen, sulphur, oxygen and nitrogen) and the total ash content of the substance (Channiwala and Parikh, 2002). Based on the experience of the analytical laboratory at KIT and the specific equipment used in determining the elemental compositions, the Channiwala correlation has proven to give the best prediction of calorific values for pyrolysis products as well as the raw biomass. This correlation was consequently used where the calorific values of specific product phases could not be determined directly using the bomb calorimeter due to either high moisture content, or the complexity and multi-phase nature of the product mixtures found for this reactor configuration.

Equation 3-13. $HHV\ (MJ/kg) = 0.3491x_C + 1.1783x_H + 0.1005x_S - 0.1034x_O - 0.0151x_N - 0.0211x_{ash}$

Methanol extraction was used to separate the liquid and solid fractions found in the product mixture of condenser K1 (please refer to **Figure 3-3**) after which elemental analysis was employed. The total organic carbon (TOC) content was determined using a Dimatoc 2000 from Dimatec. The chemical oxygen demand (COD) was measured using a Xion 500 from Hatch Lange. Char ash content was determined using a Leco 701 TGA at 550, 818 and 1000 °C. Pyrolysis gas for the 10 kg/h plant was analysed using an online Daniel 700 GC/MS by Emerson with helium (80 °C) as carrier gas and a thermal conductivity detector (TCD). Gas analysis for the 0.1 kg/h bench scale plant was carried out by an external laboratory at KIT using GC from Agilent.

4 Thermo-gravimetric Analysis

4.1 Introduction

Thermo-gravimetric analysis is used to study the thermal degradation characteristics of a substance in an either an inert or oxidative environment. A small sample, typically a few milligrams, is placed on a very sensitive balance and suspended in a furnace while the sample is heated up according to a predefined temperature program. The balance is typically isolated from the heated zone (with only the sample supporting arm protruding into the furnace) and housed in a separate chamber underneath the furnace. An additional inert gas flow is fed to the balance chamber which provides a protective barrier from the heated zone. The balance continually records the loss in sample mass relative to the temperature of the sample, which can then be used to calculate the reaction rate constants for the thermal degradation reactions.

The isoconversional method (Aboyade *et al.* 2011; Vyazovkin *et al.*, 2011) was used in this investigation to calculate the kinetic parameters associated with the thermal degradation of *E.grandis*. The isoconversional method makes use of tie-lines at equal conversion (isoconversional tie-lines) of multiple thermo-gravimetric (TG) datasets, obtained at different heating rates, to determine the activation energy (E_a) and pre-exponential constant (A) for a specific biomass as discussed in previously in section Error! Reference source not found.. The advantage of using the isoconversional method lies in the fact that it is not required to specify a reaction model or make assumptions regarding the order or nature of the chosen kinetic model when determining the kinetic parameters. It is however important to realise that even though no specific rate equation needs to be specified, it is still assumed that the reaction kinetics follow some undefined rate expression as a function of conversion (Vyazovkin *et al.*, 2011).

The purpose of this investigation was to:

- Gain an understanding of the thermal degradation behaviour of *E.grandis* and its extracted components (alpha-cellulose, holocellulose and Klason lignin) using TGA at various heating rates.

- Determine the kinetic constants (activation energy and pre-exponential constant) of *E.grandis* and its extracted components (alpha-cellulose, holocellulose and Klason lignin).

4.2 Results and Discussion

4.2.1 Repeatability of thermogravimetric results

The characteristic temperatures for each differential thermo-gravimetric (DTG) curve were used to illustrate the repeatability of the thermo-gravimetric (TG) data. These temperatures represent the start and end points of the observed thermal degradation reaction, as well as the point at which the maximum rate of degradation was achieved as schematically shown in **Figure 4-1** for a virgin biomass sample. These include the onset and offset temperatures, as well as the temperature at the maximum rate of volatilisation. All characteristic temperatures were automatically determined by the AKTS Thermokinetics software package. For some of the compounds, however, it was observed that the software reported the onset temperatures in the region of the dashed line shown in **Figure 4-1** and not at the true start of the overall peak. The shoulder peak, responsible for this deviation in the onset temperature reporting, were typically found in the DTG curves of holocellulose and the raw biomass and are known to be representative of the hemicelluloses fraction found in both holocellulose as well as the virgin biomass. The results for the onset temperatures were therefore omitted from **Table 4-1**.

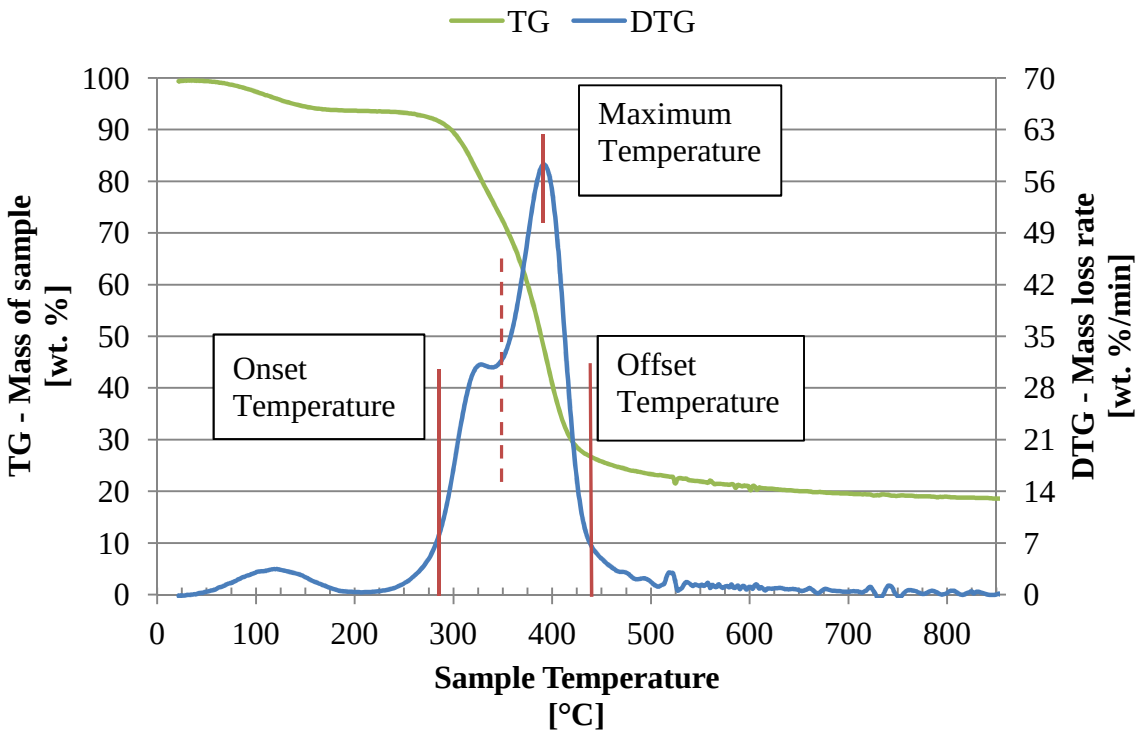

Figure 4-1: Characteristic DTG temperatures for *E.grandis*

The average values calculated for duplicate TGA runs as well as the accompanying standard deviations for each heating rate are presented in **Table 4-1**. Unfortunately, electronic data corruption resulted in the loss of one of the duplicate experimental runs conducted on lignin at 10 °C/min and the software was therefore unable to regenerate the TG and DTG curves from which the characteristic temperatures are calculated for that particular dataset. The remaining duplicate dataset was, however, used to determine the characteristic temperatures for lignin at 10 °C/min. As only a single dataset was used for this particular instance, the standard deviation was not reported for lignin at 10 °C/min as shown in **Table 4-1**. In addition to this, it was found that the offset temperature for the single available datum point could not be calculated automatically by the software. Due to the flat and wide nature of the DTG curve for this particular sample (shown in **Figure 4-5**) it was also not possible to give a reliable estimation of the offset temperature by hand.

Table 4-1: Repeatability of TGA data

	Heating rate		Temperature	
	Set point [°C/min]	**Measured [°C/min]**	**Maximum [°C]**	**Offset [°C]**
Raw biomass	10	10.76 ± 0.01	358.14 ± 0.09	382.00 ± 0.23
	20	23.83 ± 0.00	375.27 ± 0.28	404.09 ± 0.10
	30	38.65 ± 0.60	384.56 ± 0.13	420.46 ± 0.23
	50	67.86 ± 2.92	372.31 ± 22.26	425.71 ± 23.83
Lignin	10	11.03	373.80	-
	20	23.85 ± 0.25	387.80 ± 0.52	431.33 ± 6.38
	30	38.59 ± 0.36	397.09 ± 5.15	441.02 ± 2.82
	50	67.79 ± 2.33	412.57 ± 7.11	466.51 ± 9.95
Alpha-cellulose	10	10.71 ± 0.03	320.99 ± 0.01	358.24 ± 0.21
	20	23.76 ± 0.13	340.11 ± 0.45	378.85 ± 0.38
	30	38.16 ± 0.45	353.04 ± 3.03	396.17 ± 2.68
	50	68.05 ± 0.57	362.54 ± 2.63	419.21 ± 2.19
Holocellulose	10	10.80 ± 0.08	333.57 ± 0.58	355.11 ± 0.76
	20	23.90 ± 0.49	347.17 ± 0.06	372.97 ± 0.02
	30	38.10 ± 0.11	355.85 ± 0.71	388.34 ± 0.75
	50	70.43 ± 3.11	373.32 ± 25.14	425.07 ± 26.52

It was found that the measured heating rates were in all instances higher than the set point values, with the offset increasing for increasing heating rate set points. The greatest deviations were observed at the 50 °C/min set point, which resulted in the average measured heating rates deviating from approximately 67.8 to 70.4 °C/min (17.8 and 20 °C/min higher than set point of 50 °C/min). It was observed that the extent of the deviations were fairly constant for heating rates investigated at similar set points, with a standard deviation of less than 1 °C/min. The variations were, however, also found to be more significant for the 50 °C/min set point, especially for the more complex materials investigated.

The variations observed for alpha-cellulose were, in all instances, less severe than that of the other lignocellulosic components and the whole biomass investigated, as evident from **Table 4-1**. This might be a direct result of the differences in the molecular compositions of the various components investigated, because alpha-cellulose contains a single repeating

monomer arranged in linear chains, compared to the heterogeneous and amorphous nature of the hemicelluloses and lignin structures present in the other samples investigated. It is furthermore known that the thermal degradation of cellulose is endothermic while the thermal degradation of lignin and hemicelluloses tend to be exothermic in nature (Di Blasi C., 2008). It is therefore expected that greater variation in the temperature control will result from samples containing lignocellulosic compounds exhibiting both endothermic as well as exothermic reaction characteristics.

In addition, a further argument can be made for the general deviation in the heating rates observed from the set point values when considering the location where the temperature measurements were taken in the course of the experiments. As mentioned previously in **Chapter 3.3**, the thermocouple used for temperature control also supported the crucible during an experiment with the crucible fitting snuggly over the thermocouple tip. This configuration subsequently induced a temperature gradient across the crucible wall to the thermocouple. It was therefore expected that the temperature lag, and therefore also the deviation in the measured heating rate from the set point, would be greater when considering higher heating rates. An advantage of using this method of temperature control, however, was that the measurements were realistic approximations of the true evolution of the sample/biomass temperature inside the crucible and not a mere measurement of the surrounding environment due to the intimate contact of the sample with the crucible and the crucible with the thermocouple respectively.

4.2.2 Influence of biomass particle size on thermal degradation behaviour

Figure 4-2 and **Figure 4-3** show the normalised thermo-gravimetric (TG) and differential thermo-gravimetric (DTG) curves for *E.grandis* as obtained using various particle size ranges at a constant heating rate set point of 50 °C/min. As mentioned in section **3.4**, these curves were generated using the AKTS Thermokinetics software package, which expressed the data in terms of conversion, rather than sample mass, where 0 represented the dry sample mass measured at the start of the peak baseline and 1 represented the final residue/char mass measured at the end of the peak baseline. From the comparison of the normalised TG curves obtained for the various particle size ranges investigated, it was evident that the influence of

the particle size range was almost negligible, with only one of the four curves (particle size ranging from 400 to 1000 µm) deviating slightly from the others (**Figure 4-2**).

The differential form of the normalised TG data (**Figure 4-3**) accentuated the slight deviations and made the identification thereof easier. When considering the standard deviations of the characteristic temperatures calculated for the biomass, shown in **Table 4-1**, and comparing it with the standard deviations calculated for the different particle size ranges as shown in **Table 4-2**, it was clear that the deviations as a result of the differences in particle sizes were negligible and fell well within the boundary of the measured deviations at 50 °C/min inherent to the experimental procedure as shown in **Table 4-1**. It may therefore be concluded that the particle size of the biomass used had a negligible effect on the thermal degradation behaviour of *E.grandis*.

Table 4-2: Characteristic temperatures for the *E.grandis* at different particle size ranges

Particle size range	**Heating rate**	**Temperature**		
[µm]	**[°C/min]**	**Onset [°C]**	**Max [°C]**	**Offset [°C]**
0 – 224	67.9	276	394	452
224 – 400	69.6	292	396	451
400 – 1000	68.3	286	388	442
1000 - 2000	68.3	293	394	449
Standard deviation	0.74	7.9	3.7	4.4

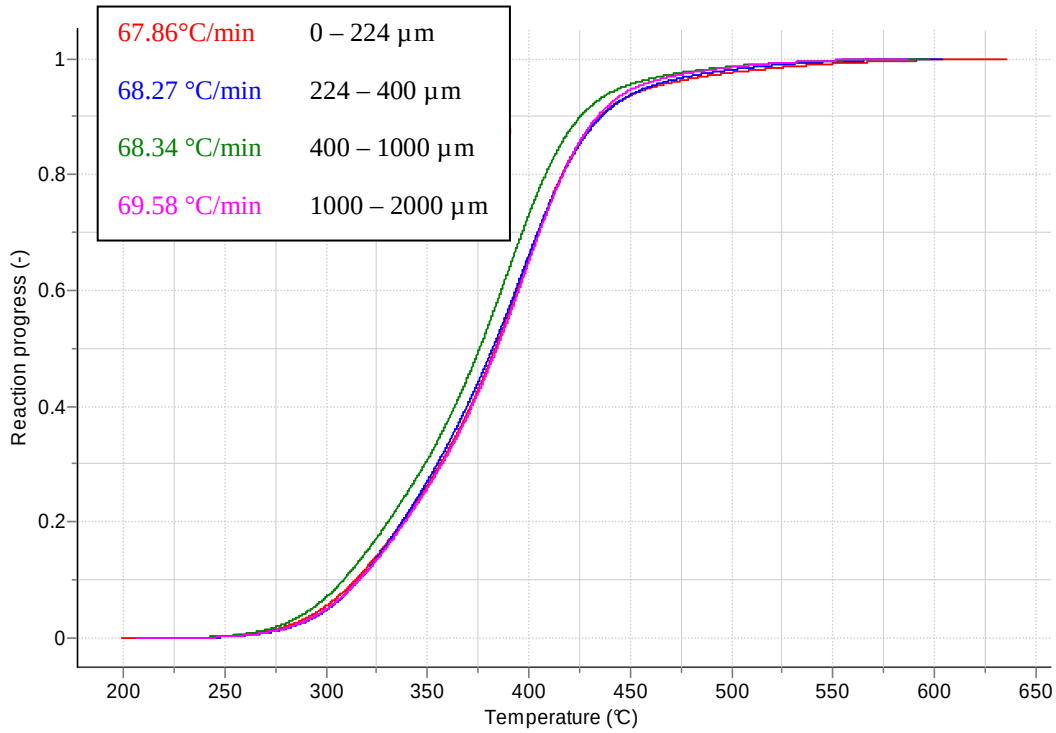

Figure 4-2: Normalized TG curve for *E.grandis* at different particle sizes

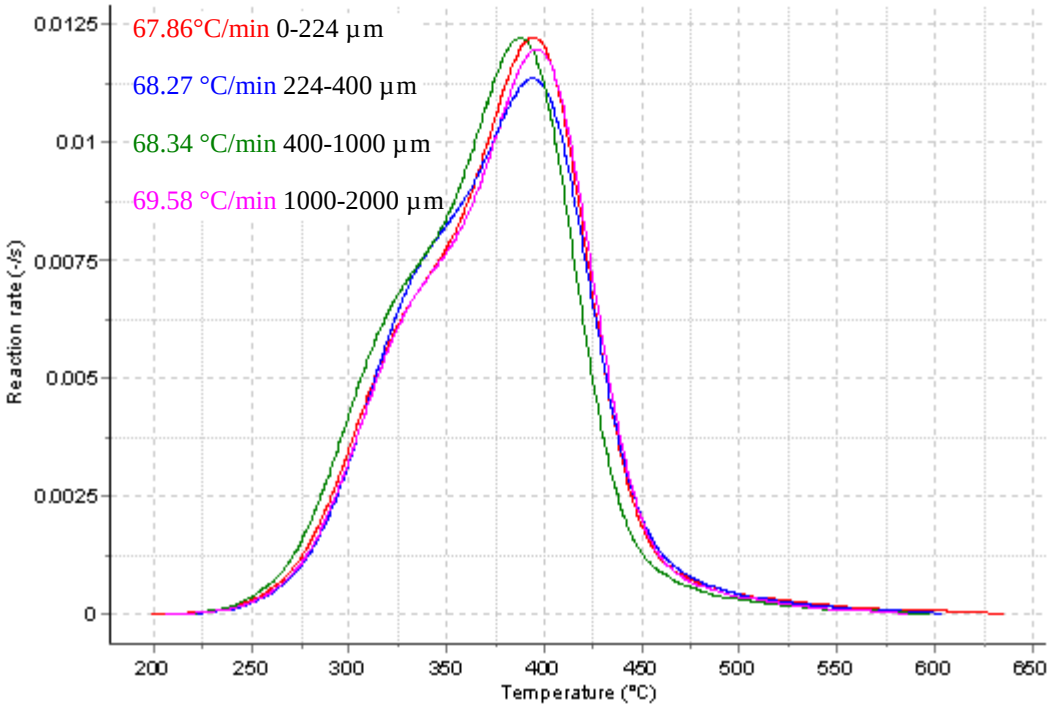

Figure 4-3: Normalized and DTG curve for *E.grandis* at different particle sizes

4.2.3 Normalised thermo-gravimetric (TG) and differential thermo-gravimetric (DTG) curves for *E.grandis* and its lignocellulosic components

The normalised TG and DTG results, as generated with the AKTS Thermokinetics software package, will be discussed in the following subsections for each of the major lignocellulosic compounds (holocellulose, alpha-cellulose and lignin) and the raw biomass.

4.2.3.1 Lignin

Figure 4-4 and **Figure 4-5** show the normalised TG and DTG curves respectively, as generated by AKTS Thermokinetics software for the extracted Klason lignin sample. It was observed that the thermal degradation reaction took place across a wide temperature range, starting in the region of 225 to 250 °C and ending between 550 and 650 °C depending on the heating rate employed. It was found that the rate of thermal degradation increased significantly at higher heating rates which also widened the observed range of thermal degradation as seen in **Figure 4-5**. From **Figure 4-5** it was also evident that higher heating rates caused a shift in the DTG curve for lignin, with the maximum reaction rate moving toward higher furnace temperatures at higher heating rates. **Table 4-3** presents the temperatures at each maximum reaction rate as well as the final char yields for each analysis. It was found that increasing heating rates had a decreasing effect on the char yield. The lowered char yield with increasing heating rate has been reported by various authors (Kumar *et al.*, 1992; Carrier *et al.*, 2011a) and is consistent with the general understanding of the influence that particle heating rate has on the thermal degradation behaviour of biomass.

Table 4-3: Char yields for thermo-gravimetric analysis of Klason lignin extracted from *E.grandis*

Heating rate set point [°C/min]	Measured heating rate [°C/min]	Temperature at maximum rate [°C]	Char yield at 850 °C [wt. %]
10	11.03	373.8	44.3 (-)
20	23.67	388.2	42.1 (± 1.7)
30	38.33	400.7	43.2 (± 0.1)
50	69.44	417.6	41.8 (-)

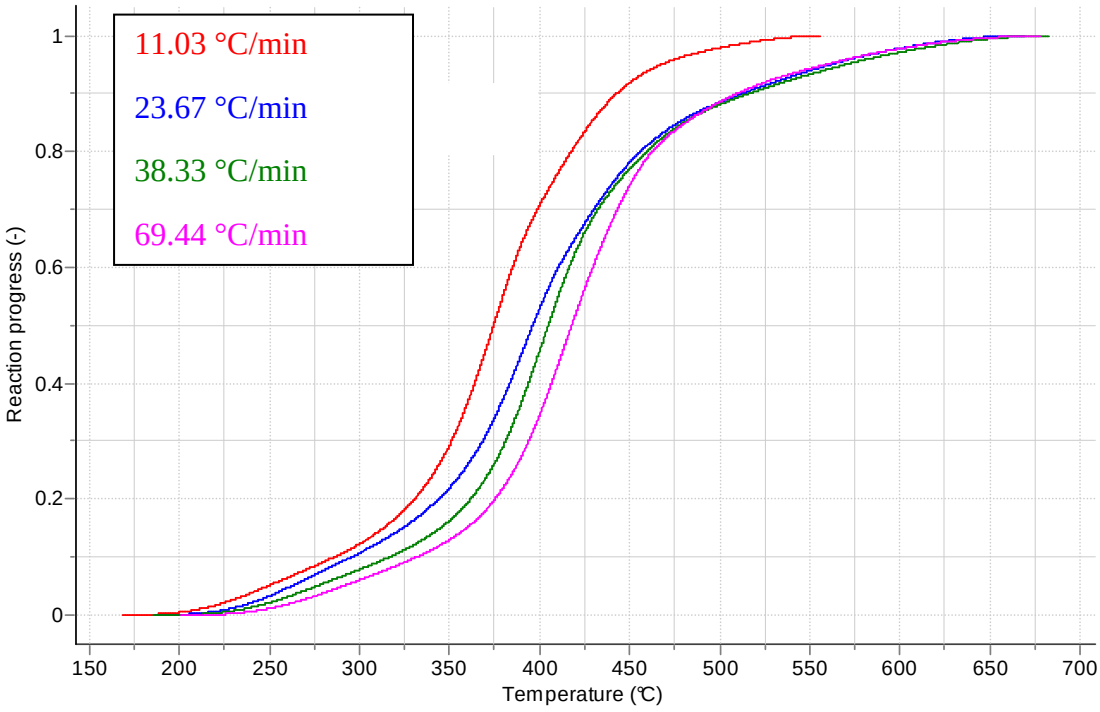

Figure 4-4: Normalised thermo-gravimetric curve for Klason lignin extracted from *E.grandis*

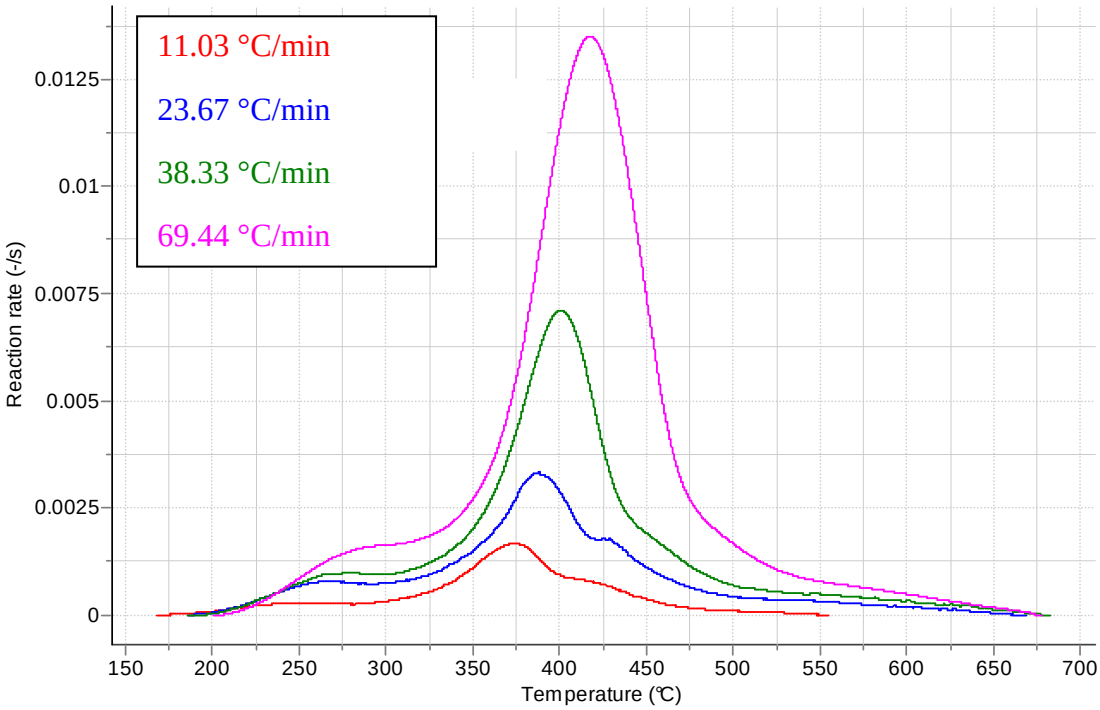

Figure 4-5: Normalised differential thermo-gravimetric curve for Klason lignin extracted from *E.grandis*

4.2.3.2 Alpha-cellulose

Figure 4-6 and **Figure 4-7** show the normalised TG and DTG curves respectively, as generated by AKTS Thermokinetics software for the extracted alpha-cellulose sample. Unlike the lignin sample, it was found that the DTG curves generated for alpha-cellulose were well defined singular peaks, within a relatively narrow temperature band ranging from 275 - 350 °C and 275 - 425 °C depending on the heating rate. These findings are consistent with those of Raveendran *et al.*, (1996) and Stenseng *et al.*, (2001) using commercial cellulose in their investigations. Similar to the findings for the lignin sample, it was observed that an increasing heating rate increased the maximum rate of reaction, while widening and shifting the DTG curve to higher furnace temperatures.

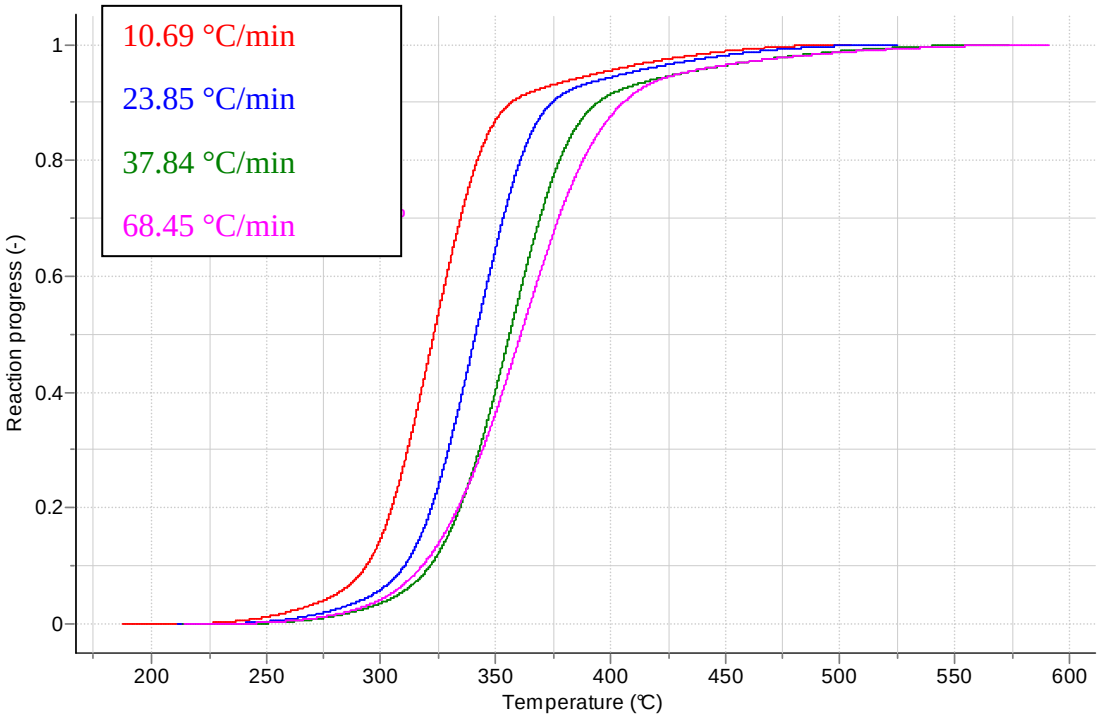

Figure 4-6: Normalised TG curve for alpha-cellulose

Table 4-4 shows the shift in the temperature at maximum reaction rate as well as the char yield found for each analysis. It was found that higher heating rates reduced the char yield resulting from alpha-cellulose. In comparison with the char yields reported for lignin (**Table 4-3**) it was observed that an increase in the heating rate affected the char yield from alpha-cellulose more significantly.

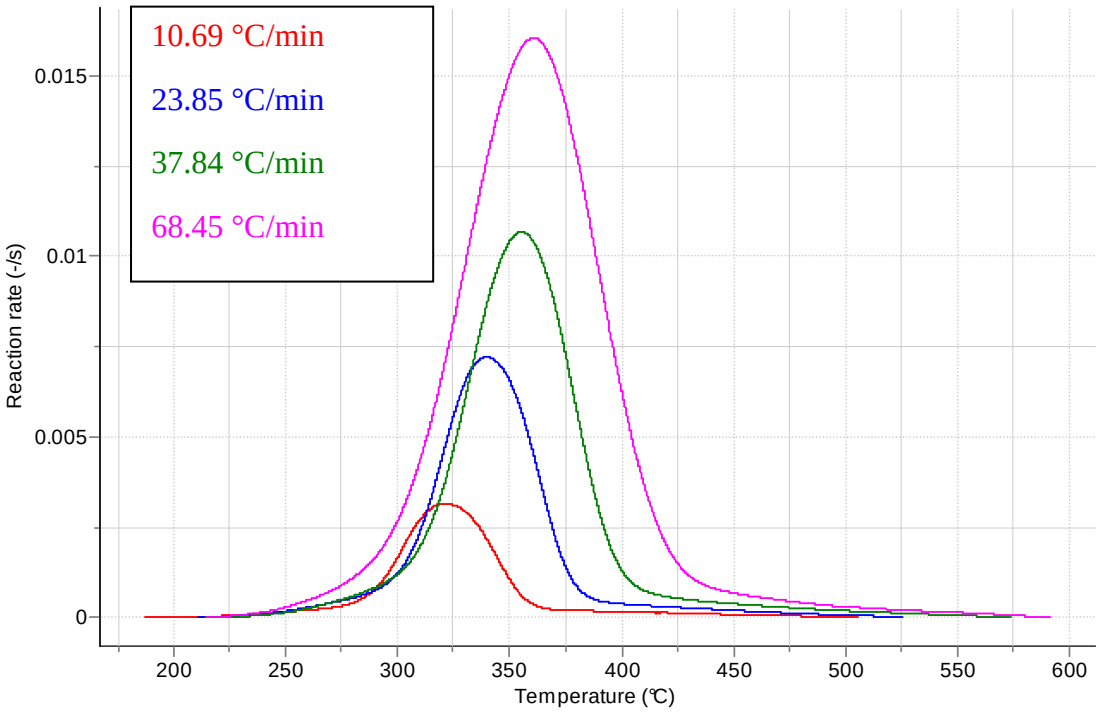

Figure 4-7: Normalised DTG curve for alpha-cellulose

Table 4-4: Char yields for thermo-gravimetric analysis of alpha-cellulose extracted from *E.grandis*

Heating rate set point [°C/min]	Measured heating rate [°C/min]	Temperature at maximum rate [°C]	Char yield at 850 °C [wt. %]
10	10.69	321.0	20.6 (± 0.1)
20	23.85	339.8	18.5 (± 0.2)
30	37.84	355.2	17.4 (± 0.6)
50	68.45	360.7	15.8 (± 3.0)

4.2.3.3 Holocellulose

Figure 4-8 and **Figure 4-9** show the normalised TG and DTG curves respectively, as generated using AKTS Thermokinetics software, for the extracted holocellulose sample. Holocellulose is a combination of alpha-cellulose and hemicelluloses, as discussed in Chapter **3**. This multicomponent nature of holocellulose was evident when considering both the TG

and DTG curves. A definite change in slope was observed in the TG curves for all the heating rates considered, indicating a change in the apparent reaction rate (**Figure 4-8**). In **Figure 4-9** the change in reaction rate was more prominent and observed as two distinct reaction rate maxima. It was found that the resolution of the two peaks deteriorated with increasing heating rate, and at the maximum set point the shoulder had disappeared completely, leaving only a single peak.

It was observed that an increase in the heating rate also shifted the DTG curves to higher furnace temperatures, but with each increase the relative shift became smaller as shown in **Table 4-5**. This phenomenon can be explained when considering the individual components of holocellulose. It is known that the characteristic shoulder peak observed in biomass DTG curve is associated with the hemicellulose fraction of the biomass, while the larger peak is primarily associated with the cellulose fraction of the biomass (Orfão *et al.,* 1999; Raveendran *et al.,* 1996). The general trend that was presented for the lignin and alpha-cellulose fractions suggest that increasing the heating rate increases the rate of reaction while also widening the DTG peak. The disappearing shoulder can therefore be explained by the merger of the two individual curves (alpha-cellulose and hemicelluloses), to form a single, larger peak that is skewed to the left by the contribution of the hemicelluloses fraction.

The char yield was found to be higher for the holocellulose sample compared to that of alpha-cellulose. The char yield from holocellulose was found to be 2.9 wt. % higher on average than the char yield from alpha-cellulose at corresponding heating rates. From the initial biomass characterisation it is known that the extracted holocellulose contained roughly 67.6 wt. % alpha-cellulose, with the remaining fraction predominantly hemicelluloses. (The biomass characterisation will be discussed in chapter **5** of this thesis, please refer to **Table 5-1** for the lignocellulosic composition of *E.grandis* used in this study). Under the assumption that the remaining 32.4 wt. % fraction was pure hemicelluloses and that no residual lignin was present in this fraction, the relative contribution of the hemicelluloses to the char yield could be calculated by weighted difference. This summative approach for calculating product yields and predicting the thermal degradation behaviour of biomass based on its lignocellulosic composition has been demonstrated successfully by Raveendran *et al.,* (1996). The calculated char yields based on pure hemicelluloses are shown in **Table 4-5**.

Table 4-5: Char yields for thermo-gravimetric analysis of holocellulose extracted from *E.grandis*

Heating rate set point [°C/min]	Measured heating rate [°C/min]	Temperature at maximum rate [°C]	Holocellulose Char yield at 850 °C [wt. %]	Hemicelluloses Char yield[a] at 850 °C [wt. %]
10	10.86	334.0	23.4 (± 2.8)	29.9
20	24.24	347.1	21.1 (± 0.2)	26.5
30	38.18	356.4	20.2 (± 0.1)	26.0
50	68.23	355.5	19.1 (± 0.1)	26.0

[a] Calculated based on average values and a 32 wt. % hemicelluloses contribution in the holocellulose sample

The calculated specific char yield for the hemicelluloses fraction of the holocellulose sample, as given in **Table 4-5**, was found to be higher than that of alpha-cellulose but lower than the specific char yield found for lignin (**Table 4-3**). Similar findings have been reported by Raveendran *et al.*, (1996), where the specific char yield from the thermo-gravimetric analysis of commercially acquired xylan and hemicelluloses were found to be 30.0 and 32.0 wt. % respectively. A different study by Raveendran and Ganesh, (1996) a lower char yield of 20.7 wt. % was reported for xylan using a packed bed reactor.

Based on the branched nature of the heterogeneous polysaccharide macromolecular structure associated with hemicelluloses, it was expected that the specific char yield of hemicelluloses would have been lower or similar to that of cellulose. This expectation of a lower char yield was due the proneness of hemicellulose for microbial and chemical attack in comparison with linear polysaccharide cellulose (sections **2.1.1** and **2.1.2**). Considering that the hemicelluloses shoulder observed in the holocellulose DTG curve (showed in **Figure 4-9**) is observed at a lower temperature interval compared to the main reaction rate peak associated with cellulose (Orfão *et al.*, 1999; Raveendran *et al.*, 1996), it can be postulated that the hemicelluloses fraction is more prone to thermal attack due to its branched structure. The increased char yield in comparison with cellulose, however, is therefore postulated to be related to the differences in the monomeric differences between hemicelluloses (mainly containing xylose and glucopyranose) and cellulose (containing only glucopyranose).

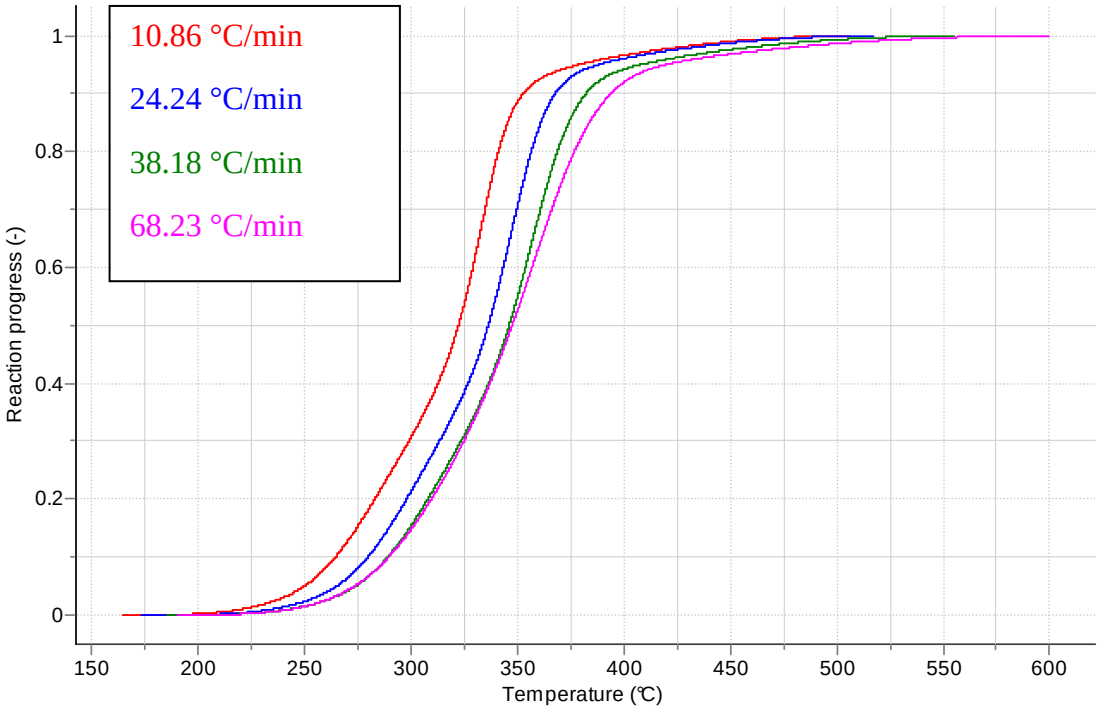

Figure 4-8: Normalised TG curve for extracted holocellulose

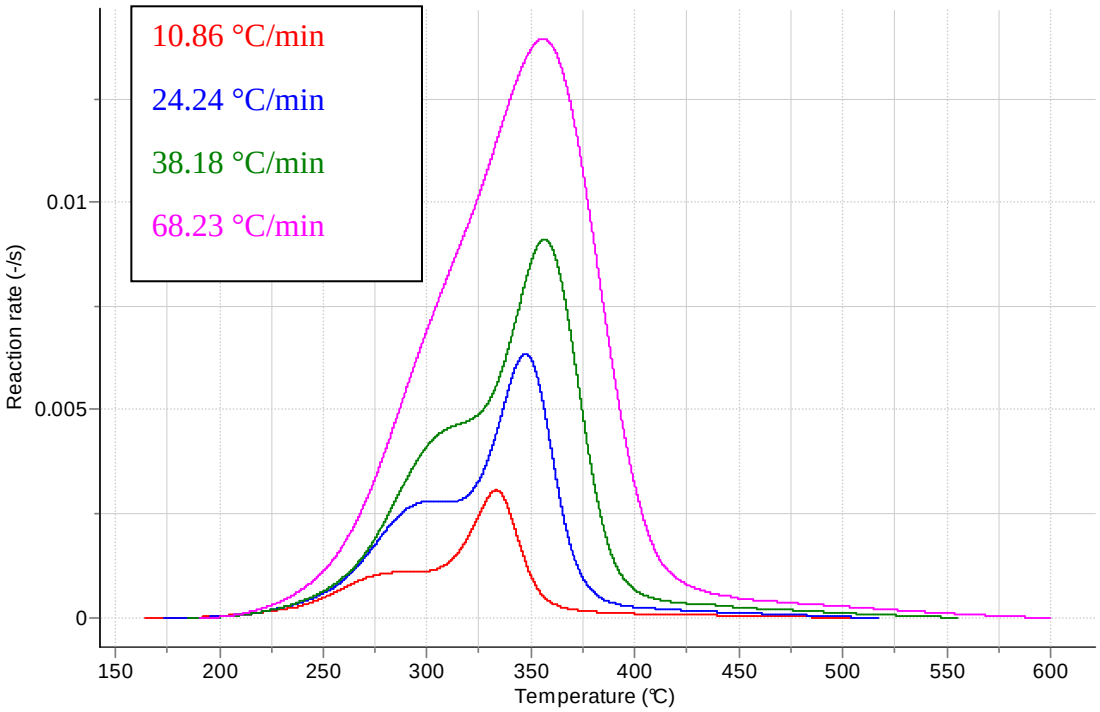

Figure 4-9: Normalised DTG curve for extracted holocellulose

4.2.3.4 *E.grandis* virgin biomass

Figure 4-10 and **Figure 4-11** show the normalised TG and DTG curves for *E.grandis* respectively, as generated using AKTS Thermokinetics software. Similar to the results discussed for holocellulose, it was observed that 2 distinct peaks formed in the DTG curve, suggesting the volatilisation of two different lignocellulosic compounds, hemicelluloses and cellulose. In comparison with the results from holocellulose, it was observed that the respective peaks were wider, and the maximum rate of reaction lower for the raw biomass compared to that of holocellulose at corresponding heating rates. This observation can be ascribed to the added effects of the lignin fraction present in the raw biomass, as it was shown in section **4.2.3.1** that lignin typically has a very wide and flat reaction rate when compared to the other samples investigated.

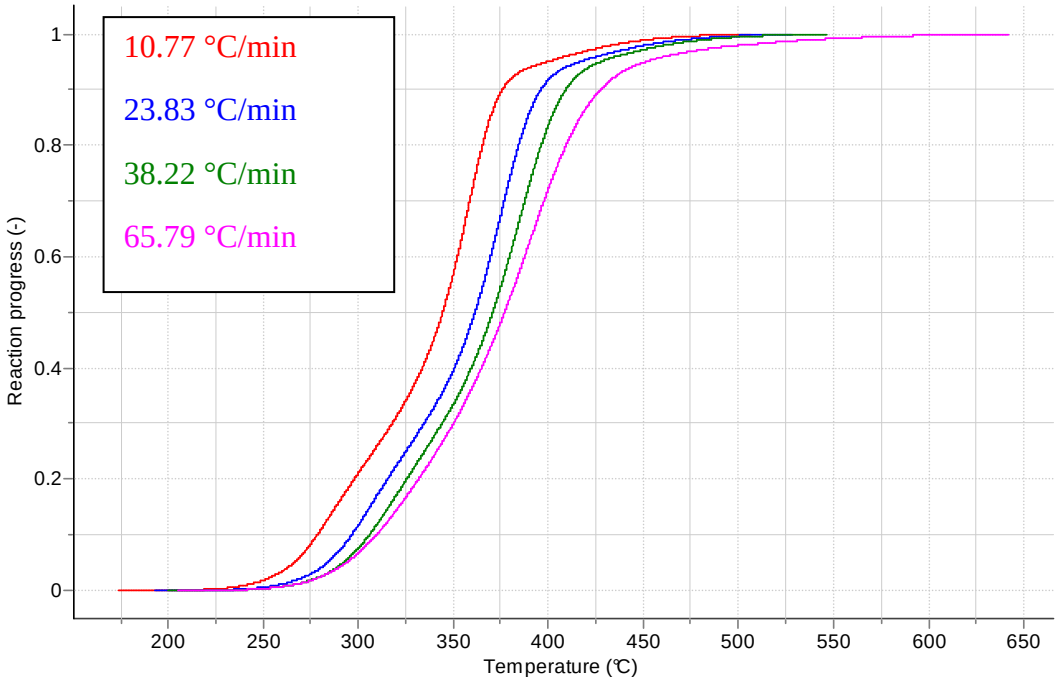

Figure 4-10: Normalised TG curve for virgin *E.grandis*

For the whole biomass as well as the individual lignocellulosic compounds investigated it was shown that higher heating rates caused a shift in the respective DTG curves toward higher furnace temperatures, accompanied by an increase in the reaction rate and widening of curve baseline. Furthermore it was observed that the resolution of the individual peaks showed in the normalised DTG curves deteriorated with increasing heating rate. Especially in the cases of the whole biomass and the holocellulose, it could clearly be seen that as the

heating rates increased, the characteristic hemicelluloses shoulder present at low heating rates merged with the larger cellulose peak to form a single, wider peak. Similar findings have been reported by various authors (Aboyade *et al.*, 2011; Poletto *et al.*, 2011; Vasile *et al.*, 2009)

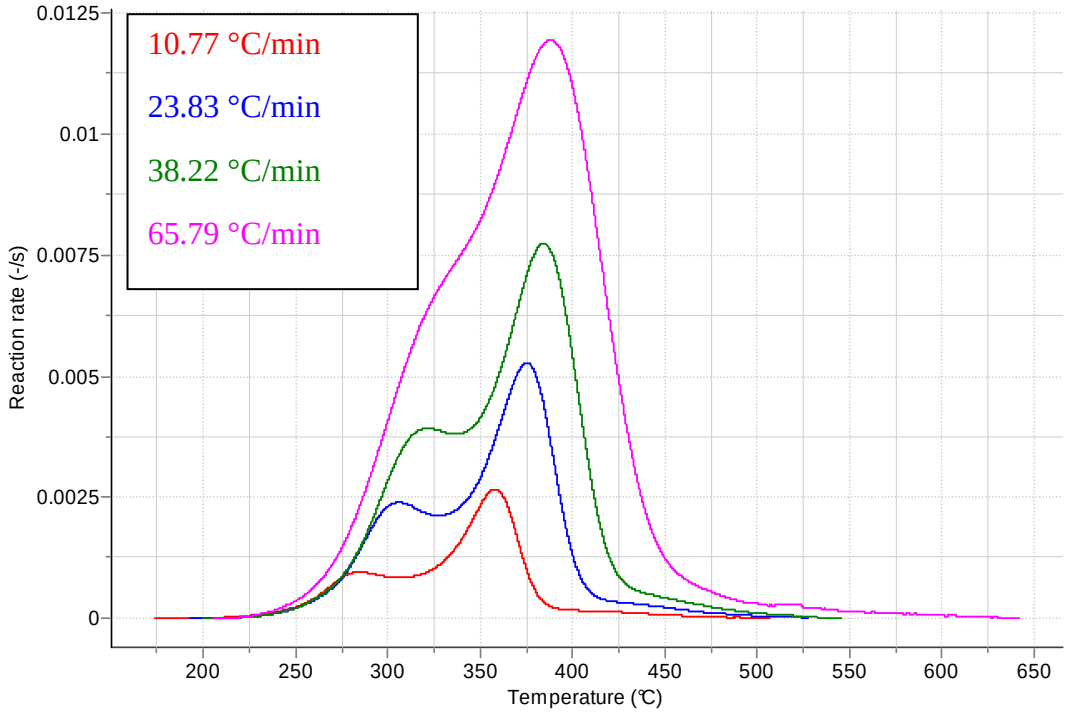

Figure 4-11: Normalised DTG curve for virgin *E.grandis*

Table 4-6: Char yields for the thermo-gravimetric analysis of virgin *E.grandis*

Heating rate set point [°C/min]	**Measured heating rate [°C/min]**	**Temperature at maximum rate [°C]**	***E.grandis* Char yield at 850 °C [wt. %]**
10	10.77	358.2	20.5 (± 0.3)
20	23.83	375.1	19.6 (± 0.1)
30	38.22	384.7	19.6 (± 0.9)
50	65.97	356.6	18.9 (± 1.5)

Raveendran and Ganesh, (1996) reported the specific char yields of commercial cellulose, xylan and lignin to be 11.1, 20.7 and 41.7 wt. % respectively using a high heating rate set point of 50 °C/min in a packed bed reactor, while Orfão *et al.*, (1999) reported char yields of 5.1, 20.5 and 38.4 wt. % for commercial cellulose, xylan and lignin respectively using TGA and a heating rate of 5 °C/min. In both instances the analyses were conducted under inert

atmosphere. Similar findings have been reported by Raveendran *et al.*, (1996), where the specific char yield from the thermo-gravimetric analysis of commercially acquired xylan and hemicelluloses were found to be 30.0 and 32.0 wt. % respectively, while the char yield of acid lignin was found to be 47.0 wt. % at a heating rate set point of 50 °C/min. The values reported in this study (**Table 4-3**, **Table 4-4** and **Table 4-5**) were found to be comparable for lignin, but not for the cellulose and hemicellulose fractions at a heating rate set point of 50 °C/min. It is however important to remember that factors such as crystallinity and the degree of polymerisation in the cellulose structure can affect the thermal behaviour of the species, which might be the reason for the deviation observed from the much lower literature values reported for commercial cellulose (Raveendran *et al.*, 1996). It should also be noted that the values reported for this study were based on the chemically extracted lignocellulosic compounds of *E.grandis* and were not sourced from the commercial market as with the abovementioned literature results.

4.2.4 Determination of reaction kinetic constants for the thermal degradation on E.grandis and its extracted lignocellulosic components

As mentioned in the literature chapter of this thesis (Section **2.3**), Friedman's and Ozawa plots were used in the determination of the activation energy (E_a) and pre-exponential constant (A) for the thermal degradation reactions for *E.grandis* and its lignocellulosic components. The following subsections will discuss the results of the kinetic constant determination for each of the lignocellulosic components extracted from *E.grandis*, as well as that of the virgin biomass.

4.2.4.1 Lignin

Figure 4-12 and **Figure 4-13** show the Friedman's and Ozawa plots for Klason lignin, as determined by AKTS Thermokinetics software. The tie-lines shown in **Figure 4-12** was found to have varying slopes and uneven spacing which was translated in the Ozawa plot as an apparent activation energy that varied significantly with conversion as shown in **Figure 4-13**. From **Figure 4-13** it was also evident that the correlation coefficient deteriorated above a conversion factor of 0.4 and could not be restored to satisfactory values (of – 0.95 or less) at higher conversions. According to Vyazovkin *et al.*, (2011) a significant variation in the

apparent activation energy with conversion is typically an indication of a multi-step reaction taking place rather than a single step reaction where the activation energy typically remains constant across the conversion range investigated (0.1 to 0.9). It may therefore be postulated that the thermal degradation of lignin does not occur in a single step and that other, possibly condensation reactions, were taking place on the char interface. It is also known that the thermal degradation of lignin and the formation of char are exothermic reactions (Di Blasi C., 2008) which might help explain the decrease in the apparent global activation energy with conversion.

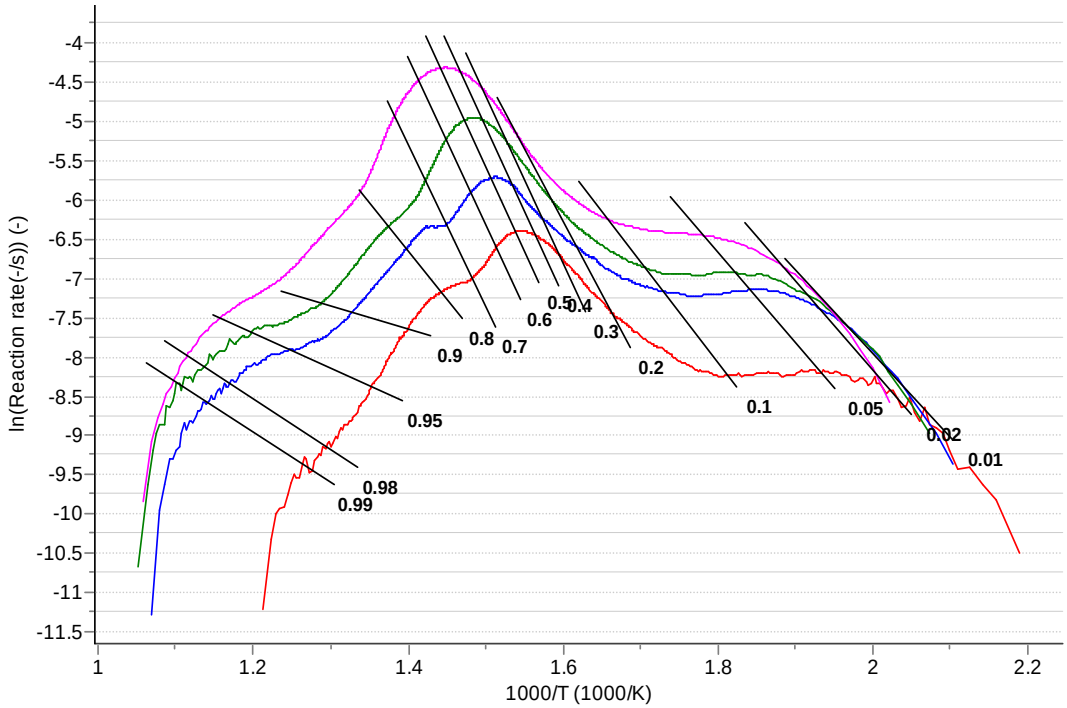

Figure 4-12: Friedman's plot for Klason lignin extracted from *E.grandis*

The average, minimum and maximum values of the activation coefficient, pre-exponential constant and correlation coefficient for Klason lignin are given in **Table 4-7** for the interval 0.1 to 0.9 conversion factor.

Table 4-7: Kinetic constants for Klason lignin extracted from *E.grandis*.

	Activation Energy	**Pre-exponential constant**	**Correlation coefficient**
	[kJ/mol]	**[s^{-1}]**	**[-]**
Average	117.02	15.14	-0.72
Minimum	0	26.53	-1.0
Maximum	176.43	-7.68	0.0

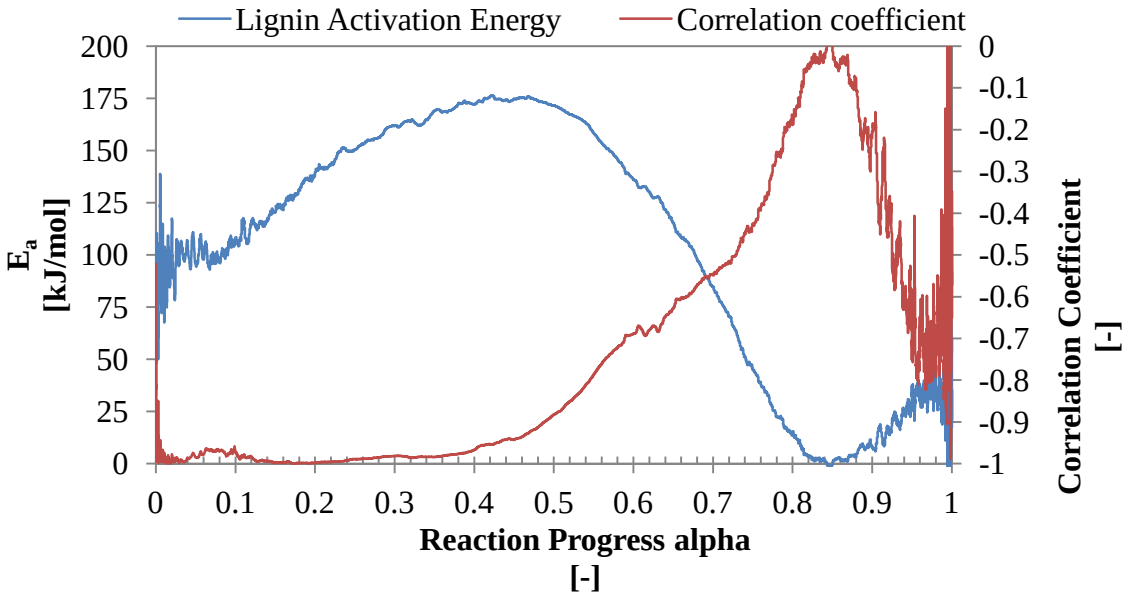

Figure 4-13: Ozawa plot for Klason lignin extracted from *E.grandis*

4.2.4.2 Alpha-cellulose

Figure 4-14 and **Figure 4-15** show the Friedman's and Ozawa plots for alpha-cellulose, as determined by AKTS Thermokinetics software. Unlike the result shown for the lignin sample, the isoconversional tie-lines for the alpha-cellulose sample were found to be more parallel. From **Figure 4-15** it was evident that the activation energy for alpha-cellulose remained fairly flat between 0.1 and 0.9 conversion factor and that a good correlation to the data was maintained for alpha-cellulose up to the 0.8 conversion factor mark before it started deteriorating. These observations were expected as the structure for alpha-cellulose is uniform and linear in nature, unlike that of hemicelluloses and lignin which are known to have a branched structure containing heterogeneous monomers.

The average, minimum and maximum values of the activation coefficient, pre-exponential constant and correlation coefficient for alpha-cellulose are given in **Table 4-8** for the reaction progress interval of 0.1 to 0.9

.

Table 4-8: Kinetic constants for alpha-cellulose extracted from *E.grandis*.

	Activation Energy [kJ/mol]	Pre-exponential constant [s^{-1}]	Correlation coefficient [-]
Average	142.22	22.43	- 0.98
Minimum	135.99	20.36	- 0.99
Maximum	170.80	25.54	- 0.71

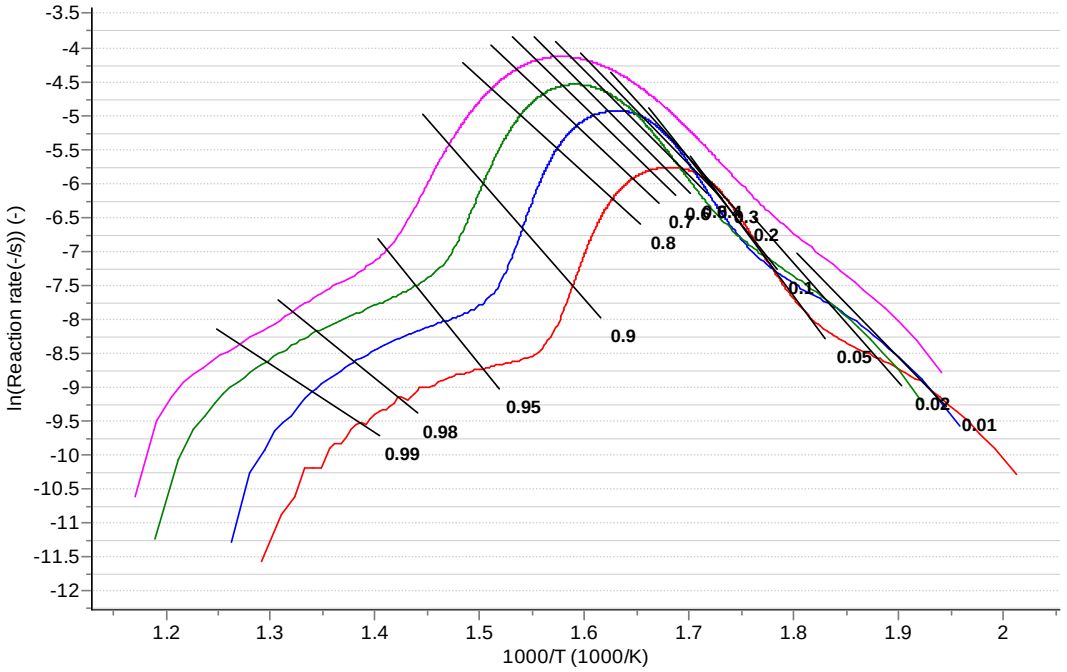

Figure 4-14: Friedman's plot for alpha-cellulose extracted from *E.grandis*

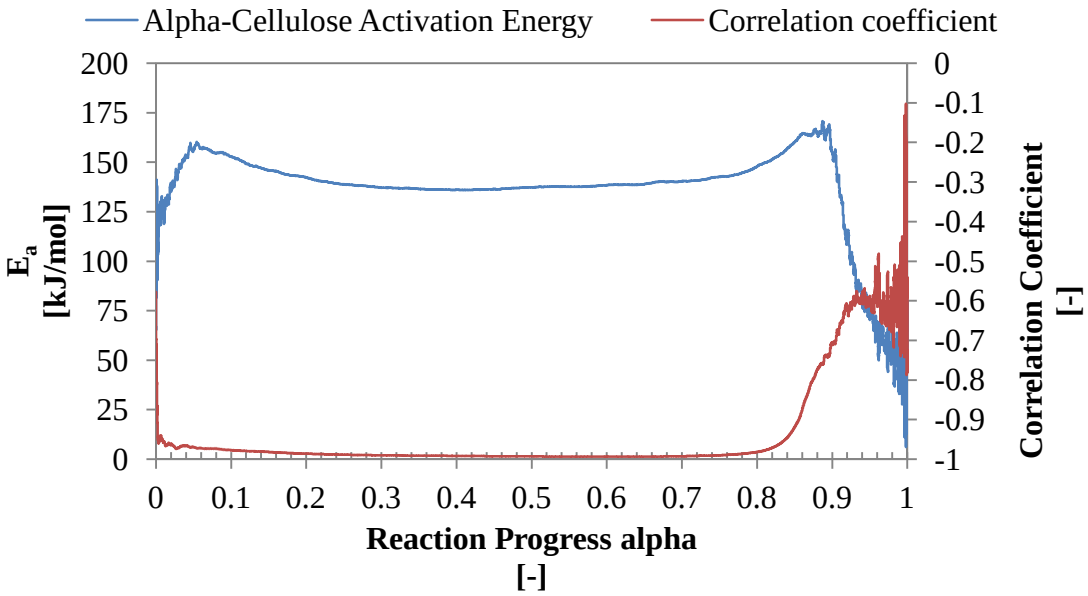

Figure 4-15: Ozawa plot for alpha-cellulose extracted from *E.grandis*

4.2.4.3 Holocellulose

Figure 4-16 and **Figure 4-17** show the Friedman's and Ozawa plots for holocellulose, as determined by AKTS Thermokinetics software. It was observed that the holocellulose sample exhibited more variation in the perceived activation energy with conversion compared to the alpha-cellulose sample. The activation energy was found to exhibit an upward trend for a conversion factor of 0.1 to 0.4, followed by a downward trend to 0.7 and then a final upward trend toward 0.9. Even though the Ozawa plot showed variation in the curve, it was observed that the correlation coefficient was under -0.9 for the entire range of conversion from 0.1 to 0.9. This deviation from the alpha-cellulose result (**Figure 4-15**) may therefore be attributed to the added effects of the hemicellulose content of the sample. The postulate that the hemicelluloses fraction in holocellulose increased the apparent activation energy observed for the holocellulose sample can then also help to explain the lower characteristic temperatures observed for alpha-cellulose sample (compared to the holocellulose sample) as was previously shown in **Table 4-4** and **Table 4-5.** With the hemicelluloses fraction present in holocellulose (32.4 wt. %), the overall activation energy of the sample is increased, and under similar temperature programs it would be expected that the holocellulose sample would start its thermal degradation at a slightly higher temperature (as observed in **Figure 4-7** and **Figure 4-9**) because more energy is needed to start the reaction.

The average, minimum and maximum values of the activation coefficient, pre-exponential constant and correlation coefficient for holocellulose are given in **Table 4-9** for the interval 0.1 to 0.9 conversion factor.

Table 4-9: Kinetic constants for holocellulose extracted from *E.grandis*.

	Activation Energy [kJ/mol]	**Pre-exponential constant [-]**	**Correlation coefficient [-]**
Average	187.36	31.72	-0.97
Minimum	160.83	28.18	-0.98
Maximum	219.93	35.32	-0.80

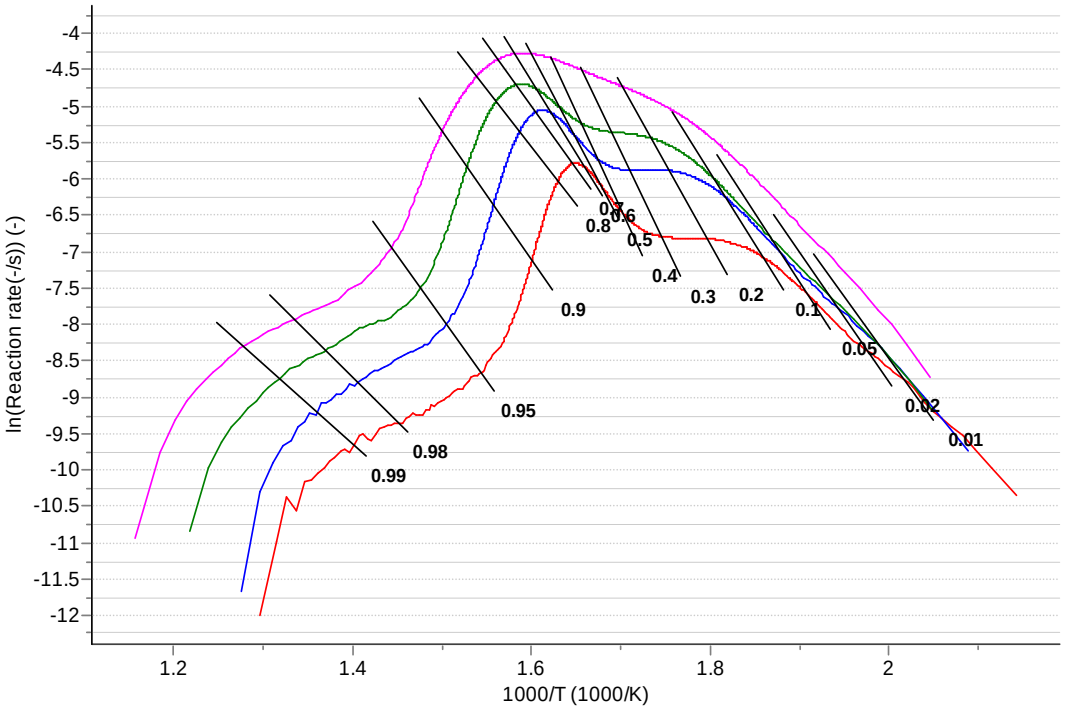

Figure 4-16: Friedman's plot for holocellulose extracted from *E.grandis*

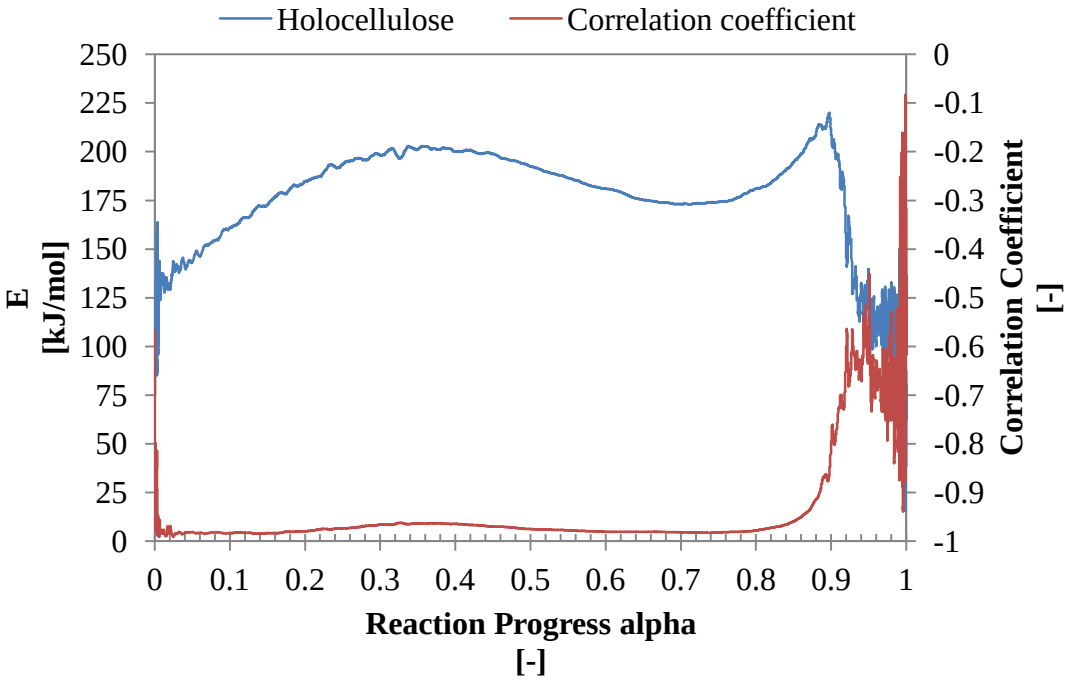

Figure 4-17: Ozawa plot for holocellulose extracted from *E.grandis*

4.2.4.4 E.grandis virgin biomass

Figure 4-18 and **Figure 4-19** show the Friedman's and Ozawa plots for *E.grandis*, as determined by AKTS Thermokinetics software. The Ozawa plot for *E.grandis* (**Figure 4-19**) was found to be very similar in nature to that of the holocellulose sample (**Figure 4-17**), showing first an increasing, then decreasing, and finally an increasing trend in the activation energy with increasing conversion factor from 0.1 to 0.9.

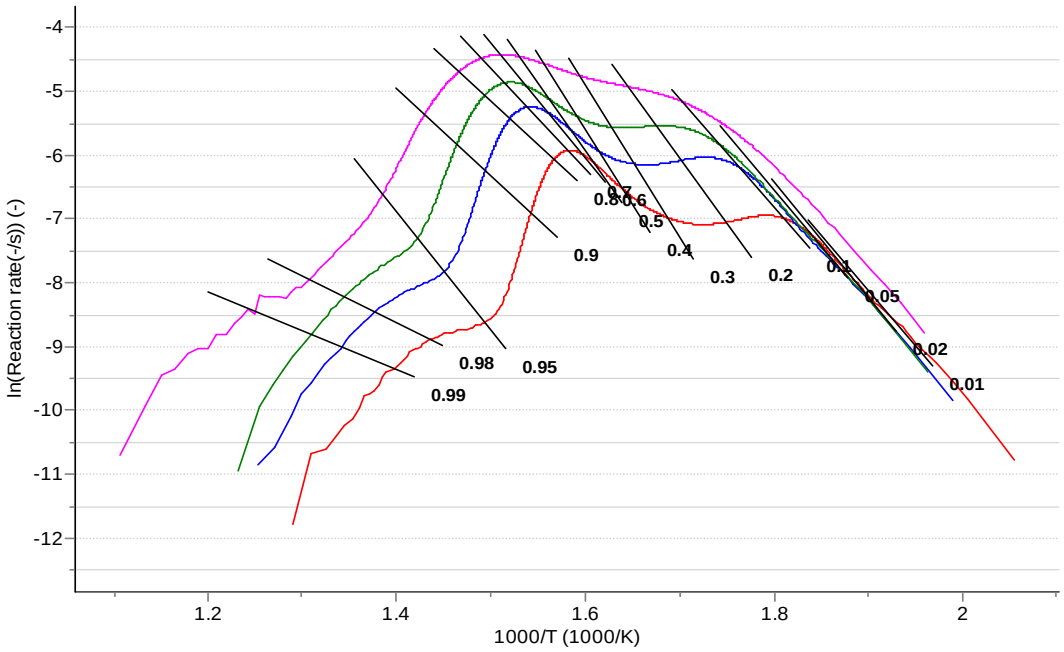

Figure 4-18: Friedman's plot for virgin *E.grandis*

Both graphs started at approximately 135 kJ/mol and increased to a local maximum of approximately 190 kJ/mol before decreasing again. It was observed that the holocellulose sample reached the local maximum at 0.35 conversion factor compared to the 0.30 of the *E.grandis* sample. A similar shift in the local minima was observed, but in the opposite direction. The holocellulose sample experienced a local minimum of 173 kJ/mol at 0.7 conversion factor, while the local minimum observed for the *E.grandis* sample was found to be 148 kJ/mol at 0.75 conversion factor. When considering the Ozawa plot of the lignin sample (**Figure 4-13**) it was evident that the lignin fraction contained in the biomass could have had a widening and lowering effect on the result shown for *E.grandis* in comparison to that of the holocellulose sample. This postulate will be discussed in more detail in section **0**. The average, minimum and maximum values of the activation coefficient, pre-exponential

constant and correlation coefficient for *E.grandis* are given in **Table 4-10** for the interval 0.1 to 0.9 conversion factor.

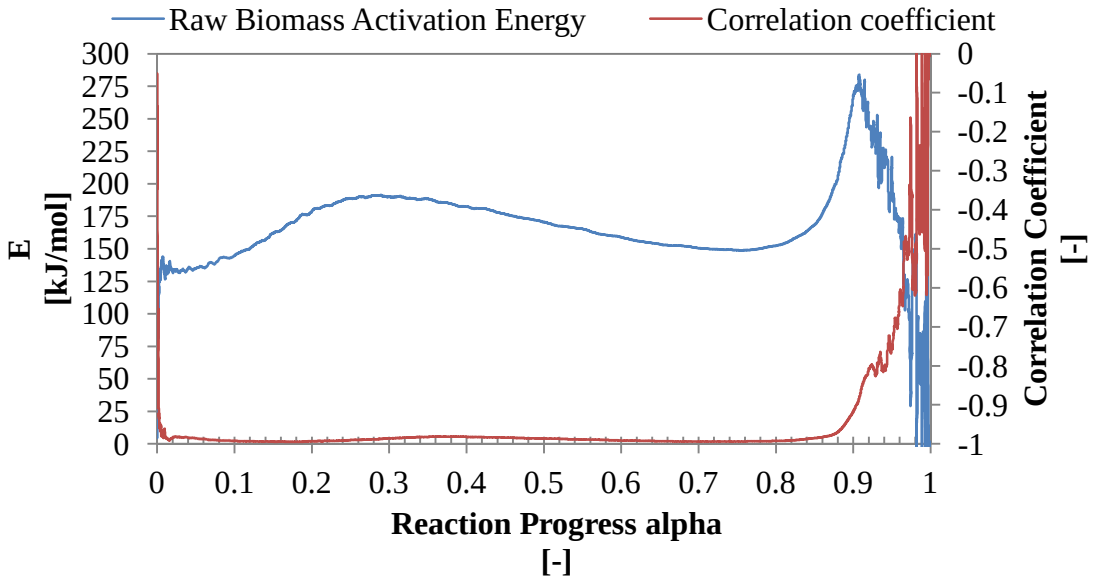

Figure 4-19: Ozawa plot for virgin *E.grandis*

.**Table 4-10:** Kinetic constants for virgin *E.grandis*.

	Activation Energy [kJ/mol]	**Pre-exponential constant [-]**	**Correlation coefficient [-]**
Average	170.30	26.94	-0.99
Minimum	144.68	21.95	-0.99
Maximum	268.31	40.67	-0.92

4.2.4.5 Comparison of average kinetic parametes

The kinetic parameters as calculated from the respective Friedman's plots discussed above for the entire range on conversion factors (0 to 1) are shown in **Table 4-11**. In an attempt to predict the activation energy of the whole biomass using the data of the individual lignocellulosic components investigated, it was required to deconvolute the holocellulose and raw biomass curves into their respective lignocellulosic components. Using AKTS Thermokinetics software, the holocellulose curve was separated into individual alpha-cellulose and hemicelluloses peaks while the whole biomass was separated into alpha-

cellulose, hemicelluloses, lignin and extractives peaks. The sum of the individual deconvoluted peaks, representing each pseudo macro-component making up the original sample, would then represent the model predicted singular peak of the original sample. A summary of the obtained kinetic parameters for the extracted curves are shown in **Table 4-12**.

Table 4-11: Average kinetic parameters

	Activation energy [kJ/mol]	Ln(A) [s^{-1}]
Holocellulose	177.8	29.5
Alpha-cellulose	141	22.1
Klason Lignin	106.2	13.2
E.grandis	170.4	26.9

Table 4-12: Kinetic parameters obtained through holocellulose and raw biomass deconvolution

Sample – individual component	**Component mass fraction in sample**	**Activation Energy**	**ln (A)**
	wt. %	kJ/mol	s-1
Holocellulose - Hemicelluloses fraction	32.4	200.1	37
Holocellulose – Cellulose fraction	67.6	168.8	27.9
Virgin biomass – Extractives fraction	2.6	81.4	12.3
Virgin biomass – Hemicellulose fraction	27.6	119.4	19.5
Virgin biomass – Cellulose fraction	57.5	145.1	22.1
Virgin biomass - Lignin fraction	15.2	63.1	5.2

The data reported in **Table 4-12** were used to try and predict the average experimental values obtained for holocellulose and raw biomass respectively, as shown in **Table 4-11**, as the weighted sum of the respective activation energies after deconvolution, multiplied with the mass fraction of the respective component. Following this summative approach of the deconvoluted pseudo components, a predicted summative value of 178.95 kJ/mol was determined for the holocellulose based on its alpha-cellulose and hemicelluloses content versus an original model prediction of 177.8 kJ/mol for the holocellulose sample. Similarly the predicted summative value for the *E.grandis* sample was found to be 128.2 kJ/mol based on the contributions of the individual deconvoluted pseudo components versus an original model prediction of 170.4 kJ/mol for *E.grandis*. The results achieved for the holocellulose sample was found to be similar for both the summative approach as well as the original

model prediction for the holocellulose sample, with a standard deviation of 0.81 kJ/mol. The large deviation observed for the raw biomass, however, might be a direct result of the chemical extractions used to isolate the individual lignocellulosic compounds investigated.

The holocellulose sample could be predicted with good accuracy, casting the focus for the deviation upon the extractives and lignin fractions as route cause for the deviations. Both these compounds are known to be made up from a variety of complex chemical families such as terpenes and terpenoids, fats, waxes, fatty acids, alcohols and phenols in the case of the extractives, and phenylpropane units in the case of lignin (Chapter **2**), but based on the relative contributions of extractives and lignin in the raw biomass, it was safe to assume that the bulk of the deviation observed would be as a result of the Klason lignin sample as it contributed to approximately 15 wt. % of the total sample in comparison to the 2.6 wt. % of the extractives. Furthermore it should be remembered that the Klason lignin extraction method relies on the total hydrolysis of a sample using concentrated sulphuric acid to dissolve the entire biomass structure (section **3.2.3.3**), before diluting the acid solution and causing the lignin to re-condense from the solution and possibly changing the chemical structure of the lignin. These considerations might also explain the poor correlation coefficient observed for the Klason lignin fraction in section **4.2.4.1**. It is recommended that future TG and isoconversional analyses make use of both Klason lignin as well as lignin extracted using other techniques such as Organosolv lignin, or milled wood lignin to evaluate the effect that the extraction method might have on the thermal degradation behaviour of lignin (Fengel and Wegener, 2003).

4.3 Conclusion

The isoconversional method was used to investigate the thermal degradation kinetics of *E.grandis* and its main lignocellulosic components. All the experimental data were generated using a thermo-gravimetric analyser at the Karlsruhe institute of Technology in Germany. From the results obtained, the following conclusions may be drawn:

- The thermal degradation behaviour of *E.grandis* and its individually extracted lignocellulosic components were investigated using thermo-gravimetric analysis. The data obtained were used to determine the isoconversional kinetic constants for the

virgin biomass as well as the individual lignocellulosic components extracted from the biomass. These are novel contributions to the scientific field of woody biomass pyrolysis.

- Good repeatability was achieved although the observed experimental deviation was found to increase with increasing heating rates.
- The influence of biomass particle size was found to be negligible at 50 °C/min when considering the standard deviations in the characteristic temperatures and the perceived reaction rates, compared to duplicate runs of the raw biomass sample.
- Increasing the heating rate resulted in a shift of the respective normalised thermo-gravimetric (TG) and differential thermo-gravimetric (DTG) curves toward higher temperature ranges. Increasing the heating rate also increased the peak reaction rates observed for the respective samples investigated and deteriorated the resolution of the resulting curves.
- Lignin resulted in the largest specific char yield, followed by hemicelluloses (as determined by difference) and cellulose in lesser quantities respectively.
- Lignin was found to degrade across the largest temperature range, while alpha-cellulose had the narrowest degradation range at corresponding heating rates investigated.
- Good correlation (above 95 %) was found for all the components investigated (except for lignin) within a conversion factor range of 0.1 and 0.9, suggesting good model fit of the experimental data.
- The average activation energies calculated for the components investigated were 177.8, 141.0, 106.2 and 170.4 kJ/mol for holocellulose, alpha-cellulose, Klason lignin and *E.grandis*, respectively.
- The predicted activation energy for holocellulose corresponded well to the measured value using a summative approach of the component compositions and deconvoluted activation energies.
- The activation energy for *E.grandis* could not be predicted accurately by the deconvolution of its lignocellulosic components due to changes in the molecular structure of the Klason lignin component inherent to the extraction procedure.

5 Fast Pyrolysis

5.1 Introduction

Fast Pyrolysis is the rapid thermal degradation of biomass followed by immediate quenching of the product vapours to produce a high yield liquid product called bio-oil. Although many different types of reactor configurations are employed and presented in the literature (Bridgwater, 2011; Meier and Faix, 1999), the main focus falls upon Bubbling Fluidised Bed Reactors (BFBR) for their superior heat transfer and mass transfer capabilities and their relative ease of scaling-up (Bridgwater, 2003). Fast pyrolysis data can be found for various eucalyptus species (*E.globulus*, *E.globulus labill*, and *E.loxophelba*) and forestry wastes (branches, stumps, bark etc.), but almost no data is available for the Fast Pyrolysis of *E.grandis* (Garcìa-Pérez *et al.*, 2007;Garcia-Perez *et al.*, 2008; Oasmaa *et al.* 2010; Shen *et al.*, 2009). The Fast Pyrolysis data that are available for *E.grandis* are not easily comparable with other literature due to reactor configurations, the scale of the operations and the process parameters employed to generate the data as explained in **section 2.9**.

The purpose of this investigation is to generate valuable Fast Pyrolysis data for *E.grandis* relating to the product yields and properties (quality), and to compare the obtained Fast Pyrolysis data from 3 different Fast Pyrolysis reactor configurations used in this study. Fast Pyrolysis experiments were conducted at Stellenbosch University (South Africa) and at the Karlsruhe Institute of Technology (Germany). Furthermore, the analysis of the product phases was conducted at the respective institutions where pyrolysis experimental work was undertaken.

5.2 Biomass characterisation results

5.2.1 Biomass particle size distribution

The typical particle size distributions (for the two size ranges of biomass chosen for this investigation) are shown in **Figure 5-1** and **Figure 5-2** respectively. **Figure 5-1** gives the distribution of the biomass resulting from 2 mm sieve milling, while **Figure 5-2** gives the

distribution of particles (greater than 1000 µm) resulting from 4 mm sieve mill milling. It was found that separation of the biomass into suitable fractions for pyrolysis was very time consuming using a small shaker seeing that only ± 100g of biomass could be fractionated at a time.

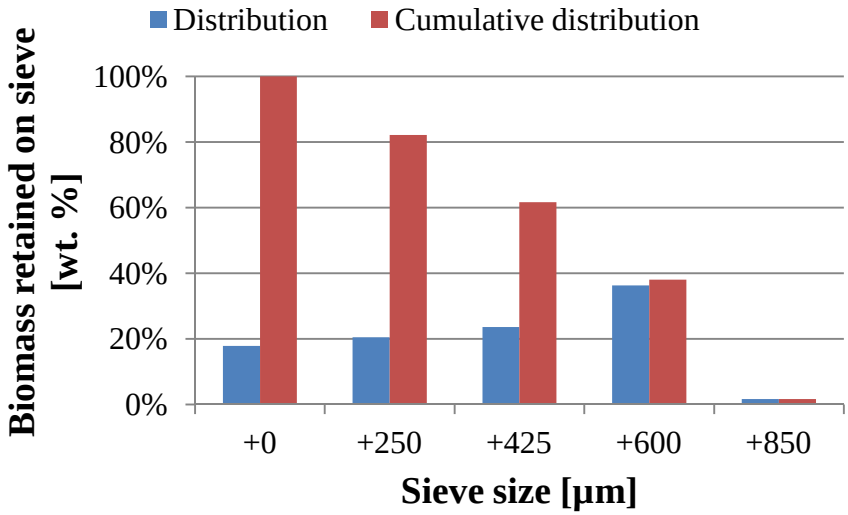

Figure 5-1: Biomass particle size distribution after 2 mm Retsch milling.

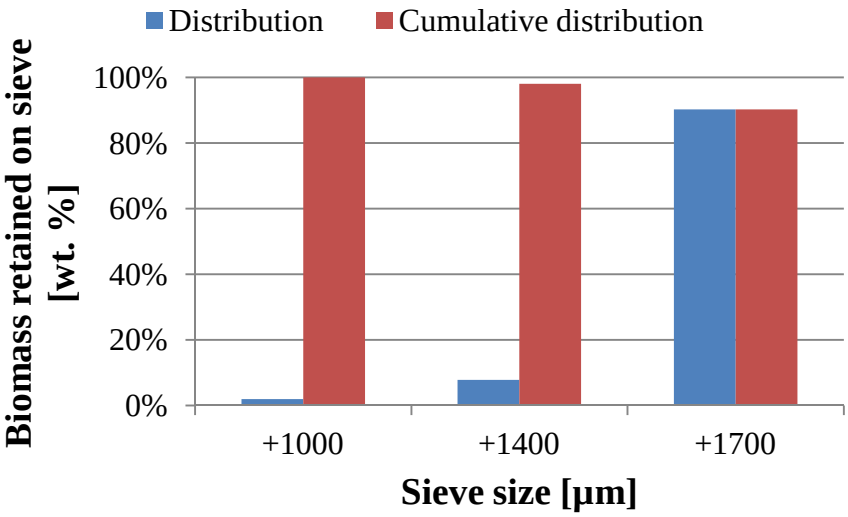

Figure 5-2: Biomass particle size distribution greater than 1000 µm after 4 mm Retsch milling.

Initial FP test runs revealed that feeding the biomass particle size distribution as shown in **Figure 5-1** resulted in downstream blockages of the condensation chain. The fines fraction (< 250 µm) was consequently removed for all subsequent experimental runs, resulting in the particle size distribution shown in **Figure 5-3**. From **Figure 5-1** it is evident that a

substantial portion of the original biomass (± 16 wt.%) was lost/removed as fines to the improve the operability of the FP plant. With the fines fraction removed, the weighted average particle sizes were found to be ± 570 µm for the 2 mm sieve milled particles and ± 1200 µm for the 4 mm sieve milled particle size range larger than 1000 µm.

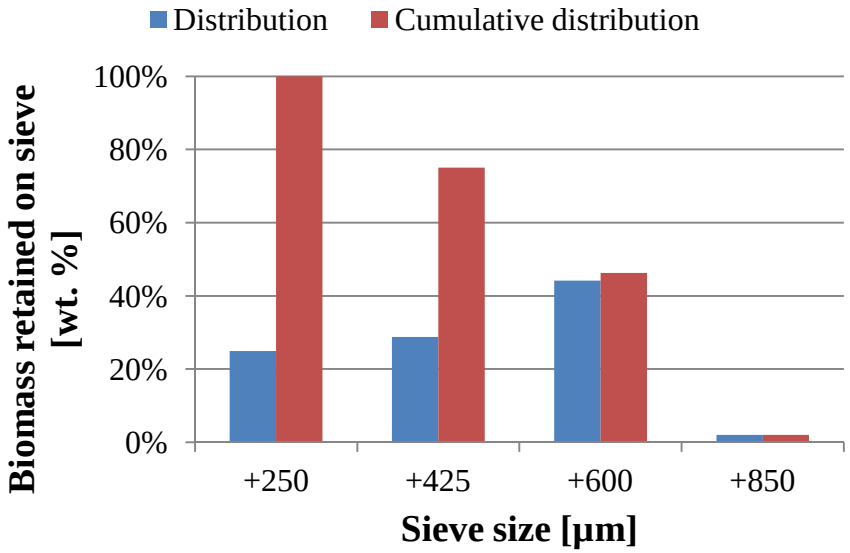

Figure 5-3: Particle size distribution of 2 mm Retsch milled biomass after removal of fines

5.2.2 Lignocellulosic composition

The lignocellulosic composition for the biomass is shown in **Table 5-1**. Subsamples were taken from batches 2 and 3 and analysed for extractives and lignin content at Stellenbosch University. As mentioned previously, the analysis of batches 2 and 3 were limited due to time constraints and only included moisture, ash, extractives and lignin content determination.

It was found that the first batch of biomass had a low lignin content compared to that of the other batches as well as that reported in literature (**Table 5-1**). Replication of the experiments confirmed the low lignin content for batch 1. Even when comparing the results from fellow students who had used the same batch of biomass for chemical analysis, it was evident that experimental error was not the cause in the low lignin content found. This deviation from the excepted norm of ± 25 wt. % (daf) could be explained after further enquiry by a fellow student (Vena, 2011). It was found that the results were plausible and within the bounds of the typical distribution of lignin content for E.*grandis* from that region,

albeit towards the lower percentile ranges (Vena, 2011). This might be a direct result of the sampling methods used for selecting batch 1 for this study.

Table 5-1: Lignocellulosic composition of *E.grandis*

	Unit	Batch 1	Batch 2	Batch 3	Oasmaa *et al.* (2010)
Moisture	**wt. %**	7.9 ± 0.3	6.4	3.9	7.6
Ash (at ± 550 °C)	**wt. % dry**	0.5 ± 0.1	0.3	0.5	0.4
Extractives	**wt. % daf**	2.6 ± 0.2	3.7 ± 0.2	4.1 ± 0.4	-
Lignin	**wt. % daf**	15.2 ± 1.5	25.0 ± 0.3	26.5 ± 2.0	± 27
Holocellulose	**wt. % daf**	85.1 ± 2.4	-	-	± 61[b]
α-cellulose	**wt. % daf**	57.5 ± 0.3	-	-	± 51
Hemicelluloses	**wt. % daf**	27.6[a]	-	-	± 10
Glucose	**wt. % daf**	37.5	-	-	-
Xylose	**wt. % daf**	11.5	-	-	-

[a] by difference; [b] sum of hemicelluloses and α-cellulose

It was further observed that poor closure and unsatisfactory repeatability resulted from the HPLC analysis to determine the carbohydrates concentrations. Furthermore it was found that the acid-soluble fraction of lignin was difficult to detect via UV spectroscopy and that this fraction was negligible compared to the acid insoluble Klason lignin. Consequently, holocellulose and alpha-cellulose extraction was conducted for comparative reasons following the methods described by Browning, 1967.

5.2.3 Proximate analysis

An example of the typical thermogravimetric (TG) curves produced for raw E.grandis is given in **Figure 5-4**, while a summary of the proximate analysis results for the different heating rates investigated are shown in **Table 5-2.** Please refer to **Figure 9-1** of Appendix **9.1**for the TGA curves of *E.grandis* at various heating rates used to determine the proximate analyses. The ash content was regrettably not determined for each thermo-gravimetric analysis and is consequently not shown explicitly here, but formed part of the reported char residue. From **Table 5-1**, however, it can be seen that the typical ash content for this biomass was in the region of 0.5 wt. % on a dry basis. The TG curves for the other heating rates are not shown here but followed the same trend. Good repeatability was observed for the results shown in **Table 5-2**, with standard deviations below 1 wt. % for duplicate analyses. Only the

analysis conducted at 50 °C/min resulted in a higher standard deviation of 1.6 wt. % for the final fixed carbon content (data not shown).

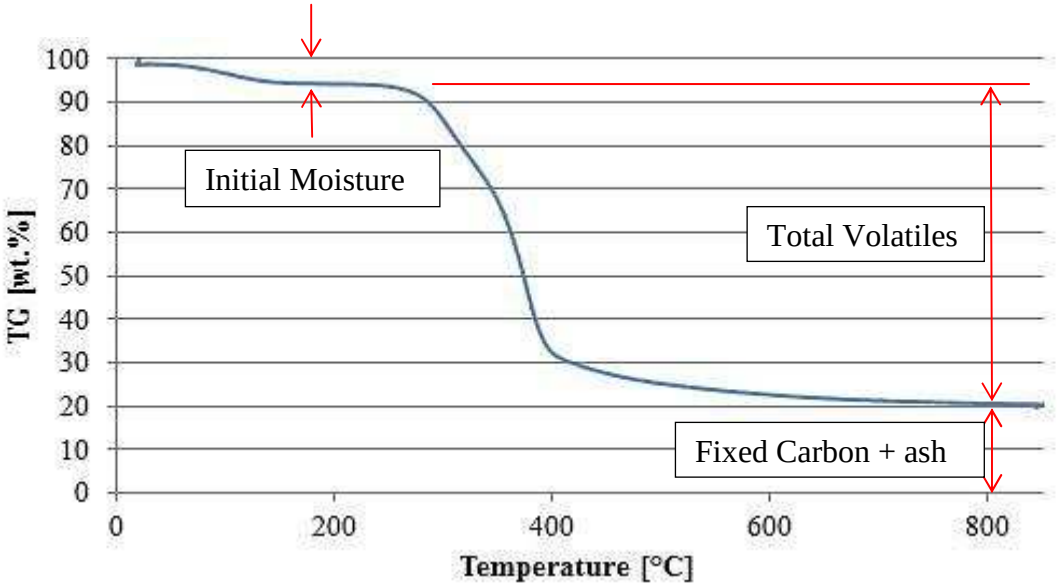

Figure 5-4: Thermo gravimetric curve at 20 °C/min

Table 5-2: Proximate analysis of *E.grandis*

	Unit	Heating rate [°C/min]			
		10	**20**	**30**	**50**
Moisture content	**wt. %**	6.0 ± 0.4	5.8 ± 0.1	5.5 ± 0.8	6.2 ± 0.2
Organic volatiles	**wt. %**	73.2 ± 0.2	74.4 ± 0.1	74.8 ± 1.0	74.7 ± 1.6
Total volatiles	**wt. %**	79.3 ± 0.6	80.2 ± 0.2	80.3 ± 1.8	80.9 ± 1.8
Fixed carbon + ash	**wt. %**	20.8 ± 0.2	19.8 ± 0.1	19.8 ± 1.0	19.1 ± 1.6

The observed fixed carbon content decreased slightly with an increase in the heating rate, which was expected when considering the work done by Guerrero *et al.*, (2008a). They reported a decrease in the char yield when comparing chars produced at low and high heating rates. At 800 °C the char yield for *E.globulus labill* was 21.8 and 18.5 wt. % for the low and high heating rate experiments respectively, and under TGA conditions the fixed carbon was calculated as 16.38 wt. % using a heating rate of 10 °C/min Guerrero *et al.*, (2008a).

5.2.4 Ultimate analysis of *E.grandis*

The elemental composition of *E.grandis* is shown in **Table 5-3** below. The results agree well with that of reported literature and small deviations may be explained by the slight variation found in the lignocellulosic compositions of the literature values and that of this study as previously shown in **Table 5-1**.

Table 5-3: Ultimate analysis of E.*grandis*

	Unit	**Batch 1**	**Batch 3**	**Oasmaa *et al.* (2010)**
C	wt. % dry	45.05	48.2	50.10
H	wt. % dry	4.24	6.20	6.00
N	wt. % dry	0.30	< 0.50	0.10
S	wt. % dry	-	< 1.00	-
O [a]	wt. % dry	50.43	44.10	44.00
C/O	-	0.89	1.09	1.13

[a] by difference

As discussed in **Chapter 2.1**, the building blocks that make up cellulose and hemicelluloses are typically cyclical sugars units with 6 carbon atoms per monomer, while lignin is typically made up of phenylpropane units which can have between 9 and 11 carbon atoms in the monomer. Similarly, the typical 6 carbon sugar will have at least 6 oxygen atoms per molecule, while the phenylpropane units will have at least 2 to 5 oxygen atoms per molecule. The ratio of carbon to oxygen can therefore be demonstrated to be higher for phenylpropane units compared to 6 carbon sugars. A higher lignin content of a specific biomass will then result in a higher carbon and lower oxygen content in the ultimate analysis of a specific biomass, and vice versa. This observation can then be used to explain the increased carbon and decreased oxygen content of runs 2 and 3 with higher lignin contents, compared to that or run 1 as shown in **Table 5-3**.

5.2.5 Higher heating value (HHV) of *E.grandis*

Table 5-4 shows the calculated and measured values (using the Channiwala correlation and a bomb calorimeter respectively) for the biomass on a dry basis. As can be seen from **Table 5-4**, the Channiwala correlation was very accurate in predicting the calorific values of the biomass used for the KIT biomass (batch 3) as well as the biomass used in the study by Oasmaa et al., (2010). The results are not so close to the measured value when considering

the SA biomass (batch 1). The poor correlation found between the predicted and measured calorific values for batch 1 can be explained by the high oxygen content of batch 1 as result of the lower than normal lignin content of the specific bath of biomass. It was found that the oxygen content of batch 1 fell outside limits of the correlation, stating a maximum allowable oxygen content of 50 wt. % (Channiwala and Parikh, 2002).

Table 5-4: Calorific values of E.*grandis*

	Moisture content [wt. %]	**Measured** [MJ/kg]	**Moisture correction** [MJ/kg]	**Theoretical (Channiwala)** [MJ/kg]
SA – batch 1	8.0	19.63	21.34	15.55
KIT – batch 3	26.5	14.29	19.44	19.59
Oasmaa *et al.*(2010)	dry	19.90	19.90	20.00

5.2.6 The influence of temperature on ash content determination

The results from the ash content determination conducted at KIT are shown in **Table 5-5**. From the results given in **Table 5-5** it was evident that the relative contribution of the overall ash content of biomass changed depending on the ashing temperature. At ashing temperatures higher than 550 °C it was observed that the total measured ash content reduced as some of the inorganics was entrained or burned off. At similar temperatures it was found that the ash content of the biomass was constant for all three batches considered and corresponds to literature values. When considering the temperatures typically employed in pyrolysis (± 500 °C), it can be seen from these results that the ash fraction of the biomass would remain in the char product, and that ash carryover into the vapour phase would be unlikely.

Table 5-5: Biomass ash content from KIT

Furnace temperature [°C]	**Ash content [wt. % dry]**
550	0.5
815	0.3
1000	0.3

5.3 Fast Pyrolysis results and discusion

5.3.1 Fast Pyrolysis conducted at Stellenbosch University

5.3.1.1 Product yields and ANOVA

A breakdown of the experimental runs conducted, and the respective yields obtained using the $SU_{1\ kg/h}$ FP plant (1 kg/h bubbling fluidised bed reactor at Stellenbosch University), are given in **Table 5-6**. In total 16 experimental runs were conducted using the $SU_{1\ kg/h}$ FP plant of which 4 runs (runs 1-4) were discarded. The discarded runs were a direct result of blockages in the equipment piping caused by the fines fraction of the biomass which resulting in dis-continuous plant operation and plant instability. Please refer to Appendix **9.2** for all the ANOVA tables associated with this chapter. Due to the constraints of the experimental design (Section **3.5.1.1**), run 0, 10 and 14 (denoted by the superscript 'b' in **Table 5-6**), were excluded from the ANOVA as these runs were performed at reactor temperatures other than those specified in the statistical analysis

Table 5-6: Overall product yields achieved with the $SU_{1\ kg/h}$ plant

Run	Reactor Temp.	Average Particle Size	Bio-Oil Yield	Char Yield	Gas Yield [a]
#	°C	µm	wt. % daf	wt. % daf	wt. % daf
12	440	570 [batch 2]	76.1	10.7	13.3
8	470	570 [batch 1]	68.7 ± 0.1	11.5 ± 1.4	19.8 ± 1.3
9	470	570 [batch 1]	68.9 ± 0.1	9.4 ± 1.4	21.7 ± 1.3
15	470	570 [batch 2]	76.3 ± 2.0	12.0 ± 1.7	11.7 ± 3.7
14 [b]	480	570 [batch 2]	73.5 ± 2.0	9.6 ± 1.7	17.0 ± 3.7
0 [b]	500	570 [batch 1]	68.1[c] ± 0.1	11.0 ± 0.4	20.9 ± 0.3
10 [b]	500	570 [batch 1]	68.2 ± 0.1	10.5 ± 0.4	21.3 ± 0.3
5	530	570 [batch 1]	63.5 ± 1.6	8.2 ± 0.3	28.4 ±1.9
6	530	570 [batch 1]	65.8 ± 1.6	8.6 ± 0.3	25.6 ± 1.9
11	440	1200 [batch 2]	70.4	14.4	15.2
13	470	1200 [batch 2]	73.0	10.0	17.0
7	530	1200 [batch 1]	56.0	9.0	35.0

[a] By difference; [b] Omitted from ANOVA; [c] Estimated

Furthermore, the tarry phase contribution typically recovered through acetone washing, was lost for run 0 before the mass could be calculated, which resulted in the under estimation of the liquid yield for run 0. The total bio-oil yield for run 0 was therefore compensated using the average contribution of the tarry phase yielded for run 10, 14 and 15 (5.95 wt. % daf) and then reported in **Table 5-6**. As indicated in **Table 5-6**, this estimated result was not used in the statistical analysis which followed, but only served as an indication of repeatability.

Good repeatability was observed throughout, with standard deviations of less than 2 % for bio-oil and char produced at similar operating conditions and with the same batch of biomass. It was noted, however, that the total bio-oil yields resulting from batch 2 were higher than that of run 0 and 10 obtained using batch 1, while the char yield remained very similar. The second batch of biomass had a slightly different chemical composition to that of the first, with a higher lignin content (25 wt. % daf compared to 15 wt. % daf) and higher initial moisture content (approximately 3 wt. % higher than batch 1) as mentioned earlier in sections 3.2.1 and 3.4.2. Experimental runs 11 – 15 were performed using batch 2, as indicated in **Table 5-6**, while all the other runs were performed using batch 1.

Closer investigation revealed that the apparent increase in overall bio-oil yield for batch 2 was primarily related to an increase in the water content of the bio-oil and to a lesser extent related to the increase in the organic fraction of the bio-oil. These findings will be discussed in section **5.4.2.2**.

Liquid product

The liquid product yielded was dark brown/black in colour with a strong pungent smell. The liquid product contained no visible solids and was free flowing at room temperature. Furthermore it was found that invisible aerosols/vapours were released when decanting the fluid into sample bottles after each experimental run, which resulted in irritation of the eyes (burning) and subsequent tearing. This might be ascribed to the known acidic nature of pyrolysis oils (Bridgwater, 2003**)**.

Figure 5-5 shows the typical trend observed for the acetone evaporation for determining the tarry phase yield for each run. A distinct change in slope was observed in the curve after a period of 4 to 5 days, changing from a polynomial to a linear trend. This sudden decrease in evaporation rate was assumed, in this investigation, as the point where the acetone had evaporated, yielding a predominantly acetone free tarry phase. This point typically

corresponded to a relative change in the sample weight of 5-8 % between two consecutive measurements. The tarry phase was dark in colour with a viscous toffee-like consistency.

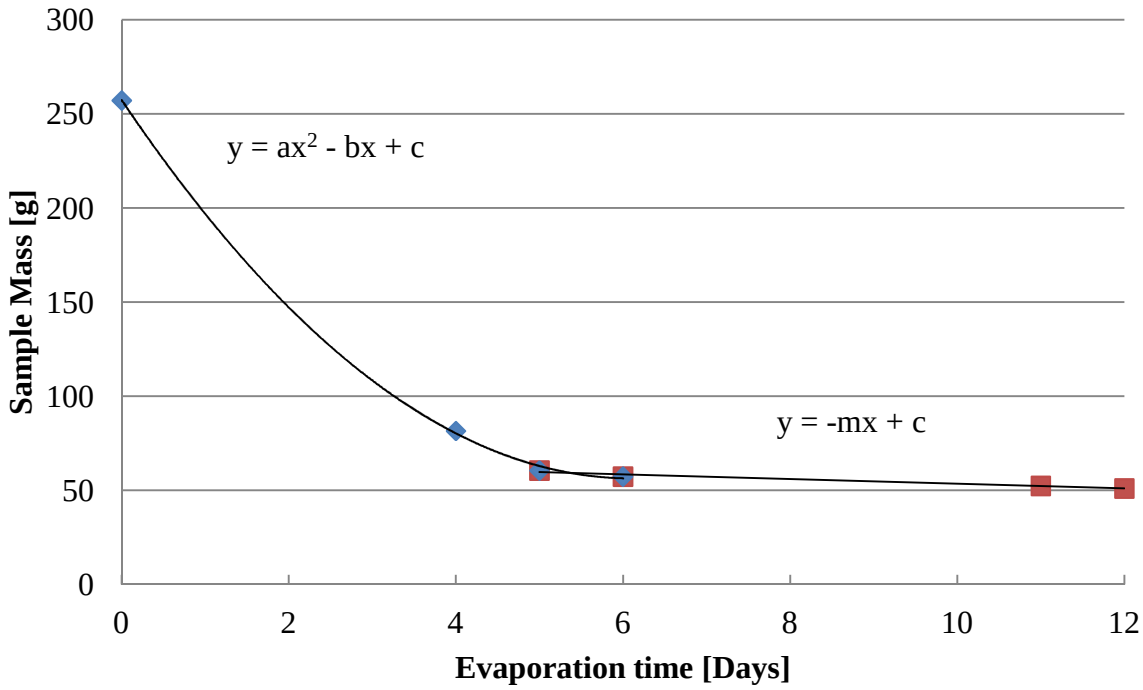

Figure 5-5: Acetone wash evaporation curve

It was found that although the typical trend of the acetone evaporation curves was similar (second order polynomial followed by a linear trend) for all the individual runs, the duration of the polynomial section varied from sample to sample (data not shown). This deviation might be explained by factors such as variations in ambient conditions due to weather changes, variations in the actual composition of the respective tarry phases, the volume of acetone required for washing and the variation in the exposed surface area of the acetone wash as different sizes of the glass beakers used to evaporate the acetone wash. The fitted surface plots for the overall liquid product yield is shown in **Figure 5-6** on dry and ash free basis of the biomass fed.

The ANOVA revealed that the reactor temperature had a significant effect on the total liquid yield at a confidence level of 95 %, but that no strong conclusions could be drawn for the effects of the particle size at the same confidence interval (**Table 9-1**). From the fitted surface plot (**Figure 5-6**) it is evident that higher liquid yield was favoured toward the lower temperatures chosen for this investigation. The component of interest in bio-oil, however, is the organic fraction which typically makes out the largest percentage of the liquid yield and gives rise to the fuel properties of bio-oil. The evolution of the organic fraction of the bio-oil

is shown in **Figure 5-7**. The ANOVA revealed that here too that the reactor temperature had a significant influence on the measured value at a 95 % confidence interval (**Table 9-2**). Similar to the findings for the total liquid yield in **Figure 5-6**, no strong conclusions could be drawn for the effects of the particle size at a 95 % confidence interval. When evaluating the p-value obtained from the ANOVA, however, it could be concluded that the particle size had a significant influence on the organic/tarry phase yield at a 90 % confidence interval (**Table 9-2**). The tarry phase yield was found to be favoured toward the lower range of reactor temperatures and the smaller particle size range investigated.

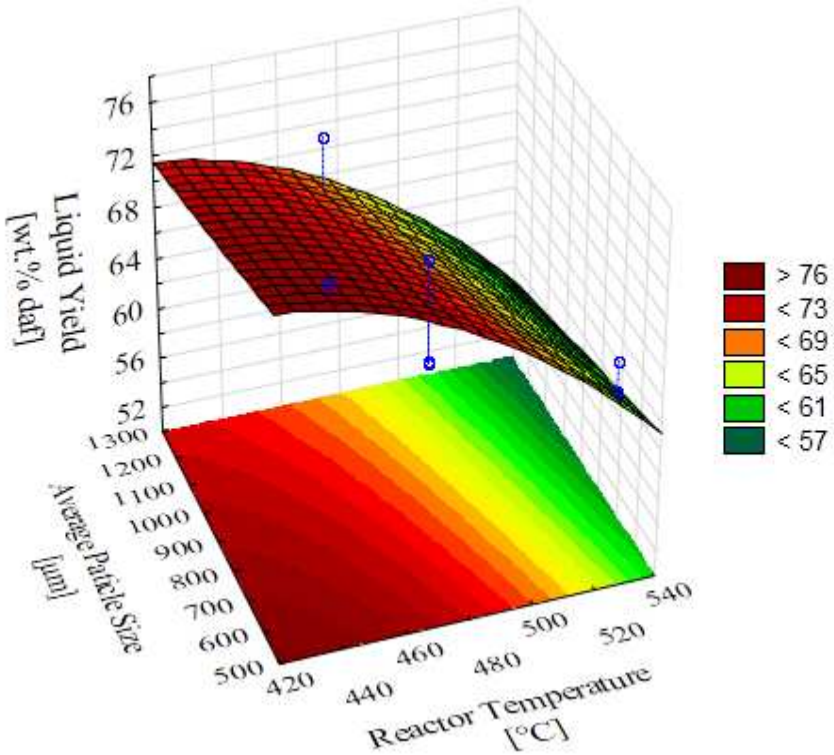

Figure 5-6: Evolution of Fast Pyrolysis bio-oil yield.

These observations are consistent with literature findings for the Fast Pyrolysis of other *eucalyptus* species (Garcia-Perez *et al.*, 2008; Kumar *et al.*, 2010; Shen *et al.*, 2009). It was found that the highest liquid yields for both the total bio-oil, as well as the organic fraction, were achieved at lower reactor temperatures (440 and 470 °C) as shown in **Figure 5-6** and **Figure 5-7** respectively. The bio-oil yields achieved in this study are comparable with the results achieved by Oasmaa et al., (2010) using debarked *E.grandis* on a 20 kg/h FP plant (70.8 wt. % mfb at 480-520 °C), but higher than those reported by Garcia-Perez et al., (2008) (54 – 63 wt. %) using oven-dry mallee eucalyptus on a 2 kg/h setup. Demirbaş, (2005) showed that the initial moisture content of the biomass used in pyrolysis has a direct

influence on the overall liquid (bio-oil) yield, mainly as a result of increased pyrolytic water formation. Using a batch type reactor, Demirbaş, (2005) showed that biomass with an initial moisture content of 12.8 %, compared to oven dry biomass, increased the overall liquid yield by ± 5 wt. % (on a dry basis) at 500 °C and a heating rate of 5 °C/s. These observations help explain the lower yields reported by Garcia-Perez *et al.*, (2008), as oven dry biomass was used in that study compared to the air dry biomass (± 7 wt. %) used both in this study and by Oasmaa *et al.*, (2010).

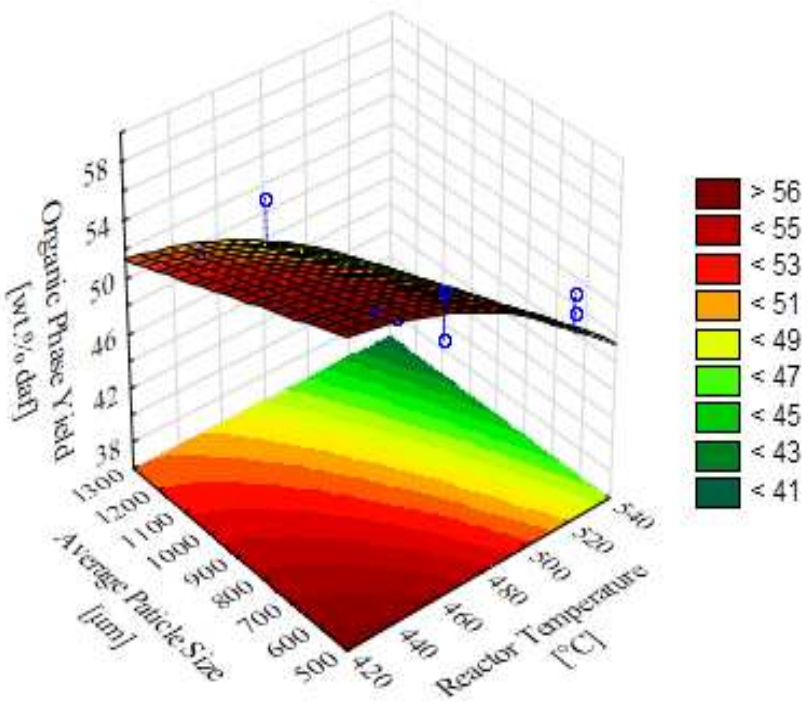

Figure 5-7: Evolution of Fast Pyrolysis bio-oil organic yield.

Solid product yield

It was found that in most instances the assumption of no sand entrainment as mentioned in section **3.5.1** held firm, but in the cases of runs 7, 11 and 12 it was found that small amounts of sand was entrained from the reactor into the char pots. The entrained sand was not visible to the naked eye when mixed with the char, but was noticeable as a white deposit (resembling the sand used in the reactor as heat transfer medium) in the crucible after determining the calorific value of the char using bomb calorimetry. No further analysis was conducted on the deposit to verify the material makeup due to time constraints and the limited occurrence of the deposit.

It was also found that for the larger biomass particles (in the range +1000 µm – 2000 µm) fed to the reactor the transport of the char from the reactor to the cyclones was impaired and that not all the char particles were successfully entrained from the reactor. From **Figure 5-8** it would appear that there is an apparent trend for more char to form at lower reactor temperatures, while the influence of the particle size seemed negligible. No strong statistical conclusions could be drawn at the 95 % confidence interval, but at a 90 % confidence interval it was clear that the reactor temperature had a significant influence on the overall char yield (**Table 9-3**).

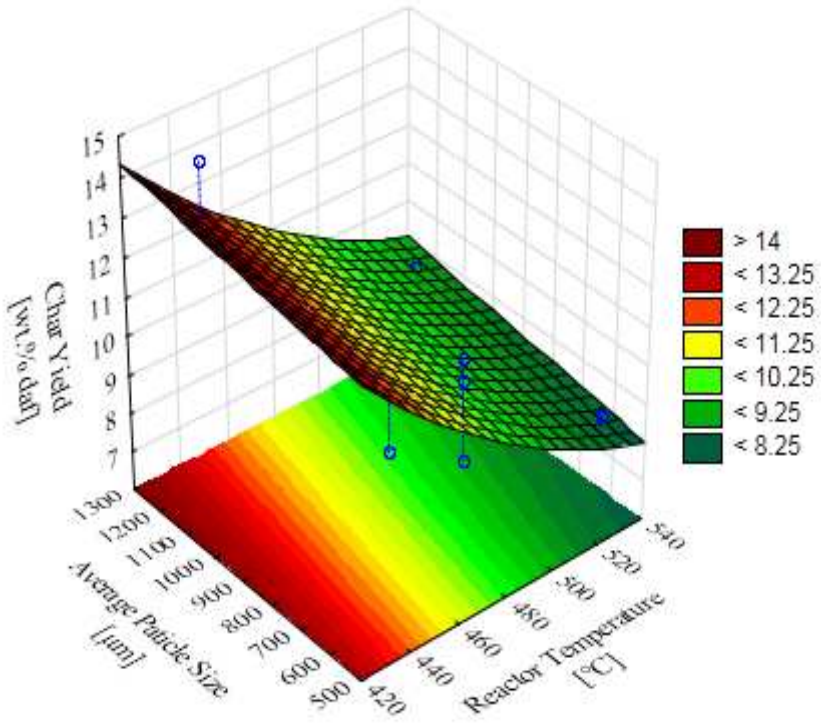

Figure 5-8: Evolution of Fast Pyrolysis char yield.

Gas product yield

The gas yield, as determined by difference, is shown in **Figure 5-9**. As the gas yield depends on the char and bio-oil yields, each with its own variance and intrinsic degree of error, **Figure 5-9** should only be used as an indication of the gas yield trend and not the true measured trend. Nevertheless, the ANOVA indicated that the reactor temperature had a significant influence on the gas yield at a 95 % confidence interval, while the particle size had not (**Table 9-4**). **Figure 5-9** indicates an apparent trend which is consistent with the findings of Bridgwater (2003), stating that the gas yield typically increases at higher reactor

temperatures. Even though the gas yields were determined by difference, it was found that the results were repeatable with standard deviations of less than 5 %, as indicated in **Table 5-6**.

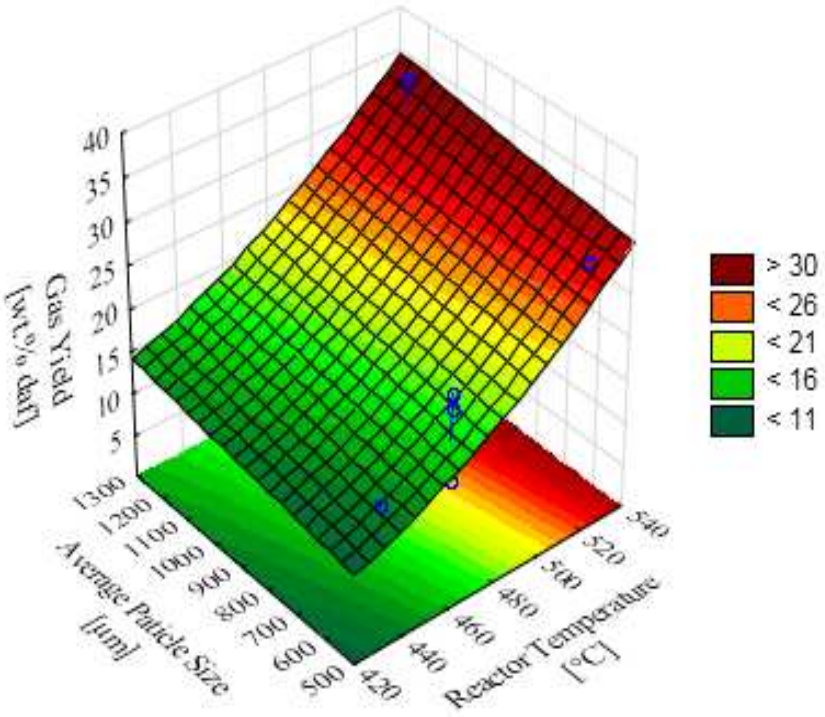

Figure 5-9: Surface plot fit and ANOVA table for gas yield.

5.3.1.2 Product quality

Water content and organic fraction

The water content of bio-oil refers to the total water fraction present in bio-oil which includes both the initial water content of the biomass used as pyrolysis feedstock, as well as the pyrolytic water which is formed as a product of pyrolysis. **Table 5-7** gives a breakdown of the bio-oil yield, with reference to the organic fraction, the pyrolytic water yield as well as biomass-derived water yield. All values are reported on a dry and ash free basis of the starting biomass used in each experimental run.

The influence of the reactor temperature and particle size on the pyrolytic water yield is given by the fitted surface plot shown in **Figure 5-10**. The surface plot showed a poor fit with an R-squared value of only 64.5 % and the ANOVA furthermore revealed no significant influences of the chosen process parameters on the pyrolytic water yield at a 95 % confidence interval (**Table 9-5**). It could however be shown that the reactor temperature had a

significant influence on the pyrolytic water yield at a confidence interval of 90 %, while the biomass particle size had not (**Table 9-5**).

Table 5-7: Bio-oil water content and pyrolytic water yield for the $SU_{1\ kg/h}$ plant

Run	Reactor Temp.	Average Particle Size	Bio-Oil Yield	Organics Yield	Pyrolytic water yield	Biomass derived water yield
#	°C	µm	wt. % daf	wt. % daf	wt. % daf	wt. % daf
12	440	570 [batch 2]	76.0	56.5	8.9	10.6
8	470	570	68.7	52.4	10.8	5.5
9	470	570	68.9	52.4	10.3	6.2
15	470	570 [batch 2]	76.3	55.6	8.4	12.3
14 [a]	480	570 [batch 2]	73.5	54.9	6.7	11.9
0 [a]	500	570	68.1 [b]	51.3	7.3	9.2
10 [a]	500	570	68.2	53.2	7.5	7.6
5	530	570	63.5	49.2	7.8	6.4
6	530	570	65.8	50.6	8.8	6.4
11	440	1200 [batch 2]	70.4	51.3	8.3	10.8
13	470	1200 [batch 2]	73.0	53.1	9.4	10.5
7	530	1200	56.0	39.6	9.8	6.6

[a] Omitted from ANOVA; [b] Estimated

Literature by Shen *et al.*, (2009) and Garcia-Perez *et al.*, (2008) suggest that a larger biomass particle size results in a slight increase in the pyrolytic water yield, but from the results generated in the ANOVA for this particular reactor configuration, it cannot be shown with statistical certainty. A possible reason for this uncertainty might be found when considering the different batches of biomass used in this investigation, with specific reference to the initial moisture content and lignin content of the biomass. It is known that variation in the initial moisture content of the feedstock can influence the total bio-oil yield as well as the pyrolytic water yield (Demirbaş, 2005). A further argument can be made for the differences in the lignin content of the different batches. In relative terms, batch 1, with the lower lignin content, would consequently have a higher holocellulose content than batch 2, which was found to have a higher lignin content. It has been suggested in literature (Azeez *et al.* 2010) that pyrolytic water is most commonly formed through the dehydration of polyoses, which is also in line with the understanding of the Waterloo-mechanism for the thermal degradation of

cellulose (Van de Velden *et al.*, 2010). Although there is merit in both arguments, it could not be observed with certainty for all the data points shown in **Table 5-7**.

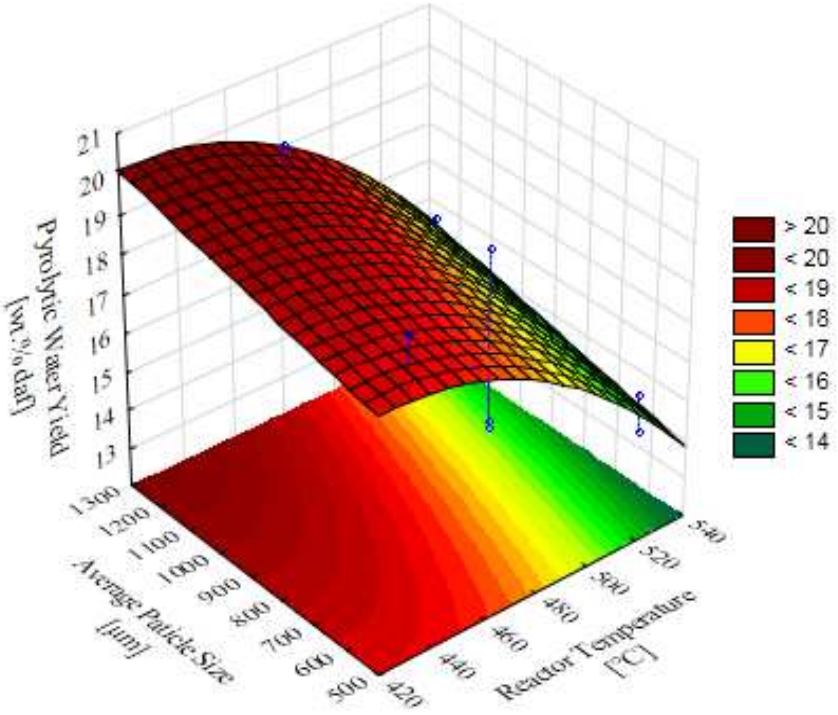

Figure 5-10: Surface plot for Fast Pyrolysis pyrolytic water yield.

Higher heating value (HHV)

The evolution of the calorific values for the char and bio-oil is presented in **Figure 5-11** and **Figure 5-12,** respectively. From the results of the ANOVA it was clear that the reactor temperature had a significant effect on the HHV of the char product at a 95 % confidence interval, while no strong conclusions could be drawn for the effects of the biomass particle size on the char calorific value of the char at the same confidence interval (**Table 9-6**). The HHV found for the char was typically higher than that of petroleum cokes (± 30 MJ/kg as reported by Van de Velden *et al.*, 2010) which makes it an attractive fuel source especially toward the lower reactor temperatures investigated. Most Fast Pyrolysis (FP) investigations focus on the characterisation of the bio-oil as main product, making data for the HHV of FP char derived from woody biomass very scarce. Azeez *et al.* 2010 have reported calculated HHVs for beech and spruce (29.1 and 28.0 MJ/kg, respectively) based on the elemental composition of the char, lower than the measured values reported in **Figure 5-11**. The HHVs of the char in this study were also found to be higher than that reported for sugarcane bagasse using the SU $_{1\ kg/h}$ FP reactor setup (Hugo, 2010).

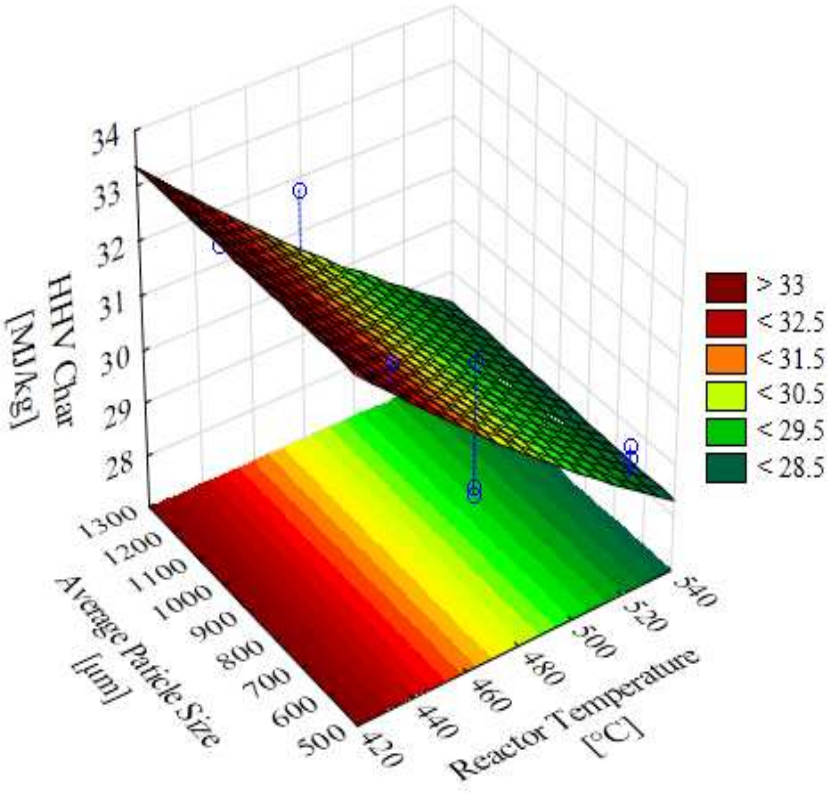

Figure 5-11: HHV of the 1 kg/h FP char.

It should be noted that the results shown in **Figure 5-12** for the HHV of the bio-oil, were measured and reported without correcting or compensating for the water content of the samples. Although no strong conclusions could be drawn at a 95 % confidence interval for influence of the process parameters on the HHV of the liquid product, an apparent trend could be observed, and at a confidence interval of 90 %, it could be shown that the biomass particle size had a significant influence on the calorific value of the bio-oil (**Table 9-7**). The observed trend can however also be explained when considering the ratio of the organic to aqueous fractions of the bio-oil samples considered, as shown in **Figure 5-13**. A higher organic to aqueous ratio gave way to a higher calorific value of the bio-oil. It would appear then that the reason for the poor surface plot fit shown in **Figure 5-12** (R^2 of 62.1%), has more to do with the ratio of the organics and water fractions of the bio-oil (**Figure 5-13**) for a specific sample and to a lesser extent to do with the process conditions employed.

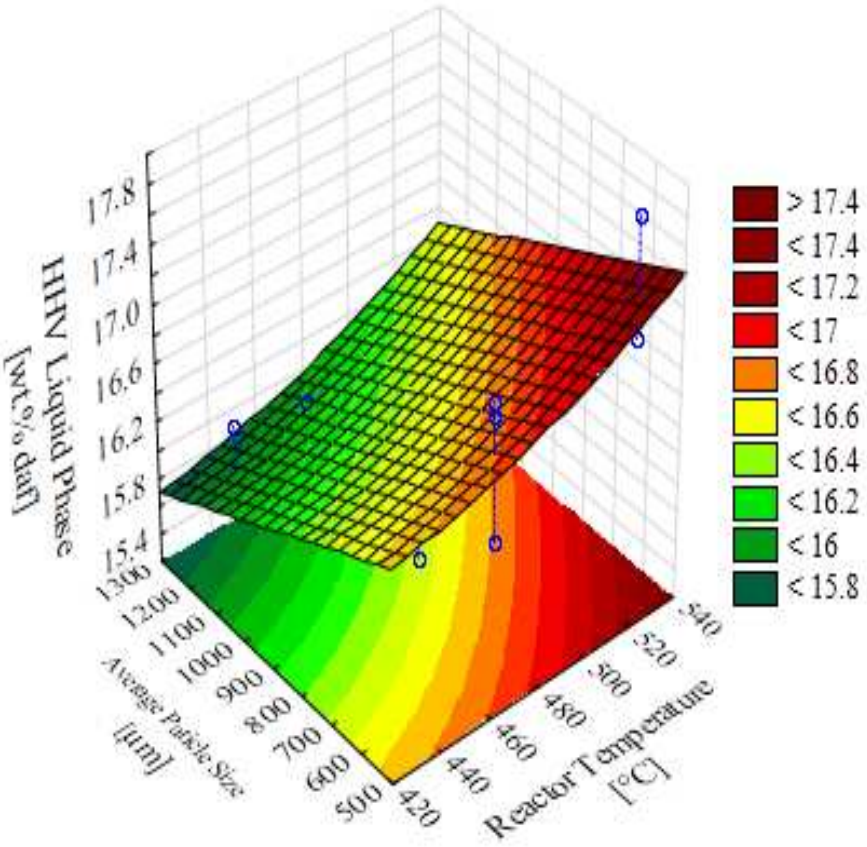

Figure 5-12: HHV of the 1 kg/h FP bio-oil.

Furthermore, it is well known that the rate of decomposition of cellulose and hemicelluloses are favoured at lower temperatures compared to that of lignin, and that the lignin fraction of biomass contributes significantly to the final char yield (Section **4.2.3.1**). It could therefore be assumed that at lower reactor temperatures more of the lignin remains intact in the solid residue compared to the higher reactor temperatures, resulting in the increase of HHV for the char product at lower reactor temperatures. The same argument may be used when considering the apparent trend presented in **Figure 5-12** for the bio-oil. The trend suggests that at higher reactor temperatures the HHV of the liquid product improves at the expense of the solid product, which agrees with the postulate that at higher reactor temperatures more of the lignin is volatilised from the char matrix and is transferred to the liquid product as heavy molecular structures such as phenols.

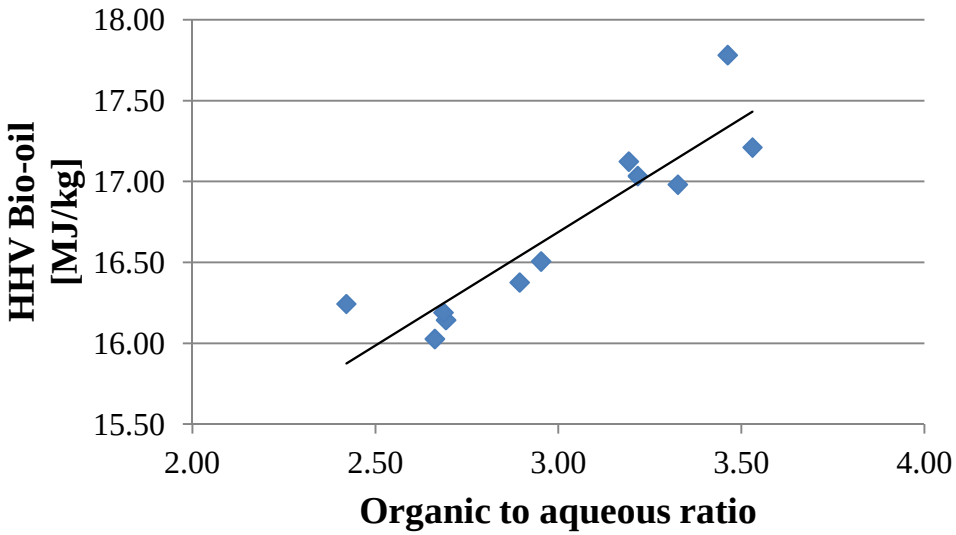

Figure 5-13: Bio-oil calorific value as a function of bio-oil organic- aqueous phase ratio

Molecular composition of liquid product using GC/MS

At the time of the GC/MS analysis of the FP bio-oil samples, no suitable compound could be sourced to act as an internal standard for the measurements. Consequently the data obtained from the analysis could not be used for direct quantitative comparison between samples for a specific compound or family of compounds, but the ratios of the relative peak areas for the respective chemical families could, however, be compared and evaluated at different process conditions.

Between 276 and 310 compounds could be detected per sample through GC/MS analysis, but only those compounds which were detected with a probability of 70 % or greater were considered further, resulting in 71 - 86 compounds detected per sample (Appendix **9.4**). These compounds were grouped according to the main chemical families present, which were aldehydes, ketones, phenols, sugars, furans and acids. A comparison of the results for bio-oil produced at similar reactor conditions showed good repeatability as shown in **Table 9-36** of Appendix **9.5**. **Table 5-8** shows the typical relative contributions found for the chemical families detected for pyrolysis runs conducted using the smaller biomass particle size (average particle size of 570 µm).

It was observed that the results of the larger particle size (average particle size of 1200 µm) were very similar to that of the small particle size when considering the chemical families as a whole (please refer to **Table 9-36** of Appendix **9.5**). The deviation from the average chemical family peak areas were found to be within 2 % for most cases, with a maximum

deviation of 5 % for phenols produced at 470 °C. In order to make a full comparison and evaluate the true influence of the particle size however, the analysis would have to be repeated while using an appropriate internal standard. **Figure 5-14** shows the trend of the ratios for the various main chemical families detected relative to Furans for the reactor temperatures investigated. The ratios of the peak area were determined using the average values for the peaks of the respective chemical families as presented in **Table 5-8**. The Furans were selected for the basis of the comparison due to the narrow band (3 – 7 %) of deviation observed for this chemical family across all the reactor temperatures as well as the constant average peak area calculated for this chemical family (5 %).

Table 5-8: Chemical families detected via GC/MC

Chemical family	Unit	Full Range	Average		
			440 °C	470 °C	530 °C
Aldehydes	%	26 – 42	32	30	41
Ketones	%	15 – 23	16	19	17
Phenols	%	21 – 38	35	35	23
Sugars	%	10 – 16	12	11	15
Furans	%	3 – 7	5	5	5
Acids	%	0.5 – 4	2	4	1

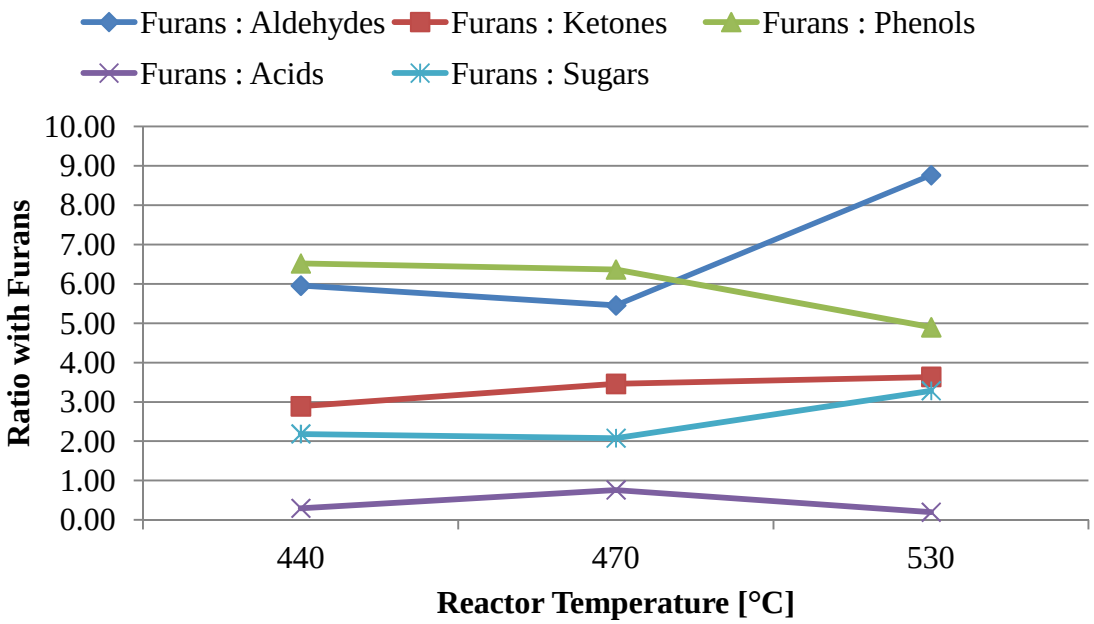

Figure 5-14: Influence of reactor temperature on the bio-oil composition

pH

Figure 5-15 shows the surface plot and apparent trend observed for the pH of the bio-oil as a function of the process parameters. According to the ANOVA, it could not be demonstrated at a confidence interval of 95 % that the particle size and reactor temperature had significant influences on the pH of the bio-oil. At a confidence interval of 90 %, however, it could be shown that the reactor temperature had a significant linear effect on the pH of the bio-oil (**Table 9-8** in Appendix **9.2**). An apparent trend was however observed for the reactor temperature. Oasmaa *et al.*, (2010) found the pH of Fast Pyrolysis oil produced at 500 °C to be 2.2 for *E.grandis*, while Azeez *et al.*, (2010) found the pH of various African woody biomass species to be within the range of 2.5 and 2.9. A recent study by Kumar *et al.*, (2010) on the slow pyrolysis of *E.globulus* reported pH values varying between 1.8 and 2.9.

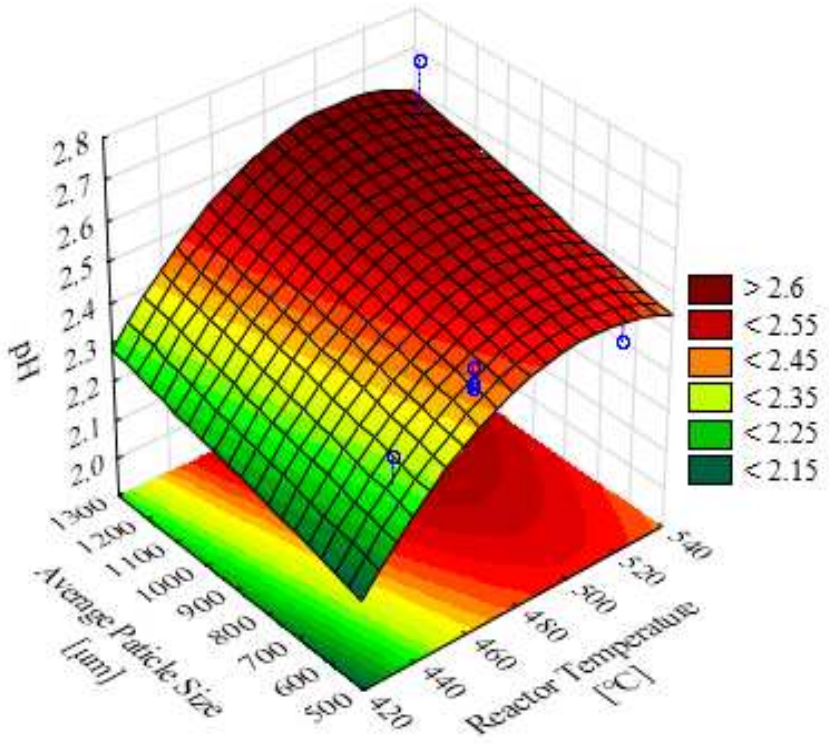

Figure 5-15: Surface plot for bio-oil pH.

Viscosity

The results from the ANOVA on the viscosity of the liquid product are shown in **Figure 5-16**. It was found that the biomass particle size had a significant effect on the viscosity of the liquid product yield with a p-value of 0.0067 (Appendix **9.2 Table 9-9**). No strong

conclusions could however be drawn for the reactor temperature at the same confidence interval.

The range of viscosities reported in **Figure 5-16** (19.6 mPa.s – 43.1 mPa.s) is higher than the point values reported in literature (16.9 mPa.s by Kumar *et al.*, (2010) for *E.globulus* and 28.3 mPa.s by Oasmaa *et al.*, (2010) for *E.grandis*), possibly due to the time elapsed between analysis of the samples and the production thereof. For organisational purposes in the analytical laboratory, the samples were sent for analysis in two batches and not analysed immediately after production. It was ensured that the samples were analysed within 30 days after production. Although the samples were stored in a fridge at 4 °C to slow the effects of ageing, it cannot be ruled out that bio-oil aging had an effect on the viscosity results.

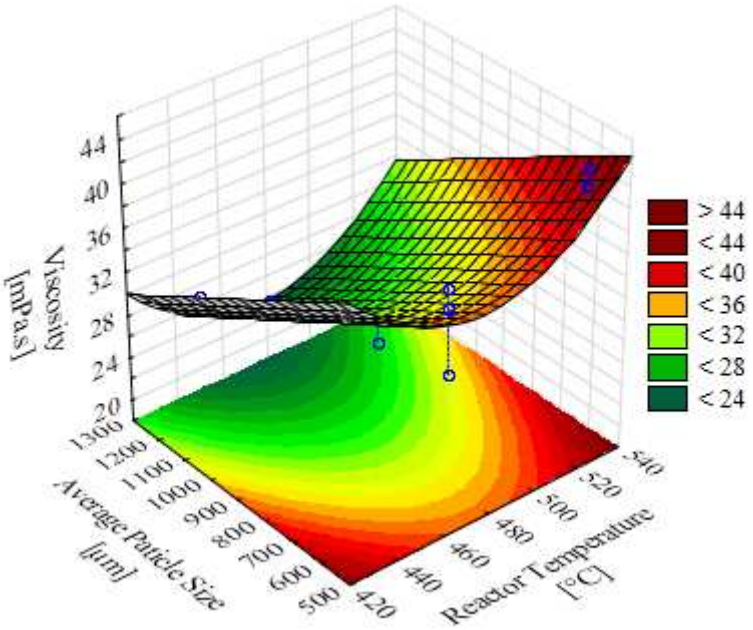

Figure 5-16: Surface plot for Fast Pyrolysis bio-oil viscosity

Elemental analysis

As no suitable technique have yet been established in Stellenbosch for determining the elemental composition of the liquid product at the time of the investigation, samples were sent to Centre for Nano-Material Science at the University of Johannesburg for trial analysis. The results for the two samples sent are given in **Table 5-9**. The oxygen contribution was determined by difference and also contained the contribution of the liquid product ash content (< 0.5 wt. %). Good repeatability was achieved with standard deviations of less than 4 % for

carbon and oxygen (+ash) relative to the average elemental compositions. A standard deviation of 12 - 20 % (or 0.5 – 0.9 wt. %) was, however, observed for elemental hydrogen. Due to the relatively small elemental contribution of hydrogen in comparison to carbon and oxygen, it was expected to see a much larger specific standard deviation for hydrogen. A blank run followed by a known calibration standard was run before and after each analysis, verifying the accuracy of the instrumentation.

Table 5-9: Ultimate analysis of liquid product

Replicate	**Weight used**	**N**	**C**	**H**	**S**	**O + ash**
	mg	wt. %	wt. %	wt. %	wt. %	wt. %
Sample 1-1	2.4	0.0	37.7	4.9	0.0	57.4
Sample 1-2	2.4	0.0	35.5	3.9	0.0	60.6
Sample 1-3	2.1	0.0	36.6	4.0	0.0	59.4
Average	**2.3**	**0.0**	**36.6 ± 1.1**	**4.3 ± 0.5**	**0.0**	**59.1 ± 1.6**
Sample 2-1	2.8	0.0	38.0	5.7	0.0	56.3
Sample 2-2	2.6	0.0	36.0	4.2	0.0	59.9
Sample 2-3	2.4	0.0	36.4	4.0	0.0	59.6
Average	**2.6**	**0.0**	**36.8 ± 1.0**	**4.6 ± 0.9**	**0.0**	**58.6 ± 1.9**

Ash composition

XRF analysis was used to evaluate the composition of the ash resulting from both the raw biomass as well as the char product as given by tables **Table 5-10** and **Table 5-11** respectively. From **Table 5-11** it is evident that the silica content of the char was very low in comparison to that of other elements reported such as potassium, magnesium and calcium, proving that under normal operation, there was no sand carryover from the reactor to the char pots. These results prove that the observation of sand carryover mentioned in section **5.3.1.1**was indeed an isolated occurrence.

Table 5-10: Ash composition of biomass using XRF

Compound	[%]	Element	[ppm]
Al_2O_3	0	Al_2O_3	0
CaO	0.2	CaO	2000
Cr_2O_3	0	Cr_2O_3	0
Fe_2O_3	0.03	Fe_2O_3	300
K_2O	0.01	K_2O	100
MgO	0.12	MgO	1200
MnO	0.02	MnO	200
Na_2O	0	Na_2O	0
P_2O_5	0.02	P_2O_5	200
SiO_2	0	SiO_2	0
TiO_2	0.01	TiO_2	100
Loss on Ignition	99.56		
H_2O	7.77		

Table 5-11: Ash composition of char using XRF

Compound	[%]	Element	[ppm]
Al_2O_3	0	Al_2O_3	0
CaO	0.73	CaO	7300
Cr_2O_3	0	Cr_2O_3	0
Fe_2O_3	0.12	Fe_2O_3	1200
K_2O	0.88	K_2O	8800
MgO	0.23	MgO	2300
MnO	0.08	MnO	800
Na_2O	0.2	Na_2O	2000
P_2O_5	0.06	P_2O_5	600
SiO_2	0.1	SiO_2	1000
TiO_2	0.02	TiO_2	200
Loss on Ignition	96.10		
H_2O	4.18		

Char BET surface area

The BET (Brunauer, Emmett and Teller) surface area was found to be greater for the 570 µm particles than for the 1200 µm particles, ranging between 337 and 372 m^2/g as shown in **Table 5-12**. This finding is in agreement with the literature suggesting that increasing the particle heating rate (in this case by using smaller particles) consequently increases the porosity of the resulting char particles (Guerrero *et al.*, 2008). The typical range of BET surface areas found in this investigation, for an average particle size of 570 µm, was similar to that found for teak sawdust in a study conducted by Ismadji *et al.*, (2005), suggesting that

the FP char produced in this study could also potentially be a suitable precursor for activated carbon. A similar increase in the BET surface area with increasing reactor temperature has been reported by Hugo (2010) for sugarcane bagasse using the $SU_{1\ kg/h}$ Fast Pyrolysis reactor. The corresponding average BET surface areas reported for sugarcane bagasse were 255 and 282 m^2/g for char produced at reactor temperatures of 495 and 526 °C respectively (Hugo, 2010), lower than those presented in **Table 5-12** for *E.grandis* at similar reactor temperatures.

Table 5-12: BET surface areas for FP char

Run ID	Reactor temperature [°C]	Average particle size [µm]	BET surface area [m^2/g]
J-01	500	570	372
J-06	530	570	348
J-07	530	570	340
J-09	470	570	346
J-10	470	570	344
J-11	500	570	338
J-12	440	1200	295
J-08	530	1200	128

5.3.2 Fast Pyrolysis conducted at KIT on bench scale

5.3.2.1 General observations and findings

It was found that, for the operating conditions employed on the bench scale FP plant, the single cyclone failed to separate all the char particles from the reactor exhaust before entering the condensation chain. Significant quantities of char were consequently found carried over to the first condenser during each run. In some cases the fouling was so severe that the entire inside diameter of the first condenser got blocked and no light could be seen through the condenser during the cleaning phase. Char deposits were also observed on the inner walls of the glassware connecting the first and second condenser after each run.

Furthermore it was observed that the liquid products yielded in each of the 4 glass condensers in series were very watery in consistency, with a gradual change in colour from the first condenser through to the cryogenic trap (condenser 4), ranging from dark brown/black to light yellow. The first electrostatic precipitator yielded a viscous product resembling a tarry phase that could only be sampled by scraping the inside of the electrostatic precipitator (ESP) during the cleaning stage. No product was yielded in the second ESP. Even though the

bench scale plant was equipped with a volumetric gas flow meter and three gas samples were taken, one every 15 minutes during each run to quantify the gas yield, it was found that the mass balance could not be closed with good repeatability using the data gathered (data not shown). Gas yields were therefore rather reported by difference.

5.3.2.2 Product yields

Figure 5-17 and **Figure 5-18** show the product yields achieved for the experimental runs conducted on the $KIT_{0.1\ kg/h}$ Fast Pyrolysis plant for two particle sizes selected. The error bars indicate the standard deviation of the results observed. All the yields were expressed on a dry and ash free basis of the initial biomass fed to the reactor.

When taking the standard deviation into consideration it would appear that the yields achieved for both particle sizes remained relatively constant across the range of initial moisture content of the biomass particle sizes fed to the reactor. The liquid yield for the 2 mm particle size however decreased with higher initial biomass moisture content. A study by Demirbaş (2005) on beech wood, however, showed that the yield of liquids should increase with increasing initial moisture content of the biomass fed. This deviation might be explained by the catalytic effect of the char on the product vapours (Bridgwater, 2003) due to the blockages found from the reactor exhaust, all the way to the first condenser. Considering that the first condenser was controlled at 18 °C, it would seem unlikely for the catalytic reactions to have taken place within the condenser. A further explanation might be found when considering the change in residence time both within the reactor and the condensation chain due to the blockage.

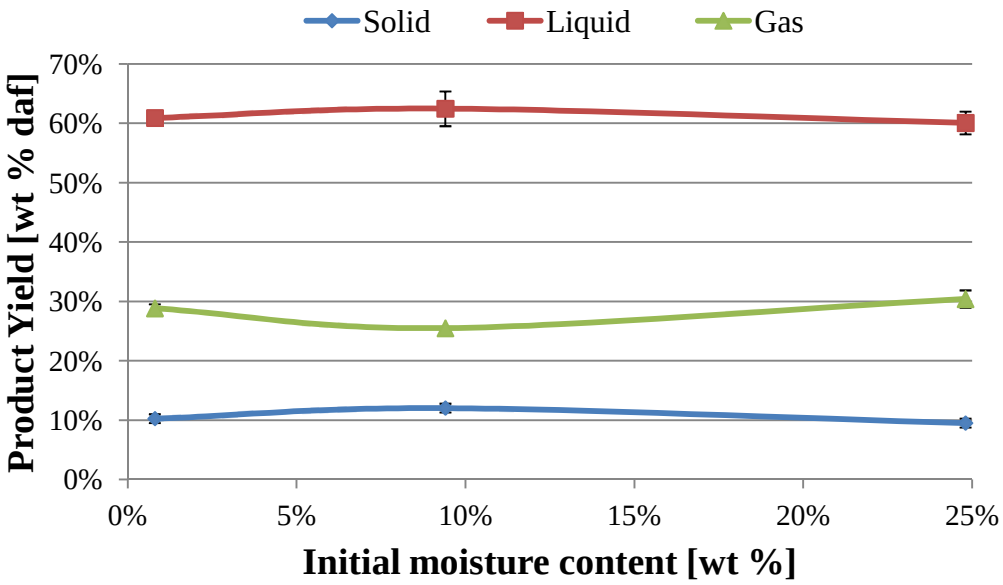

Figure 5-17: Influence of initial biomass moisture content (1 mm particle size)

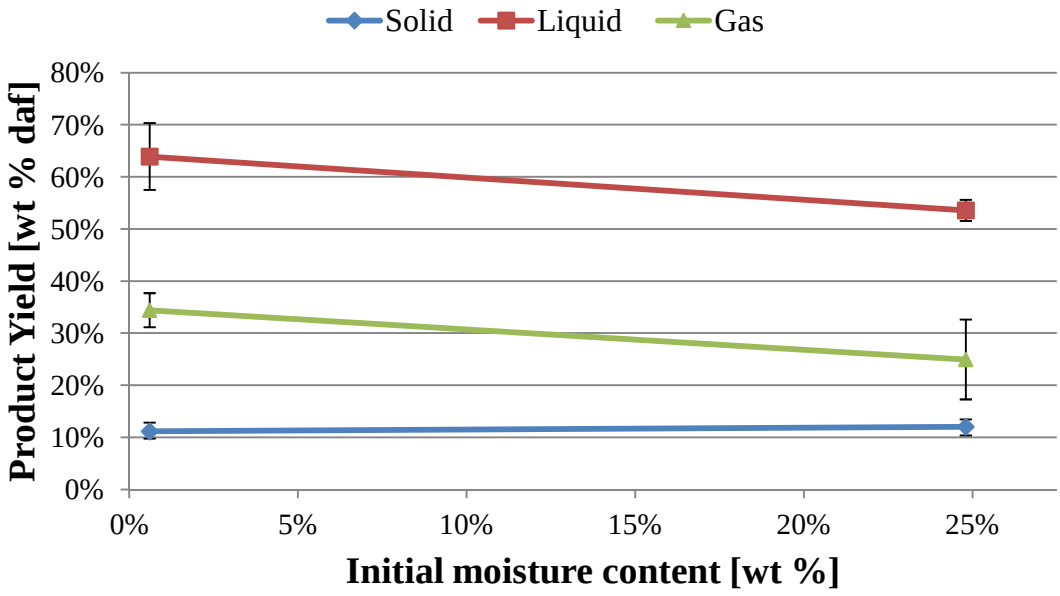

Figure 5-18: Influence of initial biomass moisture (2 mm particle size)

5.3.2.3 Product quality

Liquid product

The analytical results that were obtained for the bio-oil produced with the $KIT_{0.1\ kg/h}$ Fast Pyrolysis plant included bio-oil pH, water content, total organic carbon (TOC), and chemical

oxygen demand (COD) as listed in **Table 5-13**. No result was reported when the product volumes were insufficient to conduct the analysis.

Table 5-13: Liquid product quality results from KIT 0.1 kg/h FP plant

Run #	Particle size	Initial moisture	Analysis	Unit	Analytical results - Liquid product			
					Condenser 1	Condenser 2+3	ESP 1	Cryo trap
4,5	1 mm	24.80%	pH	-	-	2.3	-	-
			KF	wt. %	43.2	76	5.5	93.5
			TOC	mg/L	285000	108000	-	62900
			COD	mg/L	873000	312000	-	211000
1,2,3	2 mm	24.80%	pH	-	2.3	2.4	-	2.3
			KF	wt. %	54.1	76.5	4.0	84.3
			TOC	mg/L	254000	110000	-	73300
			COD	mg/L	750000	303000	-	219000
6,7	1 mm	9.40%	pH	-	-	2.3	-	-
			KF	wt. %	22.6	65.5	4.4	78.3
			TOC	mg/L	427000	159000	-	89700
			COD	mg/L	1300000	462500	-	292000
8,9	1 mm	0.80%	pH	-	-	1.9		1.9
			KF	wt. %	7.1	49.7	3	69.6
			TOC	mg/L	-	240000		129000
			COD	mg/L	1300000	686000		403000
10,11	2 mm	0.80%	pH	-	-	2.2	-	2.3
			KF	wt. %	10.7	55.9	4.3	65.7
			TOC	mg/L	509000	220000	-	145000
			COD	mg/L	1420000	627000	-	500000

From **Table 5-13** it can be observed that the liquid fractions resulting from the condensers had very high water contents, especially for the biomass fed with a high initial moisture content. It was also found that the TOC and COD results decreased with increasing initial moisture content and vice versa. For a specific experimental run it was also observed that the TOC and COD results decreased across the condensation chain, with the largest contributions detected in condenser 1 and the smallest contributions detected in the cryo-trap. This observation might be a result of the heavier volatiles condensing before the lighter compounds in the condensation chain. The high water content and small volumes of the liquid product yielded made it impossible to measure the liquid calorific value with a bomb calorimeter. Furthermore, because the samples were added together for experimental runs conducted at the same conditions, according to similar components in the condensation chain,

the apparent trends observed carry combinations of variance for each of the individual samples. Care should therefore be taken in the interpretation of the results achieved.

Solid product

From the experimental runs conducted using the bench scale FP reactor, only the char samples from 7 experimental runs could be analysed for ash content during the allotted time at KIT. Similarly, the char samples from runs conducted at the same conditions were mixed and analysed as one to reduce the total number of analyses and to be consistent with the equivalent combination of the liquid samples analysed. The ash contents of the analysed samples are given in **Table 5-14**. The moisture content reported in **Table 5-14** is that of the sample after being milled in a cryogenic ball mill prior to analysis using TGA. It was observed that at the higher furnace temperatures some of the ash was entrained, leading to lower overall ash yields at the higher temperatures. Under normal pyrolysis conditions (± 500°C), however, it was therefore expected that the ash remained in the char and was not volatilised as in the case of 815 and 1000 °C shown in **Table 5-14**.

Table 5-14: Ash content of 0.1 kg/h FP plant char product

Measurement	**Unit**	**Experimental run #**		
		1,2,3	**4,5**	**6,7**
Moisture Content	wt %	1.9	1.6	1.6
Ash Content [550 °C]	wt %	3.6	3.7	3.3
Ash Content [815 °C]	wt %	2.6	2.6	2.4
Ash Content [1000 °C]	wt %	2.5	2.5	2.3

Gas composition and calorific value

The composition of the gas product stream, as analysed via GC-MS, is given in **Table 5-15**. The results as shown are given on a nitrogen and oxygen free volume basis and report the average result obtained from three gas samples taken for each run. It was found that the gas consisted primarily of CO_2, CO and CH_4 in decreasing order, similar to the trends reported for woody and herbaceous biomasses in a study conducted by Oasmaa *et al.*, (2010).

Table 5-15: KIT 0.1 kg/h plant gas composition

Initial moisture	24.80%					9.40%		0.80%			
Particle size	2 mm		1 mm							2 mm	
Run #	1	2	3	4	5	6	7	8	9	10	11
Compound	Gas composition [wt. %]										
H2	0.1	0.1	0.1	0.1	0.1	0.1	0.1	0.1	0.0	0.0	0.0
CO	39.0	39.0	49.7	49.7	41.1	43.5	39.6	39.7	40.8	39.5	36.5
CO2	52.2	52.4	38.8	39.3	50.4	48.0	52.7	51.9	51.3	51.9	55.9
CH4	4.8	4.7	6.5	6.0	4.8	5.2	4.4	4.7	4.4	4.8	4.1
C_2H_4	1.8	1.8	2.3	2.4	2.0	1.3	1.7	1.9	1.9	1.6	1.2
C_2H_6	1.0	1.0	1.5	1.2	1.0	1.0	0.9	1.0	0.9	1.0	0.9
C_3H_8	0.4	0.3	0.4	0.5	0.0	0.1	0.1	0.1	0.1	0.2	0.2
i C_4H_{10}	0.6	0.6	0.8	0.8	0.6	0.7	0.6	0.6	0.6	0.9	1.1
n C_4H_{10}	0.0	0.0	0.0	0.0	0.0	0.1	0.0	0.0	0.0	0.0	0.0

The data in **Table 5-15**, in conjunction with the individual gas yields as determined using the difference method for each run, were used to calculate the theoretical calorific value of the gas stream on a nitrogen and oxygen free basis as shown in **Table 5-16**.

Table 5-16: Gas yields and theoretical HHV for the $KIT_{0.1\ kg/h}$ reactor.

Run #	Initial moisture content	Particle size	Gas yield	HHV
	wt. %	mm	wt. % daf	MJ/kg
1	24.80	2	27.1	8.9
2	24.80	2	34.6	8.8
3	24.80	1	29.8	11.4
4	24.80	1	28.9	11.2
5	24.80	1	25.3	8.9
6	9.40	1	22.6	9.2
7	9.40	1	20.9	8.3
8	0.80	1	26.6	8.8
9	0.80	1	26.8	8.4
10	0.60	2	28.8	8.7
11	0.60	2	15.0	7.8

It was observed that the CO and CH_4 content accounted for approximately 75 ± 9 % of the total energy content of the gas stream, with the individual gasses contributing 46.1 ± 4.8 % and 28.8 ± 4.3 % respectively. A clear trend could be observed showing the direct relation

between the mass fraction of these gas species and the calorific value calculated (data not shown). No clear trend could, however, be identified for the change in the chemical composition of the gas stream and the variables chosen for the experimental work.

5.3.3 Fast Pyrolysis conducted at KIT on process demonstration scale

5.3.3.1 Product yields

Due to the complexity of the mass balance inherent to the experimental setup of the PDU, a preliminary mass balance is given in **Table 5-17**. Unlike the other two reactor configurations used in this study, the PDU generated mixed product phases which needed chemical extraction prior to quantifying the individual product yields. The first condenser, K1, yielded a mixture of char and oil, while the second condenser, K2, yielded a mixture of aqueous condensate from the previous run combined with new condensate from the current run. The values given in **Table 5-17** are therefore calculated after taking the abovementioned limitations into consideration.

Table 5-17: Preliminary mass balance on wt. % basis of biomass as received

	Unit	**Run 1**	**Run 2**	**Run 3**	**Run 4**	**Run 5**
Biomass fed	[kg]	39.2	39.0	37.6	37.7	36.9
Moisture content	[wt. %]	10.6	21.7	23.4	22.4	9.5
Inlet Temp. K1	[°C]	20	20	40	40	60
Biomass fed	[wt. %]	100	100	100	100	100
Total oil chars K1	[wt. %]	62.9	72.7	67.8	68.7	45.3
Condensates K2	[wt. %]	11.5	8.6	15.8	12.1	16.8
ESP	[wt. %]	0.6	1.4	1.4	2.2	2.4
Total Pyrolysis gas	[wt. %]	18.8	12.6	12.0	12.5	19.2
Mass balance closure	[wt. %]	93.9	95.3	96.9	95.5	83.7

In general, good repeatability and mass balance closure was observed for the first 4 experimental runs, with run 5 as the exception. The poor closure found for run 5 might be a result of the high inlet temperature chosen for K1 (60°C), which consequently imposed additional load onto the second condenser, K2, and the electrostatic precipitator (ESP), as evident from the increased product yields observed for these units. The measured gas yield

observed for run 5 was the highest of all the runs conducted, but similar to that of run 1 which was conducted using biomass with similar initial water content. No major liquid or solid phase losses were reported for run 5, suggesting that the poor closure could have been a result of losses which could have occurred in the gas phase.

After correcting for the water content of the biomass and the liquid products, the product yields were calculated on a dry and ash free basis of the biomass fed to the reactor. These product yields are shown in **Figure 5-19**, with the gas yield determined by difference. The error bars denote the standard deviation observed for results achieved using biomass with similar initial moisture content.

Good repeatability was observed for runs 3 and 4 which were conducted at the same operating conditions. Run 2 showed similar product yields to runs 3 and 4, even though the inlet condenser temperature (K1) was set higher than for runs 3 and 4, while using the same initial biomass moisture content. From **Figure 5-19** it was evident that runs 2, 3 and 4 yielded between 5.4 and 8.4 wt. % daf more bio-oil than run 1, while the char yield decreased by less than 1 wt. % daf on average. This observation is consistent with the findings by Demirbaş (2005) who showed an increase in the overall liquid yield when increasing the initial biomass water content. Run 5 exhibited the lowest yields for both the char and liquid products, which could partly be explained by the fact that this run was conducted at the highest inlet coolant temperature for the K1 condenser (60 °C compared to 20 and 40 °C for the other runs) and partly due to the poor closure as mentioned previously.

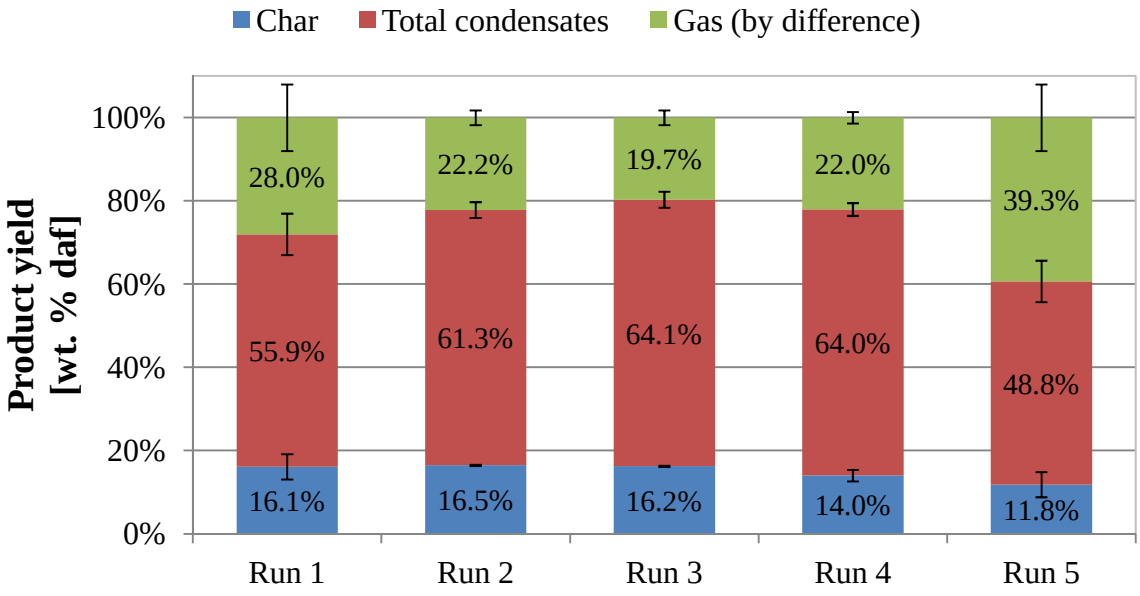

Figure 5-19: Product yields obtained from the 10 kg/h process demonstration plant

5.3.3.2 Product quality

Water content

The pyrolytic water yield is given in **Table 5-18**. The water yield was calculated as the sum of the individual water contents of the various liquid products resulting from K1, K2 and the ESP. When considering the water content of the bio-oil/liquid product as a whole, the results were comparable to literature and to the results achieved for the other two FP reactor configurations investigated in this chapter. It was found that changing the inlet temperature of the first condenser (K1) had no noticeable effect on the overall bio-oil yield or the water content of the bio-oil as a whole. The initial moisture content of the biomass, however, had an effect on the organic fraction of the overall bio-oil yield. It was observed that the overall organic yield increased when using biomass with higher moisture content.

Table 5-18: Water content of PDU condensates

	Unit	Run 1	Run 2	Run 3	Run 4	Run 5
Condensates overall	[wt. % daf]	55.9	61.3	64.1	64.0	48.8
Organic yield	[wt. % daf]	45.5	52.5	52.6	54.8	41.9
Pyrolytic water yield	[wt. % daf]	10.3	8.8	11.5	9.1	6.9
Pyrolytic water content	[wt. %]	18.5	14.4	17.9	14.3	14.2

Pyrolysis gas composition

The composition of the pyrolysis gas, after correcting for the nitrogen, oxygen and neon (internal standard) content, is given in **Table 5-19** on a mass basis. It was found that the largest contributors to the total pyrolysis gas were CO, CO_2 and CH_4. It was observed that even when the temperature of the inlet coolant stream to K1 was increased, the mass fractions of the pyrolysis gas yielded remained fairly constant when looking at runs 1 and 5, and runs 2 – 4, respectively. In both instances where the biomass with the lower initial moisture content was fed to the reactor, there was an increase in the C3, C4 and C5 gas families in the gas stream, accompanied with a slight reduction in the CO and CO_2 contributions (**Table 5-19**). It may be postulated that the increased water vapour, due to the increased biomass water content of runs 2, 3 and 4, might have facilitated the condensation of the heavier organic vapours within the condensers. This postulate might also help to explain the increased organics yield observed in **Table 5-18** for runs conducted using biomass with a high moisture content.

Table 5-19: Composition of PDU pyrolysis gas.

Compound	Unit	Run 1	Run 2	Run 3	Run 4	Run 5
H2	[wt. %]	0.3	0.2	0.2	0.2	0.1
CO	[wt. %]	34.9	37.5	37.7	37.5	34.3
CO2	[wt. %]	53.5	56.8	56.8	56.6	52.0
CH4	[wt. %]	3.8	4.3	4.2	4.2	4.4
C2H4	[wt. %]	0.4	0.0	0.2	0.4	0.7
C2H6	[wt. %]	0.5	0.8	0.7	0.6	0.6
C3H8	[wt. %]	0.8	0.2	0.2	0.2	1.0
C4's	[wt. %]	2.2	0.2	0.0	0.2	2.7
C5+	[wt. %]	3.7	0.0	0.0	0.0	4.2

Ultimate analysis

The ultimate analyses for the products found in the first (K1) and second condensers (K2) of the PDU are shown in **Table 5-20**. Char was isolated from the oil-char mixture of K1 using methanol extraction, where the organic liquid fraction of the mixture was dissolved in methanol and extracted, leaving only the char. After conducting the elemental analysis on the oil-char mixture and the extracted char, the elemental analysis of the dissolved organic phase (bio-oil from oil-char mixture) could be determined by difference and expressed on the same basis. Similarly the elemental composition of the watery product from K2 was determined by difference of results obtained from consecutive runs.

Table 5-20: Ultimate analysis of K1 and K2 products

		Unit	Run 1	Run 2	Run 3	Run 4	Run 5
Extracted Char	C	[wt. % dry]	83.1	82.1	80.9	80.1	82.4
	H	[wt. % dry]	3.6	3.6	3.6	3.4	3.5
	O [a]	[wt. % dry]	13.2	14.3	15.5	16.5	14.1
	N	[wt. % dry]	0.1	0.0	0.0	0.0	0.0
	S	[wt. % dry]	0.0	0.0	0.0	0.0	0.0
Oil char	C	[wt. % dry]	64.7	63.7	62.2	63.6	63.1
	H	[wt. % dry]	5.3	5.4	5.5	5.5	5.5
	O [a]	[wt. % dry]	29.7	30.8	32.2	30.6	31.1
	N	[wt. % dry]	0.2	0.0	0.0	0.3	0.3
	S	[wt. % dry]	0.0	0.0	0.0	0.0	0.0
Organic condensate (by difference)	C	[wt. % dry]	55.3	56.3	54.6	65.9	54.7
	H	[wt. % dry]	6.3	6.2	6.3	7.0	6.4
	O [a]	[wt. % dry]	38.2	37.5	39.0	39.9	38.5
	N	[wt. % dry]	0.2	0.0	0.0	0.5	0.4
	S	[wt. % dry]	0.0	0.0	0.0	0.0	0.0
K2 condensate	C	[wt. % dry]	44.4	47.0	49.3	51.1	49.3
	H	[wt. % dry]	9.1	7.4	7.3	6.0	6.9
	O [a]	[wt. % dry]	46.5	45.7	43.4	42.9	43.8
	N	[wt. % dry]	0.0	0.0	0.0	0.0	0.0
	S	[wt. % dry]	0.0	0.0	0.0	0.0	0.0

[a] By difference

The carbon content of the extracted char was found to decrease, while the oxygen content increased when using biomass with higher initial moisture content as were the case with runs 2, 3 and 4. This might be a result of the additional energy required to evaporate the excess water from the biomass matrix, which reduced the available energy for thermal cracking and volatilisation of organic matter from the char. This postulate is confirmed when evaluating the oxygen and carbon trends for the organic condensates. It was observed that the carbon content increased while the oxygen content decreased with increased initial water content in the biomass, inverse to the trend observed for the char. An increasing trend was observed with each consecutive run for the carbon content of the K2 condensates, while the oxygen and hydrogen contributions decreased for consecutive runs. It was observed that with each reuse of the quenching medium inventory, the organics concentration increased at the expense of the original starting inventory's fresh water (**Table 5-20**).

HHV

The high heating values (HHV) of the pyrolysis products are shown in **Figure 5-20** on a moisture free basis (mf). For the product phases containing high quantities of water, the

Channiwala correlation was used to determine the approximate/theoretical calorific value of the product, based on the elemental composition of the particular sample. For consistency and ease of comparison, all the values reported in **Figure 5-20** were calculated with the Channiwala correlation (section **3.7.2**).

As can be seen from **Figure 5-20** and **Table 5-20**, the specific calorific values for the products decreased with deceasing carbon content. When considering the energy balance, which took into account the relative mass fractions and energy densities for each product phase, it was found that the oil-char mixture from the first condenser, K1, contained the bulk of the energy put into the system as biomass. This finding is in agreement with the BioLiq strategy to use pyrolysis as a method of condensing and upgrading bulky biomass into a high energy feedstock for gasification (Henrich *et al.*, 2009).

Table 5-21 shows the relative energy contributions of the various product phases in relation to the initial biomass energy content on a dry, mass basis. With the exception of run 5, the oil-char mixture was found to contain between 70 and 80 % of the original energy input, of which 43-53 % of the energy content was concentrated in the organic liquid phase of the oil-char mixture. The pyrolysis gas and the organic condensate from the second condenser and the ESP, was found to have much lower energy densities, contributing less than 11 % each of the original biomass energy.

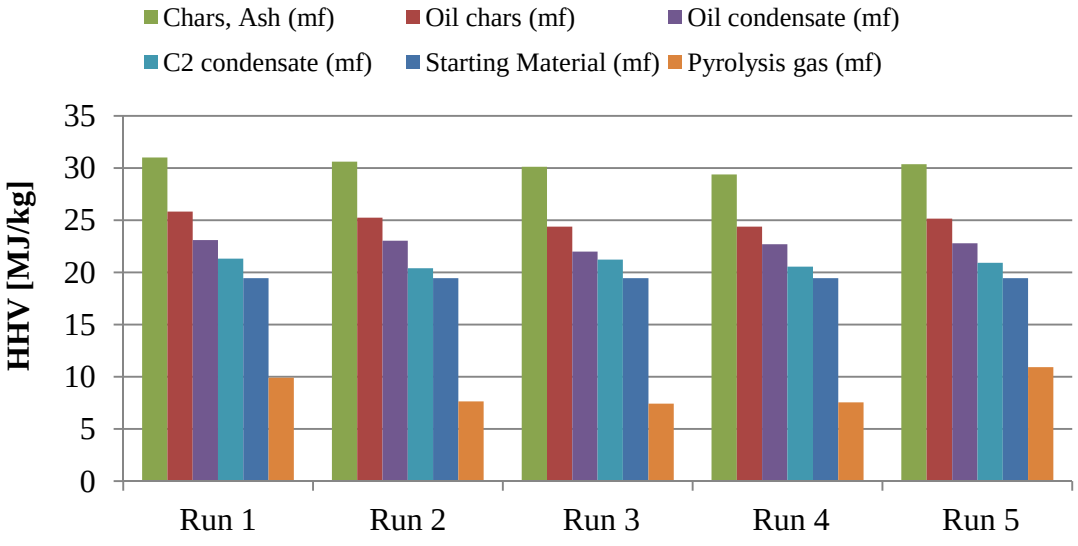

Figure 5-20: High heating values of PDU products on dry basis

Table 5-21: Energy balance for the PDU

	% Energy content relative to dry starting biomass				
	Run 1	**Run 2**	**Run 3**	**Run 4**	**Run 5**
Dry Biomass	100.00	100.00	100.00	100.00	100.00
K1 Oil-char mixture	70.73	80.20	75.98	75.10	55.04
K1 Oil condensate	43.72	53.24	49.79	53.14	35.60
K1 Char	26.23	26.44	25.67	21.71	19.03
K2 Condensate	3.96	4.37	8.08	6.53	9.00
ESP Condensate	0.87	2.11	2.16	3.40	3.34
Pyrolysis gas	10.75	6.33	5.97	6.28	11.88
Deficit	14.51	7.51	8.33	9.00	21.14

Ash

The ash content for the biomass and K1 product samples, are reported in **Table 5-22**. It was observed that the ash remained concentrated in the char.

Table 5-22: Comparison of ash content of biomass and the product from condenser K1 as obtained at 815 °C

Sample	**Unit**	**Run 1**	**Run 2**	**Run 3**	**Run 4**	**Run 5**
Biomass (dry)	[wt. %]	0.4	0.4	0.4	0.4	0.4
Oil-char mixture	[wt. %]	0.8	0.6	0.7	0.7	0.9
Extracted char	[wt. %]	2.4	2.4	2.4	2.8	3.3

Properties of K2 and ESP condensates

Additional measured properties of the liquid phases yielded by the second condenser (K2) and the electrostatic precipitator (ESP) are given in **Table 5-23** and **Table 5-24**. As these liquid fractions did not have to be separated or extracted like the products from K1, these fractions could be analysed for acidity, density, and water content, total organic carbon (TOC) and chemical oxygen demand (COD). The analysis for run 5 could not be completed.

Table 5-23: Electrostatic precipitator condensate properties

	Unit	**Run 1**	**Run 2**	**Run 3**	**Run 4**
pH	[-]	3.4	3.1	2.9	2.8
Density (at 20 °C)	[kg/l]	1.16	1.18	1.19	1.19
Water content	[wt. %]	21.8	21.1	22.7	20.7

The results shown for the electrostatic precipitator remained fairly constant when comparing the various runs. A slight increase in the pH was observed for run 1, suggesting that the relatively drier biomass reduced the formation of acidic compounds, but without the results of run 5, it was impossible to verify apparent trend.

Table 5-24: K2 condensate (filtered) properties

	Unit	Run 1	Run 2	Run 3	Run 4	Run 5
pH	[-]	3.2	3.2	3	3	-
Density (at 20 °C)	[kg/l]	1.04	1.05	1.07	1.07	-
Water content	[wt. %]	71.7	62.1	64.1	60.5	-
TOC	[mg/l]	131000	186000	190000	216000	-
COD	[mg/l]	424000	552000	560000	600000	-

A decreasing trend was observed for the pH of the respective products, with each consecutive experimental run, while the densities of the respective products increased slightly for the K2 condensates, as shown in **Table 5-24**. The observed trends for the K2 condensate density and pH changes can be explained by systematic accumulation of organic matter in the quenching medium. As mentioned previously, the content of the second condenser was continuously reused for consecutive experimental runs of the same biomass. As the starting inventory for the first run was pure water, it was expected to see accumulation of organic material after each use, as indicated by the condensate density, the total organic carbon (TOC) and the chemical oxygen demand shown in **Table 5-24**.

5.4 The comparison of FP reactor configurations

In order to compare the results from the 3 different FP reactor configurations investigated, and evaluate the influence of the respective reactor configurations on product yields and quality, data had to be generated at similar operating conditions. The data generated at a reactor temperature of ± 500 °C, a vapour residence time under 2 seconds and an initial biomass moisture content of ± 10 wt. % were considered for the comparison. It was however important to evaluate the distinct differences in the respective reactor configurations and to realise the limitations involved when making the said comparison. These aspects will be revisited and summarised briefly before evaluating the influences thereof on the results achieved.

5.4.1 Differences in equipment

The key differences of the 3 Fast Pyrolysis reactor configurations are summarised in **Table 5-25**. The full descriptions of the various reactor configurations and their respective operating conditions have been discussed in section **3.5**.

Table 5-25: Comparison of FP reactor configurations

	SU $_{1\ kg/h}$	**KIT $_{0.1\ kg/h}$**	**KIT $_{10\ kg/h}$**
Reactor type	Bubbling Fluidised Bed	Bubbling Fluidised Bed	Twin Screw
Heat carrier	sand	sand	steel balls
Atmosphere	Nitrogen	Nitrogen	Nitrogen
Temperature	± 500 °C	± 500 °C	± 500 °C
Solid separation	2 Hot cyclones in series	1 Hot cyclone	-
Condensation chain	3 units	6 units	3 units
	Direct contact - Isopar (13 ± 5 °C)	1 x Shell and tube (18°C)	Shell and tube (20 °C)
	2 ESP in series (14 and 12 kV)	2 x glass condensers (0°C)	Direct contact – water (10 °C)
	-	2 x ESP in series (8 and 4 kV)	ESP (20 kV)
	-	1 x glass condenser (-50°C)	-
Gas flow measurement	No	Yes	Yes
Product phases	Solid, liquid, gas	Solid, liquid, gas	Oil-char mixture, watery mixture, gas

Of specific interest in the comparison of the pyrolysis equipment is the treatment of the solid product immediately after pyrolysis has taken place and the configuration of the condensation chain. It was observed that poor or no solid separation was achieved for the two KIT Fast Pyrolysis plants resulting in (unwanted) prolonged contact of the char with product vapours and even product liquid phases. In the case of the KIT $_{0.1\ kg/h}$ plant this prolonged vapour char contact was a direct result of inefficient solid separation using a single hot cyclone, while in the case of the KIT $_{10\ kg/h}$ plant the aim of the configuration (with no installed hot cyclone) was to yield a slurry type product for gasification purposes in a downstream facility at KIT. Compared to the SU $_{1\ kg/h}$ FP plant, the isolation of the respective product phases and the quantification thereof was difficult and required chemical treatment to separate the respective product phases.

When considering the configurations of the respective condensation chains, it becomes apparent that there were major differences between the respective systems. In both the SU $_{1\ kg/h}$ and the KIT $_{10\ kg/h}$ plants, direct contact quenching was used in one of the condenser stages, while the smaller KIT $_{0.1\ kg/h}$ plant only made use of glass condensers submerged in cold media. Direct contact quenching imposes an extra parameter to the process, requiring additional separation and calculations in order to determine product yields and isolate the products from the quenching medium. In the case of the SU $_{1\ kg/h}$ FP plant the Isopar and bio-oil mixture could be separated with relative ease as the two fluids were not miscible, but this was a time consuming exercise. The bio-oil and Isopar mixture had to be left overnight to achieve sufficient phase separation before decanting the bio-oil into sample bottles. Furthermore, to prevent Isopar carryover into the sample bottles, the decanting was stopped a few millilitres before the visible interface in the separation funnel, increasing the experimental error in determining the bio-oil yield by a few grams (less than 15 g). Fresh Isopar is a colourless fluid at room temperature, but it was found that the colour started changing gradually as the volume were re-used, changing from colourless to a light yellow, and even light brown. The discolouration was found to be very gradual with time and no additional analyses were conducted on the discoloured Isopar. This observation raises additional questions regarding the possible interactions between the bio-oil and the Isopar or the partial miscibility of some chemical compounds in the bio-oil with Isopar. It is recommended that future studies investigate the discolouration in more detail and quantify the interaction, if any.

In the case of the KIT $_{10\ kg/h}$ plant, water was used as quenching medium in the second condenser, K2. Using water as quenching medium limits the application of the condensates formed in K2 due to the inevitable dilution of the organic yield and makes it very difficult (if not impossible) to isolate the generated condensate from the starting water inventory economically. In this investigation, the condensate yields for K2 were determined theoretically by chemical analyses of the product mixture and not as an isolated product phase, free from the initial water inventory. This modus of operation would not be a problem for continuous industrial operation, as the condensates will become saturated with organic matter over time. For experimental purposes, however, where only a few runs can be conducted, it added to the experimental error of the results.

Another major difference in the reactor configurations was the method of gas flow determination. For the SU $_{1\ kg/h}$ plant there was no equipment installed to measure the gas

flow or to take gas samples for gas analysis, while the other configurations were equipped with a volumetric gas flow measurement (with sample point) and an online gas chromatograph for the KIT $_{0.1\ kg/h}$ and KIT $_{10\ kg/h}$ plants respectively. Only the KIT $_{10\ kg/h}$ plant, however, managed to give reliable gas flow measurements with good mass balance closure using Neon as a tracer gas. The gas yields for the SU $_{1\ kg/h}$ and KIT $_{0.1\ kg/h}$ plants were consequently determined by difference.

5.4.2 Comparison of products

5.4.2.1 General

Due to the complexity of the product phases found for the KIT $_{10\ kg/h}$ FP plant and the limited overlap of analysis done for the products from the respective reactor configurations, the comparison of the products were limited to product yields, bio-oil pyrolytic water content, and the calorific values of the bio-oil as well as the char, as shown in **Table 5-26**. All the product yield results reported were calculated on a weight basis of the biomass fed to the reactor to simplify the comparison of the product yields.

The liquid yields for KIT reactor configurations were calculated as the sum of all the individual liquid fractions from each condenser stage and reported as a total bio-oil yield in **Table 5-26**. Due to the poor mass balance closure found for run 5 of the KIT $_{10\ kg/h}$ FP plant, that particular run was omitted from the comparison and only run 1 was used for the purposes of this section. The results shown for the SU $_{1\ kg/h}$ and KIT $_{0.1\ kg/h}$ plants are average values of duplicate runs, with the standard deviation shown in brackets (**Table 5-26**).

Furthermore, the higher heating values (HHV) reported for the KIT $_{10\ kg/h}$ FP plant were calculated using the Channiwala correlation, while those reported for the SU $_{1\ kg/h}$ FP plant were experimentally measured. Adjustments had to be made for the calorific values of the bio-oil for both reactor configurations to ensure that values are compared on the same basis. The measured value of the SU $_{1\ kg/h}$ FP plant was adjusted upwards to exclude the water content of the bio-oil originating from the biomass. Conversely, the HHV for the bio-oil from the KIT $_{10\ kg/h}$ FP plant had to be adjusted downward to include the relative mass of the pyrolytic water content calculated for the whole bio-oil. Both values reported in **Table 5-26** were therefore adjusted to account for the total organic and pyrolytic water fractions of the bio-oil.

Table 5-26: Comparison of FP results achieved at 500 °C with biomass of ± 10 wt. % initial water content.

	Unit	SU $_{1\ kg/h}$	KIT $_{0.1\ kg/h}$	KIT $_{10\ kg/h}$
Biomass Water Content	[wt. %]	7.7	9.4	10.1
Biomass Ash Content	[wt. % dry]	0.6	0.5	0.4
Biomass Batch	[-]	1	3	3
Bio-oil Yield	[wt. %]	68.8 ± 0.0	68.9 ± 0.8	60.4
Organic Yield	[wt. %]	47.5 ± 1.1	44.1 ± 1.2	36.7
Total Water Yield	[wt. %]	14.3 ± 1.0	24.8 ± 0.3	23.7
Pyrolytic Water Yield	[wt. %]	6.6 ± 0.0	15.4 ± 0.3	13.1
Char Yield	[wt. %]	9.8 ± 0.4	11.5 ± 0.2	14.8
Gas Yield [a]	[wt. %]	28.4 ± 0.4	19.6 ± 1.2	24.8
Calorific Value (HHV)				
Bio-oil	[MJ/kg]	19.6 [b]	-	18.8 [b,c]
Char	[MJ/kg]	32.9	-	31.0 [c]
Gas	[MJ/kg]	-	8.8 (± 0.6)	9.9

[a] by difference; [b] Corrected for biomass water content; [c] calculated using the Channiwala correlation

5.4.2.2 Comparison of product yields

It is evident from **Table 5-26** that, for the specific process conditions employed, the $SU_{1\ kg/h}$ FP plant achieved the highest organic yield and the lowest pyrolytic water yield, while the $KIT_{10\ kg/h}$ FP plant achieved the lowest organic and overall bio-oil yields. The KIT $_{0.1\ kg/h}$ plant achieved an organic yield that was slightly lower than that of the $SU_{1kg/h}$ FP plant, but when considering the standard deviations the results were found to be very similar. Curiously there was a big difference in the pyrolytic water yields between the $SU_{1\ kg/h}$ FP plant and the KIT reactor configurations. As mentioned earlier in section **5.3.1.2**, there was no strong evidence to suggest that changes in biomass particle size or the lignocellulosic composition of the biomass had any significant effects on the pyrolytic water yield. The explanation to the large increase in the pyrolytic water content for the KIT reactor configurations must therefore be found in the differences in the reactor configurations and other process related aspects.

An argument can be made that the effectiveness of solid separation of char from the vapour phase and the efficiency of the condensation chain contributed to the higher pyrolytic water content found for the KIT $_{0.1\ kg/h}$ plant, in comparison to the $SU_{1kg/h}$ FP plant. It was reported that the hot cyclone in the KIT $_{0.1\ kg/h}$ was inefficient and that char particles were entrained from the hot zone into the condensation chain (section **5.3.2.1**). In contrast, no visible traces of char carryover was found in the bio-oil of the $SU_{1kg/h}$ FP plant, meaning that all the char particles were contained within the cyclones and char pots in the hot zone for the entire duration of the experimental run as well as the cool down phase. Keeping the char in the hot zone ensures that all the volatiles are released at the desired reactor temperature, while maintaining a short vapour residence time. In the event of char carryover from the hot zone, it is possible for a char particle to leave the hot zone before releasing all of its volatile matter. For the KIT $_{0.1\ kg/h}$ plant it was observed that between 20 and 40 wt. % of the total char yield was carried over into the condensation chain and subsequently recovered through filtration of the wash liquid. Poor solids retention in the hot zone may therefore account for the slightly higher char yield (± 1.5 wt. %) found for the KIT $_{0.1\ kg/h}$ plant compared to the $SU_{1kg/h}$ FP plant.

The largest deviation in the product yields for the $SU_{1kg/h}$ and KIT $_{0.1\ kg/h}$ FP plants was observed for the gas yield and the pyrolytic water yield. From **Table 5-25** it is clear that the KIT $_{0.1\ kg/h}$ FP plant had the most elaborate condensation chain out of the three configurations considered, with 6 stages in total of which one was a cryogenic trap maintained at – 50 °C, ensuring that none of the condensable species leave the process in the gas stream. In comparison, the $SU_{1kg/h}$ FP plant only made use of a single spray cooling tower at 18 °C and 2 ESPs in series before the process gas was vented to atmosphere. As reflected by the organic yield results, it is clear that the condensation chain of the $SU_{1kg/h}$ plant was very effective in trapping the heavier, organic species from the pyrolysis vapours, but it was unclear whether all the lighter organics and the water vapour would have been trapped. The results in **Table 5-26** suggest that the decrease in the gas yield for the KIT $_{0.1\ kg/h}$ FP plant came at the cost of increasing the observed pyrolytic water yield for the KIT $_{0.1\ kg/h}$ FP plant. It is furthermore suggested that the possibility existed that water was lost via the gas stream for the $SU_{1kg/h}$ FP plant without being condensed and consequently reported as an increased gas yield.

The results reported for the KIT$_{10\ kg/h}$ FP plant can also be explained by the poor/no solid separation compared to that of the KIT $_{0.1\ kg/h}$ and the $SU_{1kg/h}$ FP plants. In comparison, the

higher char yield found for the $KIT_{10\ kg/h}$ FP plant can be ascribed to the absence of a hot cyclone in the condensation chain. A similar argument can be followed that the hot cyclone ensures complete volatilisation of the char and that, without a hot cyclone, it was expected to see an increase in the char yield at the expense of the liquid yield. When considering the organic liquid yields for all three reactor configurations investigated, it was clear that the highest organic yields accompanied the most efficient solid separation system ($SU_{1kg/h}$ FP plant) while the lowest organic yield was a result of no solid separation ($KIT_{10\ kg/h}$ FP plant). An intermediate organic yield coincided with an insufficient solid separation system which resulted in partial char carryover into the condensation chain ($KIT_{0.1\ kg/h}$ plant).

The gas yield for the $KIT_{10\ kg/h}$ FP plant was found to be higher than that of the $KIT_{0.1\ kg/h}$ plant, but similar to that of the $SU_{1kg/h}$ FP plant on a difference basis. It should, however, be noted that the overall liquid yields from the $KIT_{10\ kg/h}$ FP plant was found to be lower than that of the other reactor configurations (as a result of no solid separation) and that the gas yield was reported here on a difference basis. For the $SU_{1kg/h}$ and the $KIT_{0.1\ kg/h}$ reactor configurations, it was necessary to use the difference method to determine the gas yield due to the lack of gas flow instrumentation and the poor performance of the installed instrumentation respectively. The mass balance closure reported for run 1 in **Table 5-17** was 93.9 % with a measured gas yield of 18.8 wt. %, which was comparable to the gas yield result of the $KIT_{0.1\ kg/h}$ plant (**Table 5-26**).

When comparing the relative gas compositions as reported in **Table 5-15** (runs 6 and 7) and **Table 5-19** (run 1 and 5) for the $KIT_{0.1\ kg/h}$ and $KIT_{10\ kg/h}$ reactor configurations respectively, it was found that the gas compositions were very similar, with standard deviations of less than 5 wt. % as shown in

Table 5-27. It may be postulated that the overall efficiency of the condensation chains were similar for the two reactor configurations, even though completely different equipment was

used. The slightly higher pyrolytic water yield of the $KIT_{10\ kg/h}$ FP plant compared to that of the $SU_{1kg/h}$ FP plant might be due to the direct water quenching that was used for run1 of the $KIT_{10\ kg/h}$ FP plant.

Table 5-27: Comparison of KIT gas composition

Compound	Unit	$KIT_{10\ kg/h}$ Run 1	$KIT_{10\ kg/h}$ Run 5	$KIT_{0.1\ kg/h}$ Run 6	$KIT_{0.1\ kg/h}$ Run 7	Average
H2	wt. %	0.3	0.1	0.1	0.1	0.2 ± 0.1
CO	wt. %	34.9	34.3	43.5	39.6	38.1 ± 4.3
CO2	wt. %	53.5	52.0	48.0	52.7	51.6 ± 2.4
CH4	wt. %	3.8	4.4	5.2	4.4	4.5 ± 0.6
C2H4	wt. %	0.4	0.7	1.3	1.7	1.0 ± 0.6
C2H6	wt. %	0.5	0.6	1.0	0.9	0.8 ± 0.2
C3H8	wt. %	0.8	1.0	0.1	0.1	0.5 ± 0.5
C4's	wt. %	2.2	2.7	0.7	0.6	1.6 ± 1.1
C5+	wt. %	3.7	4.2	0.1	0.0	2.0 ± 2.3

5.4.2.3 Comparison of calorific values

In comparison, the calorific value for the overall bio-oil of the $SU_{1kg/h}$ FP plant was found to be slightly higher than that of the $KIT_{10\ kg/h}$ FP plant (**Table 5-26**). This observation was expected when considering the increased pyrolytic moisture content for the overall bio-oil yield compared to that of the $SU_{1kg/h}$ FP plant. It should be noted that both values would be lower in practice due to the added effects of the biomass moisture content also present in the overall liquid yield. For the $SU_{1kg/h}$ FP plant the measured value of the bio-oil produced at 500 °C with a total water content of 22.4 wt.% was found to be 17.2 MJ/kg, approximately 12 % lower than the adjusted value given in **Table 5-26**.

The char produced with the $SU_{1kg/h}$ FP plant was also found to have a slightly higher calorific value compared to that of $KIT_{10\ kg/h}$ FP plant, possibly due to the differences observed in the solid hold time within the heated zone. Kumar *et al.*, (1992) showed that increasing the solid residence time within the heated zone increased the carbon content of the residual char.

The calorific values of the gas were found to be very similar for the two KIT reactor configurations. As mentioned previously the observed maximum standard deviation for the relative gas contributions of the two reactor configurations were within 5 wt. %.

5.5 Conclusions and recommendations

5.5.1 Biomass characterisation

From the results presented on biomass characterisation in this chapter it may be concluded that:

- The weighted average particle size for the two biomass fractions +250-1000 µm and +1000-2000 µm were found to be 570 µm and 1200 µm respectively. Separation into these particle size ranges was found to be very time consuming when using a small shaker especially when large quantities of biomass need to be prepared.
- It has been shown that the lignocellulosic composition may differ for different batches of biomass originating from the same geographical location, climate and genus.
- It was found that although theoretically possible, the results from HPLC analysis used to estimate the holocellulose composition of a biomass after complete hydrolysis, proved to be inferior compared to the chemical extraction of holocellulose and α-cellulose.
- It was found that batches 2 and 3 had similar lignocellulosic composition and that the values were comparable to literature findings, especially with regard to the lignin content.
- Although elemental composition may be used to determine the theoretical HHV of an organic compound using the Channiwala correlation, it could only be applied within acceptable standard deviation using the analysis techniques employed at KIT.

Following the above mentioned conclusions, it is recommended that:

- Larger separation equipment is needed to speed up the particle size selection and separation of the biomass after milling, especially when large quantities of biomass is needed for continuous Fast Pyrolysis experimentation.
- Rather use alpha- and holocellulose extraction over the proposed poly-saccharide determination via HPLC.

5.5.2 Fast Pyrolysis - $SU_{1\ kg/h}$

From the results presented in this chapter it may be concluded that:

- Product yield and quality data were generated for the Fast Pyrolysis (FP) of *E.grandis* with special reference to the effects that reactor temperature and particle size have on the measurable parameters. The generated results were also compared for three different FP reactor configurations at different scale and comprising of different condensation chains. The optimisation of *E.grandis* FP and the comparison of *E.grandis* FP at different scale are both novel contributions to the field of pyrolysis research.
- It was shown that the biomass particle size and reactor temperature had significant effects on both the yield and quality of the liquid product. An optimum liquid yield of 76 wt. % (daf) could be achieved at 470 °C using the $SU_{1kg/h}$ FP plant while feeding an average biomass particle size of 570 µm. These process conditions also resulted in the optimum organic yield achieved for *E.grandis* FP bio-oil of 56.5 wt. % daf.
- Both liquid and char yields were favoured toward the lower reactor temperatures investigated (440 – 470 °C), while the gas yield increased with increasing reactor temperature.
- Bio-oil pyrolytic water yield varied from 6.7 to 10.8 wt. % showing an increasing trend with decreasing reactor temperature. The total water content of the bio-oil affected the HHV of the bio-oil adversely, where increased bio-oil water content lowered the measured HHV of the bio-oil. The HHV of $SU_{1kg/h}$ derived bio-oil ranged between 15 and 18 MJ/kg.

- FP char had a HHV of 28 – 33 MJ/kg with an increasing trend observed toward the lower reactor temperatures investigated.

Based on the findings of this investigation it may be recommended that:

- The use of Isopar as a quenching medium needs to be re-evaluated due to the colour changes observed in the Isopar with continual reuse.
- Modification to the fast Pyrolysis equipment is needed to accommodate longer experimental runs.

5.5.3 Comparison of FP reactors

From the results presented in this chapter it may be concluded that:

- Differences in the reactor configurations, especially with regard to the condensation chain, proved to be of vital importance in the results achieved for both the overall liquid yields as well as the pyrolytic water content of the bio-oil produced.
- The $SU_{1kg/h}$ FP plant produced the highest quality bio-oil with an organic content of 47.5 wt. % and a total water yield of 14.3 wt. %. The increased organic fraction and decreased pyrolytic water yield found for the $SU_{1kg/h}$ FP plant, in comparison to the KIT reactor configurations, were attributed to efficient solid separation of the char from the product vapours and the extended residence time of the separated char in the heated zone.
- The char and gas yields for the KIT reactor configurations were found to be higher than those for the $SU_{1kg/h}$ FP plant, due to extended contact time of the product vapours and char caused by inefficient solid separation for the $KIT_{0.1\ kg/h}$ FP plant and the absence solid separation for the $KIT_{10\ kg/h}$ FP plant.
- Unlike the $SU_{1kg/h}$ FP plant, the two reactor configurations at KIT produced mixed phase product streams (solid, organic and aqueous phases) requiring chemical extraction for qualitative and quantitative analyses. As a result of these complex mixtures the characterisation of the individual product phases and the direct comparison thereof with the other reactor configurations and literature were limited.

6 The comparison of Slow and Vacuum Pyrolysis of *E.grandis*

6.1 Introduction

Very little data is available for the slow pyrolysis of *E.grandis*, and to the best knowledge of the author, there are no data available for the Vacuum Pyrolysis of *E.grandis*. The data that are available can also not be directly compared to similar biomass species due to the intrinsic differences of the various reactor configurations and process parameters employed in generating the data. The purpose of this investigation was to generate Slow and Vacuum Pyrolysis data for *E.grandis* using the same reactor configuration and to compare the results achieved as a function of reactor temperature and reactor heating rate.

Slow and Vacuum Pyrolysis was conducted using a packed bed batch reactor. Vacuum pyrolysis was conducted at a reactor pressure of 7 kPa absolute and Slow Pyrolysis was conducted under an inert nitrogen atmosphere with a flow rate of 40 ml/min. A holding time of 1 hour was used for Slow and Vacuum Pyrolysis experiments.

6.2 Results and Discussion

6.2.1 General observations

It was observed that the amount of smoke/vapour produced increased dramatically for all the experimental runs at a reactor temperature of ± 375 °C, indicating a sudden onset of, or acceleration in the rate of volatilisation. It has been reported by various authors that cellulose (the main constituent of lignocellulosic biomass) and hemicelluloses primarily decompose between 300 and 430 °C, suggesting that the sudden onset of smoke/product vapours corresponded to the thermal degradation of these components (Orfão *et al.*, 1999; Raveendran *et al.*, 1996). During this increased period of smoke generation, a slight change in the system pressure could be observed with the needle of the pressure gauge vibrating slightly in some cases and indicating a slightly higher pressure (± 1-2 kPa) in other cases. Although this change in pressure could be observed easily by the needle movement, a precise quantification could not be made with the installed pressure gauge, as the pressure intervals given on the

dial were in denominations of 5 kPa and therefore not fine enough for absolute precision. A further indication of the rise in the pyrolysis reaction rate, at the said temperature interval, was a definite increase in the bubbling rate observed for the purge line partially submerged in soapy water.

De Jongh *et al*., (2011) investigated the Vacuum Pyrolysis of intruder plants using the same Vacuum Pyrolysis equipment as used in this study. It was found that raising the absolute reactor pressure from 18 kPa, to 50 kPa, had an almost negligible effect on the overall char yield achieved for 2 of the 3 biomass species investigated, showing increases in the char yield of only 1-2 wt. % (daf) at reactor temperatures of 380 and 450 °C. The influence of the reactor pressure was found to be much more dramatic for the third type biomass investigated (Asbos) at 350 °C. At the higher reactor pressure the corresponding char yield decreased by ± 10 wt. % (daf), compared to the result achieved at 18 kPa. It was also reported by the authors that condensation of the product vapours took place inside the reactor at the higher reactor pressure. No mention was made in the on the influence of the reactor pressure on the vapour residence time, or the overall liquid yield. It may be postulated that the increased pressure, or in fact the decrease in the vacuum induced across the reactor when employing a reactor pressure of 50 kPa instead of 18 kPa, reduced the vapour residence time and caused the condensation of product vapours within the reactor.

It was observed for both the Slow and Vacuum Pyrolysis runs that an amorphous product "clump" formed on the inside of the quartz reactor during pyrolysis. This clump varied for different runs with regard to its size and consistency. It was found that the consistency was never uniform for a specific run as the clump would typically contain a brittle and dry section which comprised the bulk of the clump, together with a tarry phase section. The mass of the clump was determined by difference, after removing the free flowing product char (and liquid in some cases) from the reactor for each run, and found to vary between 1 and 4 g. This contribution was added to the char yield as the majority of the clump appeared solid when rinsing with acetone, introducing a small error due to the tarry phase present in the clump.

Due to the short residence times of 2 to 3 seconds associated with Vacuum Pyrolysis in this reactor configuration (Carrier *et al.*, 2011a), liquid formation inside the reactor was limited with almost no visible tarry phase present on the reactor's inner walls. For Slow Pyrolysis however, it was found that significant quantities of liquid collected inside the reactor during pyrolysis, being both free flowing and viscous in consistency. Where possible, this liquid

fraction was collected and added to the contents of the first condenser. No appreciable liquid product could be collected from the 0 and -40 °C condensers as a result of the low nitrogen flow rate. Typical yields in these condensers were recorded below 0.5 % on a weight basis.

6.2.2 Product yields and ANOVA

An overview of the products yields achieved from Slow and Vacuum Pyrolysis are shown in **Table 6-1** and **Table 6-2**, respectively. All yields reported are on a dry and ash free basis of the biomass used, which had an average moisture content of 10.2 wt. % and an ash content of 0.3 wt. % on a dry basis. The centre point runs were used to calculate the standard deviations expected for the respective reactor configurations, as presented in **Table 6-1** and **Table 6-2**.

Table 6-1: Overall product yields achieved with Slow Pyrolysis

Reactor Temperature	**Heating Rate**	**Liquid yield**	**Char yield**	**Gas Yield**	**Pyrolytic water Yield**	**Organic yield**
[°C]	[°C/min]	[wt.% daf]	[wt.% daf]	[wt.% daf]	[wt.% daf]	[wt.% daf]
300	7	9.2	75.9	14.9	4.7	4.4
300	17	11.8	73.3	14.0	2.3	9.5
450	7	31.7	29.7	38.6	13.0	18.7
450	17	41.1	31.3	27.6	16.7	24.4
269	12	2.1	85.0	13.0	0.0	2.1
481	12	38.0	32.1	29.9	14.5	23.5
375	5	29.0	39.1	31.9	11.6	17.4
375	19	33.3	37.4	29.3	11.6	21.7
375[a]	12	24.1 ± 8.2	37.2 ± 0.1	38.7 ± 8.3	7.8 ± 4.6	16.3 ± 3.6
375[a]	12	35.7 ± 8.2	37.0 ± 0.1	27.3 ± 8.3	14.3 ± 4.6	21.4 ± 3.6

[a] Centre point

It was furthermore noted that for VP the liquid yields were slightly higher at corresponding operating conditions. This observation may be ascribed to the difference in vapour residence times between SP and VP. It is known that shorter vapour residence times promote the formation of bio-oil while longer residence time favours char product formation (Meier and Faix, 1999; Bridgwater, 2003). In the case of SP, the average residence time of the vapour in the reactor was calculated to vary from a few seconds up to 12 minutes (depending on the packing density, reactor temperature and the available head room above the biomass bed), compared to the typical sub 2 second average residence times found for VP. As a consequence of the long vapour residence time, the vapours were exposed to the heated zone

and the formed char particles in the reactor for very long time intervals (compared to VP or FP) which resulted in further secondary cracking and condensation side reactions, lowering the overall liquid yield and increasing the char yield, especially at lower reactor temperatures. This effect is also seen when considering the relative organic yields for the two reactor configurations. There was a significant increase in the organics yield for Vacuum Pyrolysis compared to that of Slow Pyrolysis at similar heating rates and reactor temperatures. Local liquid yield maxima of 41.1 and 64.4 wt. % daf for SP and VP were respectively achieved at 450 °C and a heating rate of 17 °C/min.

Table 6-2: Overall product yields achieved with Vacuum Pyrolysis

Reactor Temperature	**Heating Rate**	**Liquid yield**	**Char yield**	**Gas Yield**	**Pyrolytic water Yield**	**Organics yield**
[°C]	[°C/min]	[wt.% daf]	[wt.% daf]	[wt.% daf]	[wt.% daf]	[wt.% daf]
300	7	13.2	60.0	26.8	0.0	14.4
300	17	28.3	55.7	16.0	10.6	17.8
450	7	52.7	24.4	22.9	16.3	36.5
450	17	64.4	19.1	16.5	18.4	46.0
269	12	10.8	83.2	6.1	5.5	5.3
481	12	52.2	20.5	27.3	12.9	39.3
375	5	34.7	32.9	32.4	11.2	23.5
375	19	57.9	28.6	13.5	15.1	42.9
375[a]	12	44.4 ± 6.4	30.6 ± 0.6	25.0 ± 7.0	12.8 ± 1.3	31.7 ± 5.0
375[a]	12	53.5 ± 6.4	29.8 ± 0.6	17.0 ± 7.0	14.6 ± 1.3	38.8 ± 5.0

[a] Centre point

Pimenta *et al.,* (1998) reported a liquid yield of 45.5 wt. % for the Slow Pyrolysis of debarked *E.grandis* at 450 °C using a heating rate of ± 1 °C/min, while recent work by Kumar *et al.,* (2010) found the optimum conditions for achieving maximum liquid yield of 60.5 wt. % via SP to be at 450 °C and a heating rate of 20 °C/min. In both cases, however, the yields were reported on a weight basis and did not take into account the initial moisture, or ash content of the biomass used. Furthermore, no mention of inert atmosphere or residence time was made for either of the studies which made direct comparison of the results difficult as the effects of oxygen, possibly present in small quantities especially at the start of a particular run, cannot be overlooked. The results found for the Vacuum Pyrolysis of *E.grandis* in this study, compared well with data reported by Roy *et al.,* (1992) using Aspen Poplar as feed biomass and a heating rate of 10 °C/min.

Please refer to Appendix **9.3** for all the ANOVA tables associated with this chapter. The fitted response curves for the liquid product yields from Slow and Vacuum Pyrolysis and the accompanying ANOVA tables are given in **Figure 6-1** and **Figure 6-2** respectively. From the ANOVA it was shown that both heating rate (linear) and reactor temperature (linear and quadratic) had significant effects on the liquid yields for Vacuum Pyrolysis (**Table 9-11** Appendix **9.3**), while for Slow Pyrolysis, only reactor temperature (linear and quadratic) was shown to have a significant effect on the liquid yield at a confidence interval of 95 % (**Table 9-10**, Appendix **9.3**). It was found that the general trend of the curves were the same for both SP and VP, where the liquid yield was favoured toward the higher reactor temperatures and higher heating rates.

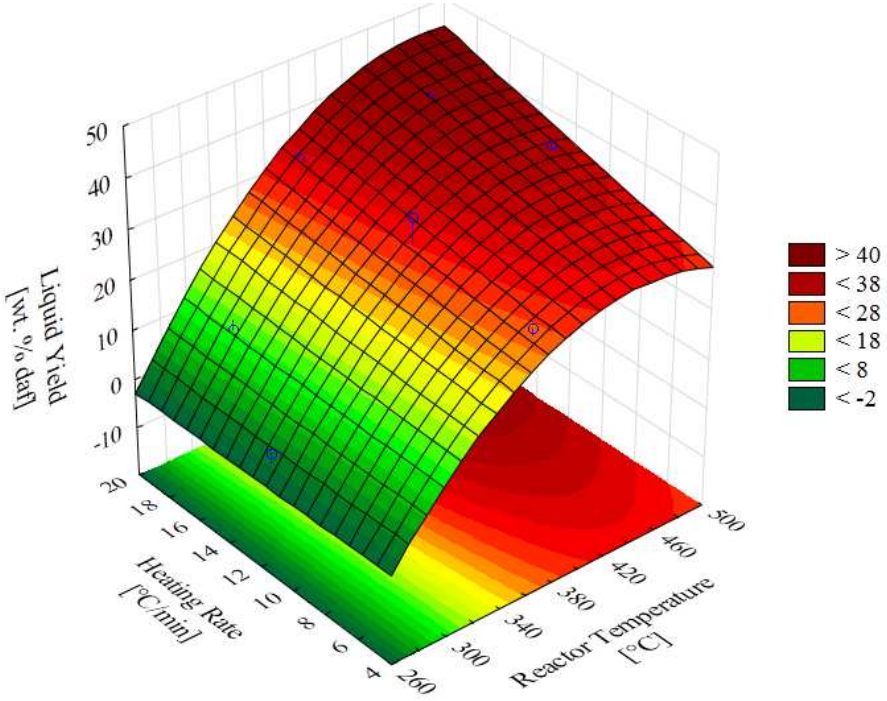

Figure 6-1: Evolution of Slow Pyrolysis bio-oil yield.

Figure 6-3 and **Figure 6-4** show the fitted response curves for the char yields from Slow and Vacuum Pyrolysis as generated using Statistica. The accompanying ANOVA results are given in **Table 9-12** and **Table 9-13** (Appendix **9.3)** for SP and VP char respectively. The ANOVA revealed that only reactor temperature had a significant effect on the char yields for both SP and VP at a confidence interval of 95 %. In the case of the VP results, the effects were found to be both linear and quadratic in nature, while only linear effects were found to be significant for SP. It was found that, for corresponding operating conditions, more char was yielded via SP, than for VP, especially toward the higher heating rates. This was

expected as significantly longer vapour residence times found for the Slow Pyrolysis runs (up to 12 minutes) compared to that of the Vacuum Pyrolysis runs (typically a few seconds). In the case of VP, the product vapours were swept from the reactor heated zone immediately after formation, limiting secondary cracking and condensation reactions occurring on the char surface.

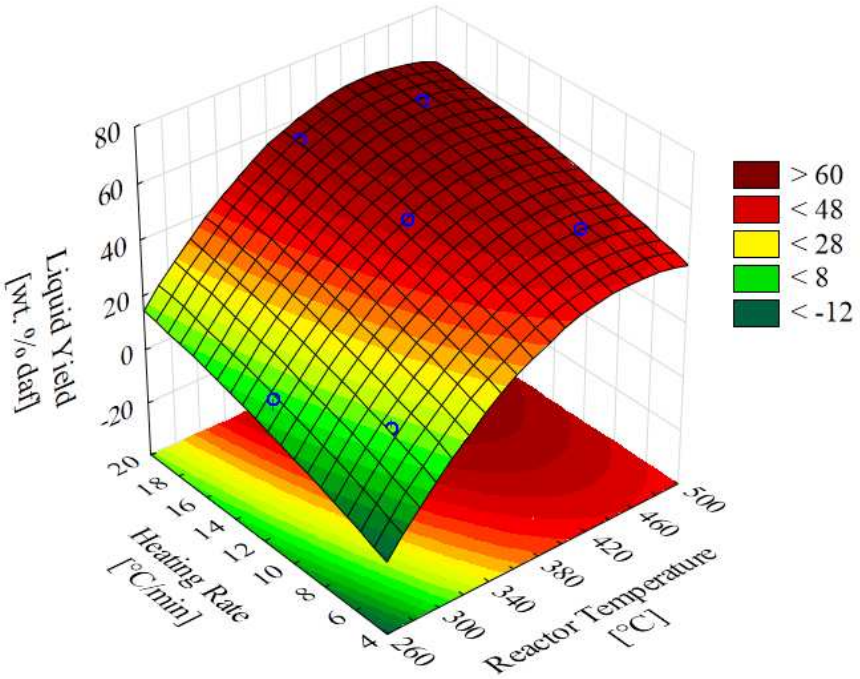

Figure 6-2: Evolution of Vacuum Pyrolysis bio-oil yield.

The gas yield surface plots for Slow and Vacuum Pyrolysis are given in **Figure 6-5** and **Figure 6-6** respectively, with the accompanying ANOVA results given in **Table 9-14** and **Table 9-15** (Appendix **9.3),** respectively. It was found that only the linear interaction for the Slow Pyrolysis had a significant effect on the gas yield at a 95 % confidence interval, as indicated in **Table 9-14** (Appendix **9.3)**. Seeing that the gas yields were calculated by difference, care should be taken in interpreting the results from the ANOVA. In general, however, it was observed that SP yielded more gas than VP at similar operating conditions and that the gas yield was favoured toward the higher reactor temperatures investigated, as the apparent trends suggest. The gas yield results of the Vacuum Pyrolysis runs also showed more erratic behaviour as evident from the poorer fit achieved for the surface plot in **Figure 6-6**.

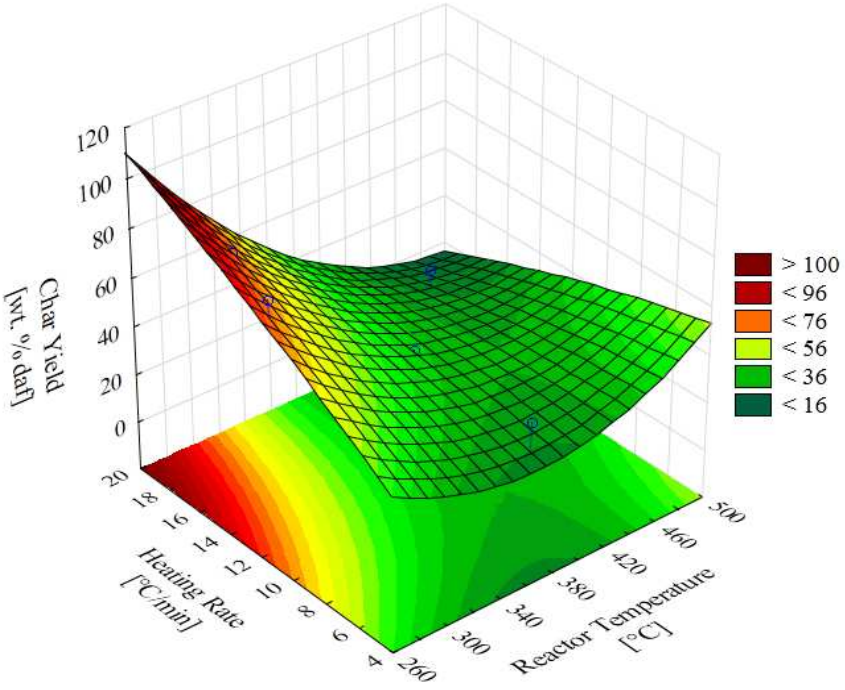

Figure 6-3: Evolution of Slow Pyrolysis char yield.

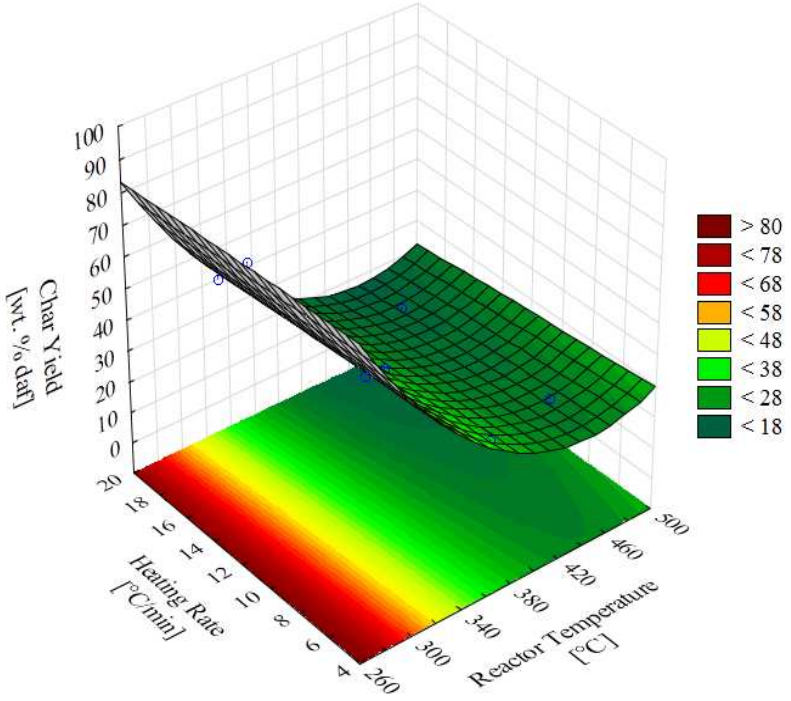

Figure 6-4: Evolution of Vacuum Pyrolysis char yield.

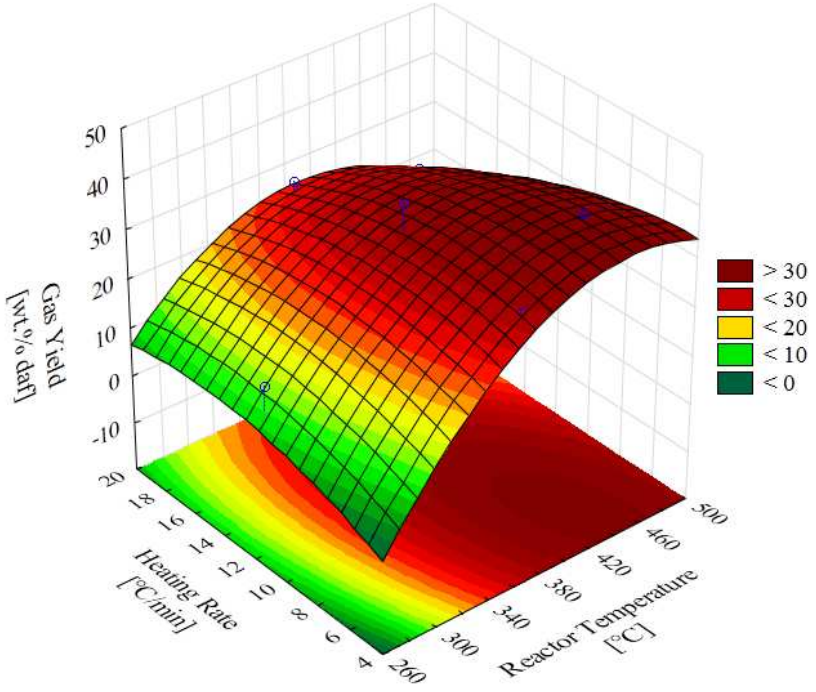

Figure 6-5: Evolution of Slow Pyrolysis gas yield.

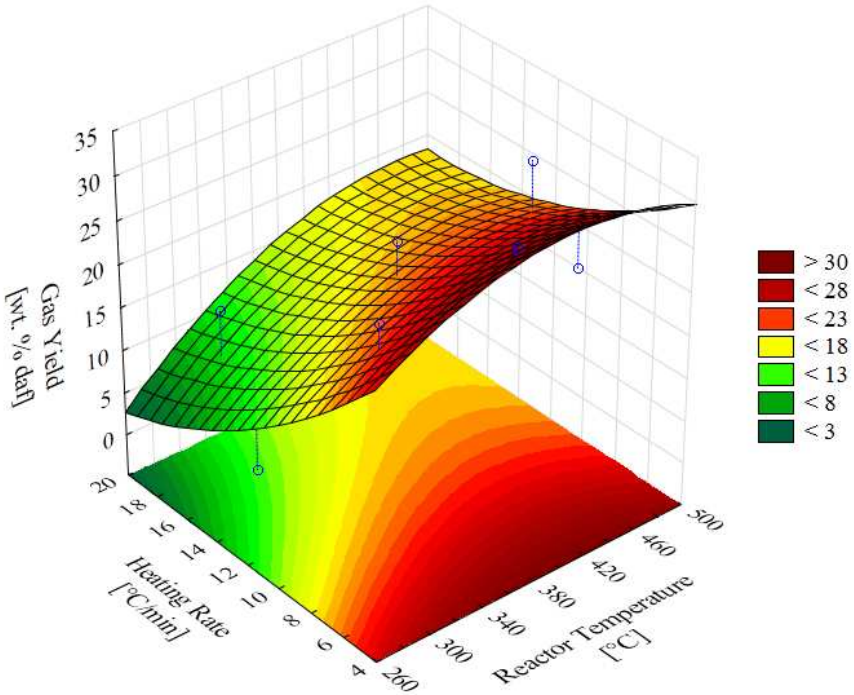

Figure 6-6: Evolution of Vacuum Pyrolysis gas yield.

6.2.3 Product quality

6.2.3.1 Pyrolytic Water Yield

A comparison of the overall pyrolytic water yield for Slow and Vacuum Pyrolysis, are given in **Figure 6-7** and **Figure 6-8**, with accompanying ANOVA tables given in **Table 9-16** and **Table 9-17** of Appendix **9.3**, respectively. Only reactor temperature was found to have significant linear effects on the overall pyrolytic water yield for the Slow and Vacuum Pyrolysis results at a confidence interval of 95 %. It was found that an increase in the reactor temperature increased the pyrolytic water yield for both reactor configurations. Furthermore it was noticed that at a confidence interval of 90 % it could be shown that the heating rate had a significant linear influence on the gas yield for Vacuum Pyrolysis, showing an increasing trend for the pyrolytic water yield with increasing heating rates.

The total water content of the respective liquid product fractions is given in **Table 6-3**. The values reported in **Table 6-3** took into account both the pyrolytic water fraction as well as the water which was added to the system as the initial moisture content of the biomass. No result was reported in the case of VP runs 5 and 7 due to the low, or no liquid product yield in the ambient and 0 °C condensers respectively.

For Slow Pyrolysis there was no fractionation observed across the condensation chain and the entire bio-oil contribution was found to have accumulated in the room temperature condenser, which explains the high moisture content of the product relative to the result found for VP (**Table 6-3**). For SP, the liquid product was found to be watery and single phase with an orange-brown colour.

A clear trend could be observed for the water content of the Vacuum Pyrolysis products across the various condensers. It was found that due to the high linear velocities accompanying Vacuum Pyrolysis (due to the short vapour residence times), the bio-oil was fractionated across the condensation chain with the heavier molecules being condensed in the first stage of the condensation chain and the lighter organic and water vapour being condensed in the 0 and sub 0°C condensers. This was evident by the dark brown and more viscous liquid found in the ambient condenser compared to that of the following stages which were yellow (-40 °C) and orange (0 °C) in colour and resembled the consistency of water at room temperature.

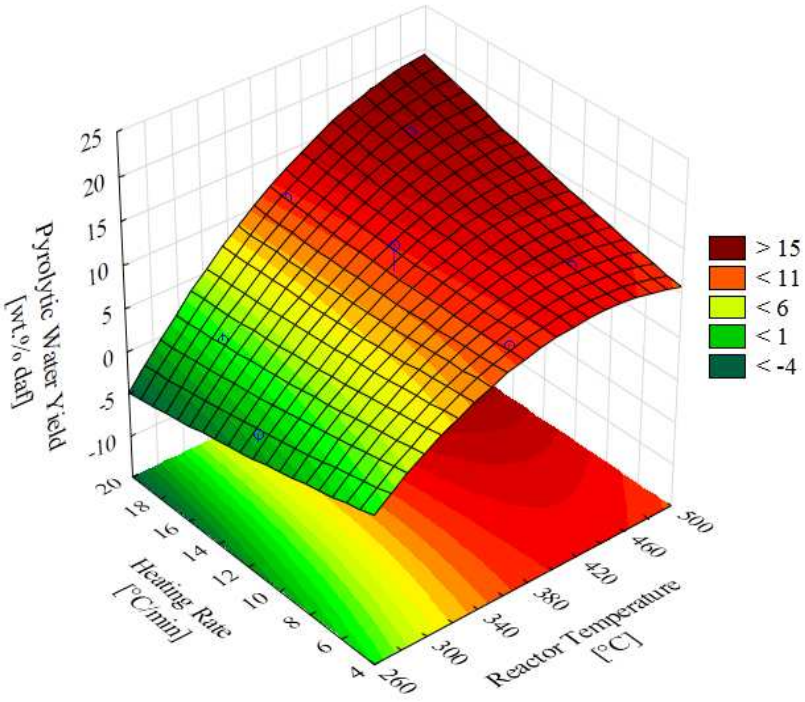

Figure 6-7: Evolution of Slow Pyrolysis pyrolytic water yield.

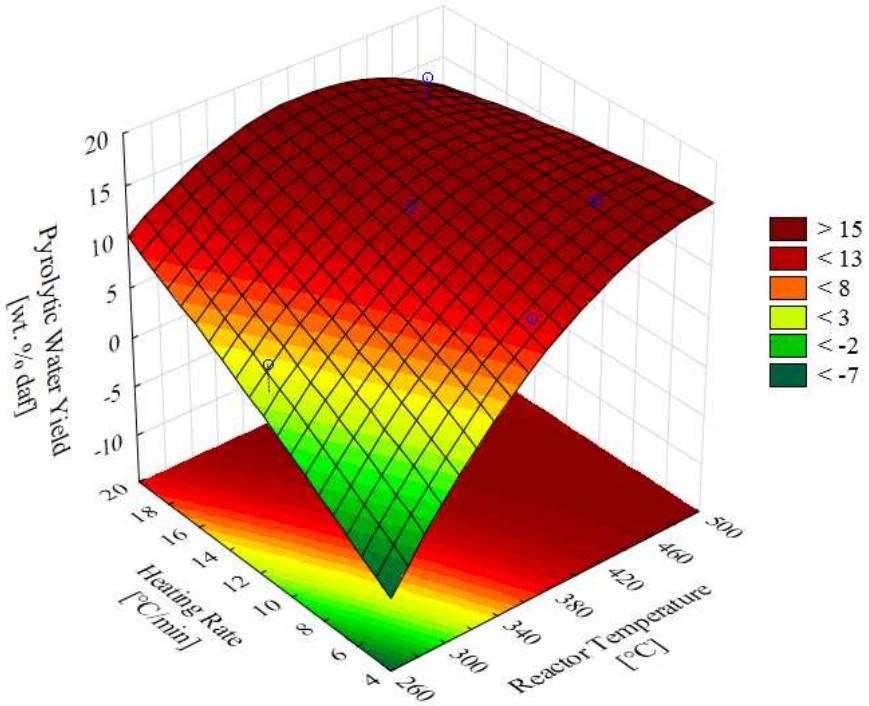

Figure 6-8: Evolution of Vacuum Pyrolysis pyrolytic water yield.

Table 6-3: Water contents or liquid product fractions via Karl-Fischer titration

Run	Reactor Temperature	Heating rate	Slow Pyrolysis	Vacuum Pyrolysis		
			Ambient	Ambient	0 °C	-40 °C
[-]	[°C]	[°C/min]	[wt. %]	[wt. %]	[wt. %]	[wt. %]
1	300	7	78.46	4.46	37.97	76.08
2	300	17	75.17	2.97	47.50	74.16
3	450	7	58.37	8.39	47.50	80.59
4	450	17	58.41	4.37	61.56	75.66
5	269	12	82.03	-	76.56	84.85
6	481	12	56.40	8.39	43.36	77.17
7	375	5	61.12	17.74	-	86.60
8	375	19	56.82	3.78	49.79	72.78
9	375	12	58.53	5.11	43.97	77.36
10	375	12	59.43	5.01	53.77	73.77

6.2.3.2 Organic Liquid Yield

Figure 6-9 and **Figure 6-10** give the respective surface plots for the evolution of the organic liquid yields for Slow and Vacuum Pyrolysis respectively. The accompanying AVONA results are given in **Table 9-18** and **Table 9-19** of Appendix **9.3** for Slow and Vacuum Pyrolysis, respectively. It could be demonstrated that reactor temperature had significant effects (linear and quadratic) on the organic liquid yield for both SP and VP at a 95 % confidence interval. Although no strong statistical conclusions could be drawn for the effects of the heating rate on the organic yield for the SP plant at 95 %, it could be shown that the heating rate had a significant linear interaction with the organic yield at a 90 % confidence interval. The result for the VP plant showed that the heating rate had a significant linear influence on the organic liquid yield.

In general, the fitted trends for both the reactor configurations were very similar, showing that the total organic yield was increased with increasing heating rate and reactor temperature. The yields achieved with the Vacuum Pyrolysis plant was found to be higher than that achieved with the Slow Pyrolysis plant, suggesting that the shorter vapour residence times typically found in VP maximised the organic yield achieved. Similar results have been reported for sugarcane bagasse (Carrier *et al.,* 2011a).This is in agreement with literature reporting that residence times below two seconds limit the secondary reactions occurring in the vapour phase, promoting liquid yield (Van de Velden *et al.,* 2010) while long residence

times promote char formation (Bridgwater, 2003) as char formed during pyrolysis has catalytic effects on the vapour phase condensation reactions (Bridgwater, 2011).

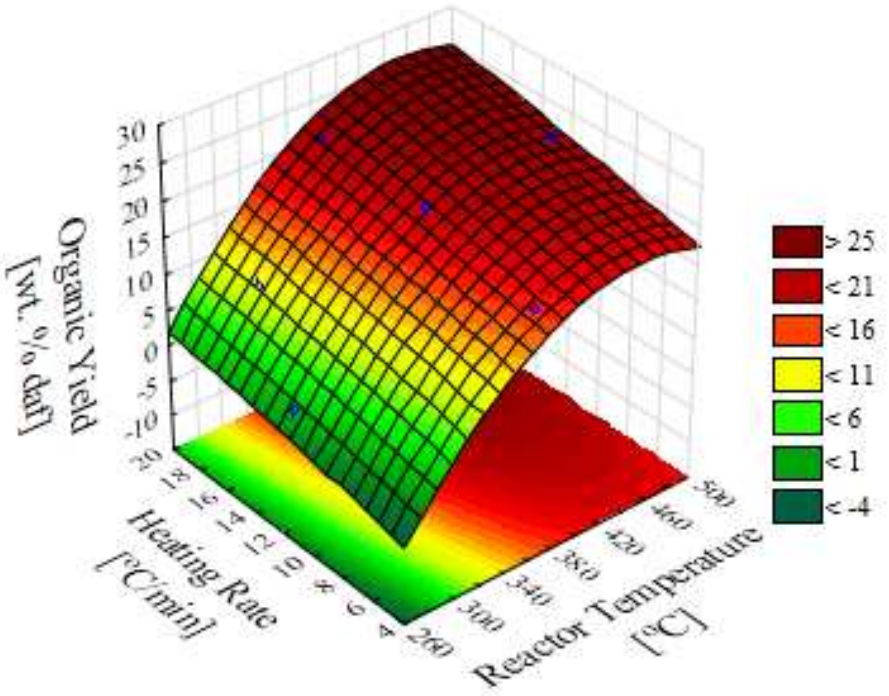

Figure 6-9: Evolution of Slow Pyrolysis organic liquid yield.

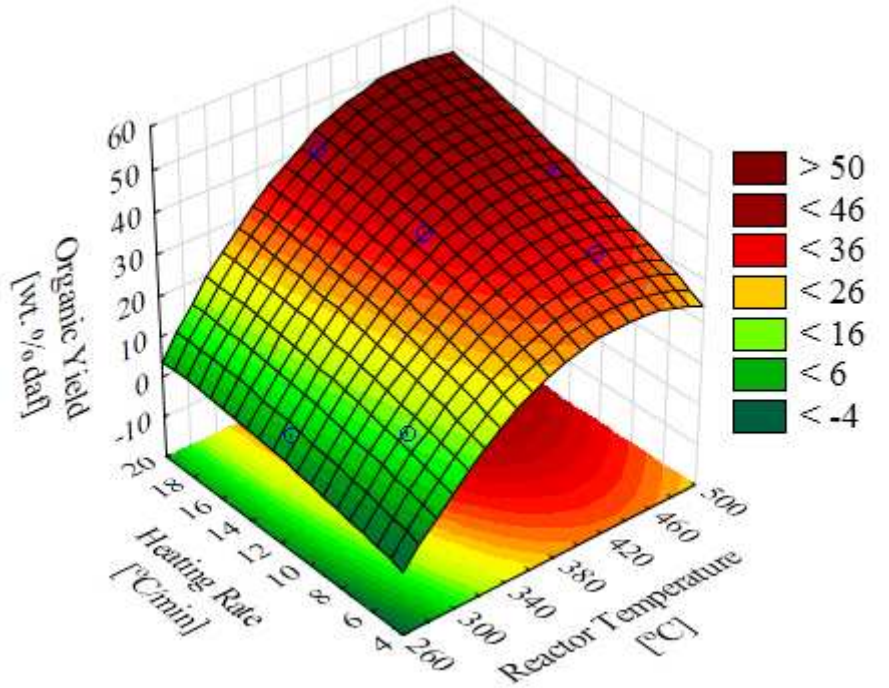

Figure 6-10: Evolution of Vacuum Pyrolysis organic liquid yield.

6.2.3.3 Chemical composition by GC/MS

The relative contributions of the main chemical families found in the bio-oil produced via Slow and Vacuum Pyrolysis are given in **Table 6-4**. The contributions were calculated as the sum of the peak areas of a specific chemical family/compound which were detected with a certainty of greater than 70 %, relative to the total peak area of all the compounds detected with a certainty of greater than 70 %. Please refer to **Table 9-35** of Appendix **9.4** for a list of all the compounds detected with a certainty of 70 % or greater for Slow and Vacuum Pyrolysis bio-oils. The result for run SP1 (Slow Pyrolysis 1) was unfortunately found to be incomplete/corrupt and was subsequently omitted from further discussion and the ANOVA. In general, the largest contributions to the total chemical families/compound detected (above 70 % certainty) came from the acids, aldehydes, ketones and phenols. It was also noted that individual components such as the Acetic Acid, Syringol and Furfural were present in large concentrations relative to the other compounds. Acetic acid was found to make up between 75 and 100 % of the total detected acid compounds, with an average contribution of 92 % (data not shown). Furfural contributed between 22 and 92 % of the total aldehydes while Syringol accounted for 50 to 82 % of the total phenol species detected, when these compound were found to be present in the bio-oil.

Table 6-4: Relative composition of Slow and Vacuum Pyrolysis bio-oil (chemical families detected at + 70 % confidence)

	Temperature	Heating rate	Furans	Acids	Ketones	Aldehydes	Sugars	C 5-ring	Phenols	Furfural	Heptane (Int. Std)	Syringol
	[°C]	[°C/min]	[%]	[%]	[%]	[%]	[%]	[%]	[%]	[%]	[%]	[%]
SP 2	300	17	3.1	53.3	3.0	32.6	0.0	0.5	8.8	28.8	0.6	4.4
SP 3	450	7	11.1	19.2	16.9	23.5	7.7	10.3	32.6	10.1	0.4	18.9
SP 4	450	17	8.5	15.8	18.5	20.3	0.0	9.1	41.6	8.8	0.4	29.1
SP 5	269	12	1.1	61.1	1.4	34.7	0.0	0.0	1.1	32.0	0.7	0.9
SP 6	481	12	7.0	13.3	17.5	12.8	0.0	9.6	45.9	7.9	0.3	31.3
SP 7	375	5	8.7	36.1	14.8	22.7	6.4	7.8	21.7	10.9	0.4	0.0
SP 8	375	19	11.3	18.0	25.2	21.3	1.3	9.4	30.1	10.9	0.5	0.0
SP 9	375	12	12.1	21.1	21.5	20.6	0.0	10.1	31.0	12.4	0.5	0.0
SP 10	375	12	10.6	21.0	18.3	28.4	7.9	8.8	26.7	11.4	0.4	16.7
VP 1	300	7	12.7	6.9	18.4	26.8	9.0	9.2	25.5	14.8	0.9	0.0
VP 2	300	17	6.8	45.2	9.6	23.4	4.8	4.2	14.0	11.5	0.6	0.0
VP 3	450	7	10.9	15.2	18.4	16.9	0.0	9.6	38.3	0.0	0.4	0.0

VP 4	450	17	5.5	31.3	16.4	24.5	9.5	9.9	21.8	5.9	0.5	0.0
VP 5	269	12	0.7	57.6	1.5	33.8	0.0	0.2	6.2	20.3	0.9	3.3
VP 6	481	12	10.7	11.7	22.8	14.6	11.7	12.7	34.0	4.1	0.5	21.4
VP 7	375	5	9.6	18.4	28.6	33.0	13.3	11.8	14.3	5.7	0.5	6.6
VP 8	375	19	8.2	22.5	20.6	27.3	10.3	8.1	23.2	6.1	0.5	15.9
VP 9	375	12	13.0	14.9	23.1	14.8	11.9	11.6	28.1	4.5	0.4	20.7
VP 10	375	12	9.1	25.8	18.1	17.3	13.2	8.3	23.1	4.6	0.4	16.1

The results shown in **Table 6-4** were subjected to an ANOVA and the families for which an acceptable surface fit could be achieved (with an R^2 value of 0.8 and higher) were selected for discussion in the following subsections. The results produced for the aldehydes were found to be outside the acceptable limit with regard to the surface plot R^2 values and the AVOVA was unable to identify any interactions of the process variables on the aldehyde concentration at 95 or 90 % confidence intervals. The ANOVA results for furfural (a major contributor to the total aldehyde family) were found to be closer to the acceptable range and the ANOVA was able to identify significant effects for both Slow and Vacuum Pyrolysis at a 95 % confidence interval.

Furans

The evolution of the furans relative to the total compounds identified with a certainty of + 70 %, is shown in **Figure 6-11** and **Figure 6-12** respectively for Slow and Vacuum Pyrolysis bio-oils. The ANOVA revealed a significant influence of the reactor temperature on the Furan yield for both the Slow and Vacuum Pyrolysis bio-oils as shown in **Table 9-20** and **Table 9-21**Error! Reference source not found. of Appendix **9.3**. According to the surface plots generated, the furan yields were favoured within the temperature range of 380 – 430 °C. No strong conclusions could be drawn at a confidence level of 95 % for the heating rates of either reactor configuration, but an apparent trend was observed for VP, suggesting that lower heating rates favoured furan yield in VP. When considering the chemical structure of Furan, it is evident that Furans originate from the thermal degradation of the hemicelluloses fraction of the biomass, which is known to contain various 4 and 5 carbon mono-saccharides in its macromolecular structure (Fengel and Wegener, 2003). It may therefore be postulated that in the region of 380 – 430 °C the hemicellulose derived product vapours are degraded to such an extent that the monomeric building blocks of the poly-saccharide are liberated from the macro structure.

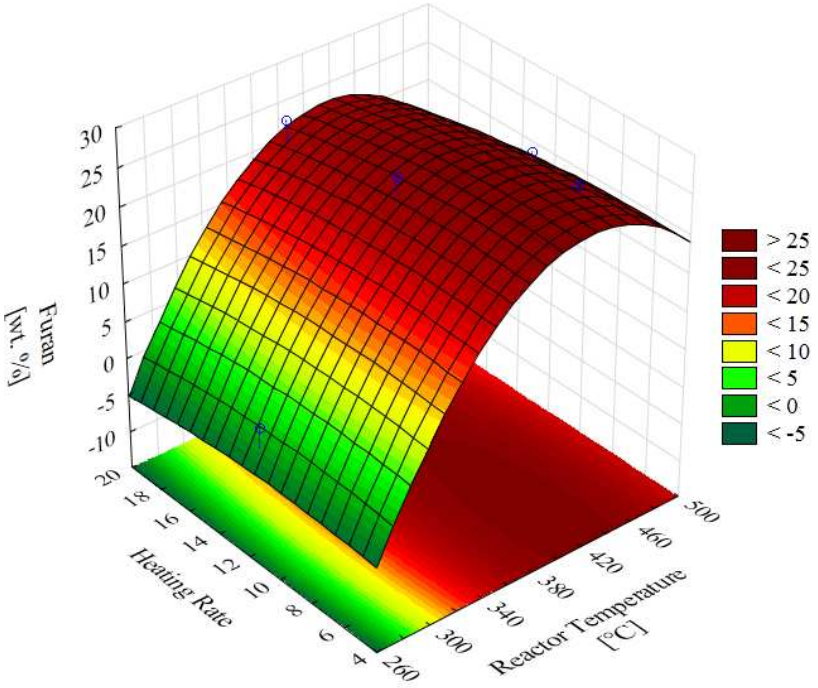

Figure 6-11: Evolution of Furan in Slow Pyrolysis bio-oil.

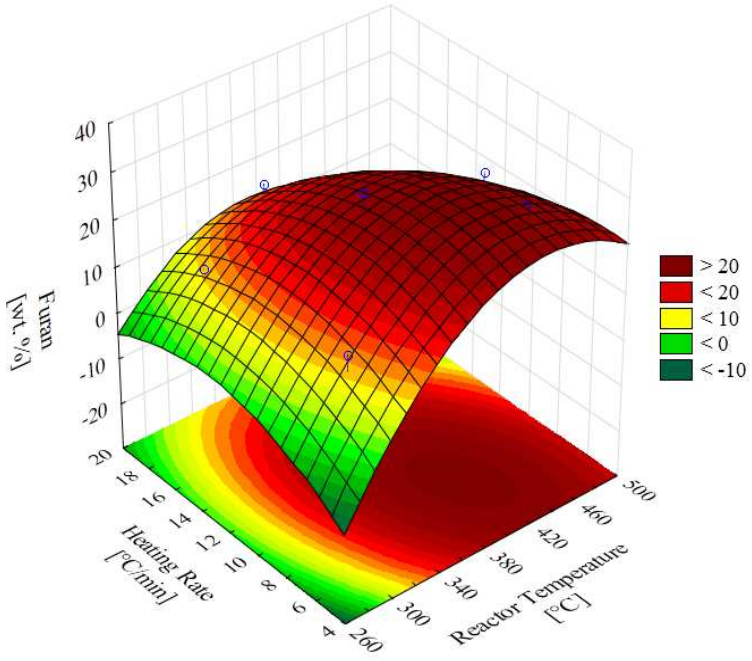

Figure 6-12: Evolution of Furan in Vacuum Pyrolysis bio-oil.

Acids

The acids family was found to be present in large proportions throughout the analyses conducted. Further investigation revealed that acetic acid contributed between 75 and 100 % of the total detected. Only the results from the Slow Pyrolysis bio-oil analysis yielded a good

surface plot fit with an R^2 value of 0.84 as shown in **Figure 6-13**. In comparison, the fit of the VP results had an R^2 value of 0.48 and was consequently omitted. Furthermore, the ANOVA found that reactor temperature had a significant linear effect on the evolution of the acid compounds yielded in the GC/MS results for the SP bio-oils, as shown in **Table 9-22** (Appendix **9.3)**.

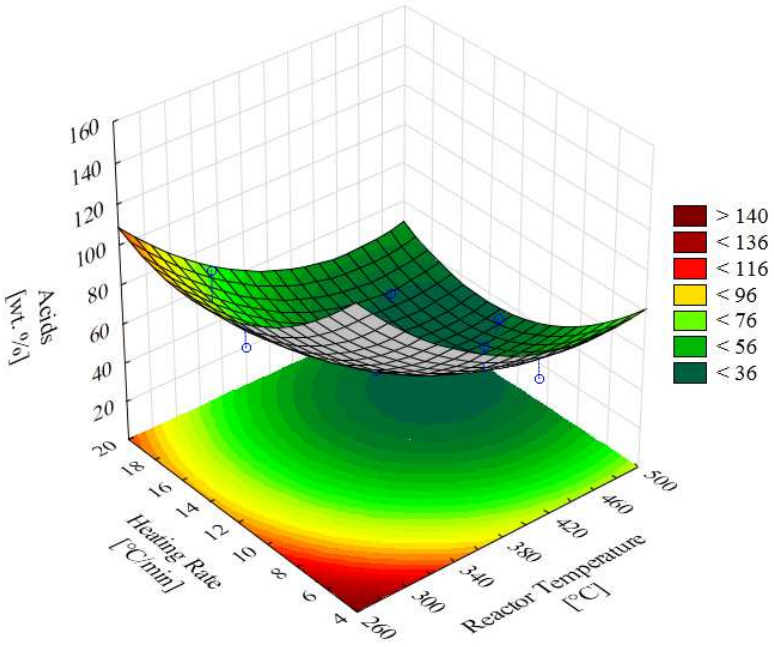

Figure 6-13: Evolution of Acid in Slow Pyrolysis bio-oil

Ketones

Figure 6-14 and **Figure 6-15** show the surface plots for the evolution of ketones as detected via GC/MS for the Slow and Vacuum Pyrolysis bio-oils respectively. The results from the ANOVA for Slow and Vacuum Pyrolysis are given in **Table 9-23** and **Table 9-24** of Appendix **9.3,** respectively. The ANOVA revealed that reactor temperature had significant effects on the ketone yields for both reactor configurations at a 95% confidence interval. Reactor temperature was found to have both linear and quadratic effects for the VP bio-oils (**Table 9-24,** Appendix **9.3)** while for the SP bio-oils only a linear interaction proved to be significant. The effect, if any, of the heating rate on the ketones formation in Slow Pyrolysis could not be shown within the 95 or 90% confidence intervals as shown in **Table 9-23** of Appendix **9.3**. For Vacuum Pyrolysis, however, it could be shown at a 90 % confidence

interval that the heating rate had a significant linear effect on the ketone formation, as suggested by the trend in **Figure 6-15**.

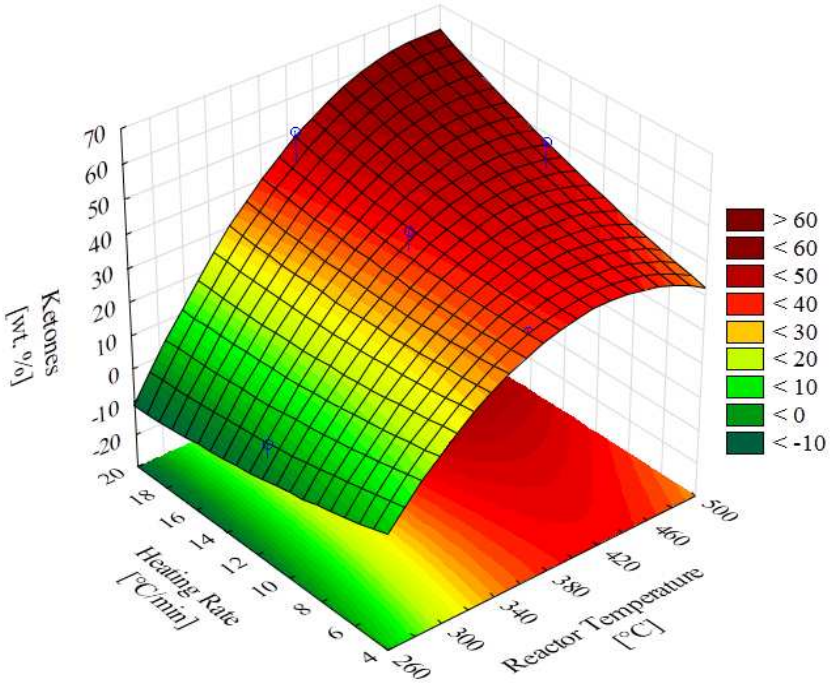

Figure 6-14: Evolution of Ketones in Slow Pyrolysis bio-oil

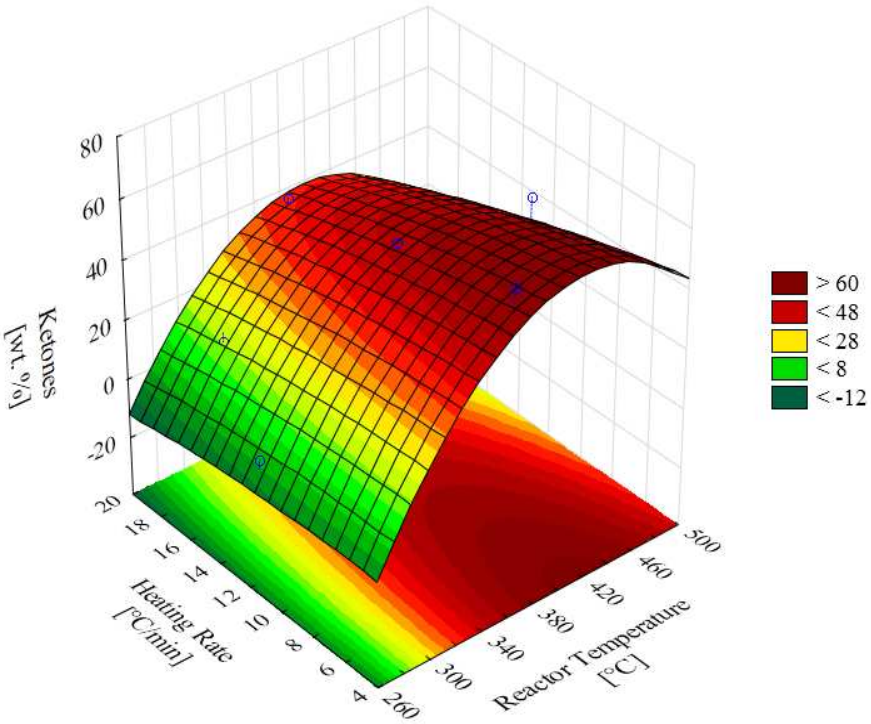

Figure 6-15: Evolution of Ketones in Vacuum Pyrolysis bio-oil

Cyclic compounds (C5)

The evolution of the 5-carbon cyclical/ring compounds are shown in **Figure 6-16** and **Figure 6-17** for Slow and Vacuum Pyrolysis bio-oils respectively. The accompanying ANOVA results are given in **Table 9-26** and **Table 9-27** of Appendix **9.3,** respectively. The ANOVA revealed significant linear influences for the reactor temperature for both reactor configurations investigated. Additional significant influences were found in the VP bio-oil results for the quadratic effects of the reactor temperature as well as the linear effects of heating rate. In both instances it was suggested by the trends observed that the formation of 5-carbon ring structures were favoured from the mid to high reactor temperatures investigated (300 – 500 °C) and that for VP, a further preference was shown toward the mid to lower heating rates (< 15 °C/min) investigated.

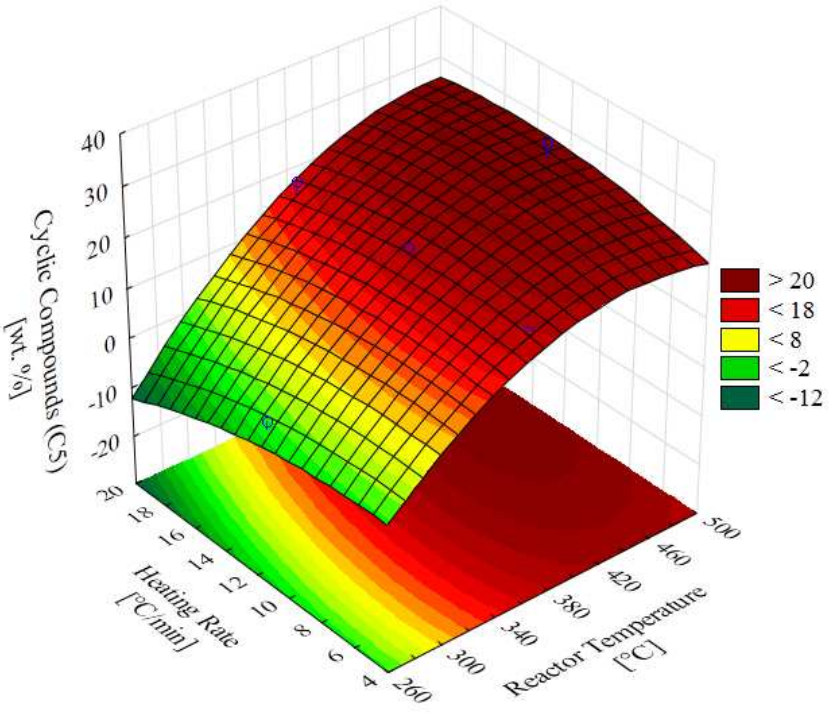

Figure 6-16: Evolution of Cyclic 5-carbon compounds in Slow Pyrolysis bio-oil

The preferred temperature range expressed by **Figure 6-16** and **Figure 6-17** furthermore correlated well with the accepted decomposition temperatures for the cellulose and hemicelluloses fractions found in biomass, as was discussed in section **6.2.1**. It is known that these lignocellulosic compounds are made up by linear and branched chains of anhydro-pyranose units (5-carbon ring sugars) as the chief monomeric structures (Fengel and Wegener, 2003). Under mild thermal degradation of these lignocellulosic compounds it was

therefore expected that 5-carbon ring structures will be formed in significant quantities as was seen in the abovementioned results.

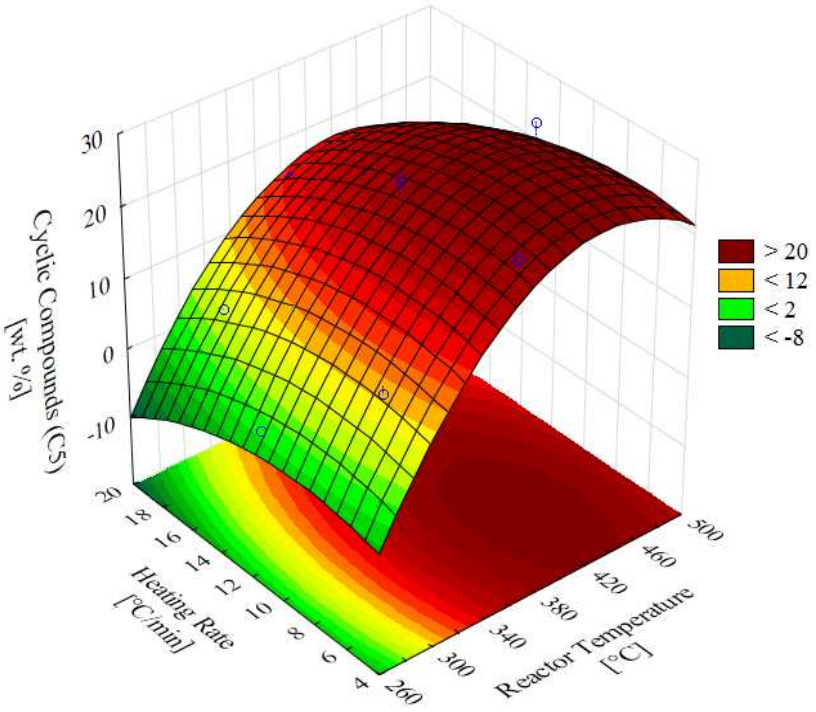

Figure 6-17: Evolution of Cyclic 5-carbon compounds in Vacuum Pyrolysis bio-oil

Furfural

Figure 6-18 and **Figure 6-19** show the evolution of furfural for the Slow and Vacuum Pyrolysis bio-oil, while the ANOVA results are presented in **Table 9-30** and **Table 9-31** of Appendix **9.3,** respectively. Even though an R^2 value of 0.8 or better could not be achieved in either of the surface plots for furfural, it was found that the ANOVA could identify significant effects at a 95 % confidence interval. Furthermore, it was shown in **Table 6-4** that furfural made out a significant portion of the total aldehyde contribution and that it was regarded as one of the most abundant individual compounds found in the pyrolysis bio-oils. Statistica was, however, not able to generate a good fit of aldehydes as a chemical family for both Slow and Vacuum Pyrolysis, nor could it identify significant interaction of the reactor temperature and heating rate at a 95 % confidence interval. It was therefore important to show the apparent trends and effects of furfural, as an indication of the behaviour of the aldehydes family.

Similar to the discussion of the Furans, it is evident that furfural originates from the thermal degradation of the hemicelluloses fraction of the biomass, which is known to contain various

4 and 5 carbon mono-saccharides in its macromolecular structure (Fengel and Wegener, 2003). This can be substantiated when considering the findings expressed in section **4.2.3.3** where it was shown that the hemicelluloses fraction of the biomass undergoes a thermal degradation rate maximum in the region of 250 – 300 °C, corresponding well with the furfural yield maxima showed in **Figure 6-18** and **Figure 6-19**.

The ANOVA revealed that reactor temperature had a significant (linear) influence on the yield of furfural for both Slow and Vacuum Pyrolysis, and that in both cases production of furfural was favoured toward the lower reactor temperatures investigated. It was also observed that the typical Furfural contribution was higher for Slow Pyrolysis compared to Vacuum Pyrolysis at the same temperature and heating rate. This might be an indication that a longer vapour residence time promotes the formation of this chemical compound.

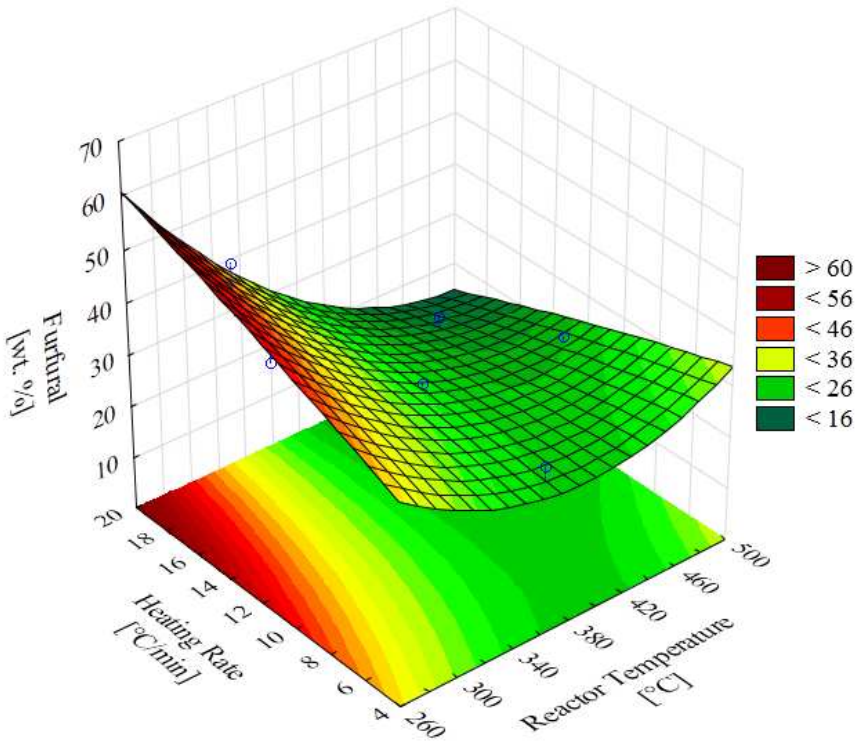

Figure 6-18: Evolution of Furfural in Slow Pyrolysis bio-oil

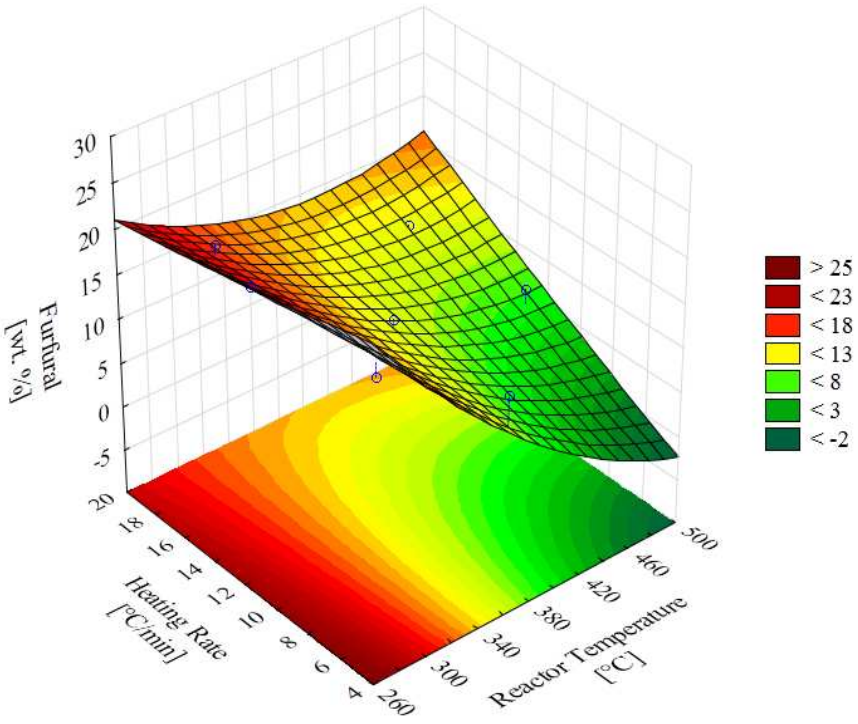

Figure 6-19: Evolution of Furfural in Vacuum Pyrolysis bio-oil

Sugars

Sugars were identified by searching for all compound names, detected with a certainty of 70 % or greater, ending with "-ose". The evolution of these sugar compounds could only be fitted with a satisfactory R^2 value (0.95) for the Slow Pyrolysis bio-oil **Figure 6-20**. It was found that the heating rate had a significant influence on the evolution of the sugars in the SP bio-oil and that lower heating rates favoured sugar yield (**Table 9-25**, Appendix **9.3**). As mentioned previously in Chapter **2.1**, the main lignocellulosic components of biomass are cellulose and hemicelluloses, which are poly-saccharide macrostructures with 4 and 5 carbon sugar molecules as their building blocks. One would then expect to see a significant sugar contribution in the bio-oil after thermal degradation had taken place, but the contrary was observed in **Figure 6-20**. This might be explained when considering the evolution of the furans and 5 carbon cyclic compounds as shown in **Figure 6-11** and **Figure 6-12**, and in **Figure 6-16** and **Figure 6-17** respectively. These curves would suggest that the majority of sugars were degraded to other functional groups under the specific process conditions employed.

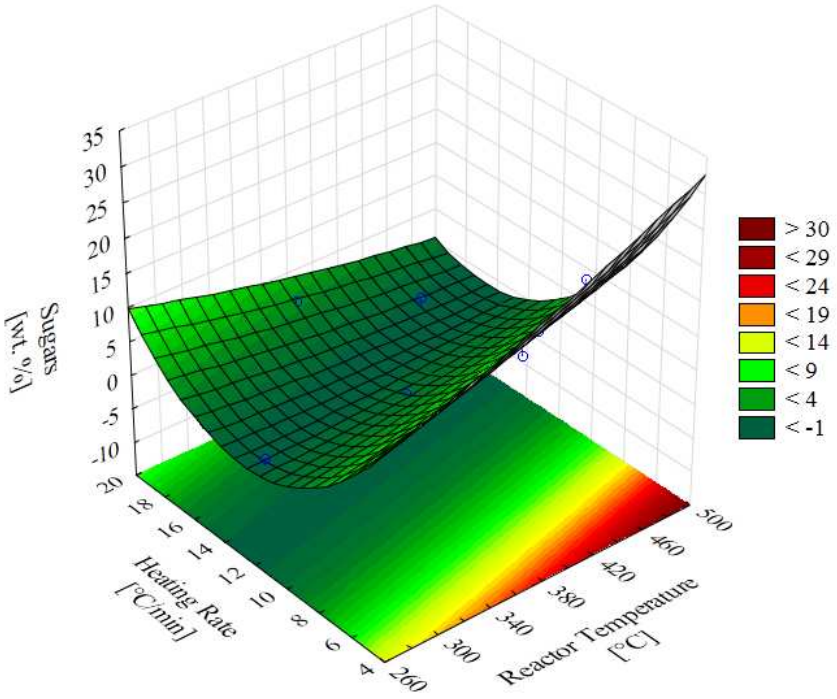

Figure 6-20: Evolution of Sugars in Slow Pyrolysis bio-oil

Phenols

The evolution of phenols is shown in **Figure 6-21** and **Figure 6-22** respectively for Slow and Vacuum Pyrolysis bio-oils. The accompanying ANOVA results are given in **Table 9-28** and **Table 9-29** of Appendix **9.3,** respectively for Slow and Vacuum Pyrolysis bio-oils. For both reactor configurations investigated, the ANOVA revealed significant (linear) interactions for the reactor temperature on the phenol yield at a confidence interval of 95 % as shown in **Table 9-28** and **Table 9-29**. The phenolic compounds typically found in bio-oil result from the decomposition of the lignin structure in biomass, as phenylpropane units are the main building blocks for this amorphous super structure (Fengel and Wegener, 2003). It has been reported that lignin decomposes over a wide temperature range and that the rate of decomposition is much lower than for the other lignocellulosic constituents (Raveendran *et al.,* 1996). The trends observed in **Figure 6-21** and **Figure 6-22** may then be explained by the known kinetics of the thermal degradation of lignin, where higher reactor temperatures will result in faster thermal degradation of lignin and a higher phenolic content of the bio-oil. A similar trend for the production of phenolic compounds in the bio-oil resulting from Vacuum Pyrolysis has been reported by Murwanashyaka *et al.,* (2001).

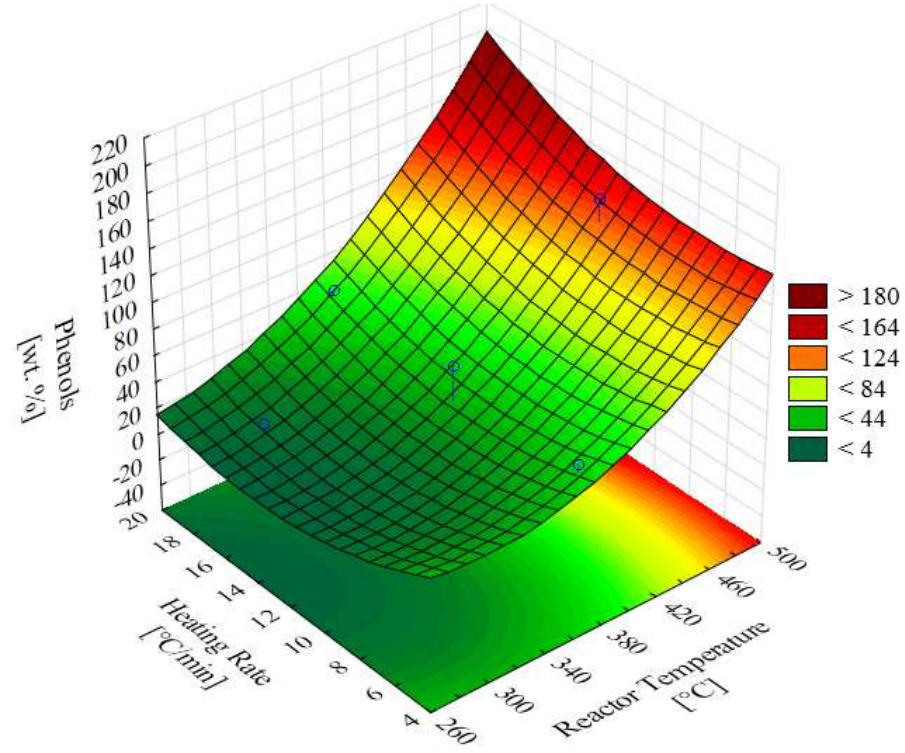

Figure 6-21: Evolution of Phenols in Slow Pyrolysis bio-oil

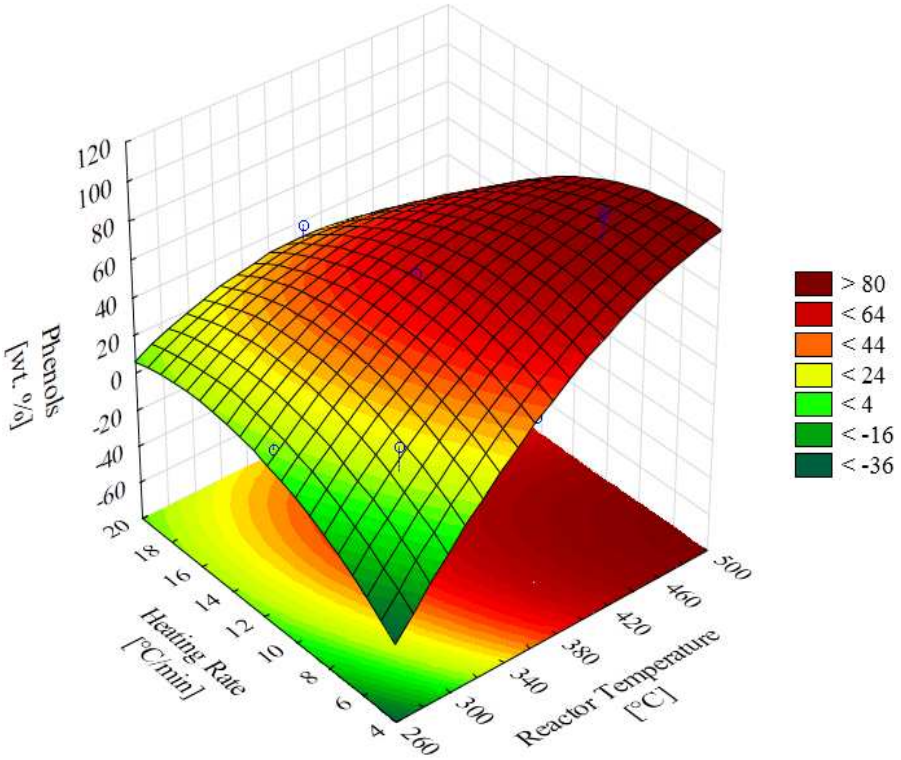

Figure 6-22: Evolution of Phenols in Vacuum Pyrolysis bio-oil

Molecular composition overview

After evaluating the evolution of the respective chemical families identified as a function of the chosen process variables, it was interesting to note the change in the relative contributions of the major chemical families. It was observed that the summative contributions of the acid, ketone, aldehyde and phenol families accounted for 77 to 99 % (91 % average) of the total chemical families detected with a certainty of + 70 %. **Figure 6-23** and **Figure 6-24** show the change in the relative composition of the bio-oil for Slow and Vacuum Pyrolysis respectively, for components detected with a certainty of + 70 %. For SP it was found that the ketone and phenol families showed a predominantly increasing trend with increasing reactor temperatures and heating rates, while the aldehyde and acid families showed a predominantly decreasing trend with increasing reactor temperatures and heating rates.

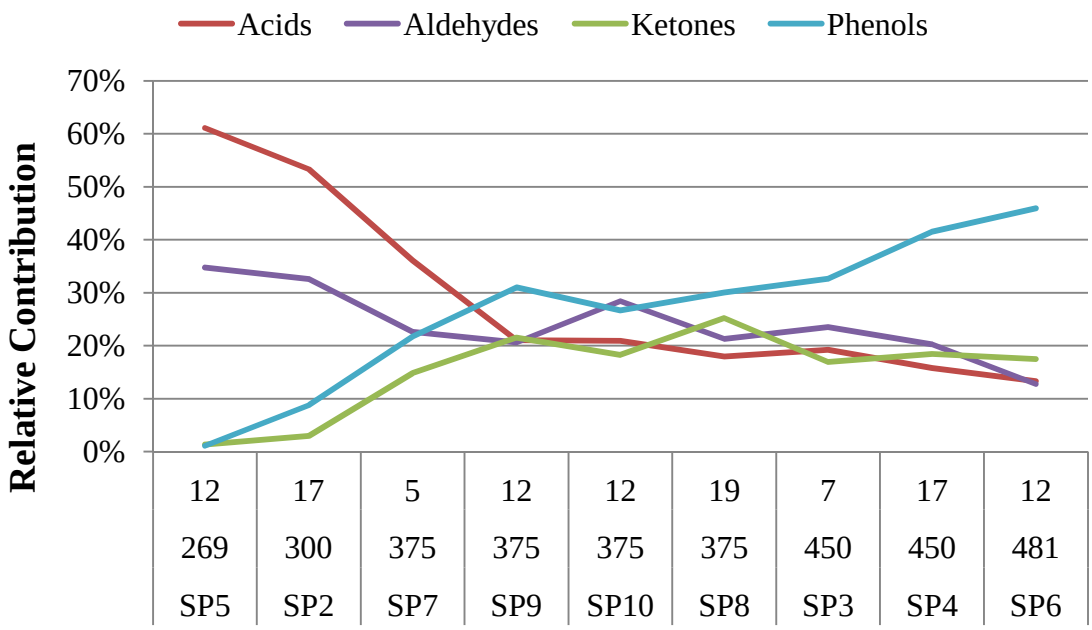

Figure 6-23: The relative contribution of chemical families in Slow Pyrolysis bio-oil

The same basic trend could be observed for the VP bio-oil composition with regard to reactor temperature, while the inverse was found the relationship with the chosen heating rates, as shown in **Figure 6-24**. For a set reactor temperature, an increase in the heating rate resulted in a decrease in the relative contributions of the ketones and phenols for the VP bio-oil, while the acids and aldehydes increased. For both the SP and VP compositions it was observed that an increase in the relative contributions of the ketones and phenols, from one run to the other, had a decreasing effect on the acids and vice versa. The general increasing phenol content, with increasing reactor temperature can be attributed to the increase in the lignin

decomposition rate at higher reactor temperatures, as the maximum rates of lignin volatilisation was found in the region of 375 to 425 °C (section **4.2.3.1**) depending on the heating rate employed.

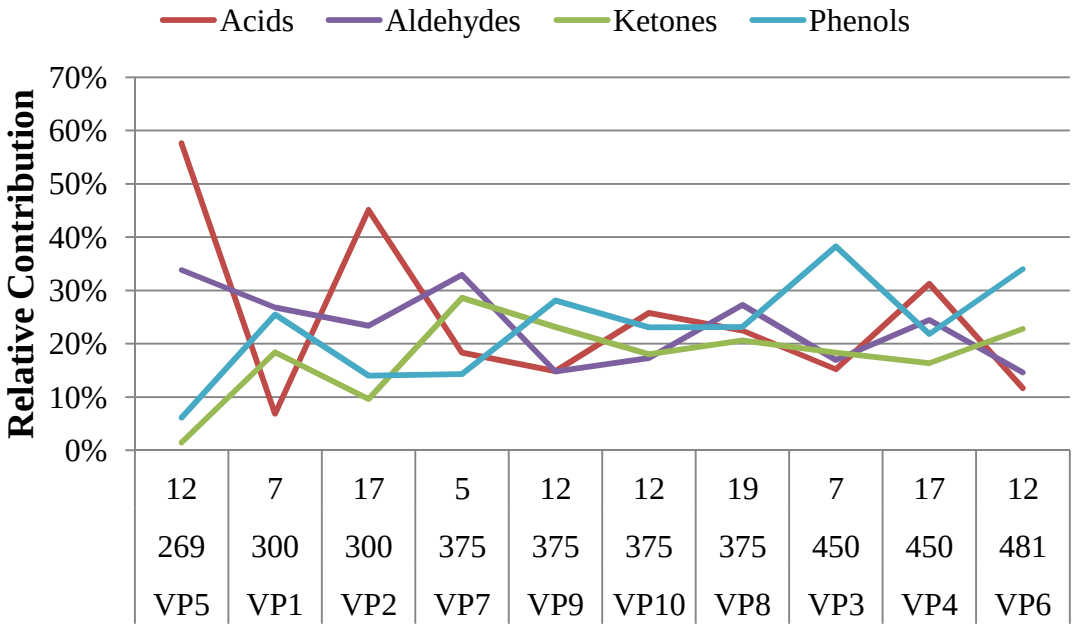

Figure 6-24: The relative contribution of chemical families in Vacuum Pyrolysis bio-oil

6.2.3.4 HHV of char

Figure 6-25 and **Figure 6-26** show the evolution of the measured HHV of the char produced using Slow and Vacuum Pyrolysis respectively. The accompanying ANOVA results are reported in **Table 9-32** and **Table 9-33** of Appendix **9.3,** respectively for Slow and Vacuum Pyrolysis char. The ANOVA showed that at a confidence interval of 95 % the reactor temperature had a significant linear influence on the calorific value of the char for Slow Pyrolysis, while for Vacuum Pyrolysis it was found that the influence of the reactor temperature was significant for both linear and quadratic interactions. Various studies have reported improved char quality with special reference to HHV at higher reactor temperatures (Carrier *et al.*, 2011a; Della Rocca *et al.*, 1999; Guerrero *et al.*, 2005; Kumar *et al.*, 1992). The HHV was found to be higher for the char produced via SP compared to char produced at similar operating conditions via VP.

This can be explained when considering the vapour residence times for the respective reactor configurations. As mentioned in previous discussions, the longer residence times found in SP facilitates secondary cracking and condensation reactions, increasing the char yield

(Bridgwater, 2003) and also increasing the HHV. It can also be postulated that the negative pressure in the reactor creates a strong driving force for the volatilisation and removal of organic vapours from the char matrix, stripping the char from more organic matter in VP compared to SP which is conducted at atmospheric pressure.

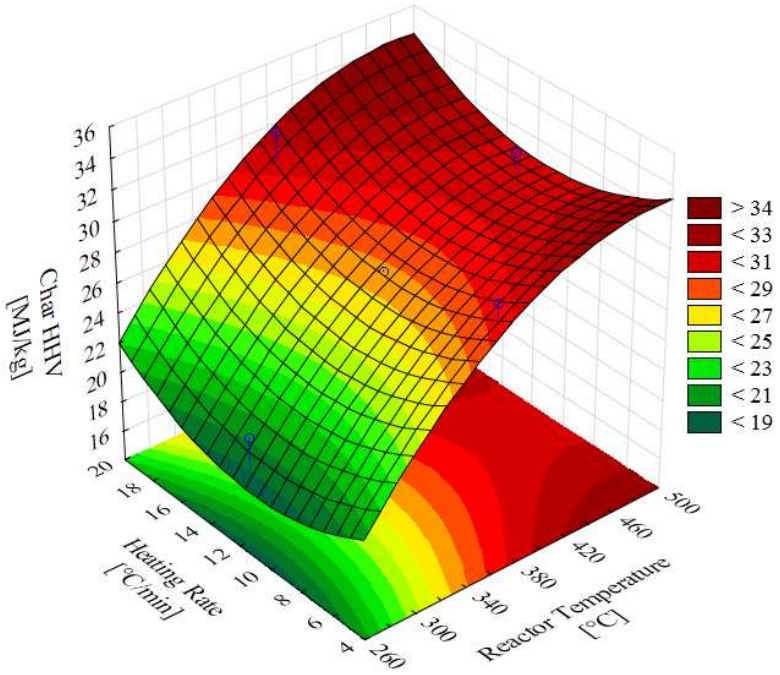

Figure 6-25: Evolution of the HHV for Slow Pyrolysis char

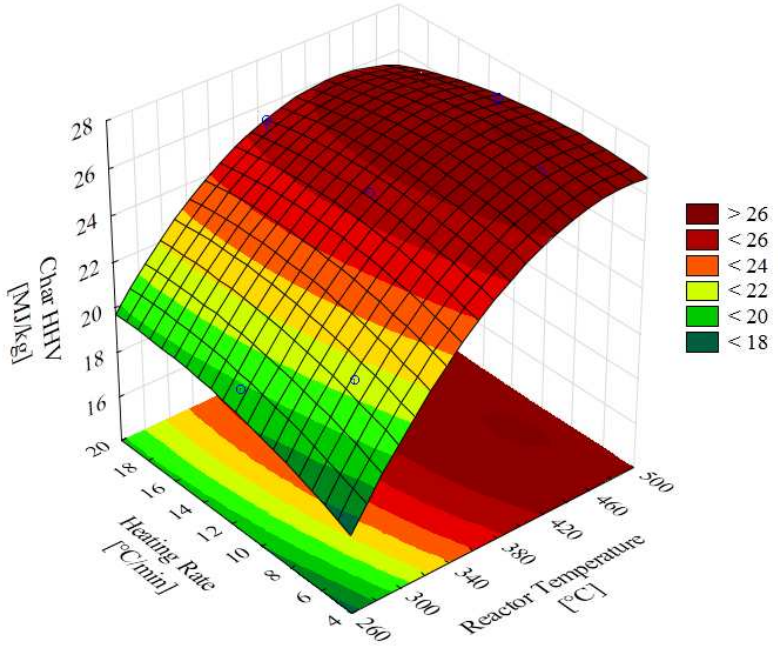

Figure 6-26: Evolution of the HHV for Vacuum Pyrolysis char

6.2.3.5 BET surface area of char

It was found during the de-gassing stage of the analysis that the char produced at low heating rates and/or low reactor temperatures, contained significant quantities of trapped organic volatiles. These volatiles contaminated the equipment and the char could not be de-gassed sufficiently in order to conduct the BET surface area determination. These effects were found to be more severe in the case of the Slow Pyrolysis chars, possibly due differences in the mass transfer gradient between Slow and Vacuum pyrolysis as a result of the differences in the absolute reactor pressures. Increased reactor pressure is believed to facilitate condensation and carbonisation reactions (Carrier *et al.*, 2011a; De Jongh *et al*., 2011) These observations support the hypothesis that the higher HHV values measured for SP, relative to VP, are partially due to the differences in the reactor pressure and retention times of the different reactor configurations as discussed in section **6.2.3.4**. In total, only 2 of the SP char samples and 6 of the VP char samples could be successfully analysed for BET surface areas; these results are given in **Table 6-5.**

The BET surface area values measured for the VP chars were much higher compared to that of the SP chars, especially for the chars prepared at reactor temperatures higher than 375 °C. The typical range of BET surface areas found for the chars produced under VP conditions at high reactor temperatures and heating rates in this investigation was similar to that found for teak sawdust in a study conducted by Ismadji *et al.*, (2005), suggesting that the VP char produced in this study could also possibly be a suitable precursor for activated carbon. Similar findings have also been reported for sugar cane bagasse using this reactor configuration (Carrier *et al.*, 2011a).

Table 6-5: BET surface areas for Slow and Vacuum Pyrolysis chars

Run ID	Reactor temperature [°C]	Heating rate [°C/min]	BET surface area [m^2/g]
VP 3	450	7	403.8
VP 4	450	17	436.0
VP 6	481	12	308.5
VP 7	375	5	154.3
VP 9	375	12	85.2
VP 10	375	12	239.4
SP 4	450	17	8.3
SP 6	481	12	12.3

6.3 Conclusions and recommendations

Based on the results achieved for the Slow and Vacuum Pyrolysis of *E.grandis* it may be concluded that:

- The rate of the overall pyrolysis reaction increased dramatically at ± 375 °C for both reactor configurations, but could not be quantified with desired precision.
- Vapour residence time played a major role as reflected in both the comparison of the product yields achieved as well as the product quality, as a result of secondary cracking and condensation side reactions.
- It was found that significant quantities of moisture accumulated in the reactor when SP conditions were employed.
- In general VP resulted in a higher bio-oil and lower char yield compared to that of SP.
- Liquid yields were maximised at high reactor temperatures and high reactor heating rates. Local liquid yield maxima of 41.1 and 64.4 wt. % daf were found for Slow and Vacuum Pyrolysis, respectively (achieved at a reactor temperature of 450 °C and a heating rate of 17 °C/min).
- Even though char yields were favoured at low reactor temperatures (269 – 300 °C), the higher heating values of the char were found to be favoured at high reactor temperatures (29 – 34 MJ/kg for 375 – 481 °C).
- Reactor temperature was found to be the most dominant process parameter investigated with significant influences found for most of the response parameters investigated. According to ANOVA the effect was more often than not a linear interaction and in some cases both linear and quadratic.
- Bio-oil was found to be rich in acetic acid and furfural.

Based on the results and conclusions of this chapter, the following recommendations are made:

- Installation of a sensitive pressure transducer and logging system can be very beneficial in monitoring and understanding the thermal behaviour of biomass under on a bench scale pyrolysis plant and is recommended for future studies.
- For future investigations the nitrogen flow rate should be increased, or modifications need to be made inside the reactor tube to prevent excessive condensation occurring

outside the heated zone during SP. A higher flow rate (possibly 100 – 200 ml/min) might prevent pyrolysis vapour pushing back the nitrogen feed and condensation taking place on the cold reactor walls outside the heated zone.

7 Conclusions and recommendations

The purpose of this study was to investigate and compare the Slow, Vacuum and Fast Pyrolysis of *E.grandis*, with specific reference to the objectives outlined in Chapter 1. The main findings and conclusions based on these objectives will now be summarised.

7.1 Objective 1:Literature review

From the literature review it was shown that the lignocellulosic composition of biomass is paramount in understanding and interpretering pyrolysis data, and that the study of the thermal degradation behaviour and pyrolysis kinetics of biomass facilitates the analysis and understanding of pyrolysis results. The literature review showed that pyrolysis data for *E.grandis* are very scarce (for Fast and Slow Pyrolysis) and difficult to compare with that of other biomass species. No data were available on the Vacuum Pyrolysis of *E.grandis*. These gaps in the literature review formed the motivation for:

- The lignocellulosic characterisation of the biomass (Chapters 3 and 5),
- Investigating the thermal degradation behaviour of *E.grandis* using TGA (Chapter4),
- Investigation and comparison of the Fast Pyrolysis of *E.grandis* using three different reactor configurations of different scale (Chapter 5), and
- Investigation and comparison of the Slow and Vacuum Pyrolysis of *E.grandis* using a packed bed reactor (Chapter 6)

7.2 Objective 2: Biomass characterisation

The lignocellulosic characterisation of *E.grandis* was carried out at the University of Stellenbosch in South Africa. It was found that the lignocellulosic composition of biomass may vary significantly between batches of biomass of the same species. It was found that batches 2 and 3 had similar lignocellulosic composition and that the values were comparable to literature findings, especially with regard to the lignin content (± 25 wt. % daf), while

batch 1 had a much lower lignin content (± 15 wt. % daf). Determining the cellulose and hemicelluloses fractions of biomass through HPLC analysis after total acid hydrolysis was found to be unreliable compared to the chemical extraction methods used for alpha-cellulose and holocellulose extractions.

7.3 Objective 3: Thermo-gravimetric analysis (TGA)

The thermal degradation behaviour of *E.grandis* and its main lignocellulosic components extracted from the biomass were studied using thermo-gravimetric analysis (TGA) at the Karlsruhe Institute of Technology in Germany. The generated data were analysed using the AKTS Thermo-Kinetics software package at the University of Stellenbosch, South Africa and used to determine the isoconversional activation energy and pre-exponential constant for virgin *E.grandis* and its lignocellulosic components – a novel contribution to the scientific field. Higher heating rates caused a shift in the thermo-gravimetric (TG) and differential thermo-gravimetric (DTG) curves. Lignin was found to generate the largest specific char yield while also having the widest thermal degradation range of all the samples investigated. Good correlation (above 95 %) was found for all the components investigated (except lignin) with average activation energies calculated as 177.8, 141.0, 106.2 and 170.4 kJ/mol for holocellulose, alpha-cellulose, Klason lignin and raw *E.grandis*, respectively.

7.4 Objectives 4 and 5: Fast Pyrolysis of *E.grandis* and reactor comparison

The Fast Pyrolysis of *E.grandis* was investigated using three reactor configurations of different scale the University of Stellenbosch ($SU_{1\ kg/h}$) and the Karlsruhe Institute of Technology ($KIT_{0.1\ kg/h}$ and $KIT_{10\ kg/h}$). With reactor temperature and biomass particle size as process variables, an optimum liquid yield of 76 wt. % (daf) could be achieved at 470 °C for the $SU_{1kg/h}$ FP plant using an average biomass particle size of 570 µm. In comparison with the reactor configurations used at KIT, it was found that differences in the condensation chain, especially with regard to solids handling had a significant effect on the quality of bio-oil produced. Extended contact of product vapour and condensates with pyrolysis char

increased the gas and char yield for the KIT reactor configurations compared to that of the $SU_{1\ kg/h}$ Fast Pyrolysis plant. The optimisation of the Fast Pyrolysis of *E.grandis* as well as the comparison of the Fast Pyrolysis of *E.grandis* at different scale have not before been conducted and are both novel contributions to the field as pyrolysis research.

7.5 Objective 6: The comparison of Slow and Vacuum Pyrolysis

The influence of reactor temperature and heating rate for the Slow and Vacuum Pyrolysis of *E.grandis* was investigated using a packed bed reactor at the University of Stellenbosch. Vacuum Pyrolysis resulted in a higher bio-oil and lower char yield compared to Slow Pyrolysis. Reactor temperature was found to have the most significant influence on the Vacuum and Slow Pyrolysis of *E.grandis*. The higher heating value of the char was optimised at higher reactor temperatures (375 – 481 °C). The bio-oil yielded from Slow and Vacuum Pyrolysis was found to be rich in acetic acid and furfural. The comparison of Slow and Vacuum Pyrolysis of *E.grandis* using the same reactor configuration has not been conducted before and is novel to the field of pyrolysis research.

7.6 Recommendations and future work

After completion of this study, the following recommendations and suggestions for future work can be made:

- In this study, the pyrolysis of *E.grandis* was investigated using biomass originating from the Mondi pulp mill in Richards Bay, South Africa. The biomass was therefore limited to the trunk section of the tree (provided as wood chips) and did not contain any branches, leaves or bark. It is recommended that future studies investigate the pyrolysis of these wood residues and compare the results to this work to gain a fuller picture of the use of *E.grandis* as a renewable energy source.
- From the thermo-gravimetric analysis done using *E.grandis* and its main lignocellulosic components, it was identified that Klason lignin was the only

component which could not be modelled by the AKTS Thermokinetics software package with acceptable correlation coefficients. It was postulated that the severity of the chemical treatment required for Klason lignin extraction caused structural changes to the macro-molecular configuration of the lignin, which affected its thermochemical behaviour. It is recommended that future studies investigate the thermal degradation behaviour of extracted lignin from *E.grandis* using alternative and less harsh extraction methods, such as milled wood lignin, or organosolv-lignin.

- The Fast Pyrolysis of *E.grandis* using the $SU_{1\ kg/h}$ reactor configuration identified the need to re-evaluate the use of Isopar as a quenching medium. The significance of the experienced colour change needs to be investigated and quantified.

- It was also found that the experimental run length using the $SU_{1\ kg/h}$ reactor configuration was limited by die nitrogen supply. It is therefore recommended that the plant be modified to accommodate longer experimental runs by including additional nitrogen cylinders to the nitrogen feed system to ensure seamless transition when one of the nitrogen cylinders runs empty.

- For future Slow and Vacuum Pyrolysis experimental work it is recommended to install a pressure transducer with accompanying logging system to quantify the extent and magnitude of volatilisation within the reactor at different heating rates and reactor temperatures.

- It is also recommended that the flow rate used for future Slow Pyrolysis experiments be increased (possibly 100 – 200 ml/min) to help prevent condensation occurring within the reactor.

- Finally, it is recommended that future studies investigate the economic feasibility and environmental impact of biomass pyrolysis in South Africa, taking into account government's directive to diversify the energy supply in the short to medium term.

8 References

Aboyade, A.O., Hugo, T.J., Carrier, M., Meyer, E.L., Stahl, R., Knoetze, J.H. & Görgens, J.F. 2011, "Non-isothermal kinetic analysis of the devolatilization of corn cobs and sugar cane bagasse in an inert atmosphere", *Thermochimica Acta*, vol. 517, no. 1-2, pp. 81-89.

Agblevor, F.A., Beis, S., Kim, S.S., Tarrant, R. & Mante, N.O. 2010, "Biocrude oils from the fast pyrolysis of poultry litter and hardwood", *Waste Management*, vol. 30, no. 2, pp. 298-307.

Azeez, A.M., Meier, D., Odermatt, J. & Willner, T. 2010, "Fast pyrolysis of African and European lignocellulosic biomasses using Py-GC/MS and fluidized bed reactor", *Energy and Fuels*, vol. 24, no. 3, pp. 2078-2085.

Barneto, A.G., Hernandez, R.B. & Berenguer, J.M. 2011, "Thermogravimetric characterization of eucalyptus wood", *O Papel*, vol. 72, no. 7, pp. 53-56.

Bridgwater, A.V. 2003, "Renewable fuels and chemicals by thermal processing of biomass", *Chemical Engineering Journal*, vol. 91, no. 2-3, pp. 87-102.

Bridgwater, A.V. 2004, *Therm.Sci.*, vol. 8, pp. 21.

Bridgwater, A.V. 2011, "Review of fast pyrolysis of biomass and product upgrading", *Biomass and Bioenergy*, , no. 0.

Browning, B.L. 1967, *Methods of Wood Chemistry*, John Wiley & Sons, Inc., United States of America.

Carrier, M., Hugo, T., Gorgens, J. & Knoetze, H. 2011a, "Comparison of slow and vacuum pyrolysis of sugar cane bagasse", *Journal of Analytical and Applied Pyrolysis*, vol. 90, no. 1, pp. 18-26.

Carrier, M., Loppinet-Serani, A., Denux, D., Lasnier, J., Ham-Pichavant, F., Cansell, F. & Aymonier, C. 2011b, "Thermogravimetric analysis as a new method to determine the lignocellulosic composition of biomass", *Biomass and Bioenergy*, vol. 35, no. 1, pp. 298-307.

Channiwala, S.A. & Parikh, P.P. 2002, "A unified correlation for estimating HHV of solid, liquid and gaseous fuels", *Fuel*, vol. 81, no. 8, pp. 1051-1063.

Commandre, J.-., Lahmidi, H., Salvador, S. & Dupassieux, N. 2011, "Pyrolysis of wood at high temperature: The influence of experimental parameters on gaseous products.", *Fuel Processing Technology*, , no. 92, pp. 837--844.

Cox Phillip (2011),"Mondi forestry operations",Personal Communication, Kwambonambi; Kwa-Zulu Natal; South Africa.

Czernik, S. & Bridgwater, A.V. 2004, "Overview of applications of biomass fast pyrolysis oil", *Energy and Fuels*, vol. 18, no. 2, pp. 590-598.

Da Silva, M., Andreia, Luiz, J., Colodette, Gomes, De Fatima, Adriana, Gouvea, Livio, J., Gomide, Dos Santos, Marcello, Coelho, Muguet & Pedrazzi, C. 2009, "Eucalyptus wood quality and its impact on kraft pulp production and use", *Tappi Journal*, , pp. 32-39.

de Jongh, W.A., Carrier, M. & Knoetze, J.H. 2011, "Vacuum pyrolysis of intruder plant biomasses", *Journal of Analytical and Applied Pyrolysis*, vol. 92, pp. 184--193.

Della Rocca, P.A., Cerrella, E.G., Bonelli, P.R. & Cukierman, A.L. 1999, "Pyrolysis of hardwoods residues: On kinetics and chars characterization", *Biomass and Bioenergy*, vol. 16, no. 1, pp. 79-88.

Demirbaş, A. 2005, "Relationship between initial moisture content and the liquid yield from pyrolysis of sawdust", *Energy Sources*, vol. 27, no. 9, pp. 823-830.

Demirbas, A. 2007, "The influence of temperature on the yields of compounds existing in bio-oils obtained from biomass samples via pyrolysis", *Fuel Processing Technology*, vol. 88, no. 6, pp. 591-597.

Di Blasi, C. 2008, "Modeling chemical and physical processes of wood and biomass pyrolysis", *Progress in Energy and Combustion Science*, vol. 34, no. 1, pp. 47-90.

dos Santos, F.J. & Goldstein Jr., L. 2008, "Experimental aspects of biomass fuels in a bubbling fluidized bed combustor", *Chemical Engineering and Processing: Process Intensification*, vol. 47, no. 9-10, pp. 1541-1549.

Elyounssi, K., Blin, J. & Halim, M. 2010, "High-yield charcoal production by two-step pyrolysis", *Journal of Analytical and Applied Pyrolysis*, vol. 87, no. 1, pp. 138-143.

Fahmi, R., Bridgwater, A.V., Donnison, I., Yates, N. & Jones, J.M. 2008, "The effect of lignin and inorganic species in biomass on pyrolysis oil yields, quality and stability", *Fuel*, vol. 87, no. 7, pp. 1230-1240.

Fengel, D. & Wegener, G. 2003, *Wood Chemistry, Ultrastructure, Reactions*, Verlag Kessel, Germany.

Garcia-Perez, M., Chaala, A., Pakdel, H., Kretschmer, D. & Roy, C. 2007, "Characterization of bio-oils in chemical families", *Biomass and Bioenergy*, vol. 31, no. 4, pp. 222-242.

Garcia-Perez, M., Wang, X.S., Shen, J., Rhodes, M.J., Tian, F., Lee, W., Wu, H. & Li, C. 2008, "Fast Pyrolysis of Oil Mallee Woody Biomass: Effect of Temperature on the Yield and Quality of Pyrolysis Products", *Ind Eng Chem Res*, vol. 47, pp. 1846-1854.

Godsmark, R. 2010, "Forestry South Africa Roundwood Sales Analysis for the 2009 Financial Year", Forestry South Africa, .

Graham, R.G., Bergougnou, M.A. & Freel, B.A. 1994, "The kinetics of vapour-phase cellulose fast pyrolysis reactions", *Biomass and Bioenergy*, vol. 7, no. 1-6, pp. 33-47.

Guerrero, M., Ruiz, M.P., Alzueta, M.U., Bilbao, R. & Millera, A. 2005, "Pyrolysis of eucalyptus at different heating rates: Studies of char characterization and oxidative reactivity", *Journal of Analytical and Applied Pyrolysis*, vol. 74, no. 1-2, pp. 307-314.

Guerrero, M., Ruiz, M.P., Millera, A., Alzueta, M.U. & Bilbao, R. 2008a, "Characterization of biomass chars formed under different devolatilization conditions: Differences between rice husk and Eucalyptus", *Energy and Fuels*, vol. 22, no. 2, pp. 1275-1284.

Guerrero, M., Ruiz, M.P., Millera, A., Alzueta, M.U. & Bilbao, R. 2008b, "Oxidation kinetics of eucalyptus chars produced at low and high heating rates", *Energy and Fuels*, vol. 22, no. 3, pp. 2084-2090.

Henrich, E., Dahmen, N. & Dinjus, E. 2009, *Biofuels, Bioprod.Bioref.*, vol. 3, pp. 28.

Hugo, T. 2010, *Pyrolysis of sugarcane bagasse*, University of Stellenbosch.

Ismadji, S., Sudaryanto, Y., Hartono, S.B., Setiawan, L.E.K. & Ayucitra, A. 2005, "Activated carbon from char obtained from vacuum pyrolysis of teak sawdust: pore structure and characterisation", *Bioresource technology*, vol. 96, pp. 1364-1369.

Kumar, G., Panda, A.K. & Singh, R. 2010, "Optimization of process for the production of bio-oil from eucalyptus wood", *Journal of Fuel Chemistry and Technology*, vol. 38, no. 2, pp. 162-167.

Kumar, M., Gupta, R.C. & Sharma, T. 1992, "Effects of carbonisation conditions on the yield and chemical composition of Acacia and Eucalyptus wood chars", *Biomass and Bioenergy*, vol. 3, no. 6, pp. 411-417.

Lehmann, J., Da Silva, J.P.J., Steiner, C., Nehls, T., Zech, W. & Glaser, B. 2003, "Nutrient availability and leaching in an archaeological Anthrosol amd a Ferrasol of the Central Amazon basin: fertilizer, manure and charcoal amendments", *Plant and Soil*, vol. 249, pp. 343-357.

Lv, D., Xu, M., Liu, X., Zhan, Z., Li, Z. & Yao, H. 2010, "Effect of cellulose, lignin, alkali and alkaline earth metallic species on biomass pyrolysis and gasification", *Fuel Processing Technology*, vol. 91, pp. 903-909.

Maggi, R. & Delmon, B. 1994, *Fuel*, vol. 73, pp. 671.

Martins, A.F., Cardoso, A.d.L., Stahl, J.A. & Diniz, J. 2007, "Low temperature conversion of rice husks, eucalyptus sawdust and peach stones for the production of carbon-like adsorbent", *Bioresource technology*, vol. 98, no. 5, pp. 1095-1100.

Meier, D. & Faix, O. 1999, "State of the art of applied fast pyrolysis of lignocellulosic materials — a review", *Bioresource technology*, vol. 68, no. 1, pp. 71-77.

Mohan, D., Pittman, , Charles U. & Steele, P.H. 2006, "Pyrolysis of Wood/Biomass for Bio-oil:â€‰ A Critical Review", *Energy Fuels*, vol. 20, no. 3, pp. 848-889.

Mourant, D., Yang, D.-., Lu, X. & Roy, C. 2005, *Wood and Fiber Science*, vol. 37, pp. 542.

Murwanashyaka, J.N., Pakdel, H. & Roy, C. 2001, "Step-wise and one-step vacuum pyrolysis of birch-derived biomass to monitor the evolution of phenols", *Journal of Analytical and Applied Pyrolysis*, vol. 60, no. 2, pp. 219-231.

Nowakowski, D.J., Bridgwater, A.V., Elliott, D.C., Meier, D. & de Wild, P. 2010, "Lignin fast pyrolysis: Results from an international collaboration", *Journal of Analytical and Applied Pyrolysis*, , pp. 53-72.

Oasmaa, A. & Czernik, S. 1999, "Fuel oil quality of biomass pyrolysis oils - state of the art for the end users", *Energy and Fuels*, vol. 13, no. 4, pp. 914-921.

Oasmaa, A., Solantausta, Y., Arpiainen, V., Kuoppala, E. & SipilaÌˆ, K. 2010, "Fast Pyrolysis Bio-Oils from Wood and Agricultural Residues", *Energy & Fuels*, vol. 24, no. 2, pp. 1380-1388.

Orfão, J.J.M., Antunes, F.J.A. & Figueiredo, J.L. 1999, "Pyrolysis kinetics of lignocellulosic materials - Three independent reactions model", *Fuel*, vol. 78, no. 3, pp. 349-358.

Órfão, J.J.M. & Figueiredo, J.L. 2001, "A simplified method for determination of lignocellulosic materials pyrolysis kinetics from isothermal thermogravimetric experiments", *Thermochimica Acta*, vol. 380, no. 1, pp. 67-78.

Peters, D. 2011, "Electricity Regulations on the Integrated Resource Plan 2010 - 2030", *Government Gazette, Republic of South Africa*, vol. 551, no. 9531, pp. 1--80.

Pimenta, A.S., Vital, B.R., Bayona, J.M. & Alzaga, R. 1998, "Characterisation of polycyclic aromatic hydrocarbons in liquid products from pyrolysis of Eucalyptus grandis by supercritical fluid extraction and GC/MS determination", *Fuel*, vol. 77, no. 11, pp. 1133-1139.

Pindoria, R.V., Megaritis, A., Messenböck, R.C., Dugwell, D.R. & Kandiyoti, R. 1998, "Comparison of the pyrolysis and gasification of biomass: Effect of reacting gas atmosphere and pressure on Eucalyptus wood", *Fuel*, vol. 77, no. 11, pp. 1247-1251.

Poletto, M., Pistor, V., Zeni, M. & Zattera, A.J. 2011, "Crystalline properties and decomposition kinetics of cellulose fibers in wood pulp obtained by two pulping processes", *Polymer Degradation and Stability*, vol. 96, no. 4, pp. 679-685.

Raveendran, K. & Ganesh, A. 1996, "Heating value of biomass and biomass pyrolysis products", *Fuel*, vol. 75, no. 15, pp. 1715-1720.

Raveendran, K., Ganesh, A. & Khilar, K.C. 1996, "Pyrolysis characteristics of biomass and biomass components", *Fuel*, vol. 75, no. 8, pp. 987-998.

Rencoret, J., Gutiérrez, A. & del Río, C., José 2007, "Lipid and lignin composition of woods from different eucalypt species", *Holzforschung*, vol. 61, pp. 165-174.

Roy, C., Pakdel, H. & Brouillard, D. 1992, "The Role of Extractives During Vacuum Pyrolysis of Wood", *Journal of Applied Polymer Science*, vol. 41, no. 1992, pp. 337.

Şensöz, S. 2003, "Slow pyrolysis of wood barks from *Pinus brutia* Ten. and product composition", *Bioresource technology*, vol. 89, pp. 307-311.

Shen, J., Wang, X., Garcia-Perez, M., Mourant, D., Rhodes, M.J. & Li, C. 2009, "Effects of particle size on the fast pyrolysis of oil mallee woody biomass", *Fuel*, vol. 88, no. 10, pp. 1810-1817.

Sipilä, K., Kuoppala, E., Fagernäs, L. & Oasmaa, A. 1998, "Characterization of biomass-based flash pyrolysis oils", *Biomass and Bioenergy*, vol. 14, no. 2, pp. 103-113.

Sluiter, A., Ruiz, R., Scarlata, C., Sluiter, J. & Templeton, D. 2005, *Determination of Extractives in Biomass*, NREL Biomass Program, Biomass Analysis Technology Team, Department of Energy, United States of America.

StatSoft, Inc. (2011). STATISTICA (data analysis software system), version 10. www.statsoft.com.

Stenseng, M., Jensen, A. & Dam-Johansen, K. 2001, "Investigation of biomass pyrolysis by thermogravimetric analysis and differential scanning calorimetry", *Journal of Analytical and Applied Pyrolysis*, vol. 58-59, pp. 765-780.

Swart (ed)(2012),"Variation in the wood composition of biomass used in the south african paper and pulp industry",Personal Communication, Department of Forestry, Stellenbosch University.

Tancredi, N., Cordero, T., Rodríguez-Mirasol, J. & Rodríguez, J.J. 1996, "Activated carbons from Uruguayan eucalyptus wood", *Fuel*, vol. 75, no. 15, pp. 1701-1706.

Van de Velden, M., Baeyens, J., Brems, A., Janssens, B. & Dewil, R. 2010, "Fundamentals, kinetics and endothermicity of the biomass pyrolysis reaction", *Renewable Energy*, vol. 35, no. 1, pp. 232-242.

Vasile, C., Popescu, C., Popescu, M., Brebu, M., Argyropoulos, D.S. & Willfor, S. 2009, "Thermal behaviour/treatment of some vegetable residues. IV. Thermal decomposition of eucalyptus wood", *The 5th ISFR*Chengdu, China, pp. 193.

Vena Phumla (2011),"Characterisation of biomass - low lignin content of *E.grandis*", Personal Communication, Department of Process Engineering, University of Stellenbosch.

Vyazovkin, S., Burnham, A.K., Criado, J.M., Pérez-Maqueda, L.A., Popescu, C. & Sbirrazzuoli, N. 2011, "ICTAC Kinetics Committee recommendations for performing kinetic computations on thermal analysis data", *Thermochimica Acta*, vol. 520, no. 1-2, pp. 1-19.

Yaman, S. 2004, "Pyrolysis of biomass to produce fuels and chemical feedstocks", *Energy conversion and management*, vol. 45, no. 5, pp. 651-671.

Zhang, Q. 2007, "Review of biomass pyrolysis oil properties and upgrading research", *Energy conversion and management*, vol. 48, no. 1, pp. 87-92.

9 Appendix

9.1 Thermo-gravimetric curves for *E.grandis*

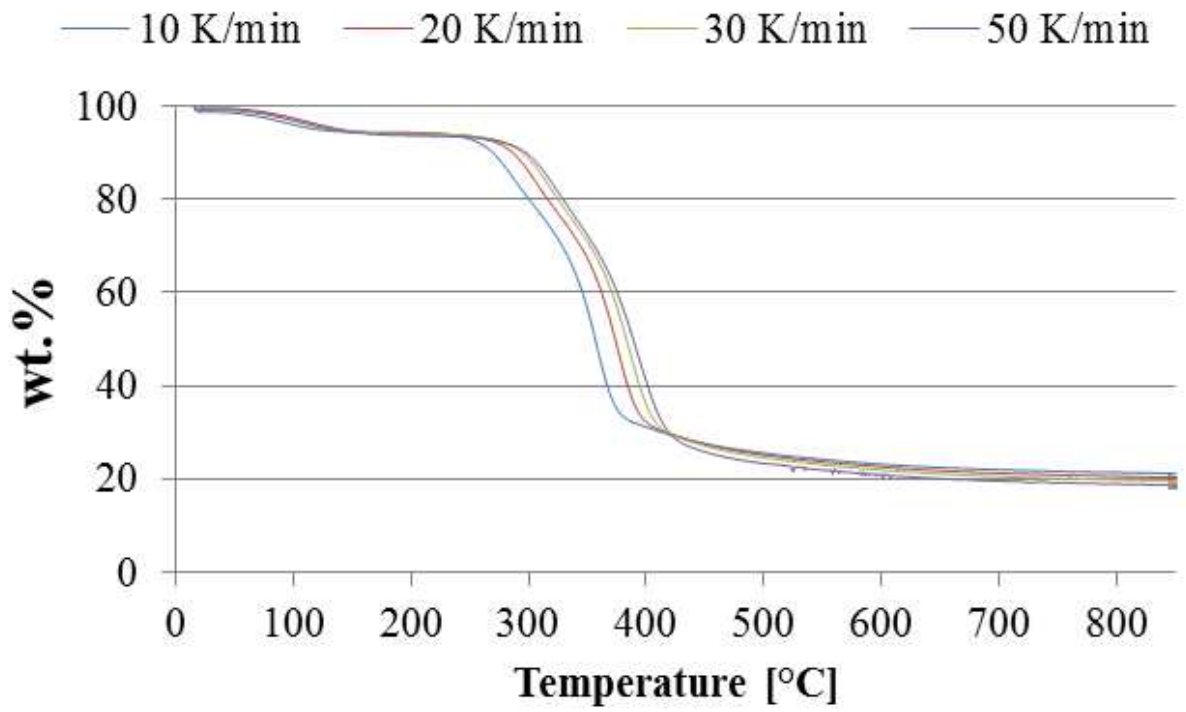

Figure 9-1: TGA curves for *E.grandis* at different heating rates

9.2 ANNOVA tables for Fast Pyrolysis

Table 9-1: ANOVA table for Fast Pyrolysis bio-oil yield

	Liquid Yield; R-sqr=.75768; Adj:.61229				
Factor	SS	df	MS	F	p
(1)Reactor Temperature L+Q	228.0227	2	114.0113	7.101266	0.034596
(2)Average Particle Size L	27.6767	1	27.6767	1.723858	0.246225
Error	80.2754	5	16.0551		
Total SS	331.2822	8			

Table 9-2: ANOVA table for Fast Pyrolysis bio-oil organic yield

Factor	Bio-oil Organic Yield; R-sqr=.78203; Adj:.65125				
	SS	df	MS	F	p
(1)Reactor Temperature(L)	81.5190	1	81.51898	9.696891	0.026431
Reactor Temperature(Q)	1.6916	1	1.69155	0.201214	0.672514
(2)Average Particle Size(L)	49.6742	1	49.67416	5.908868	0.059321
Error	42.0336	5	8.40671		
Total SS	192.8401	8			

Table 9-3: ANOVA table for Fast Pyrolysis char yield

Factor	Char Yield; R-sqr=.66166; Adj:.45866				
	SS	df	MS	F	p
(1)Reactor Temperature(L)	16.86268	1	16.86268	8.158997	0.035556
Reactor Temperature(Q)	0.24332	1	0.24332	0.117732	0.745463
(2)Average Particle Size(L)	1.20675	1	1.20675	0.583884	0.479281
Error	10.33379	5	2.06676		
Total SS	30.54296	8			

Table 9-4: ANOVA table for Fast Pyrolysis gas yield

Factor	Gas Yield; R-sqr=.81291; Adj:.70066				
	SS	df	MS	F	p
(1)Reactor Temperature(L)	298.8143	1	298.8143	17.06716	0.009074
Reactor Temperature(Q)	2.8274	1	2.8274	0.16149	0.704389
(2)Average Particle Size(L)	17.3702	1	17.3702	0.99212	0.364955
Error	87.5407	5	17.5081		
Total SS	467.9122	8			

Table 9-5: ANOVA table for Fast Pyrolysis pyrolytic water yield

Factor	Pyrolytic Water Yield; R-sqr=.64489; Adj:.43183				
	SS	df	MS	F	p
(1)Reactor Temperature(L)	17.03179	1	17.03179	5.687351	0.062789
Reactor Temperature(Q)	0.76627	1	0.76627	0.255876	0.634474
(2)Average Particle Size(L)	3.14027	1	3.14027	1.048615	0.352791
Error	14.97340	5	2.99468		
Total SS	42.16580	8			

Table 9-6: ANOVA table for Fast Pyrolysis char HHV

Factor	HHV Char; R-sqr=.70094; Adj:.5215				
	SS	df	MS	F	p
(1)Reactor Temperature(L)	15.71712	1	15.71712	10.42099	0.023254
Reactor Temperature(Q)	0.02566	1	0.02566	0.01701	0.901310
(2)Average Particle Size(L)	0.00536	1	0.00536	0.00355	0.954788
Error	7.54109	5	1.50822		
Total SS	25.21600	8			

Table 9-7: ANOVA table for Fast Pyrolysis bio-oil HHV

Factor	HHV Liquid Phase; R-sqr=.6205; Adj:.3928				
	SS	df	MS	F	p
(1)Reactor Temperature(L)	0.448891	1	0.448891	2.068354	0.209902
Reactor Temperature(Q)	0.006753	1	0.006753	0.031116	0.866905
(2)Average Particle Size(L)	1.085387	1	1.085387	5.001134	0.075563
Error	1.085141	5	0.217028		
Total SS	2.859376	8			

Table 9-8: ANOVA table for Fast Pyrolysis bio-oil pH

Factor	pH; R-sqr=.54974; Adj:.27958				
	SS	df	MS	F	p
(1)Reactor Temperature(L)	0.042579	1	0.042579	4.125919	0.097957
Reactor Temperature(Q)	0.014199	1	0.014199	1.375880	0.293638
(2)Average Particle Size(L)	0.027600	1	0.027600	2.674419	0.162900
Error	0.051600	5	0.010320		
Total SS	0.114600	8			

Table 9-9: ANOVA table for Fast Pyrolysis bio-oil viscosity

Factor	Viscosity; R-sqr=.82838; Adj:.7254				
	SS	df	MS	F	p
(1)Reactor Temperature(L)	10.7775	1	10.7775	1.04533	0.353480
Reactor Temperature(Q)	24.3078	1	24.3078	2.35765	0.185264
(2)Average Particle Size(L)	203.8545	1	203.8545	19.77215	0.006724
Error	51.5509	5	10.3102		
Total SS	300.3722	8			

9.3 ANNOVA tables for Slow and Vacuum Pyrolysis

Table 9-10: ANOVA table for Slow Pyrolysis bio-oil yield.

Factor	Liquid Yield; R-sqr=.9497; Adj:.88683 (Slow data)				
	SS	df	MS	F	p
(1)Temperature (L)	1316.192	1	1316.192	64.59455	0.001301
Temperature (Q)	137.591	1	137.591	6.75255	0.060139
(2)Heating Rate (L)	41.739	1	41.739	2.04842	0.225614
Heating Rate (Q)	0.025	1	0.025	0.00122	0.973790
1L by 2L	11.289	1	11.289	0.55403	0.498025
Error	81.505	4	20.376		
Total SS	1620.439	9			

Table 9-11: ANOVA table for Vacuum Pyrolysis bio-oil yield.

Factor	Liquid Yield; R-sqr=.97346; Adj:.94028 (Vacuum data)				
	SS	df	MS	F	p
(1)Temp (L)	2247.922	1	2247.922	107.5674	0.000488
Temp (Q)	334.504	1	334.504	16.0067	0.016119
(2)Heating rate(L)	445.424	1	445.424	21.3144	0.009905
Heating rate(Q)	5.745	1	5.745	0.2749	0.627774
1L by 2L	3.033	1	3.033	0.1451	0.722619
Error	83.591	4	20.898		
Total SS	3149.506	9			

Table 9-12: ANOVA table for Slow Pyrolysis char yield.

Factor	Char; R-sqr=.85687; Adj:.67796 (Slow data)				
	SS	df	MS	F	p
(1)Temp (L)	1750.749	1	1750.749	14.55036	0.018867
Temp (Q)	367.600	1	367.600	3.05510	0.155400
(2)Heating Rate(L)	213.923	1	213.923	1.77790	0.253274
Heating Rate(Q)	6.746	1	6.746	0.05606	0.824461
1L by 2L	408.780	1	408.780	3.39734	0.139083
Error	481.294	4	120.323		
Total SS	3362.700	9			

Table 9-13: ANOVA table for Slow Pyrolysis char yield.

Factor	Char; R-sqr=.98971; Adj:.97685 (Vacuum data)				
	SS	df	MS	F	p
(1)Temp (L)	3228.882	1	3228.882	320.6274	0.000057
Temp (Q)	498.718	1	498.718	49.5226	0.002149
(2)Heating rate(L)	31.194	1	31.194	3.0975	0.153220
Heating rate(Q)	0.085	1	0.085	0.0084	0.931321
1L by 2L	0.226	1	0.226	0.0224	0.888176
Error	40.282	4	10.071		
Total SS	3915.513	9			

Table 9-14: ANOVA table for Slow Pyrolysis gas yield.

Factor	Gas Yield; R-sqr=.87675; Adj:.72269 (Slow data)				
	SS	df	MS	F	p
(1)Temp (L)	456.6773	1	456.6773	18.53299	0.012596
Temp (Q)	182.5165	1	182.5165	7.40693	0.052901
(2)Heating Rate(L)	27.3134	1	27.3134	1.10844	0.351817
Heating Rate(Q)	13.9497	1	13.9497	0.56611	0.493663
1L by 2L	29.8037	1	29.8037	1.20950	0.333171
Error	98.5652	4	24.6413		
Total SS	799.7284	9			

Table 9-15: ANOVA table for Vacuum Pyrolysis gas yield.

Factor	Gas Yield; R-sqr=.66598; Adj:.24845 (Vacuum data)				
	SS	df	MS	F	p
(1)Temp (L)	88.5669	1	88.5669	1.886980	0.241500
Temp (Q)	16.3421	1	16.3421	0.348181	0.586867
(2)Heating rate(L)	240.8680	1	240.8680	5.131864	0.086168
Heating rate(Q)	7.2250	1	7.2250	0.153935	0.714812
1L by 2L	4.9141	1	4.9141	0.104698	0.762474
Error	187.7431	4	46.9358		
Total SS	562.0668	9			

Table 9-16: ANOVA table for Slow Pyrolysis pyrolytic water yield.

Factor	Pyrolytic water yield; R-sqr=.92328; Adj:.82738 (Slow data)				
	SS	df	MS	F	p
(1)Temp (L)	232.5197	1	232.5197	42.07522	0.002912
Temp (Q)	17.8417	1	17.8417	3.22851	0.146783
(2)Heating Rate(L)	0.2392	1	0.2392	0.04329	0.845352
Heating Rate(Q)	0.1824	1	0.1824	0.03301	0.864661
1L by 2L	9.4251	1	9.4251	1.70551	0.261608
Error	22.1051	4	5.5263		
Total SS	288.1324	9			

Table 9-17: ANOVA table for Vacuum Pyrolysis pyrolytic water yield.

Factor	Pyrolytic water yield; R-sqr=.88017; Adj:.73038 (Vacuum data)				
	SS	df	MS	F	p
(1)Temp (L)	148.0898	1	148.0898	18.71211	0.012391
Temp (Q)	22.4857	1	22.4857	2.84122	0.167155
(2)Heating rate(L)	41.6335	1	41.6335	5.26067	0.083524
Heating rate(Q)	0.3116	1	0.3116	0.03938	0.852385
1L by 2L	17.7399	1	17.7399	2.24156	0.208693
Error	31.6565	4	7.9141		
Total SS	264.1794	9			

Table 9-18: ANOVA table for Slow Pyrolysis organic liquid yield.

Factor	Organic Liquid Yield; R-sqr=.95867; Adj:.90701 (Slow data)				
	SS	df	MS	F	p
(1)Temp (L)	441.3876	1	441.3876	75.35283	0.000969
Temp (Q)	56.0814	1	56.0814	9.57410	0.036425
(2)Heating Rate(L)	35.6586	1	35.6586	6.08757	0.069147
Heating Rate(Q)	0.0758	1	0.0758	0.01294	0.914916
1L by 2L	0.0840	1	0.0840	0.01435	0.910437
Error	23.4304	4	5.8576		
Total SS	566.9023	9			

Table 9-19: ANOVA table for Vacuum Pyrolysis organic liquid yield.

Factor	Organic Liquid Yield; R-sqr=.96712; Adj:.92602 (Vacuum data (18Oct))				
	SS	df	MS	F	p
(1)Temp (L)	1211.415	1	1211.415	87.89583	0.000721
Temp (Q)	179.020	1	179.020	12.98902	0.022677
(2)Heating rate(L)	202.008	1	202.008	14.65694	0.018643
Heating rate(Q)	2.780	1	2.780	0.20169	0.676618
1L by 2L	9.543	1	9.543	0.69242	0.452135
Error	55.130	4	13.782		
Total SS	1676.697	9			

Table 9-20: ANOVA table for Furan in Slow Pyrolysis bio-oil.

Factor	Furan; R-sqr=.93184; Adj:.81823 (Slow data)				
	SS	df	MS	F	p
(1)Temp (L)	340.7257	1	340.7257	23.52410	0.016728
Temp (Q)	175.2838	1	175.2838	12.10180	0.040091
(2)Heating Rate(L)	4.0310	1	4.0310	0.27831	0.634341
Heating Rate(Q)	1.0357	1	1.0357	0.07150	0.806490
1L by 2L	0.1849	1	0.1849	0.01276	0.917189
Error	43.4523	3	14.4841		
Total SS	637.4597	8			

Table 9-21: ANOVA table for Furan in Vacuum Pyrolysis bio-oil.

Factor	Furan; R-sqr=.8828; Adj:.7363 (Vacuum data)				
	SS	df	MS	F	p
(1)Temp (L)	223.9627	1	223.9627	11.35594	0.028047
Temp (Q)	239.2052	1	239.2052	12.12880	0.025291
(2)Heating rate(L)	84.5716	1	84.5716	4.28817	0.107134
Heating rate(Q)	52.9011	1	52.9011	2.68233	0.176809
1L by 2L	45.8686	1	45.8686	2.32575	0.201938
Error	78.8883	4	19.7221		
Total SS	673.1176	9			

Table 9-22: ANOVA table for Acid in Slow Pyrolysis bio-oil.

Factor	Acids; R-sqr=.83678; Adj:.56475 (Slow data)				
	SS	df	MS	F	p
(1)Temp (L)	2747.098	1	2747.098	11.19220	0.044207
Temp (Q)	392.674	1	392.674	1.59983	0.295250
(2)Heating Rate(L)	784.266	1	784.266	3.19525	0.171815
Heating Rate(Q)	493.196	1	493.196	2.00937	0.251341
1L by 2L	2.024	1	2.024	0.00825	0.933371
Error	736.343	3	245.448		
Total SS	4511.356	8			

Table 9-23: ANOVA table for Ketones in Slow Pyrolysis bio-oil

Factor	Ketones; R-sqr=.85207; Adj:.60551 (Slow data)				
	SS	df	MS	F	p
(1)Temp (L)	1736.512	1	1736.512	11.75915	0.041564
Temp (Q)	284.193	1	284.193	1.92447	0.259460
(2)Heating Rate(L)	24.690	1	24.690	0.16719	0.710056
Heating Rate(Q)	4.031	1	4.031	0.02730	0.879276
1L by 2L	47.359	1	47.359	0.32070	0.610782
Error	443.020	3	147.673		
Total SS	2994.754	8			

Table 9-24: ANOVA table for Ketones in Vacuum Pyrolysis bio-oil

Factor	Ketones; R-sqr=.9281; Adj:.83822 (Vacuum data)				
	SS	df	MS	F	p
(1)Temp (L)	1392.262	1	1392.262	24.87705	0.007556
Temp (Q)	1019.978	1	1019.978	18.22505	0.012960
(2)Heating rate(L)	287.715	1	287.715	5.14092	0.085978
Heating rate(Q)	3.304	1	3.304	0.05904	0.819967
1L by 2L	21.849	1	21.849	0.39040	0.565961
Error	223.863	4	55.966		
Total SS	3113.361	9			

Table 9-25: ANOVA table for Sugars in Slow Pyrolysis bio-oil

Factor	Sugars; R-sqr=.95097; Adj:.86926 (Slow data)				
	SS	df	MS	F	p
(1)Temp (L)	10.8354	1	10.8354	1.49393	0.308879
Temp (Q)	0.5171	1	0.5171	0.07130	0.806758
(2)Heating Rate(L)	183.5672	1	183.5672	25.30928	0.015135
Heating Rate(Q)	115.9437	1	115.9437	15.98571	0.028041
1L by 2L	17.3098	1	17.3098	2.38658	0.220089
Error	21.7589	3	7.2530		
Total SS	443.8226	8			

Table 9-26: ANOVA table for Cyclic 5-carbon compounds in Slow Pyrolysis bio-oil

Factor	C5; R-sqr=.94469; Adj:.8525 (Slow data)				
	SS	df	MS	F	p
(1)Temp (L)	571.1572	1	571.1572	37.47564	0.008762
Temp (Q)	63.5790	1	63.5790	4.17164	0.133730
(2)Heating Rate(L)	7.3197	1	7.3197	0.48027	0.538132
Heating Rate(Q)	6.4101	1	6.4101	0.42059	0.562858
1L by 2L	6.8107	1	6.8107	0.44687	0.551662
Error	45.7223	3	15.2408		
Total SS	826.6352	8			

Table 9-27: ANOVA table for Cyclic 5-carbon compounds in Vacuum Pyrolysis bio-oil

Factor	C5; R-sqr=.96295; Adj:.91663 (Vacuum data)				
	SS	df	MS	F	p
(1)Temp (L)	494.7759	1	494.7759	72.99389	0.001030
Temp (Q)	151.3243	1	151.3243	22.32475	0.009138
(2)Heating rate(L)	55.7364	1	55.7364	8.22275	0.045582
Heating rate(Q)	14.3132	1	14.3132	2.11161	0.219846
1L by 2L	0.3198	1	0.3198	0.04717	0.838683
Error	27.1133	4	6.7783		
Total SS	731.7770	9			

Table 9-28: ANOVA table for Phenols in Slow Pyrolysis bio-oil

	Phenols; R-sqr=.85283; Adj:.60755 (Slow data)				
Factor	SS	df	MS	F	p
(1)Temp (L)	10883.51	1	10883.51	12.93177	0.036864
Temp (Q)	921.42	1	921.42	1.09483	0.372280
(2)Heating Rate(L)	95.57	1	95.57	0.11356	0.758325
Heating Rate(Q)	323.05	1	323.05	0.38385	0.579421
1L by 2L	149.39	1	149.39	0.17750	0.701895
Error	2524.83	3	841.61		
Total SS	17156.04	8			

Table 9-29: ANOVA table for Phenols in Vacuum Pyrolysis bio-oil

	Phenols; R-sqr=.82621; Adj:.60898 (Vacuum data)				
Factor	SS	df	MS	F	p
(1)Temp (L)	3905.022	1	3905.022	14.33439	0.019334
Temp (Q)	382.697	1	382.697	1.40479	0.301527
(2)Heating rate(L)	184.129	1	184.129	0.67589	0.457186
Heating rate(Q)	326.275	1	326.275	1.19768	0.335265
1L by 2L	592.502	1	592.502	2.17493	0.214296
Error	1089.693	4	272.423		
Total SS	6270.342	9			

Table 9-30: ANOVA table for Furfural in Slow Pyrolysis bio-oil

	Furfural; R-sqr=.92; Adj:.78666 (Slow data)				
Factor	SS	df	MS	F	p
(1)Temp (L)	434.4644	1	434.4644	20.45012	0.020221
Temp (Q)	78.8866	1	78.8866	3.71317	0.149612
(2)Heating Rate(L)	3.3175	1	3.3175	0.15615	0.719146
Heating Rate(Q)	0.3285	1	0.3285	0.01546	0.908907
1L by 2L	38.4429	1	38.4429	1.80950	0.271215
Error	63.7352	3	21.2451		
Total SS	796.6720	8			

Table 9-31: ANOVA table for Furfural in Vacuum Pyrolysis bio-oil

Factor	Furfural; R-sqr=.90165; Adj:.77871 (Vacuum data)				
	SS	df	MS	F	p
(1)Temp (L)	252.3709	1	252.3709	29.38259	0.005615
Temp (Q)	13.0541	1	13.0541	1.51984	0.285145
(2)Heating rate(L)	24.7526	1	24.7526	2.88185	0.164818
Heating rate(Q)	0.1115	1	0.1115	0.01298	0.914778
1L by 2L	23.0421	1	23.0421	2.68270	0.176786
Error	34.3565	4	8.5891		
Total SS	349.3276	9			

Table 9-32: ANOVA table for the HHV of Slow Pyrolysis char

Factor	Char HHV; R-sqr=.8991; Adj:.77298 (Slow data)				
	SS	df	MS	F	p
(1)Temp (L)	130.4517	1	130.4517	29.57795	0.005548
Temp (Q)	8.5410	1	8.5410	1.93655	0.236437
(2)Heating Rate(L)	1.1866	1	1.1866	0.26905	0.631345
Heating Rate(Q)	6.2359	1	6.2359	1.41390	0.300173
1L by 2L	0.0037	1	0.0037	0.00084	0.978265
Error	17.6418	4	4.4104		
Total SS	174.8500	9			

Table 9-33: ANOVA table for the HHV of Vacuum Pyrolysis char

Factor	Char HHV; R-sqr=.96575; Adj:.92295 (Vacuum data)				
	SS	df	MS	F	p
(1)Temp (L)	48.78619	1	48.78619	100.3416	0.000558
Temp (Q)	5.11738	1	5.11738	10.5252	0.031546
(2)Heating rate(L)	0.24115	1	0.24115	0.4960	0.520107
Heating rate(Q)	0.31099	1	0.31099	0.6396	0.468644
1L by 2L	0.50410	1	0.50410	1.0368	0.366141
Error	1.94480	4	0.48620		
Total SS	56.79044	9			

9.4 List of compound detected using GC-MS with a certainty greater than 70 %

Table 9-34 and **Table 9-35** list all the components detected with a certainty of more than 70 % in Fast Pyrolysis and Slow and Vacuum Pyrolysis bio-oils.

Table 9-34: Unique components detected in Fast Pyrolysis bio-oil

Fast Pyrolysis bio-oil compounds
(S)-(+)-2',3'-Dideoxyribonolactone
(S)-(+)-2',3'-Dideoxyribonolactone
[5,5-Dimethyl-7(H)-oxo-4-(2,3,3-trimethyl-5-oxopyrrolidin-2-yl)-2,3,5,6-tetrahydropyrrolo[1,2-c]pyrimidin-2-yl]acetonitrile
1,1':4',1''-Terphenyl-, 3'-methyl-
1,2-Benzenediol, 3-methoxy-
1,2-Benzenediol, 4-methyl-
1,2-Cyclopentanedione, 3-methyl-
1,2-Dimethoxy-4-n-propylbenzene
1,2-Ethanediol, diacetate
1,3,5-Benzenetriamine, 2-methyl-
1,3-Butadiene
1,3-Dimethyl-1-cyclohexene
1,3-Dimethyl-5-[1,2-dicarbethoxyhydrazino]-6-hydrazinouracil
1,3-Dioxol-2-one
1,4:3,6-Dianhydro-.alpha.-d-glucopyranose
1,4-Benzenediol, 2,3,5-trimethyl-
1,4-Benzenediol, 2-methyl-
1,4-Cyclohexanediol, trans-
1,5,8,11-Tetraazatetracyclo[7.3.1.1(3,11).0(4,9)]pentadec-4-ene, 3-methyl-
1-Butanone, 1-(2,4,6-trihydroxy-3-methylphenyl)-
1-Carboethoxypiperazine-4-thiocarboxylic acid 2-[1-[2-pyridyl 1-oxide]hydrazide
1H-Inden-1-one, 2,3-dihydro-
1H-Inden-5-ol, 2,3-dihydro-
1-Hydroxy-2-butanone
1-n-Butoxy-1-chloro-1-silacyclopentane
2(3H)-Furanone
2(3H)-Furanone, 5-methyl-
2(5H)-Furanone
Library/ID
2(5H)-Furanone, 3-methyl-
2(5H)-Furanone, 5-ethyl-
2(5H)-Furanone, 5-methyl-
2,2-Dimethyl-5,7-dinitro-1,3-diazaadamantane
2,3-Anhydro-d-mannosan
2,3-Butanedione
2,3-Dihydrofuran
2,3-Dihydroxybenzaldehyde
2,4,6,8,9,10-Hexaaza-1,3,5,7-tetraphosphatricyclo[3.3.1.1(3,7)]decane, 2,4,6,8,9,10-hexamethyl-, 1-sulfide
2,4-Dimethoxycinnamic acid
2,4-Heptadienal, (E,E)-

2,4-Hexadiyne-1,6-diol
2,5-Dimethyl-2-(2-tetrahydrofuryl)tetrahydrofuran
2,5-Furandicarboxaldehyde
2,5-Hexanedione
2,5-Methano-2H-thieno[3,2-b]thiopyran-8-ol, hexahydro-, acetate, (2.alpha.,3a.beta.,5.alpha.,7a.beta.,8R*)-
2,6,10,14-Tetramethylpentadecan-3-one
2-acetylpyridine 4-[2-Methoxyphenyl]-3-thiosemicarbazone
2-Allyl-1,4-dimethoxy-3-methyl-benzene
2-Allyl-4-methylphenol
2-Benzimidazolyl methane thiosulfuric acid
2-Butanamine, N-(1-methylpropyl)-
2-Butanone
2-Butenal
2-Butenal, 2-methyl-
2-Butenal, 2-methyl-, (E)-
2-Butenoic acid, (E)-
2-Butenoic acid, methyl ester, (Z)-
2-Cyclohexen-1-ol
2-Cyclohexene-1,4-dione
2-Cyclopenten-1-one
2-Cyclopenten-1-one, 2,3-dimethyl-
2-Cyclopenten-1-one, 2-hydroxy-
2-Cyclopenten-1-one, 2-hydroxy-3,4-dimethyl-
2-Cyclopenten-1-one, 2-hydroxy-3-methyl-
2-Cyclopenten-1-one, 2-methyl-
2-Cyclopenten-1-one, 3,4-dimethyl-
2-Cyclopenten-1-one, 3-ethyl-
2-Cyclopenten-1-one, 3-ethyl-2-hydroxy-
2-Cyclopenten-1-one, 3-methyl-
2-Cyclopentene-1,4-dione
2-Furancarboxaldehyde, 5-(hydroxymethyl)-
2-Furancarboxaldehyde, 5-methyl-
2-Furancarboxylic acid, hydrazide
2-Furanmethanol
2-Furanone, 2,5-dihydro-3,5-dimethyl
2H-Pyran-2-carboxaldehyde, 3,4-dihydro-
2H-Pyran-2-one
2H-Pyran-2-one, 5,6-dihydro-
2-Methoxy-4-vinylphenol
2-Methyl-2-vinyloxirane
2-Pentanone, 1-(2,4,6-trihydroxyphenyl)
2-Pentenoic acid, 4-hydroxy-
2-Propanone, 1-(acetyloxy)-
3-(4-Chlorobenzyl)-N-(2,5-dimethylphenyl)succinamic acid

3,3-Dimethylacryloyl chloride
3,4,5-Trimethoxybenzyl methyl ether
3,4-Dimethoxycinnamic acid
3,5-Cyclohexadiene-1,2-dione, 3,4,5,6-tetrachloro-
3,5-Dihydroxytoluene
3,5-Dimethoxy-4-hydroxycinnamaldehyde
3,6-Diazahomoadamantan-9-ol
3-Butenoic acid
3-Furaldehyde
3-Hydroxybenzoyl 2-nitrobenzylidenehydrazide
3-Isoxazolamine, 5-methyl-
4(3H)-Pyrimidinone, 2-(p-chlorophenyl)-6-methyl-
4H-Imidazol-4-one, 2-amino-1,5-dihydro-
4H-Pyran-4-one
4H-Pyran-4-one, 2,3-dihydro-3,5-dihydroxy-6-methyl-
4H-Pyran-4-one, 3,5-dihydroxy-2-methyl-
4-Hydroxy-2-methylbenzaldehyde
4-Hydroxy-3-methylacetophenone
4-Hydroxy-3-methylbenzaldehyde
4-Mercaptophenol
4-Methoxy-2-methyl-1-(methylthio)benzene
4-Methoxymethyl-6-methyl-1H-pyrazolo[3,4-b]pyridin-3-ylamine
4-Methyl-5H-furan-2-one
4-Nitro-5-hydroxy-1,2-dimethylindole
4'-Phenylpropiophenone
4-Pyridazinamine
5-(Prop-2-enylidene)-10-oxa-10,11-dihydro-5H-dibenzo[a,d]cycloheptene
5,6,7-Trimethoxy-1-indanone
5,9-Dodecadien-2-one, 6,10-dimethyl-, (E,E))-
5-Formylsalicylaldehyde
5-Hydroxymethyldihydrofuran-2-one
5-Isopropyl-3,3-dimethyl-2-methylene-2,3-dihydrofuran
5-Methyl-2-allylphenol
5-tert-Butylpyrogallol
7-Methoxybenzofuran-2-carboxylic acid
9H-Fluoren-9-ol
9H-Furo[2,3-f][1]benzopyran-9-one, 4-methoxy-7-methyl-
Acetaldehyde
Acetaldehyde, methoxy-
Acetic acid
Acetonitrile, (3-chloro-5,5-dimethyl-2-cyclohexen-1-ylidene)-, (E)-
Aminomethanesulfonic acid
Asarone
Aspidinol

Aziridine, 1,2,3-trimethyl-, trans-
Benzaldehyde, 2,4-dihydroxy-3,6-dimethyl-
Benzaldehyde, 2-ethyl-
Benzaldehyde, 2-hydroxy-3-methoxy-
Benzaldehyde, 2-hydroxy-6-methyl-
Benzaldehyde, 3-ethoxy-2-hydroxy-
Benzaldehyde, 3-hydroxy-
Benzaldehyde, 4,6-dihydroxy-2,3-dimethyl-
Benzaldehyde, 4-hydroxy-
Benzaldehyde, 4-hydroxy-3,5-dimethoxy-
Benzene, 1,2,4-trimethoxy-5-(1-propenyl)-, (Z)-
Benzene, 1,4-dimethoxy-2-methyl-
Benzene, 1-ethyl-4-methoxy-
Benzeneacetic acid, 4-hydroxy-3-methoxy-
Benzoic acid, 4-hydroxy-3,5-dimethoxy-, hydrazide
Bicyclo[4.1.0]heptan-2-one
Butane, 2,2,3,3-tetramethyl-
Butanedial
Butanoic acid
Butyrolactone
Curan-17-oic acid, 2,16-didehydro-20-hydroxy-19-oxo-, methyl ester
Cyclobutene
D-Allose
Desaspidinol
Dicyclobutylidene oxide
Ethanone, 1-(2,5-dimethoxyphenyl)-
Ethanone, 1-(2-furanyl)-
Ethanone, 1-(2-hydroxy-5-methylphenyl)-
Ethanone, 1-(3-hydroxyphenyl)-
Ethanone, 1-(3-methoxyphenyl)-
Ethanone, 1-(4-hydroxy-3,5-dimethoxyphenyl)-
Ethanone, 1-(4-hydroxy-3-methoxyphenyl)-
Ethanone, 2-(1H-imidazo[4,5-b]pyridin-2-yl)-1-(4-morpholyl)-
Eugenol
Formic acid
Furan
Furan, 2,3-dihydro-3-methyl-
Furan, 2-ethyl-5-methyl-
Furan, 2-methyl-
Furfural
Furyl hydroxymethyl ketone
Hexane, 2,2-dimethyl-
Hydrazine, (3-fluorophenyl)-
Isophthaldiamidoxime

Maltol
Methacrolein
Methyl 2-furoate
N-(4-Methoxyphenyl)-2-hydroxyimino-acetamide
Octane, 2,6-dimethyl-
Octanoic acid, 2-tetrahydrofurylmethyl ester
Pent-2-ynal
Phenol
Phenol, 2-(1-methylethyl)-
Phenol, 2,4,6-trimethyl-
Phenol, 2,4-dimethyl-
Phenol, 2,6-dimethoxy-
Phenol, 2,6-dimethoxy-4-(2-propenyl)-
Phenol, 2-chloro-4-cyclohexyl-
Phenol, 2-ethyl-
Phenol, 2-methoxy-
Phenol, 2-methoxy-3-(2-propenyl)-
Phenol, 2-methoxy-4-(1-propenyl)-
Phenol, 2-methoxy-4-(1-propenyl)-, (E)-
Phenol, 2-methoxy-4-(1-propenyl)-, (Z)-
Phenol, 2-methoxy-4-methyl-
Phenol, 2-methyl-
Phenol, 3-(1-methylethyl)-
Phenol, 3,4-dimethoxy-
Phenol, 3,4-dimethyl-
Phenol, 3,5-dimethyl-
Phenol, 3-ethyl-
Phenol, 3-methyl-
Phenol, 4-(2-propenyl)-
Phenol, 4-ethyl-
Phenol, 4-ethyl-2-methoxy-
Phenol, 4-ethyl-2-methyl-
Phenol, 4-ethyl-3-methyl-
Phenol, 4-methyl-
Propanedinitrile, (ethoxymethylene)-
Propanoic acid
Pyrazine, 2-methoxy-3-(1-methylethyl)-
Resorcinol
Silacyclohexadiene-2,5
Silane, dimethyl-
Sulfur dioxide
Tetrahydrofuran-5-on-2-methanol, .alpha.-[.alpha.-methoxy-(tetrahydrofuran-5-on-2-ylmethoxy)]-
Valeric acid, tridec-2-ynyl ester
Vanillin

Table 9-35: Unique components detected in Slow and Vacuum Pyrolysis bio-oil

Slow Pyrolysis	Vacuum Pyrolysis
(S)-(+)-2',3'-Dideoxyribonolactone	1,1'-Bicyclopentyl-1,1'-diol
1,2,4-Trimethoxybenzene	1,2,4-Trimethoxybenzene
1,2-Cyclopentanedione,-methyl-	1,2-Cyclopentanedione,-methyl-
1,3-Propanediamine, N-methyl-	1,2-Pentadiene
1,4:3,6-Dianhydro-.alpha.-d-glucopyranose	1,3-Propanediamine, N-methyl-
1,4-Benzenediol, 2-methoxy-	1,4:3,6-Dianhydro-.alpha.-d-glucop
1,4-Benzenediol, 2-methyl-	1,4:3,6-Dianhydro-.alpha.-d-glucopyranose
1,4-Benzenediol,-methyl-	1,4-Pentadiene
1,4-Dioxin,,3-dihydro-	1,6-Anhydro-.beta.-D-glucopyranose(levoglucosan)
1-Butyne	1-Cyclohexene-1-methanol
1H-Inden-1-one, 2,3-dihydro-	2(3H)-Furanone
1H-Pyrazole-4-carboxylic acid	2(3H)-Furanone, 5-methyl-
1-Hydroxy-2-pentanone	2(3H)-Furanone, dihydro-4-hydroxy-
2(3H)-Furanone	2(5H)-Furanone
2(3H)-Furanone, 5-methyl-	2(5H)-Furanone, 3-methyl-
2(3H)-Furanone,-ethyldihydro-	2(5H)-Furanone, 5-methyl-
2(3H)-Furanone,-methyl-	2,3-Anhydro-d-mannosan
2(5H)-Furanone	2,3-Butanedione
2(5H)-Furanone, 3-methyl-	2,3-Dimethoxytoluene
2(5H)-Furanone, 5-methyl-	2,3-Dimethyl-2-heptene
2(5H)-Furanone,-methyl-	2,5-Furandicarboxaldehyde
2,3-Anhydro-d-galactosan	2-Amino-3,5,7,8-tetrahydro-4,6-pteridinedione
2,3-Anhydro-d-mannosan	2-Butanone, 4-(4-hydroxy-3-methoxyphenyl)-
2,3-Butanedione	2-Butenoic acid, methyl ester, (Z)
2,5-Furandione, 3,4-dimethyl-	2-Butenoyl chloride
2,5-Hexanedione	2-Cyclohexen-1-ol
2-Acetyl-5-methylfuran	2-Cyclohexene-1,4-dione
2-Allyl-3-ethoxy-4-methoxyphenol	2-Cyclopenten-1-one
2-Butanone, 1-(acetyloxy)-	2-Cyclopenten-1-one, 2-hydroxy-
2-Butanone,-(acetyloxy)-	2-Cyclopenten-1-one, 2-hydroxy-3-methyl-
2-Butanone,,3-dimethyl-	2-Cyclopenten-1-one, 2-methyl-
2-Butanone,-hydroxy-	2-Cyclopenten-1-one, 3-ethyl-2-hydroxy-
2-Butenal	2-Cyclopenten-1-one, 3-methyl-
2-Butenal, (E)-	2-Cyclopenten-1-one,,3-dimethyl-

2-Butenoic acid, methyl ester, (Z)	2-Cyclopenten-1-one,-ethyl-2-hydroxy-
2-Butenoyl chloride	2-Cyclopenten-1-one,-hydroxy-
2-Cyclopenten-1-one	2-Cyclopenten-1-one,-hydroxy-3-methyl-
2-Cyclopenten-1-one, 2,3-dimethyl-	2-Cyclopenten-1-one,-methyl-
2-Cyclopenten-1-one, 2-hydroxy-	2-Cyclopentene-1,4-dione
2-Cyclopenten-1-one, 2-hydroxy-3-m	2-Cyclopropylcarbonyloxytridecane
2-Cyclopenten-1-one, 2-hydroxy-3-methyl-	2-Furancarboxaldehyde, 5-(hydroxymethyl)-
2-Cyclopenten-1-one, 2-methyl-	2-Furancarboxaldehyde, 5-methyl-
2-Cyclopenten-1-one, 3-ethyl-	2-Furancarboxaldehyde,-(hydroxymethyl)-
2-Cyclopenten-1-one, 3-ethyl-2-hydroxy-	2-Furancarboxaldehyde,-methyl-
2-Cyclopenten-1-one, 3-methyl-	2-Furancarboxylic acid, hydrazide
2-Cyclopenten-1-one,,3-dimethyl-	2-Furancarboxylic acid,-tetrahydrofurylmethyl ester
2-Cyclopenten-1-one,-ethyl-2-hydroxy-	2-Furanmethanol
2-Cyclopenten-1-one,-hydroxy-	2H-Pyran-2-one,,6-dihydro-
2-Cyclopenten-1-one,-hydroxy-3-methyl-	2-Methoxy-4-vinylphenol
2-Cyclopenten-1-one,-methyl-	2-Methoxy-5-methylphenol
2-Ethylacrolein	2-Methoxy-6-methylphenol
2-Furancarboxaldehyde, 5-(hydroxym	2-Pentanone, 1-(2,4,6-trihydroxyphenyl)
2-Furancarboxaldehyde, 5-(hydroxymethyl)-	2-Pentanone, 4-hydroxy-4-methyl-
2-Furancarboxaldehyde, 5-methyl-	2-Propanone, 1-(acetyloxy)-
2-Furancarboxaldehyde,-(hydroxymethyl)-	2-Propanone,-(acetyloxy)-
2-Furancarboxaldehyde,-methyl-	2-tert-Butyl-3,4,5,6-tetrahydropyridine
2-Furancarboxylic acid	3,5-Dimethoxy-4-hydroxycinnamaldehyde
2-Furancarboxylic acid, hydrazide	3-Allyl-6-methoxyphenol
2-Furanmethanol	3-Cyclobutene-1,2-dione, 3,4-dihydroxy-
2-Furanmethanol, tetrahydro-	3-Furaldehyde
2H-Pyran-3(4H)-one, dihydro-	4-Ethylbiphenyl
2-Hydroxy-3-propyl-2-cyclopenten-1	4H-Pyran-4-one, 2,3-dihydro-3,5-dihydroxy-6-methyl-
2-Hydroxy-3-propyl-2-cyclopenten-1-one	4H-Pyran-4-one, 3,5-dihydroxy-2-methyl-
2-Methoxy-4-vinylphenol	4H-Pyran-4-one,,5-dihydroxy-2-methyl-
2-Methoxy-6-methylphenol	4-Methyl-5H-furan-2-one
2-Pentanone, 4-hydroxy-4-methyl-	4'-Phenylpropiophenone
2-Pentanone,-(2,4,6-trihydroxyphenyl)	5,6-Epoxyhexanol-1
2-Pentanone,-hydroxy-4-methyl-	5,9-Dodecadien-2-one, 6,10-dimethyl-, (E,E))-
2-Propanone, 1-(acetyloxy)-	5,9-Dodecadien-2-one,,10-dimethyl-, (E,E))-
2-Propanone,-(acetyloxy)-	5-Acetoxymethyl-2-furaldehyde

3,4-Anhydro-d-galactosan	5-tert-Butylpyrogallol
3,4-Heptadiene	Acetic acid
3,5-Dimethoxytoluene	Acetonitrile, (3-chloro-5,5-dimethyl-2-cyclohexen-1-ylidene)-, (E)-
3,6,9,12-Tetraoxatetradecan-1-ol,	Adenosine, N6-phenylacetic acid
3-Buten-2-one, 3-methyl-	Benzaldehyde, 3-hydroxy-4-methoxy-
3-Penten-2-one	Benzaldehyde, 4-hydroxy-3,5-dimethoxy-
3-Pentenenitrile	Benzaldehyde,-hydroxy-3,5-dimethoxy-
3-Picoline,-amino-,-oxide	Benzene, 1,1'-ethylidenebis-
4(5H)-Benzofuranone, 6,7-dihydro-3	Benzene,,2,3-trimethoxy-5-methyl
4,4-Dimethyl-5-methylene-2-allylamino-2-thiazoline	Benzoic acid, 4-hydroxy-3,5-dimethoxy-, hydrazide
4-Chloro-2-nitrobenzyl alcohol	Benzoic acid,-(4-chloro-3-nitrobenzoylamino)-
4H-Pyran-4-one, 3,5-dihydroxy-2-me	Benzoic acid,-hydroxy-3,5-dimethoxy-, hydrazide
4H-Pyran-4-one, 3,5-dihydroxy-2-methyl-	Benzoic acid,-hydroxy-3-methoxy-, methyl ester
4H-Pyran-4-one,,5-dihydroxy-2-methyl-	Butanal, 3-hydroxy-
4-Methyl-5H-furan-2-one	Butanedial
5,9-Dodecadien-2-one, 6,10-dimethyl-, (E,E))-	Butanoic acid, 4-hydroxy-
5-Hydroxymethyldihydrofuran-2-one	Butyrolactone
5-Isopropenyloxymethylene-3,3-dimethyl-cyclohexanone	Crotonyl bromide
Acetic acid	Crotonyl isothiocyanate
Benzaldehyde, 3-hydroxy-	Cyclopropanecarboxylic acid chloride
Benzaldehyde, 4-hydroxy-3,5-dimeth	D-Allose
Benzaldehyde, 4-hydroxy-3,5-dimethoxy-	Ethanone, 1-(2-furanyl)-
Benzaldehyde,-hydroxy-3,5-dimethoxy-	Ethanone, 1-(2-hydroxy-5-methylphenyl)-
Benzaldehyde,-hydroxy-5-methoxy-	Ethanone, 1-(3-hydroxy-4-methoxyphenyl)-
Benzene, 1,4-dimethoxy-2-methyl-	Ethanone, 1-(4-hydroxy-3,5-dimethoxyphenyl)-
Benzoic acid, 4-hydroxy-3,5-dimeth	Ethanone, 1-(4-hydroxy-3-methoxyphenyl)-
Benzoic acid, 4-hydroxy-3,5-dimethoxy-, hydrazide	Ethanone,-(2-furanyl)-
Benzoic acid,-hydroxy-3,5-dimeth	Ethanone,-(3-hydroxy-4-methoxyphenyl)-
Benzoic acid,-hydroxy-3,5-dimethoxy-, hydrazide	Ethanone,-(4-hydroxy-3,5-dimethoxyphenyl)-
But-3-en-1-ynyl methyl sulfide	Ethanone,-(4-hydroxy-3-methoxyphenyl)-
Butanedial	Ethyl 5-[2-pyridyl]-4-bromopyrazole-3-carboxylate
Butyrolactone	Eugenol
Crotonic acid	Formic acid

Cyclohexanone,-ethyl-	Furan, 2,5-dihydro-
Cyclopentane, 1-methyl-2-propyl-	Furfural
D-Allose	Furfural
Dicyclobutylidene oxide	Furyl hydroxymethyl ketone
Ethanone, 1-(2-furanyl)-	Hydroquinone mono-trimethylsilyl ether
Ethanone, 1-(3-hydroxy-4-methoxyphenyl)-	Maltol
Ethanone, 1-(4-hydroxy-3,5-dimetho	Methacryloyl chloride
Ethanone, 1-(4-hydroxy-3,5-dimethoxyphenyl)-	Methanone, dicyclopropyl-
Ethanone, 1-(4-hydroxy-3-methoxyph	Methyl 2-furoate
Ethanone, 1-(4-hydroxy-3-methoxyphenyl)-	N-Methoxy-1-ribofuranosyl-4-imidazolecarboxylic amide
Ethanone,-(2-furanyl)-	o-Methylisourea hydrogen sulfate
Ethanone,-(3-hydroxy-4-methoxyphenyl)-	Perfluorotributylamine
Ethanone,-(4-hydroxy-3,5-dimethoxyphenyl)-	Phenol
Ethanone,-(4-hydroxy-3-methoxyphenyl)-	Phenol, 2,4-dimethyl-
Ethyl alcohol	Phenol, 2,6-dimethoxy-
Eugenol	Phenol, 2,6-dimethoxy-4-(2-propeny)-
Formic acid	Phenol, 2,6-dimethoxy-4-(2-propenyl)-
Furan, tetrahydro-2,5-dimethoxy-	Phenol, 2-methoxy-
Furan, tetrahydro-2-methyl-	Phenol, 2-methoxy-4-(1-propenyl)-
Furan,,4-dimethyl-	Phenol, 2-methoxy-4-(1-propenyl)-,(Z)-
Furfural	Phenol, 2-methoxy-4-methyl-
Furyl hydroxymethyl ketone	Phenol, 2-methoxy-5-(1-propenyl)-,(E)-
Hexadecanoic acid, hexadecyl ester	Phenol, 2-methoxy-6-(1-propenyl)-
Hydrazine, 1,2-dimethyl-	Phenol, 2-methyl-
Isocrotonic acid	Phenol, 3-methyl-
Maltol	Phenol, 4-ethyl-2-methoxy-
Mequinol	Phenol, 4-methoxy-3-(methoxymethyl)-
Methyl 2-furoate	Phenol, 4-methyl-
Methylenecyclopropane	Phenol, 5-methoxy-2,3-dimethyl-
Methyl-furoate	Phenol,-(3-hydroxy-1-propenyl)-2-methoxy-
Pent-2-ynal	Phenol,,6-dimethoxy-
Phenol	Phenol,,6-dimethoxy-4-(2-propenyl)-
Phenol, 2,4-dimethyl-	Phenol,-ethyl-2-methoxy-
Phenol, 2,5-dimethyl-	Phenol,-methoxy-
Phenol, 2,6-dimethoxy-	Phenol,-methoxy-3-(2-propenyl)-
Phenol, 2,6-dimethoxy-4-(2-propeny	Phenol,-methoxy-4-(1-propenyl)-
Phenol, 2,6-dimethoxy-4-(2-propenyl)-	Phenol,-methoxy-4-(1-propenyl)-,(Z)-
Phenol, 2-methoxy-	Phenol,-methoxy-4-methyl-
Phenol, 2-methoxy-4-(1-propenyl)-	Phenol,-methyl-

Phenol, 2-methoxy-4-(1-propenyl)-,	Propanoic acid
Phenol, 2-methoxy-4-(1-propenyl)-,(E)-	Propenylguaethol
Phenol, 2-methoxy-4-(1-propenyl)-,(Z)-	Pyridine, 1-acetyl-1,2,3,4-tetrahydro-5-(2-pyrrolidinyl)-
Phenol, 2-methoxy-4-methyl-	Pyrimidine, 4,6-dichloro-2-methyl-5-nitro-
Phenol, 2-methoxy-5-(1-propenyl)-,(E)-	Tetrahydrofuran-5-on-2-methanol, .alpha.-[.alpha.-methoxy-(tetrahydrofuran-5-on-2-ylmethoxy)]-
Phenol, 2-methyl-	Titanium, [(1,2,3-.eta.)-2-butenyl](.eta.8-1,3,5,7-cyclooctatetraene)-
Phenol, 3,5-dimethyl-	Triethylamine
Phenol, 3-methyl-	Vanillin
Phenol, 4-(3-hydroxy-1-propenyl)-2	
Phenol, 4-(ethoxymethyl)-2-methoxy	
Phenol, 4-ethyl-2-methoxy-	
Phenol, 4-methyl-	
Phenol,,5-dimethyl-	
Phenol,,6-dimethoxy-	
Phenol,,6-dimethoxy-4-(2-propenyl)-	
Phenol,-ethyl-2-methoxy-	
Phenol,-methoxy-	
Phenol,-methoxy-4-(1-propenyl)-	
Phenol,-methoxy-4-(1-propenyl)-,(E)-	
Phenol,-methoxy-4-(1-propenyl)-,(Z)-	
Phenol,-methoxy-4-methyl-	
Phenol,-methoxy-oxy-, hydrazide	
Phenol,-methyl-	
Propanal,-methyl-	
Propanoic acid	
Trichothec-9-en-8-one, 4-(acetyloxy)-12,13-epoxy-3,7,15-trihydroxy-,(3.alpha.,4.beta.,7.beta.)-	
Vanillin	

9.5 Repeatability of Fast Pyrolysis GC/MS results

Table 9-36: Repeatability of FP bio-oil GC/MS results

Reactor temp.	°C	**440**	**440**	**Avg.**	**470**	**470**	**470**	**470**	**Avg.**
Particle size	µm	**570**	**1200**		**570**	**570**	**570**	**1200**	
Aldehydes	%	32	29	30 ± 2	29	30	27	29	29 ± 1
Ketones	%	15	19	17 ± 3	19	15	20	16	18 ± 2
Phenols	%	35	33	34 ± 1	31	35	34	38	34 ± 3
Sugars	%	12	13	12 ± 1	12	11	10	13	11 ± 1
Furans	%	5	5	5 ± 0	6	5	5	4	5 ± 1
Acids	%	2	1	1 ± 1	4	4	4	1	3 ± 2